2014

BASES FOR BREADTH - INSIGHTS INTO HOW THE MECHANISM AND DYNAMICS OF NITROREDUCTASE CAN EXPLAIN THIS ENZYME'S BROAD SUBSTRATE REPERTOIRE

Warintra Pitsawong
University of Kentucky, warintra_p@hotmail.com

STUDENT AGREEMENT:

I represent that my thesis or dissertation and abstract are my original work. Proper attribution has been given to all outside sources. I understand that I am solely responsible for obtaining any needed copyright permissions. I have obtained needed written permission statement(s) from the owner(s) of each third-party copyrighted matter to be included in my work, allowing electronic distribution (if such use is not permitted by the fair use doctrine) which will be submitted to UKnowledge as Additional File.

I hereby grant to The University of Kentucky and its agents the irrevocable, non-exclusive, and royalty-free license to archive and make accessible my work in whole or in part in all forms of media, now or hereafter known. I agree that the document mentioned above may be made available immediately for worldwide access unless an embargo applies.

I retain all other ownership rights to the copyright of my work. I also retain the right to use in future works (such as articles or books) all or part of my work. I understand that I am free to register the copyright to my work.

REVIEW, APPROVAL AND ACCEPTANCE

The document mentioned above has been reviewed and accepted by the student's advisor, on behalf of the advisory committee, and by the Director of Graduate Studies (DGS), on behalf of the program; we verify that this is the final, approved version of the student's thesis including all changes required by the advisory committee. The undersigned agree to abide by the statements above.

Warintra Pitsawong, Student

Dr. Anne-Frances Miller, Major Professor

Dr. Dong-Sheng Yang, Director of Graduate Studies

BASES FOR BREADTH - INSIGHTS INTO HOW THE MECHANISM AND DYNAMICS OF NITROREDUCTASE CAN EXPLAIN THIS ENZYME'S BROAD SUBSTRATE REPERTOIRE

DISSERTATION

A dissertation submitted in partial fulfillment of the requirements for the degree of Doctor of Philosophy in the College of Arts and Sciences at the University of Kentucky

By
Warintra Pitsawong

Lexington, Kentucky

Director: Dr. Anne-Frances Miller, Professor of Chemistry

Lexington, Kentucky

2014

ABSTRACT OF DISSERTATION

BASES FOR BREADTH - INSIGHTS INTO HOW THE MECHANISM AND DYNAMICS OF NITROREDUCTASE CAN EXPLAIN THIS ENZYME'S BROAD SUBSTRATE REPERTOIRE

Nitroreductase from *Enterobacter cloacae* (NR) is a member of a large family of homologues represented in all branches of the tree of life. However the physiological roles of many of these enzymes remain unknown. NR has distinguished itself on the basis the diverse sizes and chemical types of substrates it is able to reduce (Koder *et al* 1998). This might be an evolved characteristic suiting NR for a role in metabolism of diverse occasional toxins. While there are numerous studies of determinants of substrate specificity, we know less about mechanisms by which enzymes can be *inclusive*. Therefore, we present a synthesis of NR's dynamics, stability, ligand binding repertoire and kinetic mechanism. We find that NR reduces *para*-nitrobenzoic acid (*p*-NBA) via a simple mechanism limited by the chemical step in which the nitro group is reduced (Pitsawong *et al* 2014). Thus, for this substrate, NR's mechanism dispenses with gating steps that in other enzymes can enforce substrate specificity. Our data demonstrate that substrate reduction is accomplished by rate-contributing hydride transfer from the flavin cofactor coupled to proton transfer from solvent, but do not identify specific amino acids with a role. This is consistent with our crystal structures, which reveal a spacious solvent-exposed active site bounded by a helix that moves to accommodate binding of substrate analogs (Haynes *et al* 2002). Because it is able to reduce TNT (trinitrotoluene), herbicides and pesticides, NR has important potential utility in bioremediation.

KEYWORDS: Nitroreductase, Flavoproteins, Enzyme Kinetics, Enzyme Mechanisms, Substrate Specificity

Warintra Pitsawong

November 24th , 2014

BASES FOR BREADTH - INSIGHTS INTO HOW THE MECHANISM AND DYNAMICS OF NITROREDUCTASE CAN EXPLAIN THIS ENZYME'S BROAD SUBSTRATE REPERTOIRE

By

Warintra Pitsawong

Dr. Anne-Frances Miller
Director of Dissertation

Dr. Dong-Sheng Yang
Director of Graduate Studies

November 24th, 2014

DEDICATION

This dissertation is dedicated to my father, my mother, and my brother for all their support, encouragement, inspiration, and love.

ACKNOWLEDGMENTS

This dissertation would not have been possible without the help and support of so many people. First I would like to thank my supervisor, Prof. Anne-Frances Miller, for the continuous support, for her motivation, patience, and knowledge while allowing me the room to work my own way, but provided me advice whenever I needed it, especially during the lab or personal meeting. She encouraged me to attend scientific meetings where I could present my research projects. She has all been fantastic in many different ways. She has supported me in every step in my research, from setting up experiment to writing up my papers and dissertation. Through the training in Miller's group, I have acquired incredibly several technical and personal skills that are indispensable in my career development. Before joining Miller's group, I hardly had any research experience in NMR spectroscopy. In the beginning, trying to learn how to run the NMR is so difficult, and the theory behind NMR is much more complicated. She spent a lot of time on training me how to process the NMR data.

I also would like to thank my dissertation committee members for their time and support, Dr. Dong-Sheng Yang who has taught me many valuable principles of computational analysis in his class, which is the starting point for my computational project. Dr. Mark Lovell who has taught me Chemical Equilibrium And Data Analysis which is very useful for data interpretation. Dr. H. Peter Spielmann who provided me fantastic suggestions during my committee meeting which is very helpful for proceeding further in my research and Dr. David W. Rodgers for his willingness to serve as my external committee and provides us crystal structures in this study.

I want to give a special thanks to Mr. John Layton, who has taught me so much about NMR maintenance and has been always available to help me with any aspect of NMR. Moreover, he has become a good friend, I have enjoyed having great discussions while helping him to fill the NMR magnets with liquid helium and nitrogen and being his NMR TA.

I would also thank Mr. A. Sebesta who has always been helped Miller's group repairing so many instruments including anaerobic glove-box, centrifuge, UV-Vis spectrophotometer, shaker, freezer, NMR, and so on.

In my daily work I have been blessed with friendly and cheerful of the previous and current lab members, Xiaonan Mei, Ting Wang, John Hoben, and Jaining Wang. They were always helpful in regards to my research as well as entertainment.

I want to thank all my friends who have made my time here more enjoyable. Staying away from home for so many years has been so challenging. I have a lot of activities I do after my workday with them and that make me feel like I am not alone.

The department of chemistry has provided the funding and equipment I needed to finish my Ph.D. Through the course of my study in the department, I have gained much more than I anticipated. I thank the people and faculty in department who gave me valuable suggestions and guidance for my degree program.

Last, but not least, I would like to thank my family, my parents, my brother, my grandmother, my uncle and my aunt for all their continued support and encouraging me in all of my pursuits and inspiring me to follow my dreams and apologize for being away so far for so long, I know you understood my decision and I know I always have you to count on when times are rough and thank you for believing in me.

With out all of you, I most certainly would not be where I am today.

Warintra Pitsawong

TABLE OF CONTENTS

ACKNOWLEDGMENTS iii

TABLE OF CONTENTS v

LIST OF SCHEMES x

LIST OF TABLES xi

LIST OF FIGURES xii

CHAPTER 1 1

GENERAL INTRODUCTION 1

1.1 FLAVOPROTEINS 1

1.1.1 CLASSES OF FLAVOENZYMES 4

1.1.1.1 FLAVOPROTEIN MONOOXYGENASES 4

1.1.1.2 ELECTRON TRANSFERASES 5

1.1.1.3 DEHYDROGENASES / TRANSHYDROGENASES 5

1.1.1.4 FLAVOPROTEIN OXIDASES 6

1.1.1.5 OXIDOREDUCTASES 6

1.2 NITROREDUCTASES 7

1.3 WHAT HAVE WE LEARNED FROM THE PAST? 18

OBJECTIVES 20

CHAPTER 2 26

UNDERSTANDING THE BROAD SUBSTRATE REPERTOIRE OF NITROREDUCTASE BASED ON ITS KINETIC MECHANISM 26

2.1 ABSTRACT 26

2.2 INTRODUCTION 27

2.3 EXPERIMENTAL PROCEDURES 31

2.3.1 Reagents 31
2.3.2 Steady-state Kinetic Experiments 32
2.3.3 Rapid Reaction Experiments 32
2.3.4 Reductive Half-reaction 33
2.3.5 Oxidative Half-reaction 34
2.3.6 Testing for the stability of *p*-HABA 35
2.4 RESULTS 35
2.4.1 Steady-state Kinetics of NR 35
2.4.2 Reductive Half-reaction of oxidized NR with NADH 38
2.4.3 Oxidative Half-reaction of Reduced NR with *p*-NBA 43
2.4.4 Oxidative Half-reaction with *p*-Nitrosobenzoic Acid 46
2.4.5 Testing for the stability of *p*-HABA 47
2.5 DISCUSSION 50
2.6 ABBREVIATIONS 53
2.7 SUPPORTING INFORMATIONS 54
CHAPTER 3 58
RATE-CONTRIBUTING PROTON TRANSFERS OF THE TWO HALF-REACTIONS OF THE FLAVOENZYME NITROREDUCTASE 58
3.1 ABSTRACT 58
3.2 INTRODUCTION 59
3.3 EXPERIMENTAL PROCEDURES 64
3.3.1 Reagents 64
3.3.2 Expression of NR 64
3.3.3 Purification of NR 65
3.3.4 Reconstitution of the Apo-nitroreductase with ^{15}N labeled FMN 65

3.3.5 Rapid Reaction Experiments 66
3.3.6 Steady-State Kinetic Experiments 68
3.3.7 Solvent deuterium kinetic isotope effect (SKIE) 68
3.4 RESULTS 69
3.4.1 Insights from the primary kinetic isotope effect (KIE) on the reductive half-reaction 69
3.4.2 Insights into the oxidative half-reaction from the primary kinetic isotope effect (KIE) 69
3.4.3 Primary, Solvent, and Double Kinetic Isotope Effects on Steady-State Kinetic Experiments 75
3.4.4 Water Accessibility 80
3.5 DISCUSSION 82
CHAPTER 4 88
AN APPROACH FOR FLEXIBILITY AND DIMERIZATION STATE OF NITROREDUCTASE 88
4.1 ABSTRACT 88
4.2 INTRODUCTION 89
4.3 EXPERIMENTAL PROCEDURES 91
4.3.1 Expression of ^{15}N Uniformly-labeled NR 92
4.3.2 Expression of ^{15}N Glycine-labeled NR 93
4.3.3 Determination of the dissociation constant (K_d) for binding of dicoumarol to NR at various temperatures 97
4.3.4 Nuclear Magnetic Resonance Spectroscopy (NMR) 97
4.3.4.1 Proton One-dimensional (1D) NMR measurements 98
4.3.4.2 Proton-Nitrogen (^{1}H-^{15}N) Heteronuclear Single-Quantum Correlated 2D NMR Spectra 98

4.3.4.3 Relaxation Dispersion Experiments 99
4.4 RESULTS 103
4.4.1 Determination of the dissociation constant (K_d) for binding dicoumarol to NR at various temperatures 103
4.4.2 Nuclear Magnetic Resonance Spectroscopy (NMR) 108
4.4.2.1 Dynamics and a possible relationship with substrate analog binding. 108
4.4.2.2 2D ^{1}H-^{15}N HSQC NMR for ^{15}N glycine-labeled NR 116
4.4.2.3 1D Relaxation Dispersion Experiments 123
4.4.3 Oligomerization state of NR in solution 133
4.5 DISCUSSION 135
CHAPTER 5 138
AN APPROACH FOR FLEXIBILITY AND DIMERIZATION STATE OF NITROREDUCTASE MUTANTS 138
5.1 ABSTRACT 138
5.2 INTRODUCTION 139
5.3 EXPERIMENTAL PROCEDURES 145
5.3.1 Site-Directed Mutagenesis 145
5.3.2 Non-denaturing (Native) Polyacrylamide Gel Electrophoresis 146
5.3.3 Determinations of the reduction midpoint potential of NR 146
5.3.4 Determination of the dissociation constant (K_d) for binding of dicoumarol to A51C-NR 148
5.4 RESULTS 149
5.4.1 Site-Directed Mutagenesis 149
5.4.2 Expression of NR mutants 149
5.4.3 Purification of NR mutants 149

5.4.4 Dimer rigidification by interactions between one monomer's C-terminus and the beta sheet of the other monomer 151
5.4.5 Effects of the N-terminus 152
5.4.6 Dimer stabilization by interactions in the dimer interface 152
5.4.7 Oligomerization state of NR in solution 159
5.4.8 Redox potential determination of wild-type and mutants NR 160
5.4.9 Determination of the dissociation constant (K_d) for binding of dicoumarol to A51C-NR 166
5.5 DISCUSSION 168
CHAPTER 6 171
CONCLUSIONS AND FUTURE WORK 171
REFERENCES 173
VITA 192

LIST OF SCHEMES

Scheme 1.1: Pathways for the reactions with oxygen in oxidases and monooxygenases……...6
Scheme 1.2: Type I and Type II nitroreductases……...9
Scheme 2.1: Reductive half-reaction of NR…… 38
Scheme 2.2: Oxidative half-reaction of NR…….43
Scheme 3.1: Kinetic mechanism of *E. cloacae* NR……59
Scheme 5.1: Xanthine/xanthine oxidase system…… 147

LIST OF TABLES

Table 1.1: Catalytic constants (k_{cat}), bimolecular rate constants (k_{cat}/K_m) of various compounds in Enterobacter cloacae nitroreductase-catalyzed reactions…… 22

Table 2.1: Kinetic parameters for NR at 4°C: comparison of steady-state, pre-steady-state, and simulation results……...42

Table 3.1: Primary, solvent, and double kinetic isotope effects on NR steady-state kinetics…….78

Table 4.1: High yield MM9 medium recipe for 15N Uniformly-labeled NR……...94

Table 4.2: Medium recipe for ^{15}N Glycine-labeled NR…… 95

Table 4.3: One-dimentional CPMG relaxation parameters for the fast time scales exchange process……...126

Table 5.1: Summary of reduction potential (E_m^0) of wild-type and mutants NR……....161

LIST OF FIGURES

Figure 1.1: The isoalloxazine ring system of flavins……...2
Figure 1.2: Redox and ionization states of the flavin ring system……...3
Figure 1.3: Spectra of *E. cloacae* NR in the oxidized (blue spectra) and fully reduced (red spectra) states…….....3
Figure 1.4: Pylogenetic tree based on deduced amino acids sequences of NfsA-FRP and NfsB-like-nitroreductase……8
Figure 1.5: Enzyme-Prodrug Cancer Therapy……..11
Figure 1.6: Nitroreductase (NR) structure…….....13
Figure 1.7: Alignment of *E. cloacae* with other nitroreductase sequences……...17
Figure 1.8: Model for entropic stabilization of NR……...19
Figure 1.9: Overlay of the active site of NR showing movement of NR upon substrate binding……..21
Figure 2.1: The reduction of nitroaromatic substrates catalyzed by nitroreductase and ribbon structure of NR…….....31
Figure 2.2: Steady-state kinetics of NR with NADH and *p*-NBA as substrates……...37
Figure 2.3: Reductive half-reaction of NR with NADH……...40
Figure 2.4: Plot of the observed rate constants of the reduction of NR…….....41
Figure 2.5: Oxidation of reduced NR by *p*-NBA……..45
Figure 2.6: Decomposition of *p*-HABA under aerobic and anaerobic conditions……....49
Figure S2.1: Oxidation of reduced NR by *p*-NBA using double-mixing stopped-flow spectrophotometry…….....56
Figure S2.2: Oxidation of reduced NR by *p*-nitrosobenzoic acid……..57
Figure 3.1: Ribbon depiction of structure of oxidized NR with flavin and substrate analog……..…….62
Figure 3.2: Schematic of two possible mechanisms for nitro-reduction…….....63
Figure 3.3: Primary kinetic isotope effect of NR……..72
Figure 3.4: Observed rate of NR oxidation by 2 mM *p*-NBA as a function of aging time…….73

Figure 3.5: ^{1}H-^{15}N HSQC NMR spectrum of ^{14}N nitroreductase reconstituted with ^{15}N-labeled FMN from flavodoxin in the fully reduced state at 25^{o}C…….74
Figure 3.6: Steady-state kinetic experiments…….....77
Figure 3.7: pH dependence of k_{cat} for NR oxidation by *p*-NBA……....79
Figure 3.8: Water accessibility of the active site of NR……....81
Figure 3.9: Overlay of oxidized (yellow) and reduced (grey) active sites of NR showing H-bonding partners within 5 Å of N(5)…….....85
Figure 3.10: Active site of oxidized NR with bound *p*-NBA showing distances from the carboxyl to N(5)-FMN and the nitro group to N(5)-FMN……....87
Figure 4.1: Spin echo pulse sequence……99
Figure 4.2: CPMG relaxation dispersion pulse sequences……...101
Figure 4.3: Absorption spectra observed at 37^{o}C during the titration of dicoumarol into a solution of wild-type enzyme…….....105
Figure 4.4: Binding of the inhibitor dicoumarol to wild-type enzyme observed over the temperature range of 4–37^{o}C…….....106
Figure 4.5: Plot of dissociation constants (K_d) of dicoumarol for WT NR as a function of temperatures……107
Figure 4.6: Crystal structure of NR showing the location of three tryptophan residues .110
Figure 4.7: A series of ^{1}H-^{15}N HSQC spectrum of wild-type enzyme at various Temperatures……..111
Figure 4.8: Overlay ^{1}H-^{15}N HSQC NMR spectra of wild-type enzyme at various Temperatures..... .112
Figure 4.9: 2D ^{1}H-^{15}N Heteronuclear Single Quantum Coherence (HSQC) spectra and proton 1D of wild-type NR at 4^{o}C and 32^{o}C…….....113
Figure 4.10: A series of ^{1}H-^{15}N HSQC spectra of wild-type enzyme with and without 1 mM dicoumarol…….....114
Figure 4.11: Overlay ^{1}H-^{15}N HSQC NMR spectra of wild-type enzyme in the presence of 1 mM dicoumarol.....115
Figure 4.12: Structure of wild-type NR bound with benzoate showing total 12 glycine residues per monomer……118
Figure 4.13: Secondary structure assignments for NR ……...119

Figure 4.14: A series of ^{1}H-^{15}N HSQC spectrum of ^{15}N Glycine-labeled NR wild-type enzyme at various temperatures……....120
Figure 4.15: Overlay ^{1}H-^{15}N HSQC NMR spectra of ^{15}N Glycine-labeled NR wild-type enzyme at various temperature.....121
Figure 4.16: Overlay ^{1}H-^{15}N HSQC NMR spectra of ^{15}N Glycine-labeled NR wild-type enzyme bound with various concentrations of dicoumarol.....122
Figure 4.17: One-dimensional CPMG relaxation NMR spectra……..127
Figure 4.18: One-dimensional CPMG relaxation data at 25ºC……....128
Figure 4.19: One-dimensional CPMG relaxation data at 32ºC……129
Figure 4.20: CPMG relaxation dispersion curves for wild-type NR enzyme at 25ºC and 32ºC.....130
Figure 4.21: One-dimensional CPMG relaxation data of wild-type NR with dicoumarol at 25ºC…….……...131
Figure 4.22: CPMG relaxation dispersion curves for wild-type NR with and without dicoumarol at 25ºC…….……...132
Figure 4.23: Temperature-dependence of hydrodynamic radius as determined by dynamic light scattering……..……..….134
Figure 5.1: Crystal structure of NR bound to benzoic acid……140
Figure 5.2: Ribbon diagrams of the structures of the nitroreductases family……..143
Figure 5.3: C-terminal residue (Cys217) cross-links to Ala51Cys……..145
Figure 5.4: SDS-PAGE (12%) of wild-type and E165L mutant NR expressed in *E. coli*…….150
Figure 5.5: Overlay 2D ^{1}H-^{15}N HSQC spectra of C217A-NR with wild-type enzyme..154
Figure 5.6: Overlay of 2D ^{1}H-^{15}N HSQC spectra of N-terminally His-tagged NR with wild-type enzyme……..….....155
Figure 5.7: Overlay of 2D ^{1}H-^{15}N HSQC spectra of S40A-NR with wild-type enzyme……..….....156
Figure 5.8: Overlay of 2D ^{1}H-^{15}N HSQC spectra of E165L-NR with wild-type enzyme……..…….....157
Figure 5.9: Overlay of 2D ^{1}H-^{15}N HSQC spectra of E165L-NR with and without FMN added at 4ºC and 32ºC…….....158

Figure 5.10: The Native gel electrophoresis (4-20%) of wild-type enzyme, C217A, S40A, and N-terminal Hig-tag at 4, 23, 32^{o}C……...…….....159
Figure 5.11: Redox potential determination of wild-type enzyme……..162
Figure 5.12: Redox potential determination of S40A-NR……...163
Figure 5.13: Redox potential determination of C217A-NR…….....164
Figure 5.14: Redox potential determination of A51C-NR……...165
Figure 5.15: Binding of the inhibitor dicoumarol to A51C-NR in the presence of H_2O_2 observed at temperature 4^{o}C and 32^{o}C…….....167
Figure 5.16: Overlay of the active site of NR and NADOX……....170

CHAPTER 1

GENERAL INTRODUCTION

1.1 FLAVOPROTEINS

Flavin containing enzymes are found in all five kingdoms of life and perform a wide variety of biochemical functions (1,2). Up to now, there are more than 2,300 crystal structures of flavoenzymes published on Protein Data Bank (PDB) (3) with several folding architectures. Flavoproteins serve as light-sensitive signals, bioluminescence, and regulators of circadian rhythm and electron carriers. Flavoenzymes typically catalyze reduction or oxidation of substrates, and can mediate one- or two-electron redox reactions. Flavin-containing enzymes play key roles in the biosynthesis of many classes of small molecules including natural product such as polyketides and peptide scaffolds (4,5). The reactions include hydroxylations, epoxidations, oxygenase reactions, disulfide oxidation and reduction, electron bifurcation reactions and even redox-neutral isomerization, all based on the chemical versatility of the tricyclic isoalloxazine ring system.

Biological flavins are derivatives of riboflavin (vitamin B2). The most common ones are FMN (flavin mononucleotide) and FAD (flavin adenine dinucleotide) (Fig. 1.1). Interactions between the isoalloxazine moeity of the flavin and the protein are key determinants of the type of functions carried out by a particular flavoenzyme. From a chemical standpoint, the isoalloxazine moiety is amphipathic. The xylene ring is hydrophobic and can interact with hydrophobic parts of the proteins whereas the pyrimidine ring is electronegative, hydrophilic, and capable of forming hydrogen bonds and electrostatic interactions with the proteins (Fig. 1.1) (6).

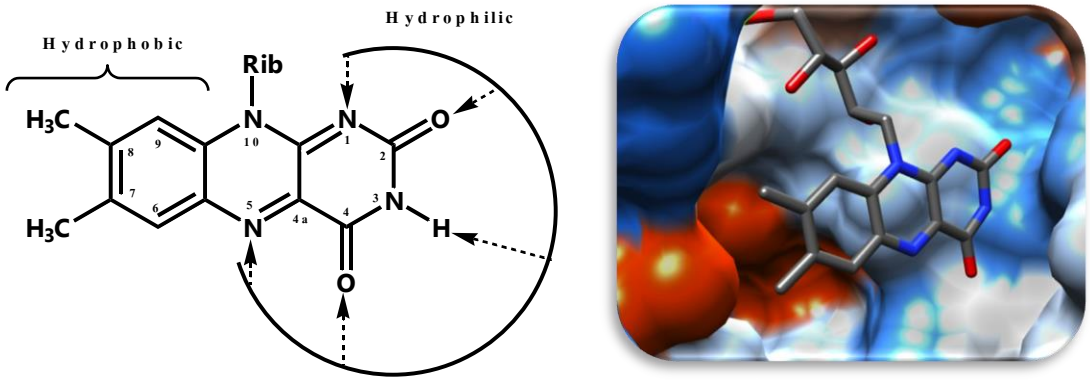

FIGURE 1.1: The isoalloxazine ring system of flavins. Left: the isoalloxazine ring showing regions amenable to different sorts of interactions with surrounding proteins. Right: molecular surface of the flavin-binding site of old yellow enzyme, color-coded by amino acid hydrophobicity (PDB: 1OYA). Most polar residues' surfaces are in dodger blue whereas the most hydrophobic residues are in orange/red with intermediate residues in white. The flavin is depicted with a gray stick model. Visualization was done with Chimera software (7).

Flavins can exist in three different oxidation states, called the oxidized, semiquinone, and fully reduced forms. Therefore flavoproteins can serve as transformers between two-electron processes (e.g. oxidation of NAD(P)H), and one-electron redox partners (e.g. Fe^{3+}/Fe^{2+}). Both the semiquinone and the fully reduced (hydroquinone) oxidation state can occur in a protonated neutral form or an anionic form (Fig. 1.2). The chemical properties of each form are distinct, particularly for the diazobenzene and uracyl rings. Reduction of flavins also causes drastic changes in their absorbance spectra, allowing convenient experimental monitoring of flavoenzymes' redox reactions (Fig. 1.3). For example, the spectrum of two-electron reduced flavin is distinct from the spectra of the neutral semiquinone ($\lambda_{max} \approx$ 360 nm and 580 nm) and the anionic semiquinone ($\lambda_{max} \approx =$ 370 nm and 480 nm) (8).

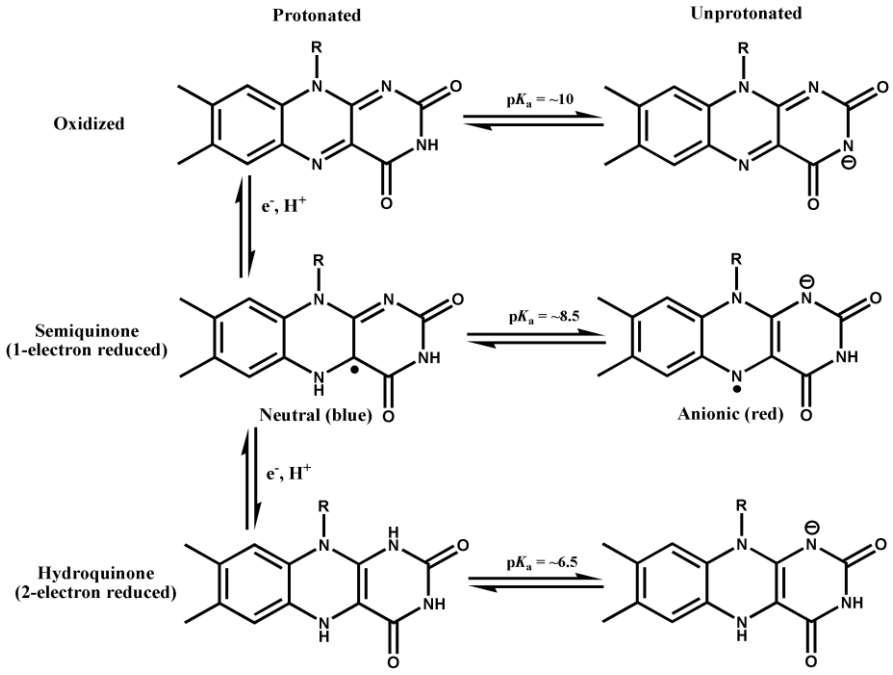

FIGURE 1.2: Redox and ionization states of the flavin ring system

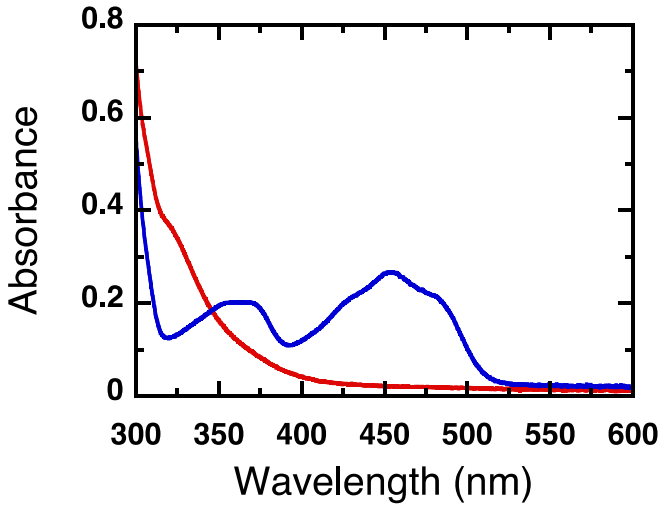

FIGURE 1.3: Spectra of *E. cloacae* NR in the oxidized (blue spectra) and fully reduced (red spectra) states

In the course of their activity, flavins typically cycle between two oxidation states, either the semiquinone and one of the oxidized or the fully reduced state (electron transfer activity) or between the oxidized and fully reduced state. The reaction in which fully reduced flavin reduces a substrate and itself becomes oxidized is called the oxidative half-reaction whereas the other half-reaction, in which oxidized flavin acquires a pair of reducing equivalents from a substrate or NAD(P)H is called the reductive half-reaction. A few flavoenzymes are recognized where the flavin does not play a redox role, but these are rare (9).

1.1.1 CLASSES OF FLAVOENZYMES

The majority of flavoenzymes can be classified as oxidases, electron transferases, flavoprotein monooxygenases or dehydrogenases. Members within the same class have been found to share several common properties including the type of reactions that they catalyze, the nature of the flavin redox properties, and their ability to use molecular oxygen as an electron acceptor, or not. The bases for classification and details of common properties were reviewed by Massey *et al*. (10) and some of the information is summarized below. Nitroreductase belongs to the class of oxidoreductases, which are described below and contrasted with the other three major classes.

1.1.1.1 FLAVOPROTEIN MONOOXYGENASES

In this class of flavoenzymes, the reduced enzyme reacts with molecular oxygen to form a readily observable flavin C(4a) hydroperoxide intermediate (10). In the absence of the target substrate for monooxygenation, the flavin hydroperoxide decays nonproductively to yield H_2O_2 and oxidized flavin. However, in the presence of the target substrate for monooxygenation, the flavin hydroperoxide transfers an oxygen atom to the substrate with concomitant formation of another intermediate, C(4a)-hydroxyflavin, which returns to its oxidized state for the next catalytic cycle upon dehydration (10). The physiological reductant of this enzyme type is usually NADH or NADPH (10,11). Two examples of the enzymes in this group are *p*-hydroxybenzoate hydroxylase (12,13) and 4-hydroxyphenylacetate 3-hydroxylase (14).

1.1.1.2 ELECTRON TRANSFERASES

In electron transferases such as flavodoxin, ferredoxin-NADP reductase and NADPH-cytochrome P-450 reductase, the enzymes react sluggishly with molecular oxygen and in the process produce O_2- and the flavin semiquinone. Enzymes from this class play roles in single-electron transfer reactions, for example in photosynthesis. Generally, they all thermodynamically stabilize the blue neutral flavin semiquinone (10). Studies replacing the natural flavin with variants that are chemically-modified, such as 8-Cl-, 8-mercapto- or 8-SCN-flavins, show that the xylene ring of the flavin is usually exposed to solvent and may serve as the route of electron acquisition by the flavin (6).

1.1.1.3 DEHYDROGENASES / TRANSHYDROGENASES

The distinction between flavoprotein dehydrogenases and flavoprotein oxidases is that in dehydrogenases the reduced flavin reacts very slowly with molecular oxygen. The physiological electron acceptors of dehydrogenases tend to be quinones, cytochromes, or nonheme-iron-sulfur clusters. In these enzymes, the rate-limiting step appears to be the initial 1-electron transfer step from reduced flavin to those acceptors. The low reactivity of dehydrogenases with molecular oxygen clearly represents a suppression of the normal chemical autoxidation (the nonenzymatic rate of O_2-dependent reoxidation of reduced flavin is about 2 s^{-1}) and promotion of electron transfer to other physiological acceptors. Either O_2 could be excluded from binding to the active site, or favorable geometry for oxidation could be avoided. Reduced flavoprotein dehydrogenases react with 1-electron acceptors to form an extremely favorable neutral semiquinone, which is stabilized by the active site environment. Because of the thermodynamic stability of the flavin semiquinone, it is a significant intermediate in enzymatic catalysis and reveals the important role of flavin coenzymes in biological oxidation. The semiquinone states permit the enzyme to release electrons one at a time, although they are acquired in a single two-electron oxidation. Thus they provide an interface between oxidation of organic substrates and reduction of cytochrome components of membrane respiratory chains. Therefore, many flavin-containing dehydrogenases are membrane-bound enzymes. Examples of enzymes in this group are acyl-CoA dehydrogenase (15), D-Lactate dehydrogenases (16), and Succinate dehydrogenase (17).

1.1.1.4 FLAVOPROTEIN OXIDASES

Flavoprotein oxidases catalyze oxidations of organic substrates to form oxidized products and H_2O_2. For example, in pyranose 2-oxidase (P_2O), the reductive half-reaction involves rupture of a substrate C-H bond with concomitant transfer of a hydride equivalent moiety to the oxidized flavin cofactor. In the oxidative half-reaction two electrons are transferred to molecular oxygen to produce hydrogen peroxide. Generally, in most flavoprotein oxidases, no intermediate is detected during the oxidative half-reaction, unlike in flavoenzyme monooxygenases where it has frequently been possible to observe formation of the C4a-(hydro)peroxyflavin intermediate resulting from bonding of a molecular oxygen to the flavin C4a (Scheme 1.1). However, an exception has been found, in an investigation of pyranose oxidase (18).

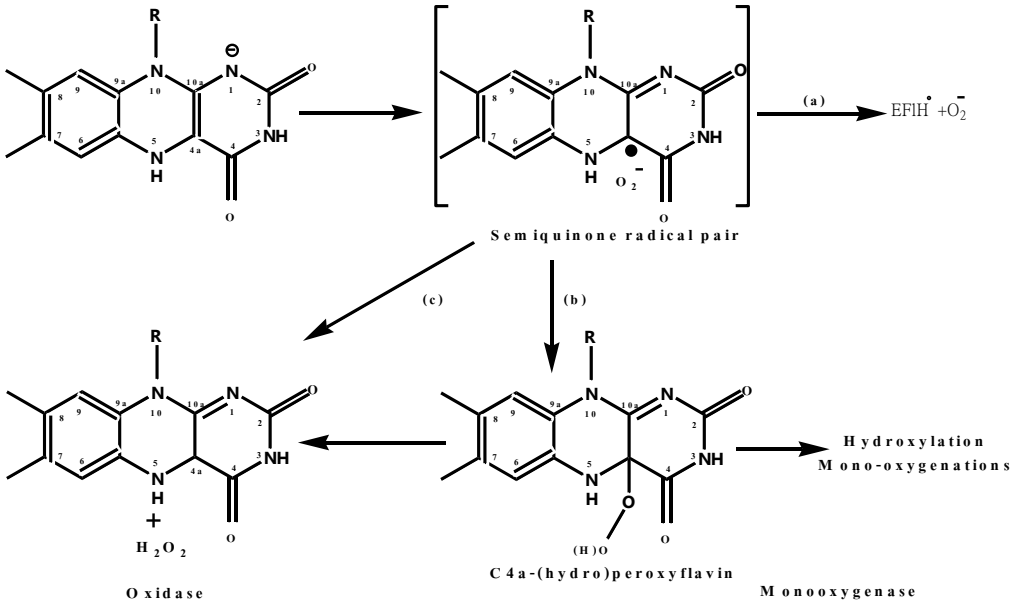

SCHEME 1.1: Pathways for the reactions with oxygen in oxidases and monooxygenases

1.1.1.5 OXIDOREDUCTASES

"Oxidoreductase" is a general term for enzymes which catalyze the transfer of electrons from a reductant molecule to another molecule (the oxidant). Oxidoreductases include the flavoprotein reductases, oxidases (above) dehydrogenases (above), hydroxylases (the monooxygenases described above), and disulfide/dithiol interconverting enzymes, which differ regarding the identities of the oxidants and

reductants employed by the reaction. For example, dehydrogenases are enzymes that oxidize a substrate by transferring a pair of hydrogen equivalents to an acceptor that is commonly either $NAD^+/NADP^+$. Thus most (but not all) flavoenzymes are oxidoreductases. Nitroreductases can be classified as NADH:FMN oxidoreductases in which the enzymes in this class use strong reducing agent (NAD(P)H) as an electron donor to donate electrons and/or protons to FMN. More details on the example of nitroreductases are discussed below.

1.2 NITROREDUCTASES

NAD(P)H:nitroaromatic reductases (Nitroreductase, EC 1.6.99.7) are flavoenzymes that catalyze the NAD(P)H-dependent reduction of the nitro groups on nitroaromatic and nitroheterocyclic compounds. Nitroreductases are homodimeric enzymes with two identical active sites each positioned between the identical subunits and containing a non-covalently bound FMN. Nitroreductases are widely distributed among bacteria (Fig. 1.4), but nitroreductase-like proteins are also found in archaea and eukaryotic organisms (19). Nitroreductases are oxygen insensitive (type I or "classical" nitroreductases) and use a two-electron reduction mechanism to catalyze sequential transfer of two electrons from NAD(P)H to a nitro group under aerobic or anaerobic condition resulting in nitroso and hydroxylamine products and finally primary amines (Scheme 1.2) (20-22). In contrast, type II or oxygen sensitive nitroreductase activity was described as stepwise single-electron reduction of nitroaromatics, initially forming a nitro anion radical (Scheme 1.2). In the presence of oxygen, the nitro anion radical may be oxidized back to a nitro group, with production of a superoxide anion ($O_2^{\cdot-}$) (23). As long as oxygen is present, a futile cycle operates, which consumes reducing equivalents through the nitroreductase without net nitro group reduction. Thus, this type II activity is only capable of net nitro group reduction in anaerobic environments (23) and in the presence of O_2 it causes oxidative stress. Type II nitroreductase activity has now been identified as a promiscuous activity of respiratory complex I (24).

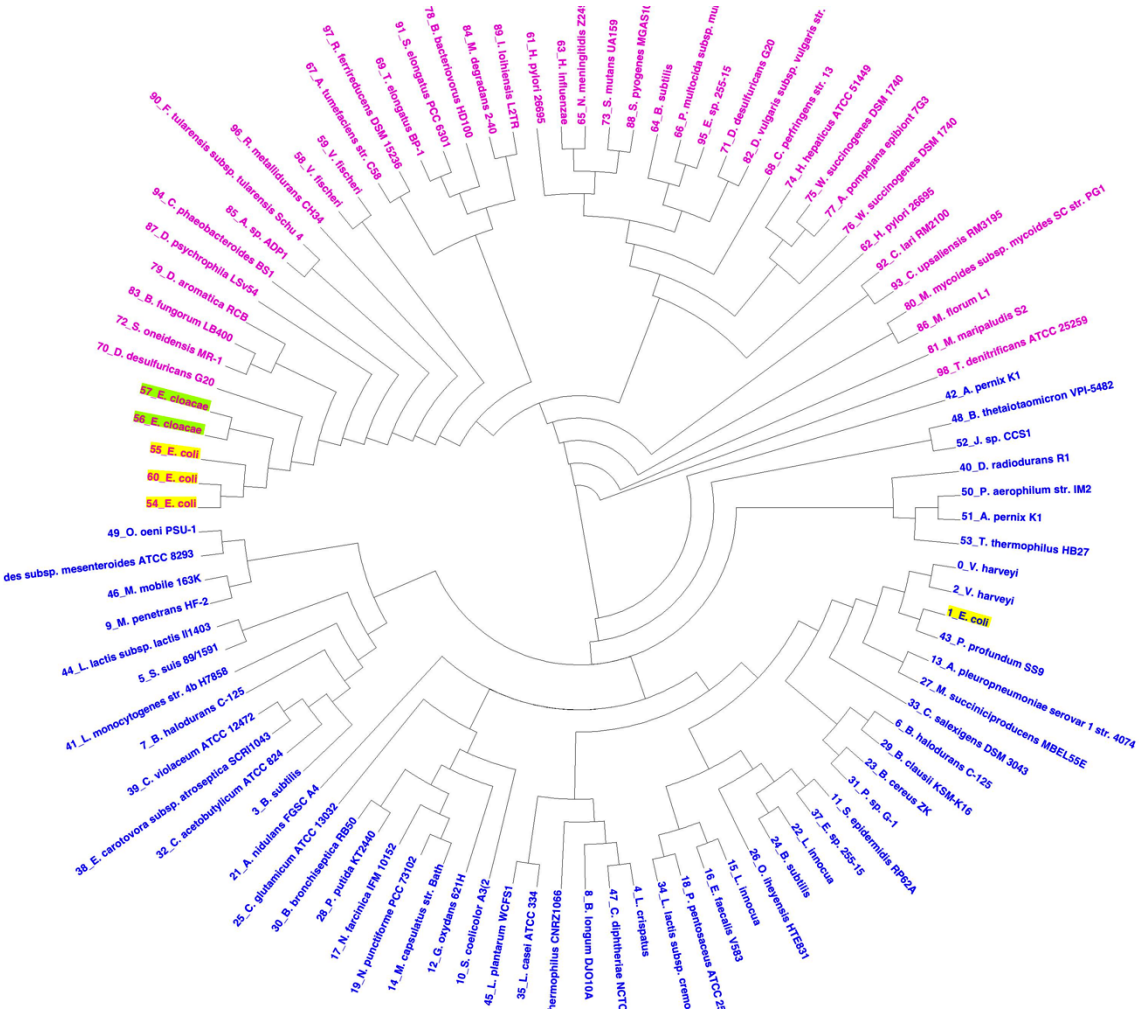

FIGURE 1.4: Pylogenetic tree based on deduced amino acids sequences of NfsA-FRP (NADPH-dependent flavin reductase and oxygen-insensitive nitroreductase) written in blue and NfsB-like-nitroreductase (FRase I in *Vibrio fischeri* and oxygen-insensitive nitroreductases) written in pink. NfsA (*E.Coli*) and NfsB (*E.Coli*) are labeled in yellow and NRs (*E. Cloacae*) are labeled in green. Phylogenetic tree generation methods provided by NCBI CDD (25) (code: cd02146 for NfsA-FRP and cd02149 for NfsB-like-nitroreductase). Software for visualizing phylogenetic trees and rooted networks provided by Dendroscope (26) (created by Warintra Pitsawong).

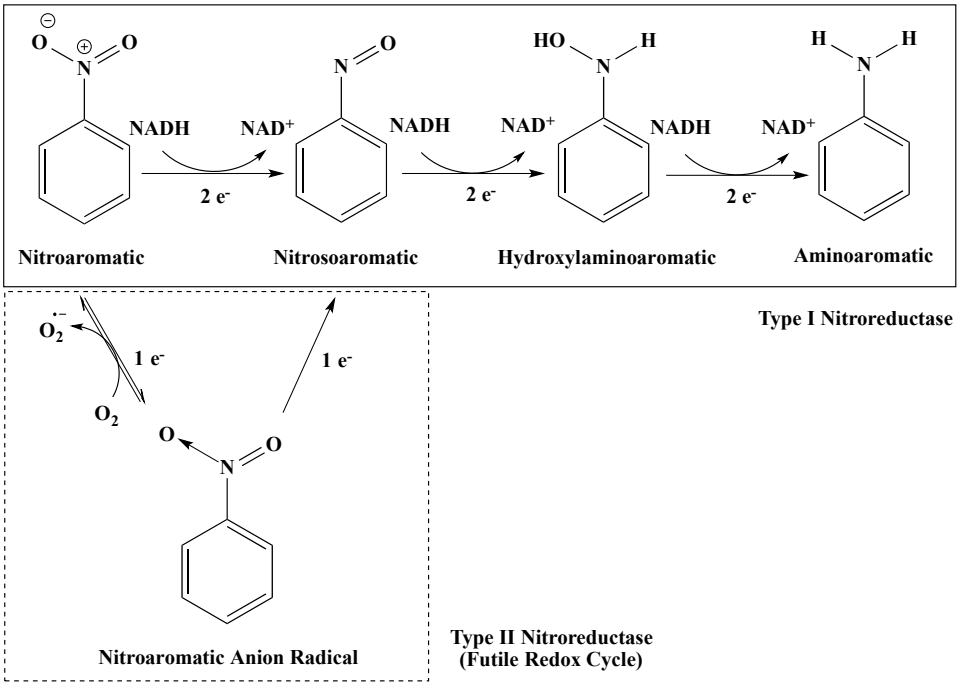

SCHEME 1.2: Type I (oxygen insensitive) and type II (oxygen sensitive) nitroreductases

Type I nitroreductases participate in reduction of several nitrocompounds ranging from nitrofuran antibiotics to nitroarene xenobiotics such as 1-nitropyrene, and also including nitroaromatic explosives such as 2,4,6-trinitrotoluene (TNT). The compounds mostly observed as a result of Type I nitroaromatic reduction are aromatic hydroxylamines (21,23,27-29). However, a few reports exist of the formation of a nitroso intermediate during biological reduction of certain nitroaromatics (30). It is difficult to isolate nitroso intermediates because nitrosos are reactive with one-another, and hydroxylamine, and the second two-electron reaction (in which nitroso is reduced to hydroxylamine) is much faster than the first two-electron transfer (in which nitroso is formed) (31).

Type I nitroreductases can be classified into 2 groups based on sequence similarity with *Escherichia coli* nitroreductase NfsA (Group A or major) and NfsB (Group B or minor) (22). Group A uses NADPH as reducing agent, whereas Group B can use either NADH or NADPH as an electron source. NR has 88% sequence identity with NfsB (32) and similar function; therefore, NR can be classified as a minor oxygen

insensitive or Group B nitroreductase. Several crystal structures have already been deposited and/or published for several members of these families (32-37).

Nitroreductases have aroused a great deal of interest due to their potential applications in bioremediation, biocatalysis, and medicine, especially as agents in prodrug activation for chemotherapeutic cancer treatments. Enzyme-prodrug cancer therapy using *E. coli* nitroreductase (NfsB) and the prodrug CB1954 (5-(aziridin-1-yl)-2,4-dinitrobenamide) (38-41) has been in clinical trials and continued development for over 30 years (42,43). CB1954 is converted to an equal mixture of 2- and 4-hydroxylamines (44), but the 4-hydroxylamine is more cytotoxic than the 2-hydroxylamine product (45). There are two major classes of delivery method for targeting enzyme to tumor tissues. Class A constitutes delivery of genes that encode prodrug-activating enzymes into tumor tissues in methods such as GDEPT (gene-directed enzyme pro-drug therapy) and VDEPT (virus-directed enzyme pro-drug therapy). Many GDEPT studies have used liposomal gene delivery to deliver a gene into the tumor cell (46-48). In contrast, in Class B delivery an active enzyme is conjugated to antibodies directed at proteins displayed on cancer cell surfaces, so as to direct the enzyme to tumor cells upon intravenous administration. As a result, the enzyme's reaction occurs specifically at tumors, where the prodrug CB1954 is enzymatically activated by reduction of a nitro group, changing the compound to a highly toxic hydroxylamine (5-(aziridin-1-yl)-4-hydroxylamino-2-nitro-benzamide), which is bifunctional alkylator, that can diffuse into surrounding cells. The cytotoxic hydroxylamine can react further with cellular thioesters such as acetyl coenzyme A to form poorly repairable DNA interstrand cross-links resulting in DNA damage and leading to cell death in both dividing and non-dividing cells with no bystander effect (49-51) (Fig. 1.5).

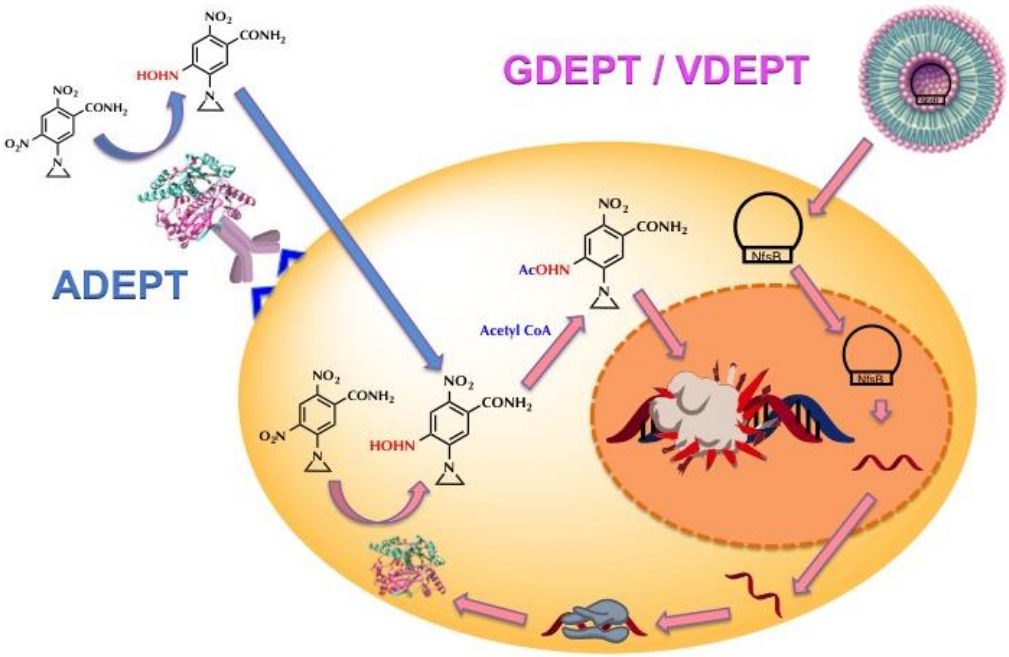

FIGURE 1.5: Enzyme-Prodrug Cancer Therapy. GDEPT: gene-directed enzyme pro-drug therapy; VDEPT: virus-directed enzyme pro-drug therapy; ADEPT: antibody-directed enzyme pro-drug therapy (created by Warintra Pitsawong).

Enterobacter cloacae nitroreductase (NR) was first isolated from a weapon storage dump for its ability to degrade highly explosive compounds like 2,4,6-trinitrotoluene (TNT), by Christopher Bryant and co-workers in 1991 (20,21). The enzyme exists as a homodimer and each of the subunits contains 217 amino acids with a reported molecular mass of 23 kDa. The dimer interface buries a large area (52) consistent with the very low dimer dissociation constant of 10 nM (53). Each active site is formed by residues from both subunits but most of the H-bonds to the flavin come from one monomer (*si face* of the flavin ring) whereas the other monomer contributes primarily steric and hydrophobic constraints to the active site, for the example of *E. cloacae* NR (Fig. 1.6) (52).

NR was first crystalized by Bryant and the structure (PDB: 1NEC) was solved based on homology with NADH oxidase (PDB: 1NOX) from *Thermus thermophilus* (33). In 2000 Haynes *et al*. reported a series of structures (1.9 Å resolution) identifying differences between the oxidized state with acetate bound, a substrate analog-bound

oxidized enzyme and the fully reduced enzyme (PDB: 1KQB, 1KQC, 1KQD) (52). The main difference between the oxidized and reduced states of the enzyme is an increase in the butterfly bend angle of FMN from 16 to 25 degrees (52). In addition, the structures of NR in the oxidized state bound with *p*-nitrobenzoic acid (*p*-NBA) (Fig. 1.6) or with nicotinic acid adenine dinucleotide (NAAD) (Fig. 1.9D), which is a NAD(P)H substrate analog, have been solved in 2005 (Haynes *et al*, unpublished structures).

The FMN cofactor is tightly bound to NR, with a K_d of 8 nM (53). Only the *re face* is accessible to substrates in the crystal structures. The plasticity of helix F creates a variable-volume cavity capable of conforming to different size of substrates (Fig. 1.6A). Interestingly, the C-terminus of one subunit wraps around the other subunit and contributes a strand to the beta sheet formed otherwise completely by the other subunit (Fig. 1.6A). In the past few years, the number of reported structures of domain-swapped proteins has increased, and some 40 proteins have been found to contribute either the N or C terminus to the structure of the other monomer. Domain swapping is interesting because it may serve as a mechanism for reversible oligomerization or may provide intrinsic flexibility for adoption of different conformations in the monomer than in the domain-swapped oligomer (54). We propose that the C-terminal domain swapping of NR may be one of the features that determines the breadth of NR's substrate specificity range by enabling conformational flexibility with minimal penalty to the stability of the dimer.

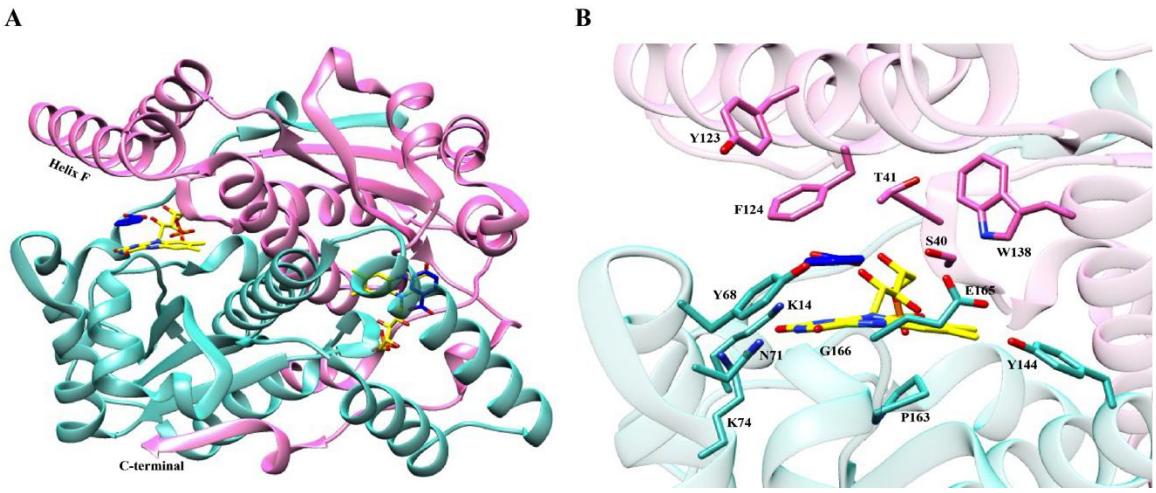

FIGURE 1.6: Nitroreductase (NR) structure. A) Ribbon representation of nitroreductase from *Enterobacter cloacae* in the oxidized state bound with FMN cofactor (yellow sticks) and benzoic acid (blue sticks). B) Interaction of FMN with amino acids from both subunits in NR active site. Both structures were generated using the program Chimera. (PDB: 1KQB) (52).

Within the active site, there are several residues from both subunits that participate in FMN and substrate binding. The side chain amine group of Lys14 weakly hydrogen bonds (3.5 Å) to N(1) of the flavin ring. In contrast, the side chain of Lys74 engages in a much stronger hydrogen bond interaction (2.7 Å) to O(2). The side chain of Asn71 participates in two hydrogen bonds with the flavin ring, with N(3) and O(4) at distances of 2.9 Å and 3.1 Å, respectively. The carbonyl oxygen of Pro163 is positioned approximately 2.8 Å from the plane of the central ring of the flavin and almost directly below its center point, where the protein backbone runs across the short axis of the flavin (Fig. 1.6B). The backbone amide NHs of Glu166 and Gly165 hydrogen bond to O(4) (3.0 Å) and N(5) (3.2 Å) of the flavin ring, respectively and they are well conserved among Type IB NRs (Fig. 1.7). The small side chain of Gly166 appears to permit binding of large substrates against the *re* face of the flavin ring. A hydrogen bond from the backbone NH of Glu165 to N(5) could increase the oxidative power of FMN. The role and mechanistic implications of hydrogen bonding interactions at the N(5) atom of the flavin in the oxidized state have not been well understood. Functional effects of hydrogen

bonding to N(5) have been studied in the Electron-transfer flavoprotein from the methylotrophic Bacterium W3A1. The results showed a significant decrease in the midpoint potential of the first couple ($E_{ox/sq}$) as a result of substitutions of the αSer254, which hydrogen bonds to N(5) (αSer254Thr, αSer254Cys, and αSer254Ala). This indicates that a hydrogen bonding interaction at N(5) increases the $E_{ox/sq}$. (55). Another example has been published concerning pyranose-2oxidase (P_2O) in which eliminating a hydrogen bond interaction by changing Thr169 to Ala produced a 100 mV decrease in the redox potential (56). In NR, the carboxyl side chain of Glu165 hydrogen bonds to hydroxyl group of Ser40 (2.7 Å) and the indole NH of Trp138 (2.9 Å) in another subunit (Fig. 1.6B). These interactions may help to allow controlled adaptability in the dimer interface. Therefore, replacement of these residues may disturb the dimerization state of the enzyme, or the flexibility of the dimer.

Molecular dynamic simulation (MD) and principle component analysis (PCA) were performed with *E. cloacae* NR in three systems including oxidized NR, fully reduced NR bound with benzoate, and fully reduced NR bound with nitrobenzene with explicit water for 20 ns each (57). Only crystal structures of oxidized NR are available (52), the reduced state of NR with bound ligand were built using the AmberTools program based on the crystal structure of the oxidized state (more detail can be found in Isayev *et al* 2012 (57)). The MD simulation results indicated that the most rigid regions are on the dimer interface and in the characteristic α+β fold of the subunits. The RMSF (per-residue root-mean-square fluctuations) of C_α of the free and bound forms of NR behaved differently, especially at the helix F and nearby loop, indicating that helix F plays a crucial role in accommodating various sizes of substrates and facilitating product release, whereas the active site remains unaffected upon substrate binding (57). During the MD simulations, benzoate and nitrobenzene remained stacked between the *re* face of the flavin ring and Phe124 making stable π-π interactions with the substituent extending out either to the ribityl chain or out of the active site, and the carboxylic group of benzoate formed a hydrogen bond with the backbone carbonyl group of Thr41 and a hydroxyl group from the ribityl chain of the flavin (57). Moreover, the MD simulation found that the nitrogroup of nitrobenzene moved away from the N(5) position of flavin to a distance greater than 5 Å suggesting a mechanism based on electron-coupled proton

transfer (two electrons transfer from flavin but one proton transfers from solution) rather than hydride transfer (concerted transfer of two electrons and one proton from flavin) (57). More detail regarding the kinetic mechanism will be provided in Chapters 3 and 4.

Molecular dynamic simulations were also performed on the closest homologue of NR, *E. coli* nitroreductase (NfsB) (58). In this paper, MD simulations were used as a tool to probe the nitroaromatic reduction mechanism and learn whether it employs a hydride transfer or an electron transfer mechanism. The crystal structure of NfsB in complex with CB1954 was used as a model for a hydride transfer mechanism. NfsB bound with CB1954 has its 2-nitro group stacked on top of N(5)-FMN in one active site but its 4-nitro group stacked on top of N(5)-FMN in another active site with the distance between nitro groups and N(5)-FMN of 3.9 Å (PDB: 1IDT), which is within the range required for hydride transfer (< ~5 Å) (59). Fully reduced NfsB was generated by adding a hydrogen atom at N(5)-FMN using the Insight II program and all parameter files were created by the AMBER 8 package (more detail can be found in Christofferson *et al* 2012 (58)). The results showed that both the 2- and the 4-nitro group of CB1954 moved away from N(5)-FMN to distances greater than 6 Å, arguing against the hydride transfer mechanism (58). Moreover, at some point during the MD simulation, CB1954 was out of the active site and re-bound with a different orientation in which the amide of CB1954 rather than the nitro group stacked on top of N(5)-FMN (58). The structural model for an E•S complex active in an electron transfer mechanism was obtained by overlaying the amide group of CB1954 with the amide group of nitrofurazone in the crystal structure of NfsB bound with nitrofurazone (PDB: 1YKI (60)), and then removing the nitrofurazone. The crystal structure of NfsB bound with nitrofurazone was used as the source of crystallographic coordinates because the amide group of nitrofurazone was stacked on top of N(5)-FMN with the nitro group pointing out of the binding pocket, supporting the electron transfer mechanism. The results showed strong hydrogen bond interactions between the amide oxygen of CB1954 and the backbone of the protein (Thr41) as well as the hydroxyl group of the ribityl chain of FMN, and between the amide nitrogen of CB1954 and the carboxyl side chain of Glu165, supporting the electrons transfer mechanism. Moreover, the MD simulation showed plenty of water moving around the nitro group within the van der Waals contact radius suggesting proton abstraction from solution (58). It is important to

note that both MD simulations of fully reduced enzyme were generated from a crystal structure of oxidized enzyme, in which the flavin ring has a different butterfly bend angle (16 degrees *versus* 25 degrees for oxidized and fully reduced flavin, respectively (52)). The electronic properties of flavin also change upon reduction (61) resulting in a large change in electron distribution (61). The different charge distributions and geometries of the flavin ring may affect the orientation in which ligands bind to oxidized *vs*. reduced enzyme. There are a couple reports of different binding orientations for ligand to different redox states of enzymes, such as the example of steroid binding to pentaerythritol tetranitrate reductase (PETN reductase) (62).

FIGURE 1.7: Alignment of *Enterobacter cloacae* with other nitroreductase sequences of from *Escherichia coli*, *Salmonella typhimurium*, *Klebsiella pneumonia*, *Vibrio fischeri*, *Bacillus licheniformis* and NADH oxidase (NADOX) from *Thermus thermophilus* using UniProt Alignment. Conserved residues are shaded in gray, and the blue rectangular box identifies the Glu165 and Gly166.

1.3 WHAT HAVE WE LEARNED FROM THE PAST?

Our group is interested understanding and manipulating the broad substrate repertoire of NR, which has a number of potential applications. Conformational flexibility may be one of the explanations for the extremely broad substrate repertoire of NR (Table 1.1) (63,64). Previous studies on the steady-state kinetics at 25^{o}C with a wide range of substrate analogs showed that NR employs a ping-pong bi-bi kinetic mechanism (two substrates and two products) in which NR reacts with first substrate (NAD(P)H) to form first product (NAD(P)$^{+}$) and modified enzyme, the latter then reacts with second substrate (nitro or quinone compounds) to form second or final product (e.g. nitroso, hydroxylamino or amino compound, or quinol) (65). Both substrates do not bind to the enzyme simultaneously. Steady-state kinetic parameters for several substrates and inhibitors have been reported by Koder *et al*. (31).

Previous studies in our group also revealed an unusual behavior for NR at low temperature based on 2D ^{1}H-^{15}N HSQC NMR spectra. At the relatively high temperature of 37^{o}C, NR's NMR resonances were well-dispersed covering a large chemical shift range in the ^{1}H dimension, while at the relatively low temperature of 4^{o}C, the amide ^{1}H chemical shifts were poorly-dispersed and confined to less than 1 ppm (7.7 – 8.3 ppm) (66). The unusual conformational behavior at low temperature was investigated in several ways, which showed that NR does not unfold or become a molten globule at lower temperature. Far-UV-CD and near-UV-CD indicated that NR retains almost the full amount of secondary structure and considerable tertiary structure at 4^{o}C compared to 37^{o}C. Visible CD was used to study the local environment around the FMN cofactor and showed no significant change from 4^{o}C-42^{o}C. Moreover FMN remained tightly bound to NR (K_d = 63 nM) at lower temperature (4^{o}C), representing a higher affinity than at higher temperature (K_d = 417 nM at 37^{o}C), based on titrations of FMN by NR apoprotein and observation of FMN fluorescence (66). Comparison of the ^{19}F NMR spectra of [(3-^{19}F)-Tyr]-labeled NR, with the control spectrum of GuHCl-unfolded [(3-^{19}F)-Tyr]-NR indicated that NR retained its native core side chain packing interactions at 4°C and that the Tyr side chains were not freely rotating on an NMR timescale, indicating that the protein core was not 'molten' and arguing further against a molten globule nature at lower temperature.

We propose that the poorly-dispersed NMR spectrum at 4°C reflects loss of persistence rather than loss of structure. In other words, NR undergoes rapid conformational averaging between different packing arrangements that are associated with different chemical shifts and this rapidly inter-conversion becomes faster than NMR time scale at lower temperatures. This proposal was supported by H/D exchange measurements. At higher temperature, the backbone amide resonances exchanged significantly more slowly with water than they did at lower temperature. These results indicated that the temperature dependent transition is related to protein hydration. We propose that release of water at higher temperature results in an increase in the entropy of water and leaves a more rigid persistent protein structure, whereas there is greater hydration of the protein backbone at lower temperatures which is equivalent to greater ordering of water molecules. Fig. 1.8 illustrates this model for the lower and higher-temperature conformational states (A-F.Miller, unpublished).

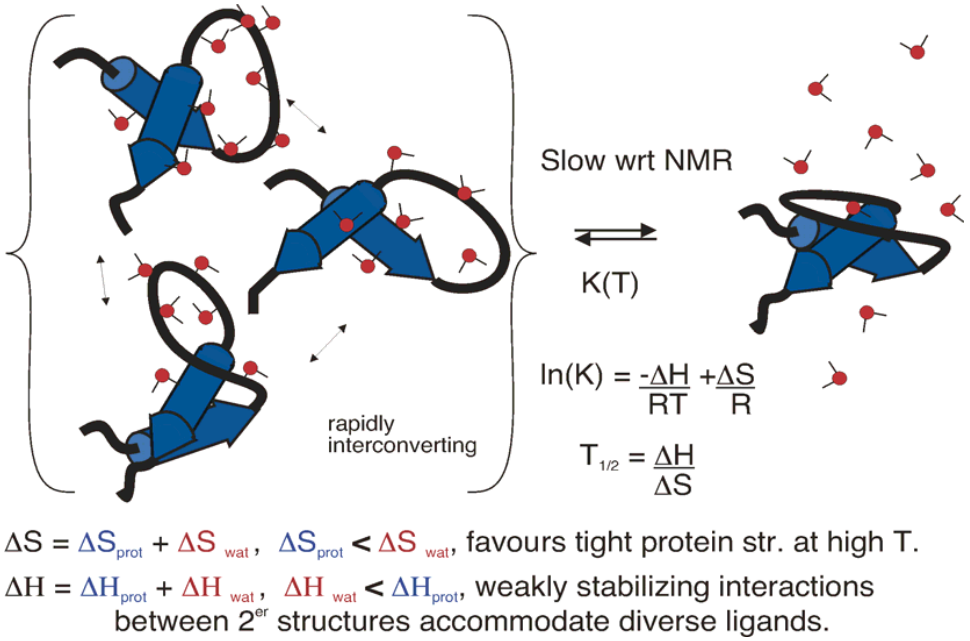

FIGURE 1.8: Model for entropic stabilization of NR. Left: Rapidly interconverting (conformational averaging and ^{1}H exchange with solvent) of NR at lower temperature, Right: Well-defined unique structure of NR at higher temperature. Protein is labeled in blue and water molecules are labeled in red (A-F.Miller, unpublished).

OBJECTIVES

Nitroreductase exhibits an unusually broad substrate repertoire (Table 1.1) (63,64) ranging from small substrates to bulky molecules. Clearly, any hypothesis for the catalytic mechanism and dynamic behavior of the enzyme must be able to explain this capability of the protein to oxidize so many different substrates. The crystal structures of NR deposited and/or published for several members of this family (33-36,52,65,67) reveal FMN bound at the interface between monomers and interacting with elements from both monomers. They also point to increased flexibility around the active site (33,34,36,37,52,67). For example, helix F moves outward to accommodate binding of nitrobenzoic acid to the NR of *E. cloacae* (Fig. 1.9). The same helix and loop (60) are displaced upon binding of substrates to the NR or *E. coli* NfsB. In the latter case extensive crystallographic studies have shown that a given substrate can bind in more than one mode (60). Thus the protein displays considerable flexibility and ability to adopt different binding interactions. In addition, the location of the active site between monomers raises the possibility that movements of one monomer relative to the other can produce considerable changes in binding site size and shape are relatively minor costs to the protein structure.

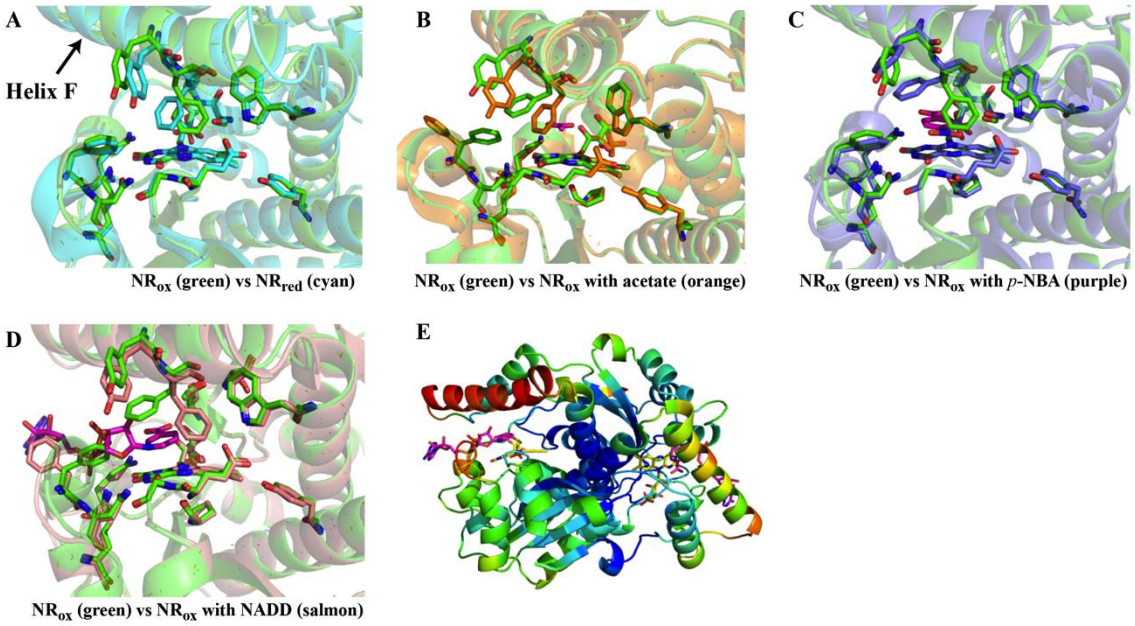

FIGURE 1.9: Overlay of the active site of NR showing movement of NR upon substrate binding. A) oxidized NR (green backbone, 1NEC) and reduced NR (cyan backbone, 1KQD). B) oxidized NR (green backbone, 1NEC) and NR bound with acetate (small size ligand, orange backbone, 1KQC). C) oxidized NR (green backbone, 1NEC) and NR bound with PNBA (medium size ligand, purple backbone, unpublished structure). D) oxidized NR (large size ligand, green backbone, 1NEC) and NR bound with NAAD (orange backbone, unpublished structure). E) B-factor of oxidized NR upon binding with NAAD (red: high B-factor value, blue: low B-factor value).

TABLE 1.1: Catalytic constants (k_{cat}), bimolecular rate constants (k_{cat}/K_m) of various compounds in *Enterobacter cloacae* nitroreductase-catalyzed reactions (0.1 M Tris-HCl, pH 7.0, 25°C) (63,64).

Compound	k_{cat} (s^{-1})[a]	k_{cat}/K_m ($M^{-1}s^{-1}$)
Tetryl	800 ± 92	$(7.3 \pm 0.51) \times 10^6$
Pentryl	620 ± 75	$(6.3 \pm 0.52) \times 10^6$
2,4-Dinitrophenyl-N-Methylnitramine	410 ± 52	$(1.0 \pm 0.15) \times 10^7$
2,4,6-Triinitrotoluene	143 ± 22	$(9.8 \pm 1.5) \times 10^6$
Nifuroxim	47 ± 4.2	$(7.8 \pm 0.5) \times 10^5$
2,4-Dinitrotoluene	(660 ± 60)	$(2.0 \pm 0.06) \times 10^5$
Nitrofurantoin	102 ± 9.2	$(5.0 \pm 0.2) \times 10^5$
p-Dinitrobenzene	305 ± 15	$(3.1 \pm 0.2) \times 10^6$
o-Dinitrobenzene	91 ± 7.0	$(1.46 \pm 0.07) \times 10^6$
p-Nitrobenzaldehyde	104 ± 8.7	$(8.02 \pm 0.80) \times 10^5$
m-Dinitrobenzene	167 ± 9.0	$(5.0 \pm 0.23) \times 10^5$
3,5-Dinitrobenzene	370 ± 21	$(4.1 \pm 0.18) \times 10^6$
p-Nitroacetophenone	100 ± 12	$(8.05 \pm 0.95) \times 10^5$
o-Nitrobenzaldehyde	83 ± 7.5	$(3.9 \pm 0.25) \times 10^5$
p-Nitrobenyl alcohol	20 ± 4.2	$(1.0 \pm 0.1) \times 10^4$
Nitrobenzene	10 ± 1.3	$(3.0 \pm 0.33) \times 10^4$
1,4-Benzoquinone	1200 ± 50	$(1.4 \pm 0.1) \times 10^8$
2-Methyl-1,4-benzoquinone	666± 37	$(5.0 \pm 0.4) \times 10^7$
2,3-Dichloro-1,4-naphthoquinone	250 ± 18	$(1.3 \pm 0.1) \times 10^7$
2,5-Diaziridinyl-1,4-benzoquinone	1610± 80	$(2.4 \pm 0.2) \times 10^7$
2,6-Dimethyl-1,4-benzoquinone	704± 82	$(1.8 \pm 0.2) \times 10^7$
5-Hydroxy-1,4-naphthoquinone	77 ± 5.2	$(1.2 \pm 0.1) \times 10^7$
5,8-Dihydroxy-1,4-napthoquinone	111 ± 8.7	$(2.5 \pm 0.1) \times 10^7$
9,10-Phenanthrene quinone	333 ±12	$(2.4 \pm 0.1) \times 10^7$
1,4-Naphthoquinone	200 ± 15	$(2.2 \pm 0.1) \times 10^7$
2-Methyl-1,4-naphthoquinone	150 ± 10	$(1.0 \pm 0.1) \times 10^6$
Trimethyl-1,4-napthoquinone	400 ± 30	$(1.0 \pm 0.1) \times 10^7$
2-Methyl-1,4-napthoquinone	50 ± 3.0	$(3.5 \pm 0.1) \times 10^6$
2,5-Dimethyl-3,6-diaziridinyl-1,4-benzoquinone	71 ± 5.0	$(2.9 \pm 0.1) \times 10^5$
9,10-Anthraquinone-2,6-disulfonate	0.83 ± 0.05	$(1.2 \pm 0.1) \times 10^4$
Tetramethyl-1,4-benzoquinone	17 ± 1.1	$(3.8 \pm 0.1) \times 10^4$
1,4-Dihydroxy-9,10-anthraquinone	1.5 ± 0.1	$(2.6 \pm 0.2) \times 10^4$
Mitomycin C	1.0 ± 0.1	$(2.3 \pm 0.2) \times 10^4$
Riboflavin	5.3 ± 0.2	$(1.0 \pm 0.1) \times 10^5$
1,8-Dihydroxy-9,10-anthraquinone	1.0 ± 0.1	$(5.0 \pm 0.3) \times 10^4$
Adriamycin	≤ 0.1	$\leq 10^3$
9,10-Anthraquinone-2-sulfonate	0.83 ± 0.1	$(2.5 \pm 0.1) \times 10^4$
1-Hydroxy-9,10-anthraquinone	1.5 ± 0.1	$(1.2 \pm 0.1) \times 10^4$
2-Hydroxy-1,4-naphthoquinone	160 ± 9	$(1.2 \pm 0.1) \times 10^7$

NADH concentration, 150 μM. The k_{cat} values in parentheses obtained at infinite concentrations of both substrates.

Very little is known about the mechanism of NR. Steady-state kinetics studies addressing modes of inhibition demonstrated that NR utilizes a ping-pong bi-bi mechanism (31) and *Race et al* (65) have used stopped-flow kinetics to tabulate rate constants for reduction of the prodrug CB1954 by a series of NR mutants. Thus studies showed that the rate of nitroaromatic reduction is much faster than the turnover rate, indicating the existence of another rate-limiting step, such as product release. No insight was proffered however as to possible formation of an initial enzyme substrate complex, a conformational equilibrium prior to the occurrence of chemistry, or an enzyme-product complex with a lifetime sufficient to contribute to the overall rate of the reaction. Moreover the half-reaction between NR and NADH has not been investigated. In monoamine oxidase, inhibitors (propargylamines, allenic amines, and cyclopropylamines) can form an ES complex but fail to undergo the reaction (68); in *p*-hydroxybenzoate (PHBH), azide inhibitor slowed the hydroxylation step (conversion of C4a-hydroperoxyflavin to C4a-hydroxyflavin) by a factor of 6.6 (69) and slowed the conversion of C4a-hydroxyflavin to the oxidized enzyme by a factor of 6.9 and in yet another case product dissociation, thus even non-chemical steps can depend on the identity of the ligand (substrate or inhibitor) and thus contribute to specificity.

Thus, in order to understand NR's very wide substrate repertoire we need to know which steps contribute to the observed overall rate and how their rate constants vary (if at all) with the identity of the substrate. It is easiest to imagine a broad substrate repertoire when relatively few steps contribute to the overall rate. We also note that specificity should not be viewed as an absolute quantity since different substrates may turn over at different rates and inefficient substrates can be viewed as representing the limits of the substrate range. A survey of substrates will be the object of another thesis; the current work seeks to lay the needed foundation by obtaining a complete description of the steps employed in the course of turnover by NR.

In order to clarify the significance of NR's structure and mechanism to NR's broad substrate repertoire we have identified the following central questions to ask:

(i) Does the enzyme use a simple transient kinetic mechanism that dispenses with steps that would depend on the size, rigidity, functional groups, etc. of substrates and thus avoids opportunities for selectivity? Other enzymes' remarkable specificity is normally

established through the use of specific intermediates and/or a complicated enzymatic reaction mechanism that restricts activity to specific substrates only.

(ii) How does the same active site accomplish both reductive and oxidative half reactions?

(iii) Do C-terminal domain swapping and interactions between monomers at the dimer interface enable NR to retain stability despite its dynamics?

In this study, we attempt to elucidate the mechanism of NR action in molecular detail. Although crystal structures of NR have been published showing that NR is able to interact flexibly with substrates or products, they do not address what NR actually does during catalysis, nor can they prove what aspects (if any) of NR's activity depend on dynamics, and how. By augmenting X-ray crystallography with NMR studies of NR's dynamics and thermodynamic and kinetic studies of NR's activity, applied to both wild-type and mutants of NR we propose to address the above three questions. This report describes advances in answering (i) what is the mechanism of NR and (ii) is NR's dynamics due to quaternary structure changes or (iii) is NR's dynamics associated with substrate binding and NR's dimeric nature.

Chapter 2, addresses the mechanistic context of NR's promiscuity by delineating the transient kinetics of the reductive half-reaction of oxidized NR with NADH, as well as the oxidative half-reaction between reduced NR and *p*-nitrobenzoic acid (*p*-NBA) or a synthetic intermediate *p*-nitrosobenzoic acid (*p*-nitrosoBA), at 4^{o}C under inert atmosphere. Steady-state kinetic experiments were used to test the kinetic and equilibrium constants obtained by pre-steady-state methods and simulation. Thus we confirm the hypothesis that NR's promiscuity reflects a very simple favourable reaction.

Chapter 3 describes the use of primary kinetic isotope effects (1^{o}KIE) and solvent kinetic isotope effects (SKIE) as tools for evaluation of the sources of protons participating in nitroaromatic reduction. The double KIE can be used to arbitrate as to whether the hydride transfer from the N(5) of reduced flavin to *p*-NBA and the proton transfer from solvent are concerted (via a single transition state) or occur in different kinetic steps (distinct steps).

Chapter 4 investigates the possible significance of dynamics to NR's promiscuity, using 1D proton, 2D ^{1}H-^{15}N HSQC NMR spectra, as well as 1D relaxation dispersion experiments at a range of temperatures to monitor NR's conformational flexibility as the stability is varied. These biophysical studies are linked to catalytic events via measurements of the dissociation constants (K_d) of the substrate analog dicoumarol. The oligomerization state of NR was also assessed over the full temperature range to ensure no dimer dissociation.

Chapter 5 describes how selected amino acid substitutions have been incorporated to test the significance of the C-terminus' intermonomer interaction and interactions in the dimer interface, which may enable the enzyme to accept many kinds of substrates. The thermodynamic driving force for oxidation and reduction of NR, of both wild type and mutants, in the form of the reduction midpoint potential were measured.

Chapter 6 assembles the conclusions of this work and records suggestions for future work.

CHAPTER 2

UNDERSTANDING THE BROAD SUBSTRATE REPERTOIRE OF NITROREDUCTASE BASED ON ITS KINETIC MECHANISM

(This chapter has been published as part of "Understanding the broad substrate repertoire of nitroreductase based on its kinetic mechanism" by Pitsawong, W., Hoben, J.P., and Miller, A.F. (2014), *Journal of Biological Chemistry*. 289, 15203-15214. This chapter reports only the work performed by me.)

2.1 ABSTRACT

The oxygen-insensitive nitroreductase from *Enterobacter cloacae* (NR) catalyzes two-electron reduction of nitroaromatics to the corresponding nitroso compounds and, subsequently, to hydroxylamine products. NR has an unusually broad substrate repertoire, which may be related to protein dynamics (flexibility) and/or a simple non-selective kinetic mechanism. To investigate the possible role of mechanism in the broad substrate repertoire of NR, the kinetics of oxidation of NR by para-nitrobenzoic acid (*p*-NBA) were investigated using stopped-flow techniques at 4°C. The results revealed a hyperbolic dependence on the *p*-NBA concentration with a limiting rate of 1.90 ± 0.09 s^{-1}, indicating one-step binding before the flavin oxidation step. There is no evidence for a distinct binding step in which specificity might be enforced. The reduction of *p*-NBA is rate-limiting in steady-state turnover (1.7 ± 0.3 s^{-1}). The pre-steady-state reduction kinetics of NR by NADH indicate that NADH reduces the enzyme with a rate constant of 700 ± 20 s^{-1} and a dissociation constant of 0.51 ± 0.04 mM. Thus, we demonstrate simple transient kinetics in both the reductive and oxidative half-reactions that help to explain the broad substrate repertoire of NR. Finally, we tested the ability of NR to reduce para-hydroxylaminobenzoic acid, demonstrating that the corresponding amine does not accumulate to significant levels even under anaerobic conditions. Thus *E. cloacae* NR is not a good candidate for enzymatic production of aromatic amines

2.2 INTRODUCTION

NAD(P)H:nitroaromatic reductases (nitroreductases) are flavoenzymes that catalyze the NAD(P)H-dependent reduction of the nitro groups of nitroaromatic and nitroheterocyclic compounds (70) (Fig. 2.1A). *Enterobacter cloacae* nitroreductase (NR)[1] was first isolated from bacteria collected at a weapon storage facility by Bryant *et al*. (20,21) based on its ability to degrade explosive compounds such as 2,4,6-trinitrotoluene (TNT). The enzyme exists as a homodimer of 217-residue monomers with two identical active sites in the dimer interface, each containing a non-covalently bound FMN that derives H-bonds from one monomer and hydrophobic contacts from both (52) (Fig. 2.1B).

Nitroreductases are widely distributed among bacteria, but NR-like proteins are also found in archaea and eukaryotes including man (19). *E. cloacae* NR is able to reduce a variety of nitroaromatics ranging from nitrofurans, nitroarene pollutants such as 1-nitropyrene, nitro-containing drugs (metronidazole), herbicides (dinoseb), and most famously nitroaromatic and nitramine explosives such as TNT (21,31,71). The Escherichia coli homologue NfsB is being developed for use as a prodrug activator for treatment of cancer (41,44,49).

The NRs from *E. cloacae* and *E. coli* reduce nitroaromatics to the corresponding nitrosoaromatics and then to the corresponding hydroxylaminoaromatics via two successive two-electron reductions (31,60) (Fig. 2.1A). It is difficult to isolate the nitroso intermediates because they react rapidly with NR, and the resulting hydroxylaminoaromatics react with their nitroso precursors to yield stable azoxy compounds (31,72,73). Nonetheless, there are reports of accumulation of a nitroso intermediate during biological reduction of certain nitroaromatics (30).

The hydroxylamine product is a basis for the toxicity of metronidazole and related antibiotics, which are activated in vivo by pathogen NRs (74,75) (in anaerobes, other mechanisms reductively eliminate the nitro group producing nitro radicals that initiate

[1] The abbreviations used are: NR, nitroreductase; NR_{ox}, oxidized NR; NR_{red}, reduced NR; MBTH, 3-methyl-2-benzothiazolinone hydrazone; NfsB, *E. coli* homologue of *E. cloacae* nitroreductase; *p*-ABA, para-aminobenzoic acid; *p*-HABA, para-hydroxylaminobenzoic acid; *p*-NBA, para-nitrobenzoic acid; *p*-NOBA, para-nitrosobenzoic acid; TNT, trinitrotoluene.

oxidative stress (76,77)). Thus chemistry of NR is being developed for clinical implementation against cancer via GDEPT (gene-directed enzyme prodrug therapy) and ADEPT (antibody-directed enzyme pro-drug therapy) wherein an NfsB-antibody fusion would be targeted to tumors where it would then reductively activate the prodrug CB1954 in ADEPT (39,41,49). Thus it is important to know what product NR produces.

Bioremediation and biocatalytic uses of NR have also been envisioned based on the possible production of aromatic amines by NR. Aromatic amines would be valuable synthons, and there are a few instances in which amine products have been detected (72,73,78,79). In particular, the NR of *Mycobacterium smegmatis* (NR-Ms) converts the nitro group of benzothiazinone to an amine (78). The NR from *Salmonella typhimurium* (NR-Sal) displays both nitroreductase and enoate reductase activity, transforming nitrobenzene to nitrosobenzene, phenylhydroxylamine, and even the fully reduced product aniline (73). Similarly, the first NR of *Klebsiella sp.* C1 (NR-I) transforms 2,4,6-TNT to 2-amino-4,6-dinitrotoluene (72). However amine products can elude detection due to their reactivity with oxygen. Thus dissolved O_2 can react with reduced products of NR including both the hydroxylamine and putative amine products in a futile cycle that will tend to diminish detected yields and mask formation of reduced products (71). This and the proclivity of the products for reactions among themselves has made it difficult to confirm accumulation of aminoaromatic products, especially given the common practice of conducting assays in air.

There are cases in which production of amines has been ruled out. For *E. coli* NfsB, it was demonstrated that only 2 eq. of NADH are oxidized per eq. of nitroaromatic reduced (60). Moreover Race *et al*. (60) showed that if reaction products were analyzed under aerobic atmosphere, hydroxylamines were converted to nitrosos. Thus full reduction of nitro groups to the corresponding amine is not a general property of the subfamily, and the identity of the substrate may be a major determinant of what final product can be achieved. Therefore, we have tested whether *E. cloacae* NR can produce para-aminobenzoic acid (*p*-ABA) from para-hydroxylaminobenzoic acid (*p*-HABA) under anaerobic conditions.

The broad substrate repertoire of nitroreductase makes it an attractive enzyme for bioremediation of nitroaromatics and for producing valuable pharmacological reagents

because this one enzyme could be used to transform a variety of related compounds (31,73). A number of enzymes are known that transform diverse substrates, including certain cytochrome P450s (80,81), and pentaerythritol tetranitrate reductase (82,83). Binding of diverse substrates appears to be associated with relatively weak and nonspecific substrate binding (for example, see Ref.(84)). Indeed, NfsB substrates have been found to bind via water molecules and to have relatively large K_m values (37). Thus one hypothesis is that the broad specificity of NR is related to its relatively high K_ms and large solvent-accessible active site (52).

However, the broad substrate repertoire of NR could also have a mechanistic basis. In several enzymes that are highly discriminating regarding their substrates, the mechanisms have been found to incorporate multiple steps in which the prospective substrate is "tested" on the basis of its ability to elicit a conformation change in the enzyme or to enhance binding of additional substrates needed for the reaction to proceed. Thus a second hypothesis is that the mechanism of NR may lack gating steps that could constrain its use of diverse substrates.

Prior steady-state kinetics studies have shown that NR employs a ping-pong bi-bi mechanism in which the flavin is alternately reduced by a nicotinamide (preferably NADH or NADPH) and then reoxidized by a nitroaromatic (or quinone) substrate (31). Pre-steady-state studies of NfsB were used to identify variants of the enzyme that enhance its activity on CB1954 and tailor the site-specificity of the reduction with respect to the two nitro groups of CB1954 (85). In these, Jarrom *et al*. (85) determined the second order rate constant k_1/K_d for the oxidative half-reaction (in which the flavin is reoxidized) but could not evaluate K_d due to the limited solubility of CB1954 as well as loss of a substantial portion of the kinetic trace in the instrument dead time for the higher CB1954 concentrations. The second-order rate constants were many times faster than the overall rate constant, indicating that the rate-limiting step is slow product release, possibly depending on conformational change (85). Thus the oxidizing substrates used in that study (CB1954 or nitrofurazone) were not able to address the possibility of a binding step preceding the chemical reaction. Nor did this study address the reductive half-reaction due to reaction times within the dead time of the instrument at 25°C.

To slow down the NR reaction we have worked at lower temperatures and performed pre-steady-state as well as steady-state analyses of each of the two half-reactions of NR to identify elements of the reaction that could participate in defining the substrate specificity of NR (and lack thereof). We have chosen a poor substrate, para-nitrobenzoic acid (*p*-NBA) to allow chemical steps to contribute more to the observed rates, and we have simulated the reactions in terms of all the participating states of the enzyme to test for possible additional steps not explicit in the observed kinetics. The higher solubility of *p*-NBA in water also enabled us to probe binding events. Knowledge of the natures and lifetimes of all the participating states for this simple substrate provides a crucial baseline for understanding the different rates and product distributions displayed by different NR substrates as well as different variants of NR produced by mutagenesis.

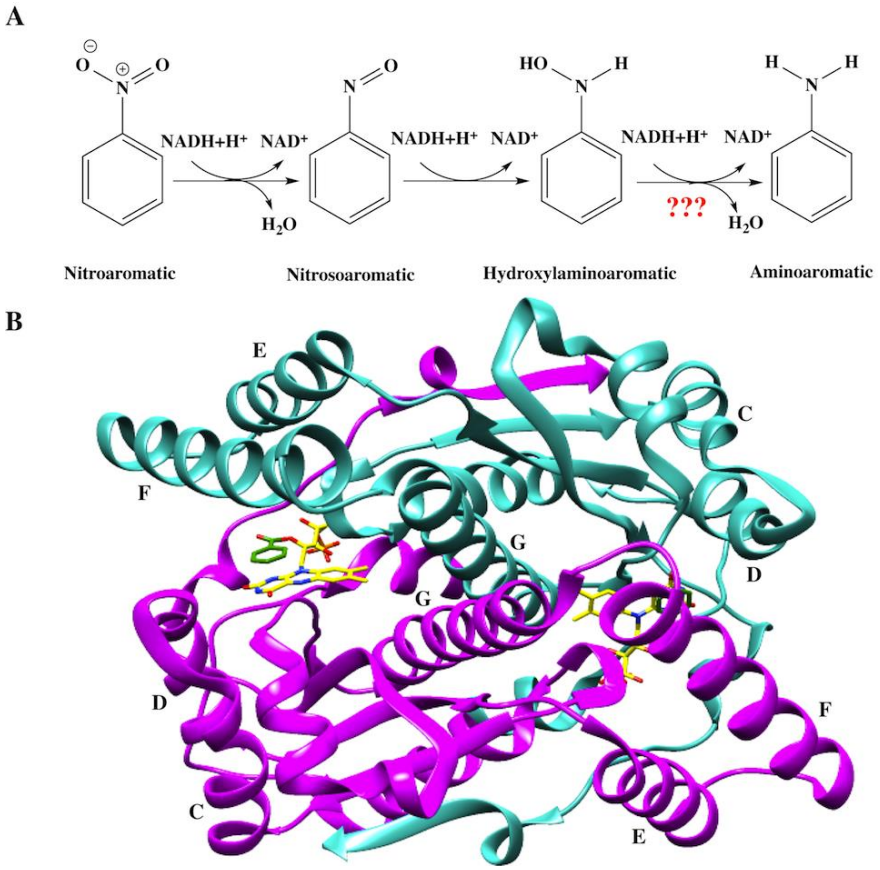

FIGURE 2.1: A) the reduction of nitroaromatic substrates catalyzed by nitroreductase for the example of nitrobenzene. B) ribbon structure of NR with lettering of the helices indicated. One monomer is in cyan, and the other is in magenta, the bound FMN is depicted with yellow sticks, and bound substrate analog benzoate is depicted with green sticks. Figure is based on 1KQB.pdb and generated using *PyMOL* (86).

2.3 EXPERIMENTAL PROCEDURES

2.3.1 Reagents

NADH (100% purity) was purchased from Roche Applied Science. *p*-NBA was from Acros Organics. *p*-Nitrosobenzoic acid (*p*-NOBA) was produced as per the procedure of Defoin (87) and validated by ^{1}H NMR spectroscopy at 400 MHz. *p*-HABA was the generous gift of K. Ferguson and A. S. Bommarius (School of Chemical and Biomolecular Engineering, Georgia Institute of Technology) and was determined to be 99% pure based on NMR. Concentrations of reagents were determined using the known

extinction coefficients at pH 7.0: ϵ_{340} = 6.22 × 103 $M^{-1}cm^{-1}$ or ϵ_{370} = 2.66 × 10^3 $M^{-1}cm^{-1}$ for NADH and ϵ_{273} = 10.1 × 10^3 $M^{-1}cm^{-1}$ for *p*-NBA. Wild-type NR was expressed and purified as previously described (70). The concentration of holo-NR was evaluated based on the extinction coefficient of the bound flavin, ϵ_{454} = 14.3 × 10^3 $M^{-1}cm^{-1}$, and rate constants reported refer to holo-enzyme (apoFMN enzyme represented <10% of the total protein based on the ratio of A_{454} to A_{280} (70).

2.3.2 Steady-state Kinetic Experiments

Initial velocities at various concentrations of NADH and *p*-NBA were measured using stopped-flow spectrophotometry at 4°C (TgK Scientific). The reactions were monitored at 370 nm to observe conversion of NADH to NAD^+. The assays contained 60 nM enzyme, various concentrations of NADH (0.1, 0.2, 0.3, and 0.4 mM) and various *p*-NBA concentrations (0.1, 0.2, and 0.4 mM) in 50 mM potassium phosphate, pH 7.50. Initial rates of the reaction were calculated using Program A (a generous gift of D. P. Ballou), and steady-state kinetic parameters were extracted using KaleidaGraph Version 3.6.2 to fit the data to the equation for a ping-pong mechanism (Eq. 2.1) (88,89) where K_m^{NADH} and K_m^{pNBA} are the K_m values for NADH and *p*-NBA, respectively

$$\frac{v}{E} = \frac{k_{cat}[NADH][PNBA]}{K_m^{NADH}[PNBA]+K_m^{PNBA}[NADH]+[NADH][PNBA]} \qquad (2.1)$$

2.3.3 Rapid Reaction Experiments

Pre-steady-state reductive and oxidative half-reactions of NR were studied using a stopped-flow spectrophotometer (TgK Scientific). The flow system was made anaerobic by rinsing with an anaerobic buffer and incubating overnight with a solution of 50 mM sodium dithionite in 50 mM potassium phosphate, pH 7.50. The buffer to be used for the sodium dithionite solution was first sparged with N2 and then equilibrated overnight to remove oxygen in an anaerobic glove box (M-BRAUN UNIlab glove box with Siemens Corosop 15 controller). Sodium dithionite was added to the anaerobic buffer inside the glove box, and the resulting solution was transferred into tonometers. These were mounted on the stopped-flow apparatus to provide reservoirs of anaerobic solutions and used to flush the flow system, which was then allowed to stand overnight with dithionite

solution throughout. Before experiments, the instrument was rinsed thoroughly with anaerobic buffer composed of 50 mM potassium phosphate, pH 7.50, equilibrated with N_2 gas that had been passed through an oxygen removal column (Labclear).

In general NR was dissolved in 50 mM potassium phosphate, pH 7.50, and experiments were performed at 4°C because the reaction rates at higher temperatures were too fast to permit detailed characterization. For single-mixing experiments a solution of ~35 μM NR was loaded in one syringe, and a concentration of substrate twice the concentration desired for the reaction, in the same buffer, was loaded in the other syringe. Equal volumes of the two solutions were co-injected into the rapid mixer (75 μl each), and the dead-time was 1 ms.

For each substrate concentration, at least four replicate measurements were made once the instrument had stabilized, and these transients were averaged. Analysis was conducted by fitting the resulting kinetic trace to exponential equations for growth and decay using the Marquardt algorithm in Program A, developed by C. J. Chiu, R. Chung, J. Diverno, and D. P. Ballou at the University of Michigan (Ann Arbor, MI) or with the Kinesyst 3 software provided with the stopped-flow spectrophotometer (TgK Scientific). Plots of observed rate constants (k_{obs}) versus the concentration of substrate used were fit with Eq. 2.2 where k is the apparent first-order rate constant (for 17.5 μM NR), and K_d is the dissociation constant for substrate and enzyme.

$$k_{obs} = \frac{k[Substrate]}{K_d + [Substrate]} \qquad (2.2)$$

Rates of background reactions between substrate and dissolved oxygen were measured and constituted <1% of the rate observed in the presence of enzyme. Kinetic traces were collected at a series of wavelengths from 340 to 700 nm at 5-nm intervals to look for the signatures of potential intermediates.

2.3.4 Reductive Half-reaction

A solution of 26 μM NR was made anaerobic by equilibration in the anaerobic glove box for 30 min then placed in a tonometer. All buffer and substrate solutions were made anaerobic by bubbling with N_2 gas that had passed through an O_2-removing

cartridge. Substrate solutions were loaded in tonometers, which in turn were mounted on the stopped-flow spectrophotometer along with the NR solution. Upon rapid mixing of the enzyme with substrate, flavin reduction was monitored by measuring loss of absorbance at 454 nm. This wavelength is the peak of the oxidized enzyme absorption and provides the maximum difference between the oxidized and the reduced enzyme. After mixing, the final concentration of the enzyme was 13 μM, whereas the concentration of the substrate was kept at least 5-fold greater than that of the enzyme, so that the pseudo-first-order condition was maintained. Analysis was carried out as described above. Rate constants k_{obs} were determined from fits of the kinetic traces obtained at 454 nm. Plots of k_{obs} versus substrate concentration were analyzed using the non-linear least-square fitting algorithms in the KaleidaGraph package (Synergy Software).

To test the presumed kinetic mechanism, simulations of reaction transients predicted by various mechanisms, rate constants, and binding equilibria were performed using Berkeley Madonna, Version 8.3 (Macey and Oster, University of California-Berkeley) refined by the Runge-Kutta 4 integration method. In brief, in the reductive half-reaction, the known parameters, which are the concentration of oxidized NR, the extinction coefficients of oxidized and reduced NR, and the reduction rate constant, were provided to the simulation, then the other parameters, which were k_1, k_{-1}, and k_3 and the extinction coefficients of E_{ox}:NADH, and E_{red}:NAD^+, were adjusted manually to produce the best agreement with experimental results based on the superposition of simulated transients with experimental transients (see Fig. 2.3). A whole set of transients was treated at once. We applied the same method to the oxidative half-reaction in which the reduced NR concentration, extinction coefficients of oxidized and reduced NR, and the oxidation rate constant from the experiments were provided to the simulation and allowed k_4, k_{-4}, and the extinction coefficients of other species to be optimized.

2.3.5 Oxidative Half-reaction

Reduced enzyme in 50 mM potassium phosphate at pH 7.50 (17.5 μM after mixing) was rapidly mixed with either *p*-NBA or *p*-NOBA in the same buffer. All substrate concentrations were at least 5-fold higher than the enzyme concentration used to maintain pseudo-first-order conditions. The reduced enzyme solution was prepared by

equilibration with the inert atmosphere in the glove box followed by reduction with a slightly substoichiometric amount of dithionite (or NADH) in the anaerobic glove box (with equivalent results). The reduction process was monitored using a spectrophotometer at 4°C. Oxidation of the enzyme by substrate was observed at 454 nm by the stopped-flow spectrometer, revealing formation of oxidized NR-bound flavin. Analysis was carried out as described above.

2.3.6 Testing for the stability of *p*-HABA

The decomposition of *p*-HABA was monitored by UV-visible spectrophotometry using a CARY-300 spectrophotometer to observe the absorbance of the final product of *p*-HABA oxidation (see Fig. 2.6C). *p*-HABA was dissolved to a concentration of 1.3 mM in 50 mM potassium phosphate, pH 7.50, that had been made anaerobic, or equilibrated with air as a control. The anaerobic sample of *p*-HABA was produced by weighing *p*-HABA (15.3 mg) and transferring it into the anaerobic glove box. The *p*-HABA powder was equilibrated in the glove box for 10 min to ensure that there was no longer oxygen associated with it. A 5-ml stock solution of 20 mM was prepared in the glove box using anaerobic buffer. For analysis, 1.3 mM *p*-HABA was transferred to a gas-tight anaerobic cuvette before removing it from the glove box.

The stability and purity of *p*-HABA in anaerobic versus air-equilibrated buffer was also characterized by 1H NMR spectroscopy at 400 MHz. p-HABA (13.3 mM) was dissolved in 50 mM potassium phosphate, pH 7.50, containing 10% v/v $^{2}H_2O$ and 0.1 mM 4,4-dimethyl-4-silapentane-1-sulfonic acid (DSS) as a chemical shift reference (δ = 0 ppm). The two samples were prepared as described above for optical samples but were transferred to NMR tubes instead of cuvettes. Wilmad NMR tubes, 5-mm diameter precision, were used to contain 600 µl of sample. For the anaerobic sample, Wilmad's gas-tight anaerobic NMR tube (535-TR-7) was used after prior degassing and incubation in the glove box overnight. The Wet1D sequence was used to achieve solvent suppression (90).

2.4 RESULTS

2.4.1 Steady-state Kinetics of NR

Although steady-state kinetic analyses of NR have been reported before (31), they were repeated as part of this effort to obtain data sets with which to test the kinetic and

equilibrium constants obtained by pre-steady-state methods and simulation (see below). The overall steady-state kinetics of NR were characterized using NADH and *p*-NBA as substrates at 4°C. Either NADH or *p*-NBA was varied at each of several concentrations of the other substrate as described under "Experimental Procedures" and the previous study (31). The data (Fig. 2.2A) were fit with Eq. 2.1 to give a K_m^{NADH} of 35 ± 8 μM, K_m^{pNBA} of 130 ± 5 μM, and a k_{cat} value of 1.7 ± 0.3 s^{-1}. The plot of initial velocity versus NADH concentration (0.02–0.33 mM) at high *p*-NBA concentration (0.4 mM) (Fig. 2.2B) and the plot of initial velocity versus *p*-NBA concentration (0.025–0.6 mM) at high NADH concentration (0.25 mM) (Fig. 2.2C) yielded similar parameters to those resulting from double-reciprocal plot (Fig. 2.2A). The complete steady-state study was repeated for two different preparations of NR. The results were within error of one another so only the parameters obtained from the larger study are reported.

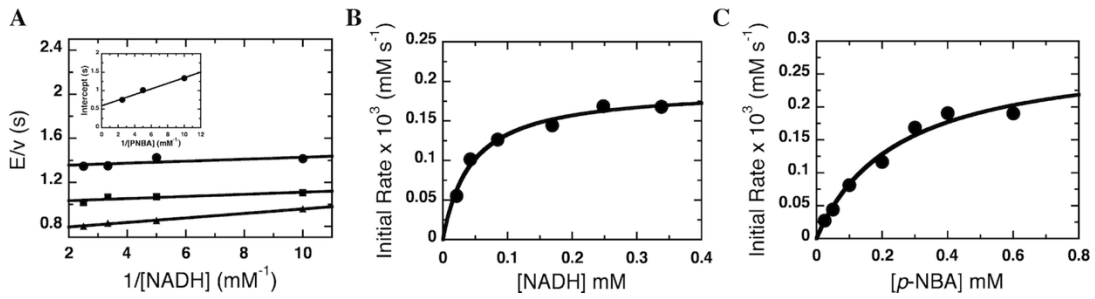

FIGURE 2.2: Steady-state kinetics of NR with NADH and *p*-NBA as substrates. A, double-reciprocal plots of the initial rates of reaction of NR with various concentrations of NADH (0.1, 0.2, 0.3, and 0.4 mM after mixing). Upper to lower lines of the primary plot are from the reactions of 0.1, 0.2, and 0.4 mM (after mixing) *p*-NBA, respectively. The assay reactions were performed using a stopped-flow spectrophotometer at 4°C. The inset shows the plot of ordinate intercepts from the double-reciprocal plot versus the reciprocal of *p*-NBA concentrations. The parameters obtained from the fits are provided in Table 2.1. B and C, used an enzyme concentration of 118 nM versus 60 nM for panel A. B, plot of initial velocity versus NADH concentration (0.02, 0.042, 0.08, 0.17, 0.25, and 0.34 mM) at a fixed p-NBA concentration (0.4 mM). The results show hyperbolic dependence on NADH concentrations with K_m^{NADH} of 44 μM and k_{cat} = 1.7 s^{-1}. C, plot of initial velocity versus *p*-NBA concentration (0.025, 0.050, 0.1, 0.2, 0.3, 0.4, and 0.6 mM) at a fixed NADH concentration (0.25 mM). The results showed hyperbolic dependence on *p*-NBA concentrations with the K_m^{pNBA} of 0.25 mM and k_{cat} = 1.7 s^{-1}.

2.4.2 Reductive Half-reaction of oxidized NR with NADH

The reaction of NR with NADH was investigated by stopped-flow spectrophotometry under anaerobic conditions at 4°C. An anaerobic solution of oxidized NR was mixed with various concentrations of NADH to yield final concentrations of 13 μM NR and 0.08, 0.16, 0.32, 0.64, 1.28, or 2.56 mM NADH (all concentrations are quoted after mixing here and below). Reduction of the enzyme-bound oxidized FMN was monitored via the loss of absorbance at 454 nm (Fig. 2.3, A and B), and formation and decay of a charge-transfer complex was monitored at 580 nm (Fig. 2.3C)

The results showed that reduction of NR by NADH is fast and the beginning of the kinetic trace (first phase) of all but the lowest concentration of NADH (0.08 mM) was within the dead time (0.001 s) of the stopped-flow instrument (Fig. 2.3B). Two rate constants were required to adequately describe the data; the use of only one resulted in systematic residuals that were eliminated by the use of a second rate constant (Fig. 2.3B). The first process (~0.001–0.01 s for 0.08 mM NADH) was characterized by decreased absorbance at 454 nm and an increase in absorbance at 580 nm (Fig. 2.3C). Therefore, the first rate constant was attributed to hydride transfer and formation of a charge-transfer complex between reduced FMN and NAD^+. The second phase (~0.01–0.1 s for 0.08 mM NADH) was attributed to dissociation of NAD^+. A plot of the observed rates of hydride transfer for reactions with 2.56 mM NADH and below yielded a hyperbolic dependence on NADH concentration and, therefore, was fit with Eq. 2.2 (Fig. 2.4A) to yield the rate constant k_2 = 700 ± 20 s^{-1} and the dissociation constant ($K_d = k_{-1}/k_1$) of 0.51 ± 0.04 mM depicted in Scheme 2.1.

$$\mathbf{E_{ox} + NADH} \underset{k_{-1}}{\overset{k_1}{\rightleftharpoons}} \mathbf{E_{ox}{:}NADH} \xrightarrow{k_2} \mathbf{E_{red}{:}NAD^+} \xrightarrow{k_3} \mathbf{E_{red} + NAD^+}$$

SCHEME 2.1: Reductive half-reaction of NR

A rate constant for the second process was estimated from the high NADH concentration asymptote of the observed rate of the second phase (65 ± 3 s^{-1}; Fig. 2.4B) and confirmed by simulations of the data using the obtained value of k_3 = 60 s^{-1} (Table 2.1).

To determine whether the observed rate constants suffice to fully describe the observed behavior, simulations of the behavior predicted by the model in Scheme 2.1 with the parameters in Table 2.1 were performed, and the parameters were refined to obtain the best visual agreement with the experimental observations. The optimized simulation results (red dashed lines in Fig. 2.3, A and B) provide a good description of the observed kinetics (black lines in Fig. 2.3, A and B) and yield a "simulated" dissociation constant ${}^{sim}K_d$ of 0.48 mM (comparable to the K_d obtained from the experiments of 0.51 ± 0.04 mM). The simulated reduction rate constant (${}^{sim}k_2$) was 700 s^{-1} (versus 700 ± 20 s^{-1} from the experiment), and the rate of dissociation of NAD^+ from NR_{red} (${}^{sim}k_3$) was found to be 60 s^{-1} (Table 2.1). The study of NR reduction kinetics was repeated for two different preparations of NR. The results were again within error of one another so only the parameters obtained from the larger study are reported.

Thus we are able to report the first numerical values for the rate of reduction of the FMN of NR by NADH, which we find to occur very rapidly. Moreover these experiments yield a limiting value for the K_m of NADH that is not complicated by concurrent operation of the other half-reaction.

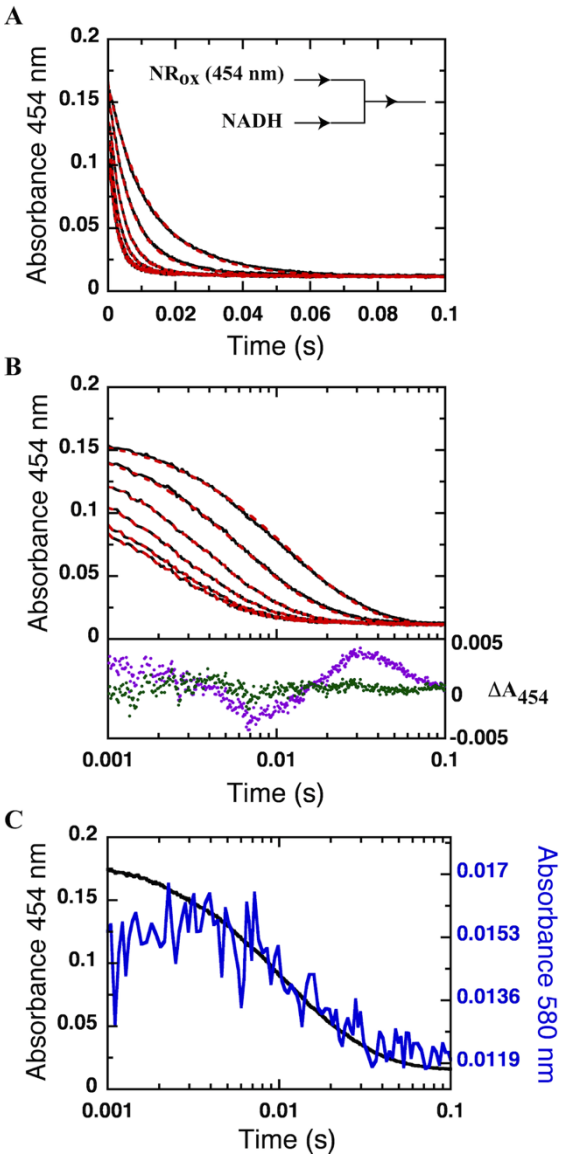

FIGURE 2.3: Reductive half-reaction of NR with NADH. Shown are the linear time scale (A) and log time scale (B) kinetic traces of the reaction of NR (13 μM) with various concentrations of NADH (0.08, 0.16, 0.32, 0.64, 1.28, and 2.56 mM) in 50 mM potassium phosphate pH 7.50 at 4°C. Reactions were monitored in the stopped-flow spectrophotometer under anaerobic conditions. All concentrations are reported as final concentrations after mixing. Dashed red lines are simulated traces obtained using the kinetic constants listed in Table 2.1 and Scheme 2.1. Residuals of fitting the reduction of NR with 0.08 mM NADH using one exponential (magenta dots) and two exponentials (green dots) are shown below with a vertical ΔA454 axis on the right. C, kinetic traces of the reduction of NR at 454 nm (black line) and formation and decay of the charge-transfer complex observed at 580 nm (blue line) with a concentration of 0.08 mM NADH.

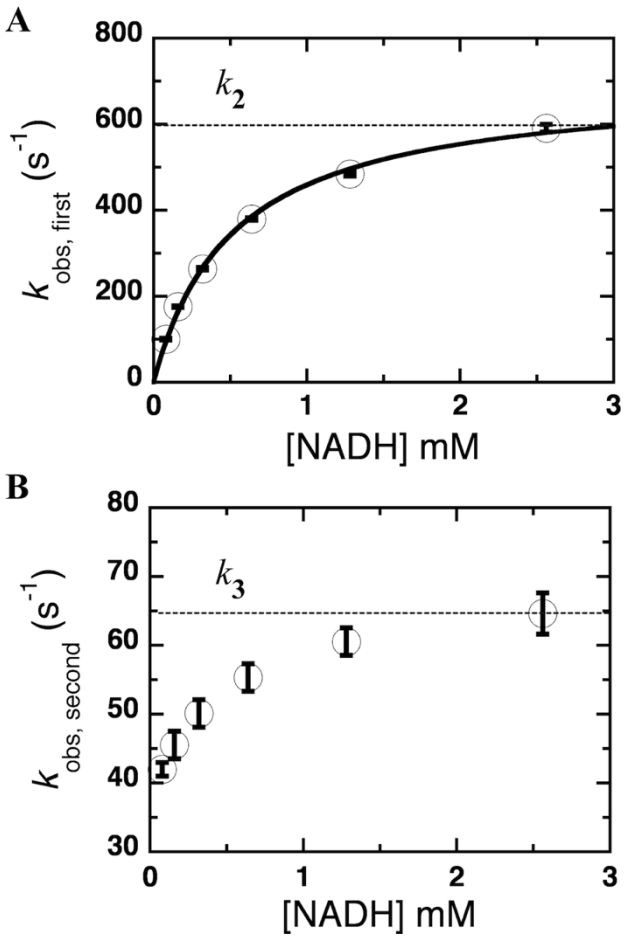

FIGURE 2.4: Plot of the observed rate constants of the reduction of NR. A, plot of the observed rate constants from the first phase; 100 ± 2, 176 ± 2, 264 ± 3, 380 ± 3, 484 ± 5, and 590 ± 9 s^{-1} (from low to high NADH concentrations; 0.08, 0.16, 0.32, 0.64, 1.28, and 2.56 mM) versus NADH concentration. The data including their error bars are well described by a rectangular hyperbola, which is the source of the values of k_2 and K_d. B, plot of observed rate constants from the second phase; 42 ± 1, 46 ± 2, 50 ± 2, 55 ± 2, 61 ± 2, and 65 ± 3 s^{-1} (from low to high NADH concentrations as described above). The k_3 value was estimated from the NADH asymptote as indicated by the *dotted line.*

TABLE 2.1: Kinetic parameters for NR at 4°C: comparison of steady-state, pre-steady-state, and simulation results. The values were obtained from the experimental data performed in 50 mM potassium phosphate, pH 7.50, at 4°C under anaerobic conditions using stopped-flow spectrophotometer or kinetic simulations. The kinetic parameters (steady-state kinetics) are as follows: k_{cat} 1.7 ± 0.3 s^{-1}, K_m^{NADH} 35 ± 8 μM; K_m^{pNBA} 130 ± 5 μM.

Kinetic parameters; pre-steady state		Extinction coefficients (M^{-1} cm^{-1})		
From experiment	From simulation	Chemical species	From experiment	From simulation
-	k_1[a] = 1.3 × 10^7 M^{-1} s^{-1}	E_{ox}	14,300	14,340
-	k_{-1}[a] = 6250 s^{-1}	E_{ox}:NADH	-	10,200
k_2 = 700 ± 20 s^{-1}	k_2 = 700 s^{-1}	E_{red}:NAD^+	-	1,940
K_3 = 65 ± 3 s^{-1}	k_3 = 60 s^{-1}	E_{red}	931	920
K_d^{NADH} = 0.51 ± 0.04 mM	K_d^{NADH}, k_{-1}/k_1 = 0.48 mM	E_{red}:*p*-NBA	-	2,850
-	k_4[a] = 6.8 × 10^5 M^{-1} s^{-1}	E_{ox}:Nitroso	-	18,240
-	k_{-4}[a] = 181 s^{-1}			
k_5 = 1.9 ± 0.09 s^{-1}	k_5 = 2 s^{-1}			
K_d^{PNBA} = 0.33 ± 0.04 mM	K_d^{PNBA}, k_{-4}/k_4 = 0.27 mM			

[a]The values provided are not necessarily unique but are able to fully explain the data observed in conjunction with the model we provide. The values of k_1 and k_{-1} are inversely correlated, as are the values of k_4 and k_{-4}.

2.4.3 Oxidative Half-reaction of Reduced NR with *p*-NBA

These reactions were investigated using stopped-flow experiments at 4°C by rapidly mixing the reduced enzyme in 50 mM potassium phosphate, pH 7.50, with the same buffer containing different concentrations of *p*-NBA to yield a final NR concentration of 17.5 μM and *p*-NBA concentrations of 0.1, 0.2, 0.4, 0.8, and 1.6 mM (after mixing). The experiment was limited to a maximum *p*-NBA concentration of 1.6 mM by the modest solubility of *p*-NBA. The reduced enzyme was prepared by stoichiometric reduction with dithionite as described under "Experimental Procedures." Kinetic traces at wavelengths from 340 to 700 nm at 5-nm intervals were collected. The kinetics at all wavelengths were the same, indicating that only formation of oxidized flavin contributes to optical spectrophotometric changes, and no transient intermediate was detected (data not shown).

The oxidation of NR the flavin of NR by *p*-NBA exhibited monophasic kinetics at 454 nm (Fig. 2.5). The observed rate constant (kobs) displayed saturation with respect to the *p*-NBA concentration as evinced by the hyperbolic curve (inset to Fig. 2.5). Therefore, the plot of kobs versus *p*-NBA concentrations was fit using Eq. 2.2 yielding the limiting value of k_5 = 1.90 ± 0.09 s^{-1} (Scheme 2.2). The intercept of the plot (k_{-5}) approached a value of zero, indicating that the reverse reaction rate is negligible (inset to Fig. 2.5). The dissociation constant ($K_d = k_{-4}/k_4$) obtained from the inset in Fig. 2.5 and Eq. 2.2 is 0.33 ± 0.04 mM. The hyperbolic dependence on substrate concentration indicates simple one-step binding before the flavin oxidation step (Scheme 2.2). The product of the oxidative half-reaction in this experiment was *p*-NOBA as no reductant was present to regenerate reduced enzyme and support a second cycle. The product was still bound to the active site at the end of the reaction (30 s) as indicated by a red shift of the final spectrum to 466 nm (from 454 nm for free oxidized enzyme) (data not show). The oxidative rate (1.90 ± 0.09 s^{-1}) was close to the turnover value measured in steady-state kinetic experiments (k_{cat} = 1.7 ± 0.3 s^{-1}).

$$\mathbf{E_{red} + S} \underset{k_{-4}}{\overset{k_4}{\rightleftharpoons}} \mathbf{E_{red}{:}S} \xrightarrow{k_5} \mathbf{E_{ox}{:}P} \xrightarrow{k_6} \mathbf{E_{ox} + P}$$

SCHEME 2.2: Oxidative half-reaction of NR

Kinetic simulation of the model in scheme 2.2 and optimization of the kinetic parameters (Table 2.1) produced excellent agreement with the experimental data as shown in Fig. 2.5 (dashed lines versus solid, respectively). The simulations yielded ${}^{sim}K_d$ (=${}^{sim}k_{-4}/{}^{sim}k_4$) of 0.27 mM and an oxidation rate constant (${}^{sim}k_5$) of 2 s^{-1} that are within error of the values determined directly from the data, indicating that this simple model and the parameters we report suffice to describe the optically perceptible events in the oxidative half-reaction of NR. All rate and equilibrium constants from the experiments and simulations are summarized in Table 2.1. These results reveal that oxidation of reduced flavin by *p*-NBA could be the rate-limiting step for overall turnover (k_5).

The above results were confirmed using double-mixing stopped-flow spectrophotometry to first produce reduced NR by mixing oxidized NR with 20 μM NADH allowing an aging time of 0.5 s for complete reduction of NR and then combining the result with various concentrations of *p*-NBA (0.2, 0.4, 0.8, and 1.6 mM *p*-NBA and 17.5 μM NR were the final concentrations) in the second mix. The reactions were monitored at 454 nm to detect flavin reoxidation. The oxidation rate constant and dissociation constant were observed to be k_5 = 2.00 ± 0.06 s^{-1} with an intercept close to zero and K_d = 0.20 ± 0.02 mM, respectively (not shown). The oxidative half-reaction of enzyme in the absence of NAD^+ was studied using single-mixing stopped-flow spectrophotometry by reducing NR using stoichiometric sodium dithionite and rapidly mixing it with various concentrations of *p*-NBA as above. The observed rate constants were hyperbolically dependent on the *p*-NBA concentration. The limiting value was k_5 = 1.90 ± 0.07 s^{-1}, and the K_d value was 0.30 ± 0.04 mM (data not shown). These results confirm that dissociation of NAD^+ from the active site of wild-type enzyme is complete within 0.5 s, and its presence in the reaction medium does not significantly affect the kinetics of the enzyme reaction with *p*-NBA. This supports a simple ping-pong bi-bi mechanism (31).

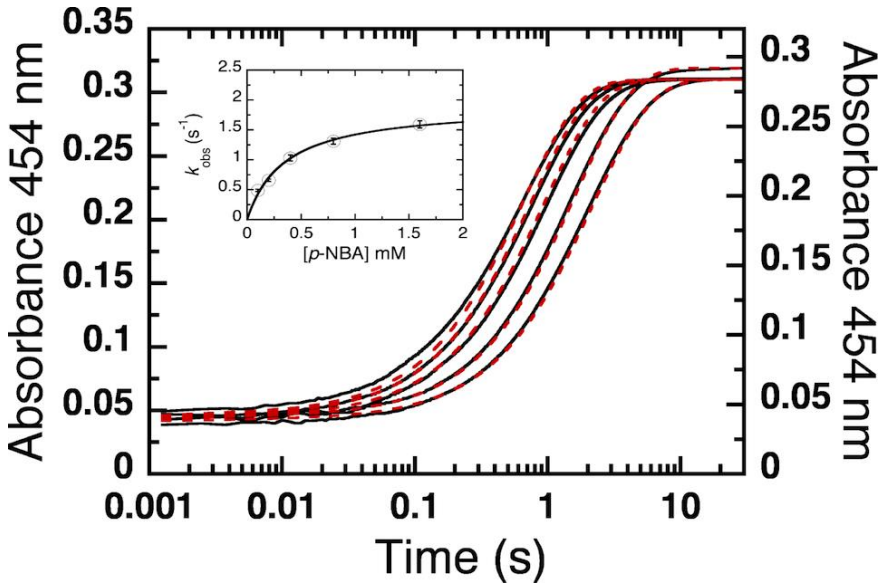

FIGURE 2.5: Oxidation of reduced NR by *p*-NBA. A solution of reduced NR (17.5 μM after mixing) was prepared by the stoichiometric addition of NADH, and this was then mixed with various concentrations of *p*-NBA to produce 0.1, 0.2, 0.4, 0.8, and 1.6 mM *p*-NBA in 50 mM potassium phosphate, pH 7.50. The reaction was monitored using the absorbance at 454 nm at 4°C. The plot of kobs versus *p*-NBA concentration (inset) was fit with Eq. 2.2 for a rectangular hyperbola. The calculated oxidation rate constant k_5 and K_d are 1.90 ± 0.09 s^{-1} and 0.33 ± 0.04 mM, respectively. The k_{obs} values from low to high *p*-NBA concentrations obtained from the transients are 0.49 ± 0.02, 0.66 ± 0.02, 1.03 ± 0.05, 1.31 ± 0.05, and 1.60 ± 0.06 s^{-1}. The vertical line at each data point represents the S.D. of the fit from the experiments. The 0.2 mM and 1.6 mM *p*-NBA samples were slightly oxidized at the start of the transient, so a smaller fraction of the sample reacted with *p*-NBA. This is manifested by a slight deviation between the t = 0 absorbance of the sample (1.6 mM) and the need to employ a modified vertical axis for the sample containing 0.2 mM *p*-NBA. Dashed red lines are simulated traces obtained using the kinetic constants listed in Table 2.1 and defined in Scheme 2.2.

2.4.4 Oxidative Half-reaction with *p*-Nitrosobenzoic Acid

The dominant product resulting from reduction of nitroaromatics by NR is the corresponding hydroxylamino aromatic (31,60). However, a few reports exist of the formation of a nitroso intermediate during biological reduction of certain nitroaromatics (30). It is difficult to isolate nitroso intermediates because they are reactive with hydroxylamines and rapidly reduced by NR (31). Thus reports of kinetic parameters are scarce.

To characterize the kinetics of nitroso aromatic reduction by NR, *p*-NOBA was generated by oxidation of *p*-ABA (see "Experimental Procedures") and used as the substrate in a study of the kinetics of NR oxidation. An anaerobic solution of reduced NR was mixed with *p*-NOBA in 50 mM potassium phosphate, pH 7.50, to yield final concentrations of 17.5 μM NR and 0.1 mM *p*-NOBA. The kinetic trace was monitored at 454 nm and 4°C using stopped-flow spectrophotometry. Most of the transients occurred during the dead time of the instrument (0.001 s) even with the lowest concentration of substrate (0.1 mM) at 4°C, so the oxidation rate constant could not be determined directly. Based on the portion of the transient we could detect, the observed rate constant was roughly estimated to be ≈650 s^{-1} (at 0.1 mM *p*-NOBA) using Program A. This result is consistent with prior work.

2.4.5 Testing for the stability of *p*-HABA

Several groups have shown that NR produces hydroxylamino products in multiple turnover reactions of nitroaromatic substrates (31,60,72,73), but there are also a few reports of amine production (72,73,78,79). Thus the capacity to produce amines may depend on the specific enzyme and substrate in use and require testing in each case. We have, therefore, optimized an assay for detecting *p*-ABA

Low yields of anything are very difficult to ascertain; moreover use of multi-turnover assays beginning with a nitroaromatic substrate could produce the amino aromatic in the presence of the corresponding nitroso, which would react with the amine (91,92). In addition, some of the prior studies were performed under air, whereas careful work has shown that hydroxylamino aromatic products can react with dissolved O_2 to regenerate more oxidized precursors and establish a futile cycle (71) that would compete with further reduction and suppress formation of amine product. Finally, sample preparation and workup for detection can expose hydroxylamine and labile enzymatic products to O_2. Again, hydroxylamino aromatics would be readily oxidized, and the resulting nitroso aromatics could then react with and mask amine products (93,94). Therefore, to detect the possible formation of aromatic amines at low concentration, we reacted NR with *p*-HABA instead of *p*-NBA to focus directly on the reaction in question, and we have refined a sensitive direct chromogenic probe for aminoaromatic products that can be applied in the presence of hydroxylamines without any workup or exposure to air (95,96).

To assess possible complications due to side-reactions and/or impurities, we first characterized the purity and stability of our *p*-HABA under the anaerobic conditions of our reaction by NMR and UV-visible spectrophotometry and compared the results with those obtained for *p*-HABA in conventional air-equilibrated solutions.

NMR spectra collected after incubation at room temperature for times ranging from 10 min to 24 h demonstrate that *p*-HABA is converted to another species in air-equilibrated buffer on a time scale of minutes to hours, but no reaction occurs under an inert atmosphere (Fig. 2.6). The *p*-HABA concentration was chosen to be 1.3 mM, 5 times the concentration of dissolved oxygen in air-saturated buffers (0.26 mM), to obtain pseudo-first order conditions. Within 5 h, the intensity of signals from 1.3 mM *p*-HABA

had begun to visibly diminish, and new signals appeared and increased in successive ^{1}H NMR spectra (Fig. 2.6A). The new signals at δ = 8.01, 8.03, 8.26, and 8.28 ppm match those of the aromatic protons of authentic *p*-NOBA, indicating that this is one of the oxidation products of *p*-HABA. Additional features in the spectrum are attributable to a small amount of contaminant (<5%) present in the *p*-HABA, and a compound that forms with the same time dependence as *p*-NOBA and that also forms when *p*-HABA is combined with *p*-NOBA under inert atmosphere, which we therefore tentatively assign to 4,4'-azoxydibenzoic acid (73). The decrease in the quantity of *p*-HABA present is fully accounted for by the sum of the increase in *p*-NOBA and putative azoxy product at all time points (Fig. 2.6B). Thus the optical signature of the proposed azoxy product could be used to monitor decay of *p*-HABA (Fig. 2.6C).

Azoxy compounds are intensely colored, whereas neither *p*-NOBA nor *p*-HABA absorbs in the visible range, so we monitored formation of the putative 4,4'-azoxydibenzoic acid at 400 nm. This was found to increase with a rate constant compatible with the growth of the new peaks in the NMR spectrum after accounting for concentration differences. Thus the initial oxidation rate constant was 3.0×10^{-2} h^{-1} for *p*-HABA. In contrast, for *p*-HABA in anaerobic solution the rate constant for appearance of the azoxy product was $\approx 3.2 \times 10^{-5}$ h^{-1} (Fig. 2.6C). These results show that our anaerobic solutions of *p*-HABA do not spontaneously react to form any other products on a time scale extending to a day.

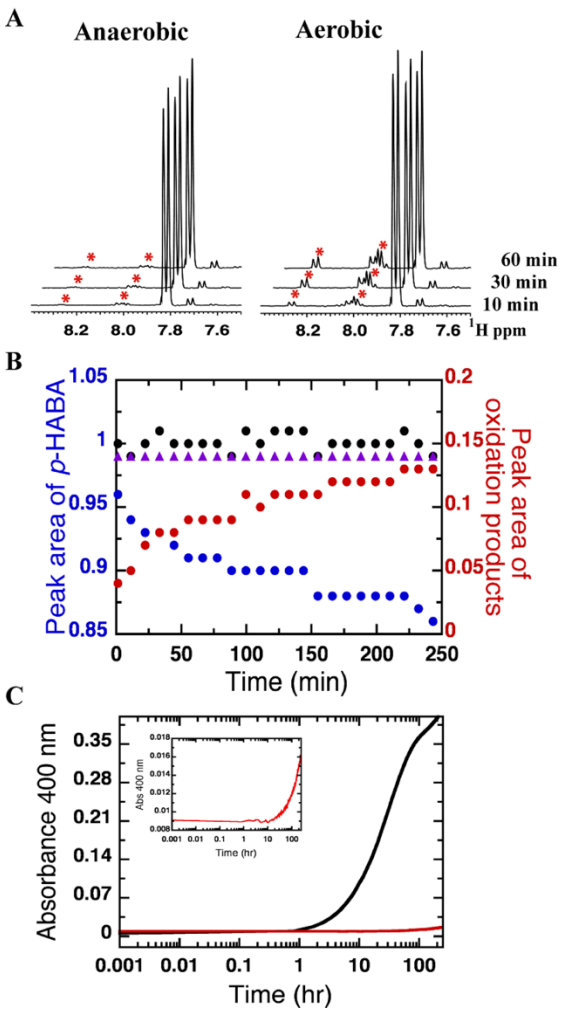

FIGURE 2.6: Decomposition of *p*-HABA under aerobic and anaerobic conditions. A, ^{1}H NMR spectra of 13.3 mM *p*-HABA in 50 mM potassium phosphate, pH 7.50, 10% D_2O, 0.1 mM 4,4-dimethyl-4-silapentane-1-sulfonic acid under aerobic and anaerobic conditions after 10, 30, and 60 min. Asterisks indicate signals that increase with time. B, total integrated NMR peak area corresponding to *p*-HABA (at δ = 7.04, 7.06, 7.81, and 7.83, blue circles) or *p*-NOBA plus 4,4'-azoxydibenzoic acid (at δ = 7.99, 8.00, 8.01, 8.03, 8.26, and 8.28 ppm, red circles) as a function of time. Black circles represent the sum of the area corresponding to *p*-HABA and oxidation products. Purple triangles represent the total integrated NMR peak area corresponding to *p*-HABA under anaerobic conditions. C, kinetic traces of formation of decomposition product of *p*-HABA under aerobic (black trace) and anaerobic (red trace) conditions. The reactions were monitored via the absorbance at 400 nm at 25°C. The inset shows a vertical expansion of the anaerobic reaction of *p*-HABA. The observed decomposition rates were calculated to be 3.0×10^{-2} h^{-1} and 5.4×10^{-4} h^{-1} for aerobic and anaerobic decomposition, respectively.

2.5 DISCUSSION

Nitroreductases are best known for their ability to catalyze reduction of the nitro groups of a wide range of aromatic substrates, but the biological function and the natural substrate of most nitroreductases are unknown. The prevalence of NR-family genes among bacteria nonetheless suggests that NRs confer a significant advantage on the organisms that bear them, and recent appreciation of the wide range of reactions conducted by members of the larger superfamily opens even wider the range of possibilities to be considered (19,97). Recent data suggest a role as a dihydropteridine reductase for the NR homologue of Rhodobacter capsulatus (98).

Structural explanations for the broad substrate repertoires of NR homologues have been discussed (52,99). The active site of NR is a large cavity between helices E and F, which extend out from the structural core of one monomer, and helix D and the preceding loop of the other monomer (Fig. 2.1). Diverse substrates bind by stacking on the flavin ring system (52); many exploit electrostatic interactions with the side chain of Lys-14 or employ water-mediated interactions with protein residues that are too far away for direct contact (99). The side chain of Phe-70 (helix D) was found to adopt diverse orientations and thereby accommodate different substrates (60,99). Helix F also moves due to interactions between Phe-124 and substrate analogs (37,52). The generally small number of interactions between substrate analogs and the enzyme is consistent with the generally large (>0.1 mM) K_d and K_m values observed for oxidizing substrates (above and Refs. (31) and (60)).

In other enzymes with broad substrate repertoires, the active site has been observed to alter its conformation to bind different substrates. The active site of the sulfotransferase SULT1A1 adopts different conformations to bind two molecules of nitrophenol at once versus estradiol (100), and isopropylmalate isomerase of Pyrococcus horikoshii was proposed to be able to bind either homocitrate or isopropylmalate due to the flexibility of a loop that replaces the helix that discriminates between similar substrates in the homologous aconitase (101). Similarly, a more flexible and accessible active site was credited with the expanded substrate repertoire of an evolved metallo-β-lactamase (102) and a glutathione S-transferase (GST) with a broader repertoire was

found to be more flexible than a GST with greater substrate selectivity on the basis of H/D exchange as well as fluorescence lifetime analyses (103).

In contrast, mechanistic bases for specificity include conformational changes required as part of the catalytic cycle. For example, *p*-hydroxybenzoate hydroxylase (PHBH) exhibits substrate specificity in the formation of a reaction intermediate. For reducing equivalents to pass from NADPH to the tightly bound FAD flavin ring, the enzyme must undergo a conformational change. This only occurs in the WT enzyme when a substrate is bound and only when that substrate can be deprotonated (104,105). α-Ketoglutarate-dependent dioxygenases also incorporate a similar "substrate trigger" (106): the substrate to be oxidized must be bound for a coordination site for O_2 to become available on the catalytic Fe^{2+} ion (107). These and many other examples underscore the use of mechanistic intermediates in mediating substrate specificity. We have tested the corollary that an enzyme with a very broad substrate repertoire might be expected to employ a much simpler mechanism that does not include multiple events that could depend on different features of the substrate.

To test this we have attempted to elucidate all the rate-contributing steps of the NR mechanism of NR through analysis of the steady-state and pre-steady-state kinetics of the reductive and oxidative reactions of NR. We find that both the reductive and oxidative half-reactions of NR employ simple kinetic mechanisms with one-step binding and concluding with simple product release. There is no evidence for distinct binding steps in which specificity might be enforced. Release of product NAD^+ does not appear to be rate-contributing for the simple substrate *p*-NBA, and the re-oxidation rates and dissociation constants of the reduced enzyme prepared by reduction with dithionite (1.90 ± 0.07 s^{-1} and 0.30 ± 0.04 mM, respectively) or NADH (2.00 ± 0.06 s^{-1} and 0.20 ± 0.02 mM, respectively) were comparable supporting a simple ping-pong bi-bi mechanism.

For NR, we find that oxidation of reduced flavin by *p*-NBA (1.90 ± 0.09 s^{-1}) is likely an important contributor to the overall rate (1.7 ± 0.3 s^{-1}) based on comparison of the steady-state turnover number k_{cat} with the rate constants obtained by transient kinetics. For NfsB, product release (either NAD^+ or nitroso aromatic) or steps other than the chemical reaction were found likely to be rate-limiting (85). The difference can be explained by the different substrates used, as the substrates CB1954 and nitrofurazone

turn over at $k_{cat} \approx 140$ s^{-1} and 230 s^{-1}, respectively (85), much faster than the k_{cat} for *p*-NBA of 1.7 s^{-1}. We chose the poor substrate, *p*-NBA, to be able to look for mechanistic steps that might define the substrate repertoire. Despite the very slow chemical conversion of this substrate, we were unable to observe any intermediates or evidence for additional steps. Thus, we have ascertained that the broad substrate repertoire of NR rests not only upon the structure of the enzyme but also on the very simple mechanism it employs.

The relatively high K_d of NR for NADH of 0.51 mM (±0.04) is in excellent agreement with the results of Koder and Miller (31). The K_d for *p*-NBA of 0.33 ± 0.04 mM is also consistent with the mM values obtained for other substrates in previous work (31). The large magnitudes of both these K_d values are compatible with binding via relatively few and water-mediated contacts as indicated by crystal structures of the enzyme complexed with other substrates (99).

The value of k_{cat} = 1.7 ± 0.3 s^{-1} obtained from steady-state kinetics agrees well with k_5 = 1.90 ± 0.09 s^{-1} obtained from pre-steady-state kinetics. Similarly, when a value is calculated for K_m^{pNBA} from the individual rate constants measured via pre-steady-state kinetics, the resulting K_m^{pNBA} = 0.27 mM agrees well with the experimental K_m^{pNBA} = 0.13 mM produced by the double-reciprocal plot (Fig. 2.2A) and the 0.25 mM describing the hyperbolic plot (Fig. 2.2C). However, the K_m^{NADH} = 1.5 μM we calculated from our individual rate constants is significantly different from our experimental values of 44 μM from the double-reciprocal plot and 35 μM from the hyperbolic plot. This may reflect the fact that genuinely saturating *p*-NBA concentrations could not be used due to their inhibitory effect (31). However, for k_{cat} and K_m^{pNBA} our primary rate constants succeed well in accounting for observed overall behavior.

Using the substrates nitrobenzene and its two-electron reduced product nitrosobenzene, Koder *et al*. (31) found that the nitroso substrate was reduced some 720 times faster than was the nitro substrate. Race *et al*. (31) confirmed analogous behavior for NfsB and nitro/nitroso toluene or nitro/nitrosobenzene. For *p*-NOBA, we could only estimate the apparent rate of reduction at 0.1 mM to be 650 s^{-1}, whereas the rate of *p*-NBA reduction is 0.50 s^{-1} at the same concentration so we find that reduction of the nitroso is some 1300 times faster than reduction of the nitro.

One reason for interest in NR is the hope that it might be useful for producing aromatic amines from the corresponding nitroaromatics (73). However, our current results confirm earlier findings that significant quantities of aromatic amines do not necessarily accumulate under the action of *E. cloacae* NR (31).

Further work is called for to understand the basis for the ability of *M. smegmatis* nitroreductase to reduce benzothiazinone 043 to the corresponding amine (78) and the success of *Klebsiella* nitroreductase in fully reducing one nitro group of TNT, (72) in contrast with the common reduction of nitroaromatics only as far as the hydroxylamine followed by use a hydroxylamino mutase to produce the corresponding aminophenol (108,109). We find that the *M. smegmatis* nitroreductase has a flavin midpoint potential very similar to that of NR,[3] arguing against greater reducing power on the part of the enzyme (53). Instead, the substrates in question may be more amenable to full reduction by virtue of additional functionalization of the aromatic ring by a trifluoromethyl group in the case of benzothiazinone 043 and two additional nitro groups that are not reduced in the case of TNT. Our refinement of a sensitive selective chromogenic assay to detect aromatic amines affirms that *p*-HABA and thus also *p*-NBA is not converted to *p*-ABA by *E. cloacae* NR. However, this assay provides a valuable tool for determining whether the same enzyme can produce aromatic amine products from different substrates.

2.6 ABBREVIATIONS

ADEPT, antibody-directed enzyme pro-drug therapy; ANOVA, analysis of variance; DSS, 4,4-dimethyl-4-silapentane-1-sulfonic acid; GDEPT, gene-directed enzyme prodrug therapy; GST, glutathione s-transferase; MBTH, 3-methyl-2-benzothiazolinone hydrazone; NfsB, *Escherichia coli* homologue of *Enterobacter cloacae* nitroreductase; NR, nitroreductase; NR_{ox}, oxidized NR: NR_{red}, reduced NR; *p*-ABA, *para*-aminobenzoic acid; PETN, pentaerythritol tetranitrate reductase; *p*-HABA, *para*-hydroxylaminobenzoic acid; *p*-HBH, *para*-hydroxybenzoate hydroxylase; *p*-NBA, *para*-nitrobenzoic acid; *p*-NOBA, *para*-nitrosobenzoic acid; TNT, trinitrotoluene; WT, wild-type.

2.7 SUPPORTING INFORMATIONS

Proton 1D NMR measurement – The WET water suppression pulse sequence was used to suppress the large NMR signal from water (110). Following the wet pre-sequence a 90^{o} pulse was used to excite proton resonances which were recorded over a 1s acquisition time using a 1s relaxation delay time between scans. The pandora's box (Pbox) component of the Agilent NMR software was used to create eburp1 waveforms producing on-resonance excitation over a bandwidth of 300 Hz. The number of scans (nt) was 16 and was arrayed for 5 hours. *p*-HABA (13.3 mM) was dissolved in 50 mM potassium phosphate buffer pH 7.50 containing 10% v/v $^{2}H_2O$ for locking and tracking the magnetic field and 0.1 mM DSS as a ^{1}H chemical shift reference (δ = 0 ppm). Wilmad NMR tubes, 5 mm diameter, precision, were used to contain 600 µL of sample.

Initial rate equation for ping-pong mechanism – Considering *p*-NBA as substrate:

$$\frac{e}{v} = \emptyset_o + \frac{\emptyset_{NADH}}{[NADH]} + \frac{\emptyset_{pNBA}}{[pNBA]}$$

$$\frac{e}{v} = \frac{1}{k_2} + \frac{1}{k_5} + \frac{1}{k_8} + \left(\frac{(k_{-1} + k_2)}{k_1 k_2}\right)\frac{1}{[NADH]} + \left(\frac{(k_{-4} + k_5)}{k_4 k_5}\right)\frac{1}{[pNBA]}$$

$$\emptyset_o = \frac{1}{k_2} + \frac{1}{k_5} + \frac{1}{k_8}$$

$$k_{cat} = \left[\frac{1}{k_2} + \frac{1}{k_5} + \frac{1}{k_8}\right]^{-1}$$

$$k_{cat} = \left[\frac{1}{700} + \frac{1}{2} + \frac{1}{>650}\right]^{-1}$$

$$k_{cat} = 2\ s^{-1}$$

$$\emptyset_{PNBA} = \frac{(k_{-4} + k_5)}{k_4 k_5}$$

$$K_m^{pNBA} = \frac{\frac{(k_{-4}+k_5)}{k_4 k_5}}{\frac{1}{k_2}+\frac{1}{k_5}+\frac{1}{k_8}}$$

$$K_m^{pNBA} = \frac{\frac{181+2}{(6.8\times10^5)(2)}}{\frac{1}{700}+\frac{1}{2}+\frac{1}{>650}}$$

$$K_m^{pNBA} = 0.27\ mM$$ (K_m^{pNBA} from steady-state kinetic experiment = 0.27 mM)

$$\emptyset_{NADH} = \frac{(k_{-1} + k_2)}{k_1 k_2}$$

$$K_m^{NADH} = \frac{\frac{(k_{-1} + k_2)}{k_1 k_2}}{\frac{1}{k_2} + \frac{1}{k_5} + \frac{1}{k_8}}$$

$$K_m^{NADH} = \frac{\left[\frac{6250 + 700}{(1.3 \times 10^7)(700)}\right]}{\frac{1}{700} + \frac{1}{2} + \frac{1}{> 650}}$$

$K_m^{NADH} = 1.5\ \mu M$ (K_m^{NADH} from steady-state kinetic experiment = 35 μM)

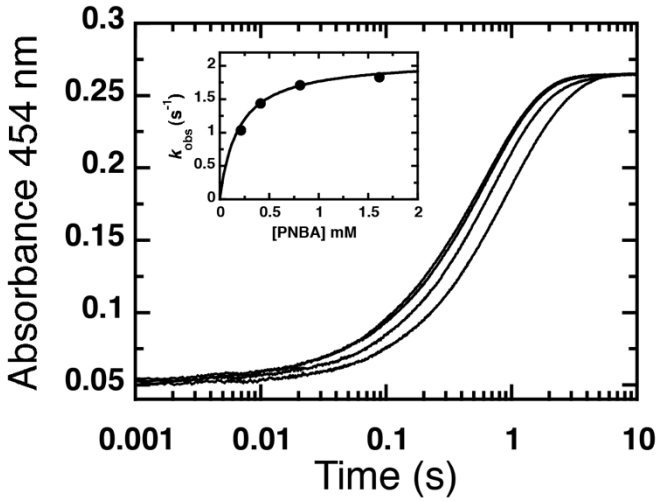

FIGURE S2.1: Oxidation of reduced NR by *p*-NBA using double-mixing stopped-flow spectrophotometry. A solution of reduced NR (17.5 μM after mixing) was first mixed with NADH (17 μM). After NR was fully reduced by NADH, using an aging time of 0.5 s, the solution resulting from the first mix was allowed to react further with various concentrations of *p*-NBA in the second mix (0.1 mM, 0.2 mM, 0.4 mM, 0.8 mM, and 1.6 mM) in 50 mM potassium phosphate buffer pH 7.50. The reaction was monitored using the absorbance at 454 nm, at 4°C. The plot of k_{obs} versus *p*-NBA concentration (inset) was fit with Eq. 2.2 for a rectangular hyperbola. Calculated oxidation rate constants and K_d are 2.0 ± 0.06 s^{-1} and 0.2 ± 0.02 mM, respectively.

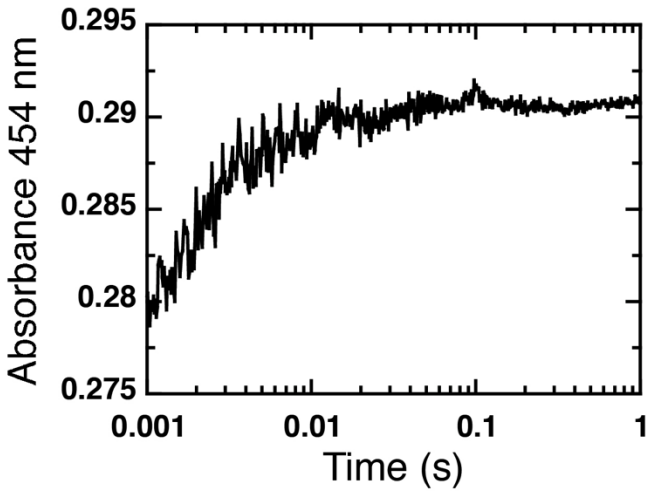

FIGURE S2.2: Oxidation of reduced NR by *p*-nitrosobenzoic acid. A solution of reduced NR (17.5 μM after mixing) was mixed with *p*-nitrosobenzoic acid (0.1 mM after mixing) in 50 mM potassium phosphate buffer pH 7.50. The reaction was monitored using the absorbance at 454 nm, at 4ºC. The observed rate constant was roughly estimated to be ≈ 650 s^{-1} (at 0.1 mM *p*-nitrosobenzoic acid) using Program A.

CHAPTER 3

RATE-CONTRIBUTING PROTON TRANSFERS OF THE TWO HALF-REACTIONS OF THE FLAVOENZYME NITROREDUCTASE

(This chapter will be submitted as part of "Rate-Contributing Proton Transfers Of The Two Half-Reactions Of The Flavoenzyme Nitroreductase" by Pitsawong *et al* to *Journal of Biological Chemistry*. This chapter focuses on the work performed by me.)

3.1 ABSTRACT

The nitroreductase of *Enterobacter cloacae* typifies numerous related enzymes found to reduce nitroaromatics to corresponding nitroso and hydroxylamino aromatics via two sequential two-electron reductions (31,60). However each reduction also requires the transfer of two protons, resulting in effective transfer of two H-atom equivalents. The electrons are known to transfer from enzyme-bound reduced anionic FMN. One proton has been proposed to be transferred with the electrons from reduced flavin as hydride (111), or alternately to be transferred as a proton from solvent in electron-coupled proton transfer (111). The other proton must derive from solvent. To gain insight into the sources of protons participating in nitroaromatic reduction, the primary and solvent kinetic isotope effects (KIEs) on different steps of the nitroreductase have been measured (and two new crystallographic structures have been determined modeling the enzyme-substrate complexes for each of the two half-reactions). Analyses of transient kinetics revealed that a large primary KIE of 3.2 applies to flavin reduction by NADH (reductive half-reaction) suggesting hydride transfer directly from NADH to the flavin N(5). For the oxidative half reaction a primary KIE of 1.6 ± 0.1 under pre-steady state and steady-state conditions indicates hydride transfer from the flavin N(5) atom to *p*-NBA (*para*-nitrobenzoic acid). The modest size of the latter is consistent with exchange of the N(5)H on the time scale of the measurements. Measured solvent KIEs are consistent with solvent as the source of the second proton. The results revealed a synchronous mechanism in which hydride transfer from the flavin to *p*-NBA and proton transfer from solvent are coupled. Thus we have been able to characterize electron transfer events via

the optical signatures of the flavin, and proton transfer steps via KIEs, to document the fundamental steps of NR's mechanism.

3.2 INTRODUCTION

Nitroreductase (NR) from *Enterobacter cloacae* is a promiscuous enzyme that catalyzes the reduction of nitroaromatics to yield hydroxylaminoaromatics via the intermediary of nitrosoaromatics (31,60). Our previous studies described transient kinetics experiments, which establish a simple kinetic mechanism in both the reductive and oxidative half-reaction, as shown in scheme 3.1 (112). This accomplishment lays the groundwork for addressing fundamental chemical steps involved in the reduction of nitroaromatic substrates. Thus we are now in a position to probe natures and rates of the individual electron and proton transfer events.

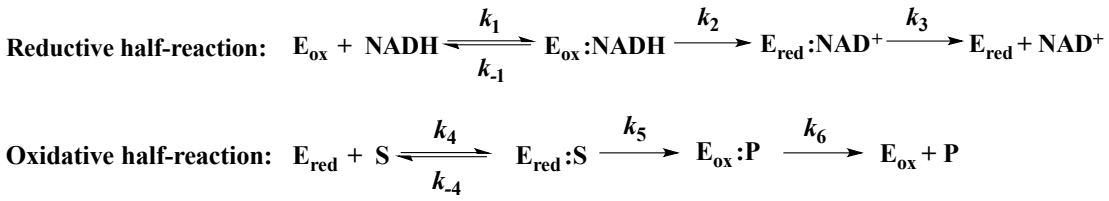

SCHEME 3.1: Kinetic mechanism of *E. cloacae* NR

To understand the molecular basis of this FMN-mediated reaction, the crystal structures of two substrate analog complexes of NR were solved. A model of the ES (Enzyme-Substrate) complex of the reductive half reaction was NR_{ox}:NAAD, where NAAD is nicotinic acid adenine dinucleotide, a substrate analog of NADH (Fig. 3.1A and 3.1B). As a model of the ES complex for the oxidative half-reaction, the structure of the NR_{ox}:*p*-NBA (*p*-NBA; para-nitrobenzoic acid) complex was solved (Fig. 3.1C) (unpublished structure). In the former, the nicotinic acid ring was found to stack against the flavin isoalloxazine ring, placing the nicotinic acid C(4) 3.6 Å from the flavin N(5). This distance is within the range (3.0 – 3.8 Å) considered ideal for hydride transfer (113). Therefore, the chemical mechanism of the reductive-half reaction was proposed to involve the formation of reduced flavin via a hydride transfer from NADH. In contrast, the crystal structure of the NR_{ox}:*p*-NBA complex (Fig. 3.1C), which provides a model of

the oxidative-half reaction, revealed a distance of 5.6 Å between the N(5) of FMN and the nitro group of *p*-NBA. Such a large distance argues against hydride transfer from the N(5) position of flavin to the nitro group of substrate. Thus, of the two prevailing mechanisms that have been proposed, our crystal structure argues against the first one (direct transfer of one proton and two electrons as a hydride ion from the reduced flavin to the nitroaromatic nitro group, step a in Fig. 3.2A). Therefore we have sought to test the second mechanism, which calls for proton transfer from solution and sequential transfer of two electrons from reduced flavin via electron-coupled proton transfer (step a in Fig. 3.2B). This second mechanism does not require that the nitroaromatic group be stacked on top of the flavin ring or that the nitro group be as close to N5, but would require that the nitro group be within ≈14Å of the flavin for efficient electron transfer (114). In both cases, electron transfer would be followed by acquisition of an additional proton from solution (possibly via a protein residue, step b in Fig. 3.2A and 3.2B) to achieve net reaction by two protons and two electrons. The steps involving electron transfer to and from the flavin can be monitored directly via the strong and informative optical signatures of oxidized flavin and the two possible semiquinone states. Steps involving proton transfer can be probed via the effect of replacing proteum with deuterium, to the extent that these steps contribute to the observed rates. Thus we have sought to arbitrate between the two proposed mechanisms.

Detailed analysis of the mechanism is a crucial complement to crystallographic studies, since it is frequently not possible to obtain crystal structures of the actual ES complex. Indeed, the NR_{ox}:*p*-NBA complex employs the oxidized state of NR so as to have a stable complex, but this procedural simplification introduces the interpretational complication that it represents a substrate-inhibited complex not the competent NR_{red}:*p*-NBA complex. These two species can be expected to differ in electronic properties at least. For example, the different charge distribution in the flavin ring system of reduced FMN vs. oxidized FMN could modulate the substrate binding orientation (115). Crystal structures of many nitroreductases from *E. cloacae* and *E. coli* (NfsB) bound with several substrate analogs have been published (33-36,52,65,67). In all cases, there were catalytically incompetent complexes, and therefore could suffer from the same complication. However the findings were that NR can accommodate diverse substrates in

a surprisingly large range of orientations. A common theme is stacking of the aromatic ring of substrate on the *re* face of the FMN, but distances between the flavin N(5) and the nitro group range from 3.9 - 7.7 Å and the, binding modes, orientations also vary considerably (60,99). These structures thus reinforce a sense that electron transfer from the flavin to the nitro group could occur via electron transfer coupled to proton transfer instead of hydride transfer. Therefore, complementary information is required to resolve this issue.

Recently, MD (molecular dynamics) simulations have provided insight into the catalytic mechanism of the reduction of prodrug CB1954 by *E. coli* NfsB (58). During the simulation, CB1954 reoriented to a position placing the amide group within van der Waals contact with N(5)-FMN whereas the nitro group pointed away from the N(5) atom. MD simulations were also performed on NR, and found that the nitro group of nitrobenzene always orients to the position away from the N(5) of FMN (57). Due to the large resulting distance between the nitro group and the N(5)-FMN, the authors suggested that two protons transfer from solution via an electron-coupled proton transfer pathway, as the preferred mechanism for CB1954 (58) and nitrobenzene (57) reduction. It is important to note that all the MD simulations were performed based on oxidized state structures of nitroreductases, for both NfsB and NR, where flavin ring has different electrostatic properties and geometries.

To shed light on the fundamental steps of electron and proton transfer that are central to the activities of both NR and NfsB, the catalytic mechanism of NR was investigated via study of the kinetic isotope effect (KIE) on the transients and on the steady state reaction. The kinetic data are used to identify the redox mechanism for nitroaromatic reduction.

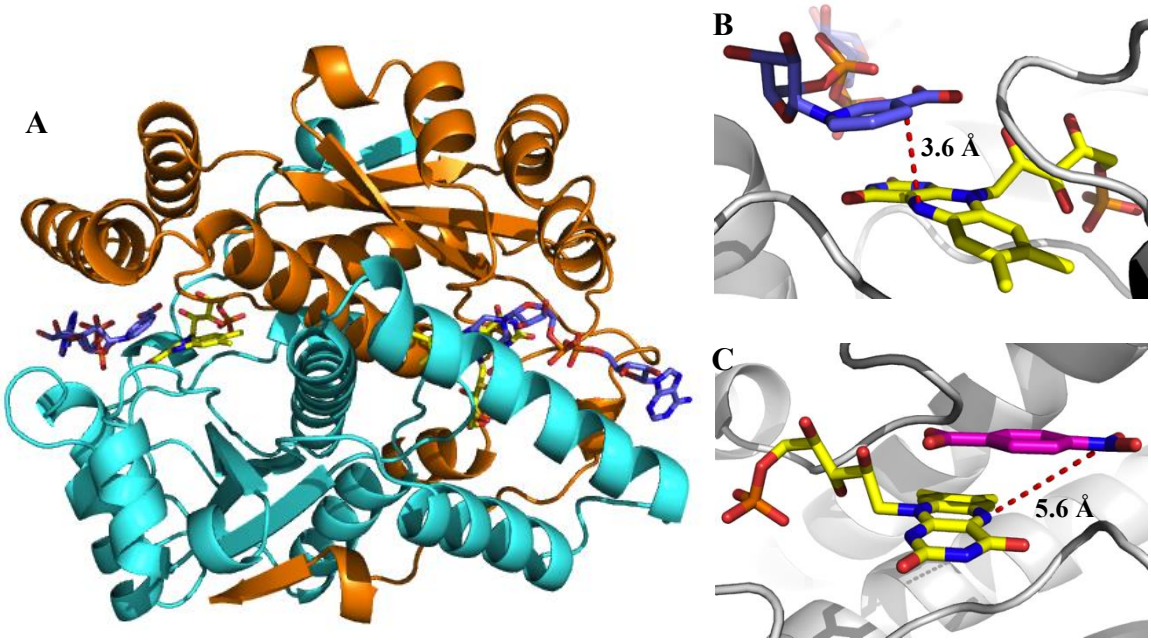

FIGURE 3.1: (A) Ribbon depiction of structure of oxidized NR with flavin and substrate analog as stick models. (B) The nicotinamide ring of NAAD (purple carbons) is stacked over the *re*-face of the isoalloxazine ring (yellow carbons) of FMN with a distance of 3.6 Å between N(5)-FMN and nicotinamide C(4). This distance allows hydride transfer between NADH and FMN (unpublished data).

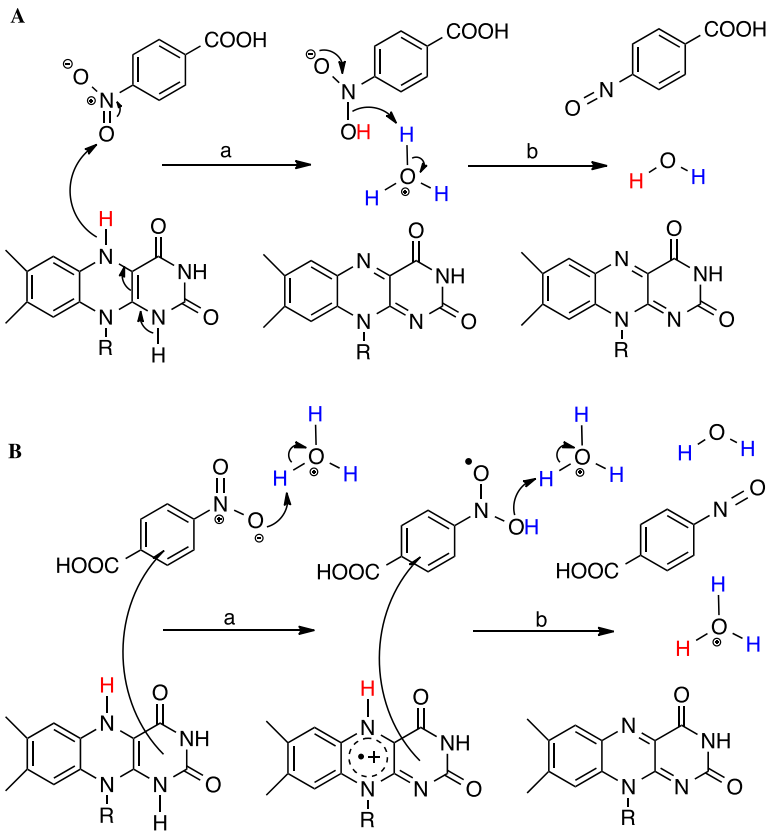

FIGURE 3.2: Schematic of two possible mechanisms for nitro-reduction. (A) two electrons and one proton (hydride transfer) from reduced flavin and another proton from solvent transfer to nitro-compound. (B) Two electrons from reduced flavin but two protons from solvent transfer to nitro-compound.

3.3 EXPERIMENTAL PROCEDURES

3.3.1 Reagents

NADH (100% purity) was purchased from Roche. NAD^+ (100% purity) was from Boehringer Ingelheim, Germany. *p*-nitrobenzoic acid was from Acros Organics. Deuterium oxide (99.9% purity), ethanol-d6 (99% purity), and sodium deuteroxide solution were from Cambridge Isotope Laboratories. [4R-^{2}H]NADH was synthesized according to the procedures of Gassner *et al* (116) and Nijvipakul *et al* (117). In brief, 25 mg of yeast alcohol dehydrogenase from *Saccharomyces cerevisiae* (Sigma-Aldrich) and NAD^+ were combined in 5 mL of 0.1 M NH_4HCO_3 buffer, pH 8.0 containing 0.3 mL ethanol-d6 and incubated at 37ºC for 1 hour or until the reaction was complete. The formation of [4R-^{2}H]NADH was monitored at 340 nm. Amicon® Ultra Centrifugal Filters – 10K (Millipore) were used to remove alcohol dehydrogenase from the resulting solution. The filtrate was diluted 5-fold with deionized water and loaded onto a 40 ml DEAE-Sepharose column, DE52 (GE Healthcare) pre-equilibrated with deionized water. [4R-^{2}H]NADH was eluted using a 300 mL gradient of 0-0.2 M NH_4HCO_3, pH 8.0. Pooled fractions containing [4R-^{2}H]NADH with $A_{260}/A_{340} \leq 2.6$ were combined. The purified [4R-^{2}H]NADH was analyzed by ^{1}H NMR spectroscopy (400 MHz), lyophilized to a dry powder and stored at -20ºC until used. Concentrations of reagents were determined using the known extinction coefficients at pH 7.0: $\varepsilon_{340} = 6.22 \times 10^3\ M^{-1}cm^{-1}$ for NADH and [4R-^{2}H]NADH, $\varepsilon_{260} = 17.8 \times 10^3\ M^{-1}cm^{-1}$ for NAD^+. The concentration of substrate *p*-NBA was determined from extinction coefficient, $\varepsilon_{273} = 10.1 \times 10^3\ M^{-1}cm^{-1}$.

3.3.2 Expression of NR

E. coli BL21(DE3) cells harboring the plasmid pRK1 containing the NR gene were used to inoculate 50 mL of Luria-Bertani broth medium (LB) containing 50 μg / mL kanamycin and cells were grown at 37°C overnight at 220 rpm, then 5 mL were added into 2 L of LB medium until their OD_{600} reached ~0.8, before protein expression was induced by addition of IPTG to a final concentration of 1 mM. The culture was incubated for a further 3 h at 37°C and then the cells were harvested by centrifugation at 9,000 rpm and 4ºC for 10 min and stored at -20°C after washing once with lysis buffer. All mutant enzymes were expressed using the same procedure used for the wild-type enzyme.

3.3.3 Purification of NR

Preparation of cell extractions; frozen cell paste (~20 mg) was thawed, re-suspended with lysis buffer containing 100 mM Tris-HCl buffer pH 7.5, 1 mM EDTA, 1 mM DTT (Dithiothreitol), 0.1 mM AEBSF (4-(2-Aminoethyl) benzenesulfonyl fluoride hydrochloride (an irreversible serine protease inhibitor) and lysozyme and disrupted (10 times) by using Ultrasonication. The suspension was centrifuged at 18,000 rpm for 45 min and the pellet was discarded. The supernatant referred to hereafter as the crude extract contained overexpressed NR.

DEAE-Sepharose chromatography; all purification steps were performed at 4°C. A 150 mL (2.5 × 31 cm) DEAE-sepharose (fast flow) chromatographic column was pre-equilibrated with 1 L of 10 mM Tris-HCl, 1 mM DTT, 0.2 mM EDTA, 0.02% NaN_3 pH 7.50. The enzyme was loaded onto the column. The loaded column was washed with 1 L of 10 mM Tris-HCl, 1 mM DTT, 0.2 mM EDTA, 0.02% NaN_3 pH 7.50. The enzyme was eluted by a gradient (0.5 L) of 0-500 mM NaCl in 10 mM Tris-HCl, 1 mM DTT, 0.2 mM EDTA, 0.02% NaN_3 pH 7.50. The fractions containing NR were identified based on absorbance at 280 (protein) and 445 nm (FMN) and SDS-PAGE (sodium dodecyl sulfate polyacrylamide gel electrophoresis). Pooled NR-containing fractions were concentrated until the enzyme volume was less than 10 mL using a Millipore Amicon® Ultra-15 Centrifugal Filter Device (10 kD cutoff).

Sephacryl S-200 Gel-filtration; the concentrated enzyme was loaded onto a Sephacryl S-200 gel filtration column (450 mL, 2.5 mm in diameter) pre- equilibrated with 50 mM KH_2PO_4, 50 mM KCl, 1 mM DTT, 0.2 mM EDTA, 0.02% NaN_3, pH 7.50. NR-containing fractions were identified based on absorbance at 280 and 445 nm and SDS-PAGE, and pooled. The pooled fractions were then concentrated until the enzyme concentration was 1 mM by using a Millipore Amicon® Ultra-15 Centrifugal Filter Devices 10K. The enzyme was stored at 4°C. Purity of the enzyme in each step was judged by SDS-PAGE. FMN content was assessed via the absorbance at 454 nm.

3.3.4 Reconstitution of the Apo-nitroreductase with ^{15}N labeled FMN

Unlabeled apo-NR was generated by method previously described in Koder *et al* (53). In brief, unlabeled holo-NR was mixed with 1.7 M ammonium sulfate, 1 M potassium bromide, 50 mM potassium phosphate pH 7.50. The solution was then applied

to a 2.5 × 5 cm column of phenyl sepharose equilibrated with the same buffer at room temperature. FMN was removed by elution with the same buffer adjusted to pH 5.0. Unlabeled apo-NR was then eluted using 50 mM potassium phosphate pH 7.50 and immediately cooled at 4^{o}C. The unlabed apo-NR was quantified based on Abs_{280} (ε_{280} = 40.73 $mM^{-1}cm^{-1}$).

^{15}N FMN was obtained from overexpressed and purified uniformly ^{15}N-labeled *Desulfovibrio vulgaris* flavodoxin (FD) by the method previously described in Mayhew *et al* (118) and Cui *et al* (119). In brief, ^{15}N FMN was dissociated from ^{15}N uniformly-labeled FD by dilution into 0.1 M sodium acetate, 2 M potassium bromide, pH 3.9. The solution was centrifuged at 4^{o}C and 14,000 × g for 10 min. The yellow supernatant was retained. The remaining ^{15}N uniformly-labeled FD in the supernatant was removed by ultrafiltration using Millipore Amicon® Ultra-15 Centrifugal Filter Devices (10 kD cutoff).

Reconstitution of unlabeled apo-NR with ^{15}N FMN was accomplished by mixing unlabeled apo-NR (2 mM) with a solution containing one stoichiometric equivalent of ^{15}N FMN (2 mM). After incubation at 4°C for overnight any unbound ^{15}N FMN was removed by ultrafiltration using a Millipore Amicon® Ultra-15 Centrifugal Filter (10 kD cutoff). The product was exchanged into 50 mM potassium phosphate pH 7.50 by G-25 gel-filtration.

3.3.5 Rapid Reaction Experiments

^{2}H kinetic isotope effects (KIEs) on NR's reductive and oxidative half-reactions were studied using a stopped-flow spectrophotometer (TgK Scientific). The flow system was made anaerobic by rinsing with an anaerobic buffer and incubating overnight with a solution of 50 mM sodium dithionite in 50 mM potassium phosphate buffer pH 7.50. The buffer used for the sodium dithionite solution was sparged with N_2 and then equilibrated overnight to remove oxygen, in an anaerobic glove-box (The M BRAUN UNIlab glovebox with Siemens Corosop 15 controller). Sodium dithionite was added to the anaerobic buffer inside the glove-box and the resulting 50 mM solutions were transferred into tonometers. The dithionite solution-containing tonometers were mounted on the stopped-flow apparatus and used to flush the flow system, which was then allowed to stand overnight with dithionite solution throughout. Prior to experiments, the instrument

was rinsed thoroughly with anaerobic buffer comprised of 50 mM potassium phosphate pH 7.50 equilibrated with N_2 gas that had been passed through an oxygen-removal cartridge (Labclear). Reductive half-reaction experiments were performed at 4°C to slow down the reduction rate whereas oxidative half-reactions were carried out at 25°C.

The kinetics of reduction of NR were investigated at 4°C using stopped-flow spectrophotometry. A solution of 52 μM NR was made anaerobic by equilibration in the anaerobic glove-box for 30 min then placed in a glass tonometer. All buffer and substrate solutions (NADH or [4R-^{2}H]NADH) were made anaerobic by bubbling with N_2 gas that had passed through an O_2-removing cartridge. Substrate solutions were loaded in tonometers, which in turn were mounted on the stopped-flow spectrophotometer along with the NR solution. Upon rapid mixing of the enzyme with NADH or [4R-^{2}H]NADH, flavin reduction was monitored by measuring loss of absorbance at 454 nm. After mixing, the final concentration of the enzyme was 26 μM, and the concentration of NADH or [4R-^{2}H]NADH was 0.1 mM.

The oxidative half-reaction of NR was monitored at 25°C using the double-mixing mode of the stopped-flow spectrophotometer, under anaerobic conditions. A solution of 52 μM oxidized NR was first mixed with 52 μM of NADH or [4R-^{2}H]NADH to generate proteated or deuterated reduced flavin, respectively. The solution was aged for 0.01 s or 1 s, respectively, to allow for full reduction of the NR flavin. In the second mixing step the solution from the first mix was reacted with 8 mM *p*-NBA. After mixing, the final concentration of the enzyme was 13 μM, the concentration of NADH or [4R-^{2}H]NADH was 13 μM, and the concentration of *p*-NBA was 2 mM. The reactions were monitored via the increase in absorbance at 454 nm that accompanies reoxidation of the flavin.

Analyses were conducted by fitting kinetic data using exponential equations for growth and decay using the Marquardt algorithm as implemented by Program A, developed by C. J. Chiu, R. Chung, J. Diverno, and D. P. Ballou at the University of Michigan (Ann Arbor, MI) or using the Kinesyst 3 software provided with the stopped-flow spectrophotometer (TgK Scientific).

3.3.6 Steady-State Kinetic Experiments

steady-state kinetic measurements were monitored spectrophotometrically by oxidation of NADH or [4R-^{2}H]NADH to NAD^+ at 370 nm with the known extinction coefficient of NADH at pH 7.50; $\varepsilon_{370} = 2.56 \times 10^3\ M^{-1}cm^{-1}$ using a Varian Cary 300 Bio UV-Visible Spectrophotometer (Agilent Technologies) at 25^{o}C. For determination of kinetic parameters, the reaction mixture contained 280 μM NADH or [4R-^{2}H]NADH, 60 nM NR, and the concentration of *p*-NBA was varied (25, 50, 100, 200, 400, and 500 μM) in 50 mM potassium phosphate buffer pH 7.50 (H_2O buffer) or pD 7.50 (where pD = pH meter reading + 0.4 to correct for the acidity of the pH electrode itself (120,121) and adjustments were made using sodium deuteroxide). Initial velocity was plotted against the *p*-NBA concentrations used and the data were fit with the Michaelis-Menten equation.

3.3.7 Solvent deuterium kinetic isotope effect (SKIE)

In studies of the solvent kinetic isotope effect on flavin oxidation, 99.9% D_2O was used to make 50 mM potassium phosphate buffer (D_2O buffer). In brief, potassium phosphate powder was dissolved in 99.9% D_2O and incubated overnight (~12 hours), then the solution was evaporated to dryness at 60^{o}C, 50 mm Hg for 3 hours using a rotary evaporator. The entire process was repeated three times to obtain a buffer containing 99.9% D_2O. The D_2O buffer was adjusted to pD 7.50 using sodium deuteroxide. Enzyme was exchanged into D_2O buffer twice using Econo-Pac® 10DG chromatography columns (Bio-Rad Laboratories) preequilibrated with D_2O buffer pD 7.50 and reduced by a adding stoichiometric equivalent of sodium dithionite in D_2O in an anaerobic glovebox.

To compensate for the higher viscosity of D_2O than H_2O, H_2O buffers were augmented with glycerol to 9 % (w/v) to relative viscosity equivalent to that of D_2O at 25°C (η = 1.24) (122-127). Therefore observed differences can be attributed to the isotopic composition. *p*-NBA was dissolved in 75% ethanol-d_6 and 25% D_2O with gentle warming.

3.4 RESULTS

3.4.1 Insights from the primary kinetic isotope effect (KIE) on the reductive half-reaction

Primary kinetic isotope effects on the reductive half-reaction were investigated by comparing the observed rate constants for the reduction of oxidized NR by [4R-^{2}H]NADH or by NADH at 4°C. Flavin reduction was monitored at 454 nm upon mixing with nicotinamide at a final concentration of 0.1 mM, as described in the experimental procedures. Kinetic traces of the reaction with [4R-^{2}H]NADH were similar to those obtained using NADH. Data were analyzed according to the model in scheme 3.1 giving rise to observed rate constants of 75 ± 2 and 238 ± 3 for [4R-^{2}H]NADH and NADH, respectively (Fig. 3.3A). Thus the observed primary kinetic isotope effect on flavin reduction (k_2^H/k_2^D) is 3.2. This value is very close to those obtained for morphinone reductase (MR) and pentaerythritol tetranitrate (PETN) and indicates that like them, NR employs hydride transfer from NADH to the N(5) position of flavin and this step is the rate limiting step in the reductive half-reaction.

3.4.2 Insights into the oxidative half-reaction from the primary kinetic isotope effect (KIE)

The oxidative half-reaction was studied via double mixing experiments at 25^{o}C to test possible sources of protons transferred to substrate. To test for H transfer from the flavin N(5), oxidized NR (13 μM) was first mixed with either 13 μM NADH or [4R-^{2}H]NADH to generate reduced flavin proteated or deuterated at the N(5) position, respectively. After allowing for full reduction of NR's flavin (0.01 s or 1 s aging time for generating FMNH$^-$ or FMND$^-$, respectively), the solution was mixed with 2 mM *p*-NBA. (Concentrations are reported as final concentrations.) Comparison of the kinetic traces recorded at 454 nm for flavin re-oxidation after reduction using NADH and [4R-^{2}H]NADH are shown in Fig. 3.3B and analysis to extract the rate constants yielded rate constants of 16.4 ± 0.06 s^{-1} and 11.5 ± 0.05 s^{-1}. Thus the observed primary kinetic isotope effect (k_5^H/k_5^D) is 1.4, which is somewhat smaller than expected for a hydride transfer. Since no partially-oxidized flavin intermediate is observed the flavin oxidation involves loss of a pair of electrons. Thus the H nucleus transfer from N(5)H represented by this primary KIE is assigned to hydride transfer.

To investigate the possibility that exchange of the reduced flavin N(5)H with proteated solvent dilutes the actual primary KIE to produce a diminished observed primarily KIE, we carried out double-mixing experiments in which a range of aging times from 10 ms to 50 s were used to allow the proposed solvent exchange to decrease deuteration at N(5) by varying amounts. A solution of oxidized NR was mixed with [4R-^{2}H]NADH to yield 26 μM of each. The reaction mixture was aged for 0.01, 0.1, 1, 2, 4, 10, or 50 s before mixing with *p*-NBA (2 mM final, NR and NAD^+ 13 μM) all under anaerobic conditions. Kinetic traces reflecting flavin oxidation were monitored at 454 nm, 25^{o}C. The longer aging times can allow more complete exchange between protium from solvent and deuterium at the N(5) of flavin. The kinetic traces of various ageing times yielded observed rate constants which increased with the increasing ageing time; 0.01 s (k_{obs} = 11.4 ± 0.03 s^{-1}), 0.1 s (k_{obs} = 11.4 ± 0.05 s^{-1}), 1 s (k_{obs} = 11.6 ± 0.05 s^{-1}), 2 s (k_{obs} = 11.9 ± 0.04 s^{-1}), 4 s (k_{obs} = 12.4 ± 0.05 s^{-1}), 10 s (k_{obs} = 13.5 ± 0.06 s^{-1}), and 50 s (k_{obs} = 16.5 ± 0.05 s^{-1}) in accordance with rate of solvent exchange of 0.048 ± 0.001 s^{-1}, a [N(5)-^{2}H]-FMN oxidation rate of 11.4 ± 0.02 s^{-1} and an FMN oxidation rate of 17.0 ± 0.08 s^{-1} (Fig. 3.4). These results indicate a 'intrinsic' primary KIE of 1.50 upon accounting for solvent exchange.

We also used two-dimensional ^{1}H-^{15}N HSQC NMR spectroscopy to test for proton exchange on N(5)-H of reduced NR at pH 7.50, 25^{o}C. In the limit of slow exchange with solvent two HN correlations are expected from reduced ^{15}N-FMN: from N(3)H and N(5)H. However for reduced NR, the HN-HSQC shows only one ^{1}H-^{15}N correlation (Fig. 3.5). This is attributable to N(3)-H based on agreement between the chemical shifts and those consistently observed for N(3)H (128) and demonstrates that our NMR methodology can detect slowly-exchanging N-bound Hs on NR's bound FMN (the H of N(3)H exchanges slowly with solvent consistent with its high pK_a). In contrast, we are unable to observe the correlation peak of N(5)-H, expected near 6.5 ppm (^{1}H) and 60 ppm (^{15}N) (128). Based on the above exchange rate of ≈ 0.048 s^{-1} we would have expected that the slow-exchange condition should apply and we could expect to see a resonance for N(5)H. We speculate that the exchange rate affecting the kinetics reflects the upshot of a series of exchanges that bring a H from solution into the active site via a series of steps or conformational events, whereas in the NMR experiment a single

exchange event that changes the chemical shift of the H on N(5) will suffice to shorten the transverse relaxation time. The signal associated with N(1) is not expected because the reduced state of NR possesses anionic reduced FMN which is not protonated at N(1) (53).

Overall, we are able to account for the contribution of exchange to the small primary KIE on the oxidative-half reaction of NR with *p*-NBA. We find that even the intrinsic primary KIE is modest compared to the values of 3.5 and 3.1 reported by Basran *et al* (129) and Pudney *et al* (130) for morphinone reductase (MR) with NADH and 2-cyclohexenone at 25^{o}C and pentaerythritol tetranitrate reductase (PETNR) with NADPH and 2-cyclohexanon at 25^{o}C, respectively. Thus we surmised that transfer of hydride from the flavin to *p*-NBA is only partially rate-determining.

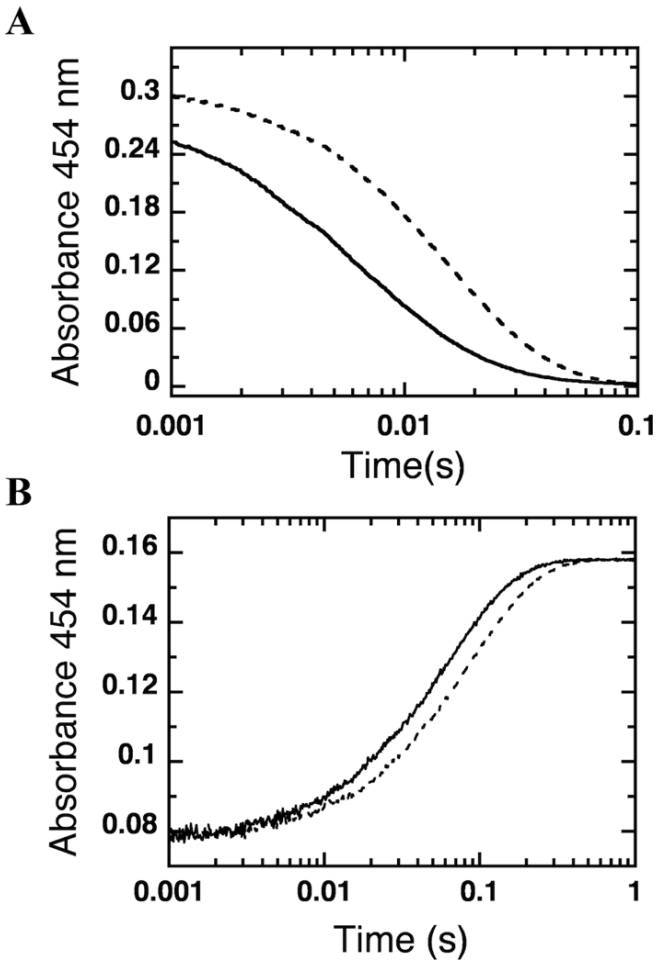

FIGURE 3.3: Primary kinetic isotope effect of NR (A) KIE of reductive half-reaction of NR. Kinetic traces of the reduction of NR (17.5 μM) with 0.1 mM NADH (solid line) or [4R-^{2}H]NADH (dotted line) in 50 mM potassium phosphate pH 7.50 at 4^{o}C. The observed rate constants (k_{obs}) were obtained from the traces of absorbance change at 454 nm to be 238 ± 3 s^{-1} and 75 ± 2 s^{-1}, respectively, showing KIE of 3.2. (B) KIE of oxidative half-reaction of NR. The reaction was performed by double mixing stropped-flow spectrophotometry at 25^{o}C under anaerobic conditions. The first mix added 13 μM NR to 13 μM NADH (solid line) or [4R-^{2}H]NADH (dotted line), the mixing solution then was added to 2 mM *p*-NBA. The age-time between mixes was 1 s to ensure complete formation of reduced flavin and the reactions were monitored at 454 nm for flavin oxidation. The observed oxidation rate constant for reaction using NADH was calculated to be 16.4 ± 0.06 s^{-1} and reaction using [4R-^{2}H]NADH was calculated to be 11.5 ± 0.05 s^{-1}, showing a KIE of 1.4.

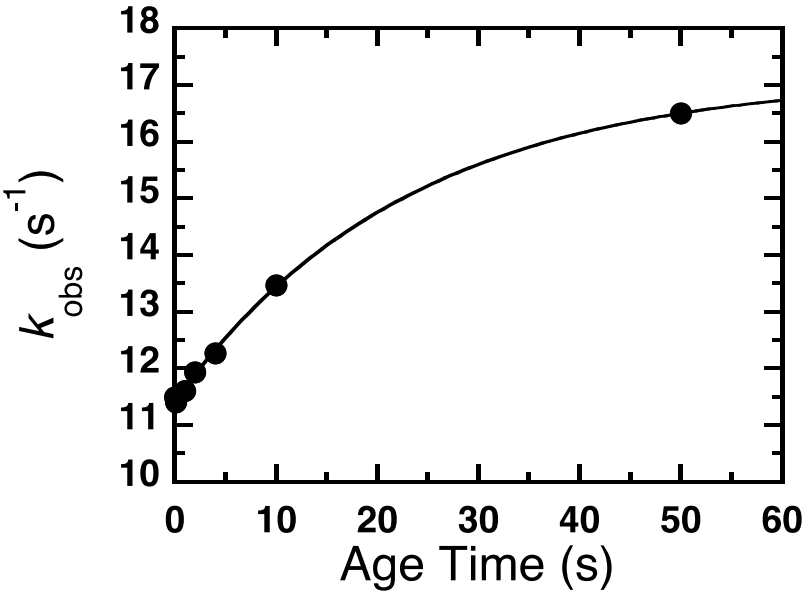

FIGURE 3.4: Observed rate of NR oxidation by 2 mM *p*-NBA as a function of aging time, since mixture of original oxidized NR with [4R-^{2}H]NADH under anaerobic conditions. Upon initial mixture the FMN of NR accepts deutero-hydride from [4R-^{2}H]NADH and becomes reduced. Once reduced the [N(5)-^{2}H]-FMN is subject to H/D exchange with excess H from the H_2O solvent, yielding FMN that is no longer deuterated at N(5). At the end of the age time the partially deuterated reduced NR reacts with *p*-NBA and the rate of flavin reoxidation was measured. The observed oxidation rate was plotted as a function of the age time revealing faster reoxidation of NR in which more of the deuterium had exchanged for proteum. The data were fit with the equation for single exponential decay of the population of [N(5)-^{2}H]-FMN_{red}-NR with an oxidation rate of $k^D_{ox\,(obs)}$ and production of proteated FMN_{red}-NR with an oxidation rate of $k^H_{ox\,(obs)}$, where the rate of H/D exchange is $k_{H/D}$: $k_{ox\,(obs)} = k^D_{ox\,(obs)} + k^H_{ox\,(obs)} * (1 - e^{(-k_{H/D} * t)}$. The best-fit was produced by $k_{H/D}$ = 0.048 ± 0.001 s^{-1}, $k^D_{ox\,(obs)}$ = 11.38 ± 0.02 s^{-1} and $k^H_{ox\,(obs)}$ = 17.02 ± 0.08 s^{-1}.

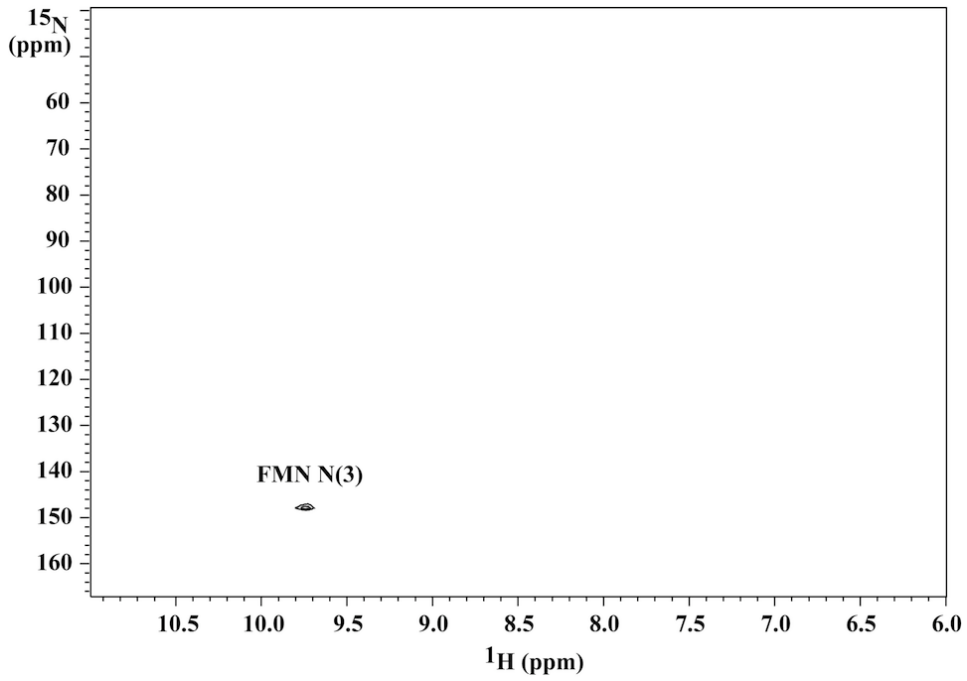

FIGURE 3.5: ^{1}H-^{15}N HSQC NMR spectrum of ^{14}N nitroreductase reconstituted with ^{15}N-labeled FMN from flavodoxin in the fully reduced state at 25°C.

3.4.3 Primary, Solvent, and Double Kinetic Isotope Effects on Steady-State Kinetic Experiments

Since our primary KIE for the oxidative half reaction of NR is small, we also evaluated it via steady-state kinetic measurements, exploiting the fact that the oxidative half reaction is the rate-limiting step in overall turnover (112). The primary KIE values were calculated as the ratio of the rates of catalytic turnover ($k_{cat}^{NADH}/k_{cat}^{NADD}$) and are listed in Table 3.1. The kinetic parameters (k_{cat} and K_m^{pNBA}) of reaction using NADH and *p*-NBA as substrates were determined by varying the concentrations of *p*-NBA (100 – 550 μM) at fixed concentrations of 280 μM NADH or [4R-^{2}H]NADH in 50 mM potassium phosphate buffer pH 7.50, 25ºC. The K_m^{pNBA} values from the plots of initial velocities versus *p*-NBA concentrations (Fig. 3.6A) were calculated to be 0.28 ± 0.04 mM and 0.26 ± 0.03 mM for NADH and [4R-^{2}H]NADH, respectively and the k_{cat} values were 10.7 ± 0.7 s^{-1} and 6.8 ± 0.3 s^{-1}, respectively, yielding a primary KIE ($k_{cat}^{NADH}/k_{cat}^{NADD}$) of 1.6. The primary KIE was found to be 1.5 (Table 3.1) when the experiment was carried out in D_2O buffer pD 7.50 (Fig. 3.6B). These primary KIEs are in agreement with the value obtained for the oxidative half-reaction from pre-steady-state kinetics after accounting for exchange (KIE = 1.5). Moreover, the steady-state-derived k_{cat} of NR is pH-independent in the range of pH 7.0 – 8.25 (Fig. 3.7) indicating that differences in the degree of ionization of deuterated vs. proteated groups is not the basis for the small primary KIE we observe at our working pH (and pD). Thus we confirm a primary KIE of only 1.4-1.6 for the oxidative half reaction.

Steady-state kinetics were also used to investigate the small solvent KIE and thereby re-test for participation of a solvent-derived proton in a rate-contributing step of the reaction in which substrate is reduced (step "b" in Fig. 3.2A). The catalytic turnover number of NR using NADH and *p*-NBA as substrates in H_2O buffer with 9% (w/v) glycerol pH 7.50 ($^{H_2O}k_{cat}^{NADH}$) was 9.1 ± 0.4 s^{-1} which was 1.3-fold higher than the value of $^{D_2O}k_{cat}^{NADH}$ (6.8 ± 0.3 s^{-1}). The lower turnover rate for proteated buffer in this experiment than in the experiment described above reflects the use of 9% (w/v) glycerol to produce the same viscosity as that of ^2H_2O. A somewhat larger solvent KIE was observed when KIE was measured with [4R-^{2}H]NADH (SKIE = 1.4). In both cases the

SKIE was >1, again indicating that a proton from solvent participates in a rate-contributing step during the reduction of *p*-NBA.

The double KIE can be used to arbitrate as to whether the hydride transfer from the N(5) of reduced flavin to *p*-NBA and the proton transfer from solvent (Fig. 3.2A) are concerted (via a single transition state) or occur in different kinetic steps (distinct transition states) (131,132). A double KIE of 2.0 can be calculated by dividing the catalytic turnover rate obtained from the experiment using NAD**H** in $\mathbf{H}_2O$ buffer (with 9% glycerol, pH 7.50) by the catalytic turnover rate of the experiment using [4R-^{2}**H**]NADH in $\mathbf{D}_2O$ buffer (pD 7.50) provided in Table 3.1 $\left({}^{H_2O}k_{cat}^{NADH}/{}^{D_2O}k_{cat}^{NADD} = 2.0\right)$. The obtained value was within error of the product of the primary and solvent KIEs (KIE × SKIE = 2.0) (Table 3.1) suggesting that hydride transfer from N(5) of reduced flavin to the nitro-group of *p*-NBA and proton acquisition by *p*-NBA from solvent are a single concerted reaction.

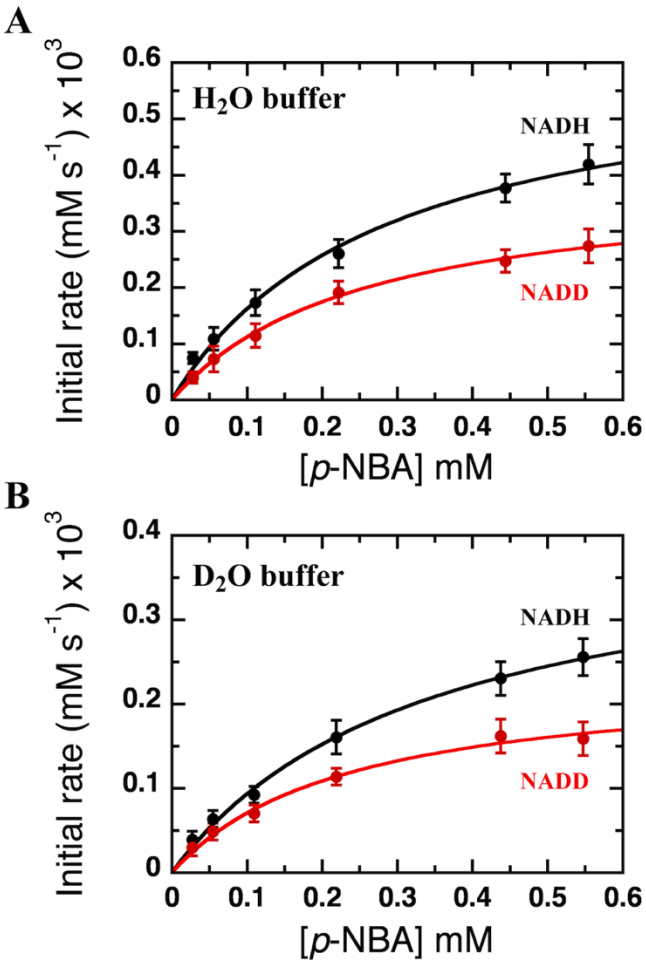

FIGURE 3.6: Steady-state kinetic experiments. Reactions were performed in (A) 50 mM H_2O buffer with 9% (w/v) glycerol pH 7.50 at 25°C and (B) 50 mM D_2O buffer pD 7.50 at 25°C. Plots of initial velocity versus *p*-NBA concentrations (0.028, 0.055, 0.11, 0.22, 0.44, 0.55 mM) at a fixed NADH concentration (280 μM, black circles) or [4R-^{2}H]NADH concentration (280 μM, red circles) showed hyperbolic dependence on *p*-NBA concentrations. The kinetic parameters of reactions carried out in H_2O buffer with 9% (w/v) glycerol were calculated to be K_m^{pNBA} of 0.28 ± 0.04 mM, K_m^{NADH} of 0.28 ± 0.04 mM and K_m^{NADD} of 0.26 ± 0.03 and the k_{cat} values were calculated to be k_{cat}^{NADH} of 9.1 ± 0.4 s^{-1} and k_{cat}^{NADD} of 6.3 ± 0.3 s^{-1}. In D_2O buffer the kinetic parameters were calculated to be $K_{m,}^{pNBA}$ of 0.30 ± 0.05 mM, K_m^{NADH} of 0.33 ± 0.05 mM, and K_m^{NADD} of 0.23 ± 0.05 and the k_{cat} values were calculated to be k_{cat}^{NADH} of 6.8 ± 0.3 s^{-1} and k_{cat}^{NADD} of 4.5 ± 0.2 s^{-1}.

TABLE 3.1: Primary, solvent, and double kinetic isotope effects on NR steady-state kinetics. Assays were performed in proteated (H_2O) with 9% (w/v) glycerol or deuterated (D_2O) 50 mM potassium phosphate buffer pH(D) 7.50 at 25°C using 0.28 mM NADH or NADD and various concentrations of *p*-NBA (0.025, 0.05, 0.1, 0.2, 0.4, and 0.5 mM). The decrease in absorbance at 370 nm ($\varepsilon_{370} = 2.56\ mM^{-1}cm^{-1}$) was observed.

k_{cat} (H_2O buffer), s^{-1}		**k_{cat} (D_2O buffer), s^{-1}**		
NADH (*a*)	NADD (*b*)	NADH (*c*)	NADD (*d*)	
9.1 ± 0.4	6.3 ± 0.3	6.8 ± 0.3	4.5 ± 0.2	
Primary KIE		**Solvent KIE**		**Double KIE**
NADH/NADD (H_2O buffer) (*a/b*)	NADH/NADD (D_2O buffer) (*c/d*)	H_2O/D_2O (NADH) (*a/c*)	H_2O/D_2O (NADD) (*b/d*)	(a/d)
1.5	1.5	1.3	1.4	2.0

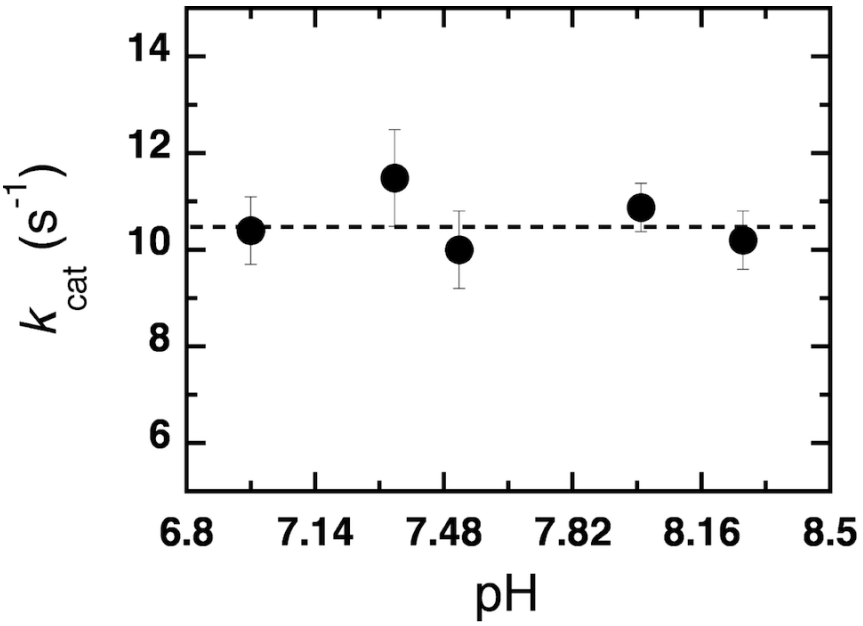

FIGURE 3.7: pH dependence of k_{cat} for NR oxidation by *p*-NBA. Initial rates were determined with 60 nM NR and various *p*-NBA concentrations (0.03, 0.06, 0.11, 0.22, 0.43, 0.52, and 0.61 mM) at a fixed NADH concentration (280 μM), pH 7.0 – 8.2, at 25°C.

3.4.4 Water Accessibility

To learn whether a proton could be acquired from bulk solvent on the time scale of the reaction, vs participation of only protons already present in the active site, single mixing stopped-flow experiments were used. 17.5 μM reduced NR equilibrated in H_2O buffer with 9% (w/v) glycerol was mixed at 25ºC with 2 mM *p*-NBA equilibrated in either H_2O with 9% (w/v) glycerol or D_2O buffer pH(D) 7.50 and kinetic traces were monitored at 454 nm. (The foregoing are final concentrations after mixing.) When reduced NR was mixed with *p*-NBA in H_2O buffer with 9% (w/v) glycerol (k_{obs,H,H_2O} = 11.5 ± 0.1 s^{-1}) the rate of NR oxidation was faster than when reduced NR was mixed with *p*-NBA in D_2O buffer (k_{obs,H,D_2O} = 9.0 ± 0.1 s^{-1}) (Fig. 3.8). The slower oxidation rate in D_2O indicated that transfer of a proton derived from the buffer with which NR was mixed contributes to the rate of the oxidative reaction. Thus the proton transferred to nascent product need not be already present in the active site prior to mixing.

The same conclusion was supported by mixing reduced NR (in D_2O buffer) with 2 mM *p*-NBA equilibrated in either H_2O with 9% (w/v) glycerol or D_2O buffer pH(D) 7.50 at 25 ºC. The oxidative reaction rate was again faster when the enzyme was mixed with *p*-NBA in H_2O (with 9% (w/v) glycerol) than with *p*-NBA in D_2O buffer (k_{obs,D,H_2O} = 7.2 ± 0.1 s^{-1} and k_{obs,D,D_2O} = 6.1 ± 0.1 s^{-1}, data not shown). While we cannot calculate KIEs from the experiments that produced mixtures of H_2O and D_2O, it is nonetheless clear that the isotopic content of bulk solvent affected the reaction rate regardless of whether NR's flavin was proteated or deuterated at N(5). Since the solvent exchange rate of N(5)H was found to be 100 times slower than the reaction in our double-mixing experiments, the reaction rates observed here represent the other H, the proton.

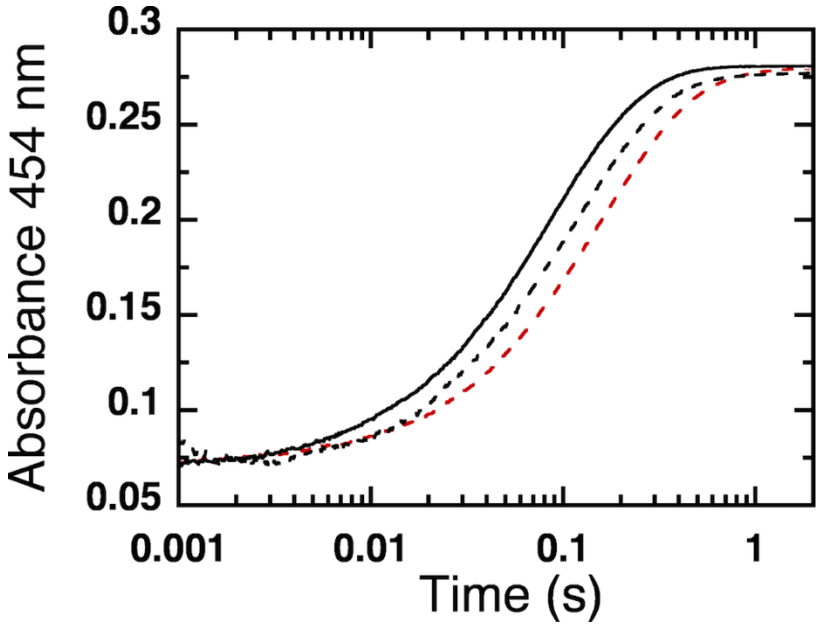

FIGURE 3.8: Water accessibility of the active site of NR. The black solid line represents the kinetic trance obtained from the reaction of reduced NR (13 μM) equilibrated in H_2O buffer with 9% (w/v) glycerol pH 7.50 mixed with *p*-NBA (2 mM) equilibrated in the same buffer with the oxidative rate constant of 11.5 ± 0.1 s^{-1}. The black dotted line represents the reaction of reduced NR equilibrated in H_2O buffer with 9% (w/v) glycerol pH 7.50 mixed with *p*-NBA (2 mM) equilibrated in D_2O buffer pD 7.50 with the oxidative rate constant of 9.0 ± 0.1 s^{-1}. The red dotted line showed the kinetic trance of 13 μM reduced NR (in D_2O buffer pD 7.50) mixed with 2 mM *p*-NBA (in D_2O buffer pD 7.50) with the oxidative rate constant of 6.1 ± 0.1 s^{-1}. The reactions were monitored on the stopped-flow spectrophotometer at 454 nm, 25°C.

3.5 DISCUSSION

This work has provided the first evidence of the source of electrons and protons transferred as part of the catalytic mechanism of NR. In this study, we used both pre-steady state and steady state kinetics to monitor the flavin oxidation state during catalytic turnover. Pre-steady state kinetic methods were used to measured the primary KIE on the reductive rate constants for NADH and [4R-^{2}H]NADH. The large KIE of 3.2 on the observed reductive rate constant at 4^{o}C suggests that the two electrons are transferred from C(4) of NADH to the N(5)-FMN$_{ox}$ as a hydride ion and this step is a rate-limiting step for flavin reduction.

Hydride transfer from NAD(P)H to flavin is a common reaction among flavoenzymes and examples include a novel flavin reductase from *Photobacterium leiognathi* (Lux G) for which the primary KIE is above 3.9 at 4^{o}C (117), morphinone reductase (MR) with the primary KIEs of 4.4 at 25^{o}C (129,133), NADPH-Cytochrome P450 with a primary KIE of 2.7 at 28^{o}C (134), and plant-type ferredoxin-NADP^{+} reductase from *Pisum sativum* with the primary KIE of 4.1 (135). The primary KIE of NR thus falls in the range expected based on other characterized, enzymes confirming the hydride transfer mechanism in the reductive half-reaction of NR. Moreover, X-ray crystal structures showed that upon binding the NADH analog NAAD, the nicotinamide ring forms a stacking interaction with the isoalloxazine ring of FMN with a C(4) to N(5) distance of only 3.6 Å (Fig. 3.1B), thus providing a favorable geometry for hydride transfer.

In contrast, a small KIE of 1.4 on the oxidative half-reaction was observed in double mixing stopped-flow experiments at 25^{o}C. The small size may be due in part to H/D exchange at N(5)-FMN$_{red}$ during the age time of the experiment (1 s), and the rate of exchange derived from experiments varying the age time was not consistent with the absence of a resonance from N(5)H in the ^{1}H-^{15}N-HSQC spectrum. Therefore, since previous studies had shown that the oxidative half-reaction (nitroaromatic reduction) was the rate-limiting step during catalytic turnover of NR (112), the steady-state kinetics were used to obtain a second measure of the KIE.

In steady-state kinetic experiments, primary KIEs of 1.5 – 1.6 were observed from the reactions carried out in both H_2O and D_2O buffer, in good agreement with the results

obtained from pre-steady state kinetics (KIE = 1.4). The small primary KIEs were not due to the pH effect because the k_{cat} values were the same between pH 7.0 and 8.25 (Fig. 3.7) indicating pH independence. Therefore the presence of a primary KIE effect on k_{cat} suggests that hydride transfers from N(5)-FMN_{red} to the *p*-NBA and the small size of the effect argues that other factors also contribute to the rate.

Lower magnitudes for primary KIE are observed if the motion along the reaction coordinate of hydrogen / deuterium transfer proceeds through an activation complex with bending motions rather than stretching motion, and therefore the change in ZPEs (zero point energy) between reactant and transition state are small (136,137). The nitro group of *p*-NBA points away from the N(5)-FMN in our crystal structure, due to the preferential interaction of carboxylate group of *p*-NBA with the backbone amide group of Thr41, as also observed in the structures of the complexes of oxidized NR with acetate or benzoate (52). However this structure represents oxidized NR, not the catalytically competent reduced state. In the reduced state, changes in the electron distribution and geometry of reduced FMN in conjunction with active site flexibility could change the binding mode of the substrate, *p*-NBA. Many binding orientations possibly occur, with one binding mode placing the nitro group close to N(5)-FMN, and that one mode leading to the proposed hydride transfer. However the nitro group may not be perfectly positioned relative to the N(5)-FMN, necessitating a bending motion along the reaction coordinate for hydride transfer and leading to the small primary KIE. Multiple binding orientations have been observed in the *E. coli* nitroreductases's active site based on the crystal structures of oxidized *E. coli* NfsB bound with CB1954 in which the 2-nitro group closest to N(5)-FMN was 4.2 Å from N(5)-FMN whereas the 4-nitro group closest to N(5)-FMN in another active site was 3.9 Å from N(5) (99). Another example was found in the crystal structure of *E. coli* NfsB bound with a dinitrobenzamide prodrug in which the nitro group faces toward N(5)-FMN in one active site at a distance of 4.1 Å but points away from N(5)-FMN in another active site (99). Another possible explanation for the small KIE is the rapid exchange of H/D at the N(5)-FMN indicated by the NMR data. A small primary KIE of ~1.5 was also observed in the flavin-oxidizing half-reaction of choline oxidase (138).

We were not able to observe the HSQC resonance of N(5)H in reduced NR, although the resonance of N(3)H was strong. We attributed this to more rapid exchange of the N(5)H proton, since correlations are expected only when the H exchange rate is smaller than the $^{1}J_{HN}$ coupling (≈ 88 Hz, (139)). In the case of free reduced FMN, the rate at which solution H exchanges into the N(5)H position is pH dependent, being rapid (100-500 s^{-1}) at both low and high pH where exchange is acid- and base catalyzed, respectively (140). At intermediate pHs exchange rates between 50 s^{-1} and 10 s^{-1} were measured and the ^{15}N resonance displayed clear coupling to ^{1}H (140). This is consistent with our estimates of exchange at a rate of 0.048 s^{-1} (exchange from bulk into the N(5)H position of NR-bound reduced FMN) yet still compatible with a rate > 90 s^{-1} (rate of detachment of H bonded to N(5) of reduced FMN bound to NR). However one normally expects that a flavin bound in a protein active site will be protected from solvent exchange by H-bonds involving the N-bound Hs. Chang and Swenson observed resonances from each of N(3)H and N(5)H for fully reduced flavodoxin from *Clostridium beijerinckii* (Chang & Swenson 1999). They found that flavodoxin variants with weaker H-bonding between the protein and N(5)H lacked the N(5)H resonance from HSQCs collected at higher temperatures, consistent with accelerated decay of the magnetic resonance correlation, due to solvent exchange for these NH groups. In the WT enzyme active site, which is known to accept an H-bond from N(5)H, the corresponding NH correlation was observed at all temperatures tried. In the case of NR, N(5)H does not appear to have good H-bonding partners as the nearest candidate is a crystallographic water 3.0Å from N(5) and 72° from the N(10)-N(5) vector (Fig. 3.9). The stretch of backbone that donates an H-bond to N(5) in oxidized NR is not observed to reorient upon reduction of the enzyme, so unlike flavodoxin wherein a carbonyl O is to proffered to the N(5)H, the N(5)H of reduced NR instead appears to encounter steric conflict producing an increase in butterfly bend and directing N(5)H to interact with a water molecule. Thus we can expect considerable accessibility to water, and efficient H exchange, consistent with the absence of an N(5)H correlation from NR's HSQC.

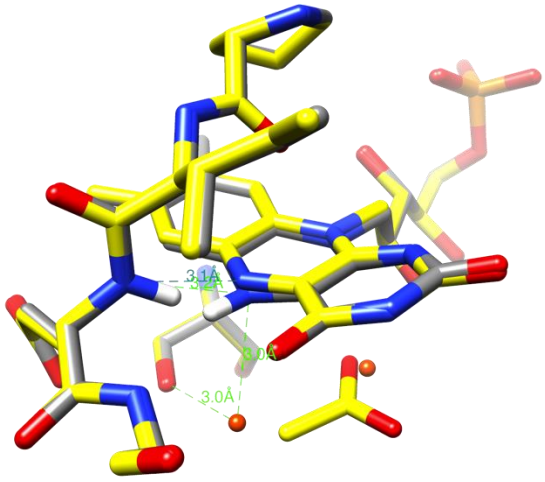

FIGURE 3.9: Overlay of oxidized (yellow) and reduced (grey) active sites of NR showing H-bonding partners within 5 Å of N(5). H atoms were added to amide N of Glu165 within Chimera. The N(5)H of the reduced state is also shown, based on the structure calculated by Spartan for the hydroquinone anion of lumiflavin, which has the same flavin ring as FMN but has a methyl group instead of the ribityl phosphate. The calculation employed the B3LYP functional and the 6-311G* basis set, while other H atoms are present in lumiflavin hydroquinone anion, only the N(5)H is shown, for simplicity. PDB coordinates are 1KQD (reduced) and 1KQC (oxidized with acetate in the active site). Water molecules specific to the reduced state are colored orange.

Solvent isotope effect studies were undertaken in order to probe for another source of a proton required for nitroaromatic reduction. When enzymatic reactions were carried out in D_2O, values of $^{D_2O}k_{cat}^{NADH}$ were smaller than the corresponding rates for reactions done in H_2O ($^{H_2O}k_{cat}^{NADH}$) with SKIE of 1.3 and 1.4 when using [4R-^{2}H]NADH in place of NADH, indicating that a proton is derived from the solution. Moreover, a multiple deuterium KIE was observed (Table 3.1) with the value equal to the product of substrate and solvent confirming the solvent effect. The multiple deuterium KIE method was also used to distinguish between concerted and stepwise mechanisms of hydride transfer and proton transfer. Within the same family of enzymes, or even for a given enzyme but comparing different substrates, the mechanism of substrate reduction might be different as witnessed by the examples of pentaerythritol tetranitrate reductase (PETN)

which executes 2-cyclohexanone reduction via a concerted reaction without transition state stabilization (129) whereas old yellow enzyme undergoes stepwise reaction with nitrocyclohexene in which hydride transfer occurs before proton transfer and a nitronate intermediate can be detected during the catalytic reaction (141). If the reaction was concerted and involved a single transition state, hydride transfer from N(5)-FMN_{red} and proton transfer from solution would be independent of one another or possibly enhanced by the presence of the second isotope. The value of our double KIE ($^{H_2O}k_{cat}^{NADH}/\ ^{D_2O}k_{cat}^{NADD}$) of 2 is equal to the product of our primary KIE and our SKIE (KIE × SKIE = 2) indicating that the transfer of hydride from the flavin (step "a" in Fig 3.2A) and a proton from solution (step "b" in Fig 3.2A) to the nitroaromatic substrate occur in the same kinetic step, in a synchronous fashion, and the proton responsible for the SKIE was not pre-localized in the enzyme active site, but could be acquired from bulk solvent, as confirmed by the water accessibility experiment.

Our studies have shown that like many other flavoenzymes, hydride transfer is the predominant pathway for flavin reduction in NR. The short distance between donor (NADH) and acceptor (flavin) in combination with the large observed KIE strongly support this mechanism. In contrast, the larger distances between N(5)-FMN and the nitro groups of nitroaromatics in available crystal structures seem to be too far for hydride transfer during the oxidative half reaction. Nonetheless, deuterium KIEs provide good evidence supporting the occurrence of hydride transfer from reduced flavin coupled to proton transfer from solution to yield the net 2-electron and 2-proton reaction, without any intermediates.

It is important to note that NR has a broad substrate repertoire including substrates ranging from small such as our substrate (*p*-NBA) and nitrofurazone, to the larger and bulkier substrates such as CB1954 and dinitrobenzamide. Thus active site flexibility and substrate dynamics within the active site may also play important roles in substrate binding and orientation. The small substrate used in the current studies may have many binding modes, and one of them might orient the nitro group close to the N(5)-FMN in a pose which is suitable for hydride transfer. In contrast, the larger and bulkier substrates have less binding possibilities and substrate reduction may occur via electron-coupled proton transfer in these cases.

In the current case, our kinetic data enable us to conclude that the substrate orientation that undergoes reduction must have its nitro group close to the flavin N(5). This would be readily accomplished if the substrate were rotated 180° from the orientation shown, so as to place the nitro group in the position shown for the carboxyl (and vice versa). The result would be a distance of 4.2 Å from nitro N to N(5) instead of 5.6 Å in the structure as solved (Fig. 3.10). The rotation we propose here is consistent with the fact that more negative charge will be concentrated in the region of N(1) to O(2) upon flavin reduction and this will tend to repel the carboxyl group that sits nearby in the crystal structure as solved, for the oxidized state of NR. Thus we propose that the necessary use of oxidized enzyme to form a model of the enzyme-substrate complex has resulted in a long nitro to N(5) distance but that the catalytically active complex brings these two much closer together consistent with demonstrated hydride transfer.

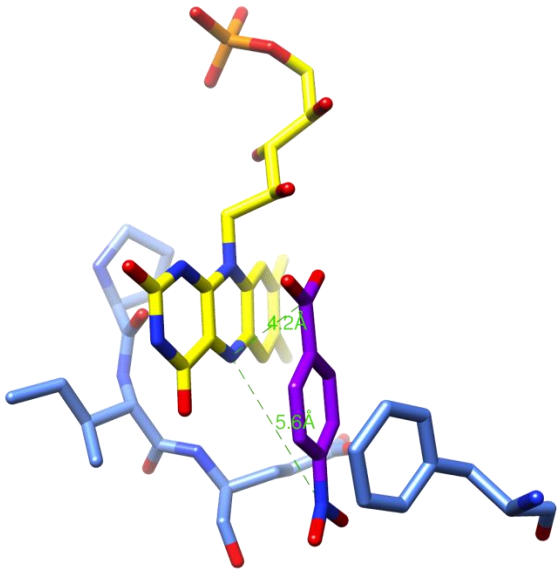

FIGURE 3.10: Active site of oxidized NR with bound *p*-NBA showing distances from the carboxyl to N(5)-FMN and the nitro group to N(5)-FMN, with the substrate oriented as per the crystal structure solved by Haynes and Rodgers (unpublished). Note that this orientation of substrate places the carboxyl group close to N(1) and O(2), whereas upon reduction of the flavin, negative charge in this region is likely to disfavour placement of the carboxyl so nearby, and favor instead the nitro group in this position. Distances were measured in Chimera.

CHAPTER 4

AN APPROACH FOR FLEXIBILITY AND DIMERIZATION STATE OF NITROREDUCTASE

4.1 ABSTRACT

To address the potential that NR's conformation is flexible, the temperature dependence of NR was investigated using 2D ^{1}H-^{15}N HSQC NMR from 4°C to 37°C. The results showed a well-resolved 2D ^{1}H-^{15}N HSQC NMR spectrum at the higher temperatures (32°C), but revealed a much less intense spectrum characterized by broader lines at 4°C, suggesting intermediate exchange. Both 2D ^{1}H-^{15}N HSQC and proton 1D NMR spectra suggest that NR undergoes more conformational averaging at 4°C. Interestingly, binding of the substrate analog dicoumarol produces qualitatively similar results: at intermediate temperatures the ^{1}H-^{15}N-HSQC resonances are broadened and less dispersed, indicating that NR is more dynamic when dicoumarol is bound.

Relaxation dispersion measurements were performed to learn whether the rate constants associated with NR's dynamics correspond to those of processes that contribute to turnover.

To test for possible linkage between increased dynamics and substrate analog binding, the temperature dependence of binding of dicoumarol was characterized over the temperature range of 4°C–37°C. Consistent with increased conformational averaging upon dicoumarol binding, the low temperature (= dynamic) form of NR displayed a higher affinity for dicoumarol with a K_d value (4°C) of 22 ± 4 μM compared with the K_d value of 62 ± 3 μM for the highest temperature (37°C). Thus for one substrate analog at least, binding is coupled to increased dynamics.

4.2 INTRODUCTION

Each enzyme must strike a compromise between two opposing requirements, for activity and stability. The active site of an enzyme has to have a certain flexibility to accommodate the incoming substrate and to release the products for high catalytic activity, while the stability is needed to apply strain to the substrate and favour its formation of a transition state (142-144). Chapter 2 and Pitsawong *et al* (112) already discussed insights into NR's promiscuity provided by transient kinetics, which provide details of the mechanism of enzymatic activity. In this section, we step back to ask whether NR may also accommodate diverse substrates via conformational flexibility.

NR binds substrates and analogs stacked against the *re* face of the flavin, in the interface between monomers of the NR dimer. Thus, movement of one monomer relative to the other can accommodate substrate binding without requiring any changes to the monomer's core or crucial structural units. Thus, conformational adaptations can make maximal use of the flexibility of loops and NR's quaternary structure, and need not be associated with large energy costs or destabilization of the fold. In this connection it is noteworthy that NR has a unique quaternary structure characterized by a 'domain-swapped dimer' motif wherein the termini of each monomer interact closely with the body of the other monomer. Indeed, the C-terminal 4 amino acids (Val214 – Cys217) contribute to a β sheet of the other monomer. These interactions far from the active sites act to hold the dimer together while allowing that the actives sites can flex and breathe.

Proteins undergo conformational fluctuations on a wide range of time scales ranging from ps to days and longer (145-150). X-ray crystallographic analysis has provided highly valuable insights into the structural properties of NR and related enzymes (33-36,52,65,67). A superposition of the structures solved with a range of different substrates reveals that certain regions of the protein can adopt difference conformations (53,65,99). Moreover, we also learn that B-factors (thermal factor) increase for certain regions, upon binding of substrate analog (Fig. 1.9E in Chapter 1). Thus they show that the protein is flexible, and indicate that certain regions in particular can be positioned differently relative to the rest of the molecule in response to substrate binding. However since all the structures deposited appear to have been determined on crystals that were preformed and then allowed to bind ligands, the pre-existing crystal

packing forces may limit the extent to which the protein is free to adapt to the ligand. Moreover the crystal structures provide only snapshots. We know they are not complete because even for a single substrate, multiple binding modes, with distinct protein adaptations, have been reported (99). Therefore we take the crystallographic findings as evidence that is it worth looking into protein dynamics directly. For this we have chosen NMR spectroscopy, since it allows for the investigation of protein structure and dynamics under close-to-natural conditions. It also provides techniques for determining the time scale of motions as well as the amino acids affected (145,150). At this point we have devoted our effort to identifying the best protein constructs for more detailed study, but are pleased to present the results of these initial surveys, which will be followed by the more time-consuming relaxation and exchange rate measurements that can give more detailed and quantitative descriptions (148).

The flexibility of NR has been surveyed initially by taking advantage of its temperature dependence. Depending on whether data are collected at a lower (4^{o}C) or higher temperature (32^{o}C), NR displays different 2D ^{1}H-^{15}N HSQC NMR spectra (Fig. 4.7). The diminution of dispersion and enlargement of line widths observed at lower temperature suggest greater dynamics and the contrast between these two temperatures are modulated by modifications to the protein's N- and C-termini. Another insight is provided by the diminished signal to noise obtained at 4°C. This suggests shorter T_2 relaxation at the lower temperature, which in turn is compatible with internal motions on relatively long molecular time scales.

To address another possible interpretation of the altered NMR spectrum at lower temperature, the oligomerization state of NR was determined over the full range of temperatures used. Thus we are able to rule out formation of higher-order aggregates as a cause of broadened lines, as well as dimer dissociation as a plausible cause for the poor dispersion of the 2D ^{1}H-^{15}N HSQC NMR spectrum at lower temperature.

We have also tested the prediction that if dynamics is needed for substrate (or analog) binding, then binding of an analog should increase dynamics. In order to study binding of substrates without the complications of reaction, we have used the oxidized state of NR in conjunction with oxidizing substrates, taking advantage of the crystallographic finding that the structure of NR is only very slightly affected by

oxidation state (52). Alternately we have exploited substrate analogs that are known inhibitors, choosing competitive inhibitors when possible. Since tight-binding inhibitors are more convenient for NMR study than weak binding inhibitors, we chose dicoumarol, for which previous work reported a dissociation constant of 62 nM (31) and there is also a crystal structure of this complex with *E. coli* NfsB (99).

The relationship between protein dynamics and their catalytic function has emerged as a topic of great scientific interest, which have been proposed to be important for various functions such as substrate binding, product release, and chemical transformation. For example, *E. coli*'s dihydroforate reductase (DHFR) undergoes large conformational changes during enzyme turnover (151) and the structural dynamics play a direct role in catalysis. NMR spin relaxation techniques including the Carr-Purcell-Meiboom-Gill (CPMG)-based R_2 relaxation dispersion experiment (147) can be used to monitor structural changes occurring in the μs to ms regime, corresponding to frequencies consistent with the catalytic turnover rate. The pre-steady-state kinetics of DHFR indicate that product release is rate-limiting and occurs at a rate of 12.5 s^{-1} at 298 K. This is similar to the conformational exchange rate constant of 12-18 s^{-1} determined by R_2 relaxation dispersion at 300 K (152). This correlation suggests that the protein motions necessary for catalysis are intrinsic properties of the enzyme and may even limit the overall turnover rate. Motion is not restricted to the active site but also affects a wider dynamic protein network.

A correlation between the overall turnover rate and protein dynamics has also been reported in cyclophilin, wherein NMR studies showed that conformational changes of the enzyme coincide with substrate turnover (153). Thus NMR insights into the nature and rates of interconversion of intermediates, along with structural information, can be used as bases for understanding the incredible catalytic efficiency of enzymes.

4.3 EXPERIMENTAL PROCEDURES

This section describes efficient methods for the production of uniformly ^{15}N-labeled proteins for our 1D proton and 2D ^{1}H-^{15}N HSQC NMR studies, and methods used to assess the integrity and suitability of proteins for further structural studies. 1D

proton NMR spectra suffer from far too much overlap to permit detailed interpretation, consistent with the fact that NR has more than 1500 distinct protons per monomer. 2D ^{1}H-^{15}N HSQC spectra of ^{15}N labeled proteins are more useful for initial characterization of proteins because each non-proline amino acid can be directly detected via its backbone amide NH peak, so the spectrum includes signals from almost every amino acid, and because the 2D format in combination with signals from only the NH groups results in fewer signals that are more spread out so that most are individually resolved under optimal conditions (Fig. 4.7).[2] Due to the small magnetic moments of ^{13}C and ^{15}N compared to ^{1}H (1/4 and 1/10 th that of ^{1}H, respectively), protein biochemists employ pulse sequences that detect these nuclei indirectly, via ^{1}H, combining their chemical shifts on one axis with those of the attached ^{1}H on a second to achieve dispersion in two dimensions. Although the abundant isotope of N is NMR active, ^{14}N has complicated spectroscopy due to its nuclear quadrupole and general practice is to produce proteins enriched to ≈ 100 % with ^{15}N, which has a nuclear spin of 1/2 and therefore has much simpler NMR properties (the natural abundance of ^{15}N is 0.37%). The abundant C isotope, ^{12}C is an S=0 nucleus that is not amenable to NMR and the NMR active S=1/2 isotope ^{13}C is only 1.1% abundant so enrichment is necessary to obtain strong NMR ^{13}C NMR spectra in reasonable amounts of time at the low concentrations achievable for proteins. ^{15}N enriched proteins can be produced in good yield by overexpression in bacteria growing on $^{15}NH_4Cl$ as the sole source of ^{15}N.

4.3.1 Expression of ^{15}N Uniformly-labeled NR

E. coli BL21(DE3) cells harboring the plasmid pRK1 containing the NR gene were used to inoculate 50 mL of LB medium containing 50 μg / mL kanamycin and cells were grown at 37°C overnight at 220 rpm, then 5 mL were added into 2 L of MM9 medium (Table 4.1, (154)). The cells were grown at 37°C until their OD_{600} reached ~0.8, before protein expression was induced by addition of IPTG to a final concentration of 1 mM. The culture was incubated for a further 3 h at 37°C and then the cells were

[2] HN occur as backbone amides once per amino acid for most amino acids although Trp, Gln, Asn, His and Arg have HN units in their side chains that are also visible, most of these occur in distinct spectral and do not overlap with the backbone amide signals.

harvested by centrifugation at 9,000 rpm and 4°C for 10 min and stored at -20°C after washing once with lysis buffer. All mutant enzymes were expressed in the same way.

4.3.2 Expression of ^{15}N Glycine-labeled NR

E. coli BL21(DE3) cells harboring the plasmid pRK1 containing the NR gene were used to inoculate 50 mL of LB medium containing 50 μg / mL kanamycin and cells were grown at 37°C overnight at 220 rpm, then 5 mL were added into 2 L unlabeled LB medium and cells were grown at 37°C until their OD_{600} reached ~0.5. The cells were corrected by centrifugation and were then wash and resuspended in ^{15}N Glycine medium (Table 4.2, (155)). The new culture was incubated at 37°C until it OD_{600} reached ~0.8 followed by addition of IPTG to the final concentration of 1 mM. The culture was incubated for a further 3 h at 37°C and then the cells were harvested by centrifugation at 9,000 rpm and 4°C for 10 min and stored at -20 °C after washing once with lysis buffer.

TABLE 4.1: High yield MM9 medium recipe for ^{15}N Uniformly-labeled NR

1. MM9 medium	per 1 L
KH_2PO_4	6 g/L
Na_2HPO_4	12 g/L
NaCl	0.5 g/L
$^{15}NH_4Cl$	1 g/L
2. 10 mL/L micronutrient solution (sterilized by Millipore syringe filter)[a]	per 100 mL
$FeSO_4$ ($7H_2O$)	0.60 g
$MnCl_2$ ($4H_2O$)	0.12 g
$CaCl_2$ ($2H_2O$)	0.60 g
$CoCl_2$ ($6H_2O$)	0.08 g
$ZnSO_4$ ($7H_2O$)	0.07 g
$CuCl_2$ ($2H_2O$)	0.03 g
H_3BO_3	2 mg
$(NH_4)_6Mo_7O_{24}$ ($4H_2O$)	0.025 g
EDTA	0.5 g
3. 10 mL/L of 1M MgCl2 (sterilized by Millipore syringe filter)	
4. 6 mL/L of 5 mg/mL Thiamine hydrochloride (sterilized by Millipore syringe filter)	
5. 0.5 mL/L of 100 mg/mL Kanamycin (sterilized by Millipore syringe filter)	
6. 10 mL/L of 100% D-glucose (autoclaved)	

[a]Recipe modification from Cia *et al* (1998) (154)

TABLE 4.2: Medium recipe for ^{15}N Glycine-labeled NR

1. Group 1 (adjusted to pH 7.50, autoclaved)	per 1 L
Sodium acetate	1.5 g
Succinic acid	1.5 g
NH_4Cl	0.75 g
NaCl	0.85 g
K_2HPO_4	10.5 g
2. Group 2 (added to media prior to autoclaving)	per 1 L
Adenine	0.5 g
Guanosine	0.65 g
Thymine	0.2 g
Uracil	0.5 g
Cytocine	0.2 g
3. Group 3 (amino acid, add to media prior to autoclaving)	per 1 L
L-Ala	0.5 g
L-Arg	0.4 g
L-Asp	0.4 g
L-Asn	0.05 g
L-Cys	0.05 g
L-Gln	0.4 g
L-Glu	0.65 g
L-His	0.1 g

L-Ile	0.23 g
L-Leu	0.23 g
L-Lys (hydrochloride)	0.42 g
L-Met	0.25 g
L-Pro	0.1 g
L-Ser[a]	2.1 g
L-Thr	0.23 g
L-Val	0.23 g
L-^{15}N Glycine	0.55 g
4. Group 4 (adjusted to pH ~2.0, autoclaved separately and added to media prior to inoculation	per 1 L
L-Trp	0.05 g
L-Phe	0.13 g
L-Tyr	0.17 g

5. Group 5 (added to media prior to inoculation)

10 mL/L of 100% D-glucose (autoclaved)

1 mL/L of 10 mM $FeCl_2$ (sterilized by Millipore syringe filter)

4 mL/L of 1 M $MgSO_4$ (autoclaved)

0.1 mL/L of 1 M $CaCl_2$ (sterilized by Millipore syringe filter)

0.5 mL/L of 100 mg/mL Kanamycin (sterilized by Millipore syringe filter)

10 mL/L of micronutrient solution (sterilized by Millipore syringe filter)[b]

[a]For ^{15}N-Glycine labeled NR: 2.1 g of L-Ser was used instead of 0.5 g to suppress metabolic migration of the ^{15}N-label into serine residues.
[b]Recipe is the same as described in Table 4.1.

4.3.3 Determination of the dissociation constant (K_d) for binding of dicoumarol to NR at various temperatures

Binding of dicoumarol to wild-type NR was monitored via changes produced to the optical signal of NR's flavin, using a Hewlett-Packard HP8452A diode array spectrophotometer with the temperature maintained at 4, 10, 15, 20, 25, 32, and 37°C by means of thermospacers and a circulating water bath. Various concentrations of dicoumarol (substrate analog), 4.4, 8.8, 13.2, 17.5, 21.7, 26.0, 30.2, 34.3, 38.5, 42.6, 46.6, 50.6, 54.6, 58.6, 62.5, 66.4, 70.2, 74.1, 77.9, and 81.6 µM, were produced by titration into a solution of 35 µM wild-type enzyme in 50 mM KH_2PO_4, 50 mM KCl, pH 7.50 in a quartz cuvette with a 1 cm path length. At each temperature, enzyme solutions were thermoequilibrated for at least 30 min before titrating with small increments of dicoumarol (10 mM stock solution) and equilibrated at least 5 min after each addition. The absorption spectrum for each titration was recorded from 300 nm to 800 nm. The plot of the maximum absorbance change at 530 nm versus dicoumarol concentrations was fitted to Eq. 4.1 to obtain K_d.

$$\frac{\Delta A}{\Delta A_{max}} = \frac{L_0 + nP_0 + K_d - \sqrt{(L_0 + nP_0 + K_d)^2 - 4nP_0L_0}}{2P_0} \qquad (4.1)$$

ΔA: the absorbance change observed at each concentration of ligand at 530 nm

ΔA_{max}: the maximum change at the saturating concentration of ligand at 530 nm

P_0 and L_0: the total concentration of enzyme and ligand, respectively

K_d: the dissociation constant of enzyme-ligand complex

4.3.4 Nuclear Magnetic Resonance Spectroscopy (NMR)

All NMR samples contained 1 mM wild-type or mutant NR (^{15}N Uniformly-labeled NR) in 50 mM KH_2PO_4, 50 mM KCl, 1 mM DTT, 0.2 mM EDTA at pH 7.50. All samples were augmented with 10% (v/v) ^2H_2O for locking and tracking the magnetic field, and 0.02% sodium azide (NaN_3) to protect against bacterial degradation. Wilmad NMR tubes, 5 mm diameter precision, were used to contain 600 µL of sample. The samples were degassed by blowing high purity argon or nitrogen gas into them for 10

minutes to remove oxygen (the paramagnetic properties of which can broaden NMR lines). Both one-dimensional (1D) and proton-nitrogen (^{1}H-^{15}N) correlated 2D HSQC NMR spectra (HSQC = heteronuclear single quantum coherence) were acquired on a Varian INOVA 600 MHz NMR spectrometer using a ^{1}H (^{13}C/^{15}N) 5 mM PFG Triple Resonance probe with Z gradients, operating at an observed temperature ranging from 4^{o}C to 37^{o}C. The sample was equilibrated at each temperature for at least 30 min and probe was re-tuned by minimizing reflected power (channel 1 and 3 for ^{1}H and ^{15}N, respectively) on the sensitivity scale 9 upon adjustment of the probe tune and match circuitry (reflected power levels of 000 or 001 were typical). The ^{1}H 90° pulse width was then determined and used for the spectra collected at that temperature. However these optimizations were repeated each time a sample was brought to a new temperature.

4.3.4.1 Proton One-dimensional (1D) NMR measurements

The Wet1D sequence was used to suppress the large water signal by creating a shaped pulse that excites only the solvent resonance followed by the use of gradients to suppress the excited resonance. Following the wet pre-sequence a 90^{o} pulse was used to excite protein resonances which were recorded over a 1s acquisition time using a 1s relaxation delay time between scans. The pandora's box (Pbox) component of the Agilent NMR software was used to create eburp1 waveforms producing on-resonance excitation over a bandwidth of 300 Hz. The spectral width was 10000 Hz and the number of scans (nt) was 128. Data were zero filled, weighted with a Gaussian or squared sine bell function, and Fourier transformed. Details and any deviations from the foregoing are described in the figure legends.

4.3.4.2 Proton-Nitrogen (^{1}H-^{15}N) Heteronuclear Single-Quantum Correlated 2D NMR Spectra

Heteronuclear **S**ingle-**Q**uantum **C**oherence (HSQC) spectra for wild-type and mutant NR were collected at various temperatures and referenced relative to the chemical shift of water at the temperature used for ^{1}H (4.9735 ppm (4^{o}C), 4.9162 ppm (10^{o}C), 4.8684 ppm (15^{o}C), 4.8207 ppm (20^{o}C), 4.7729 ppm (25^{o}C), 4.7061 ppm (32^{o}C), and 4.6583 ppm (37^{o}C)) (156) and external ^{15}N urea in DMSO (77 ppm) for ^{15}N. The ^{1}H-^{15}N HSQC experiments incorporated pulse field gradients and coherence pathway selection to effect suppression of the water resonance. The spectral widths of 10000 and 2400 Hz

were used for ^{1}H and ^{15}N dimensions, respectively. A total of 852 t_2 data points and 128 t_1 increments were collected and all spectra were recorded with 800 transients (this was necessary only for the lower-temperature spectra, but retained for consistency when collecting spectra at higher temperatures. Directly detected data were weighted with a shifted sine bell and zero-filled to 1k prior to Fourier transformation. Indirect dimension data were doubled by linear prediction then weighted with a shifted sine-bell and zero filled to 1K before Fourier transformation. The recycle delay between scans was set to 1 second.

4.3.4.3 Relaxation Dispersion Experiments

The principal of CPMG is to refocus the exchange broadening due to dynamic process such as protein conformational change ($A \leftrightarrow B$), protein ligand binding ($P + L \leftrightarrow PL$), monomer-dimer and protonated-deprotonated conversion, using a series of spin-echoes $[\tau - 180^{\circ}_{x} - \tau\,]$ applied to transverse magnetization during the relaxation delay (Fig. 4.1). The frequency of application of 180°_{x} pulses in the CPMG sequence, $1/(\tau_{cp})$ where $\tau_{cp} = 2\tau$, is called the CPMG frequency, ν_{CPMG} (Eq. 4.2). Where τ_{cp} is the interval between 180° pulses and 180 is the 180° radiofrequency (RF) pulse applied along the ±x or ±y axis. In general, a spin echo can refocus the spin magnetization vectors if each individual vector has the same average chemical shift during successive time intervals, τ, between 180° pulses. Exchange of conformations or protein dynamic leads to a difference in the magnetic environment of the spin. Therefore, each magnetization component acquires a different phase before and after τ leading to signal broadening and the resonance intensity decreases relative to the case of no exchange.

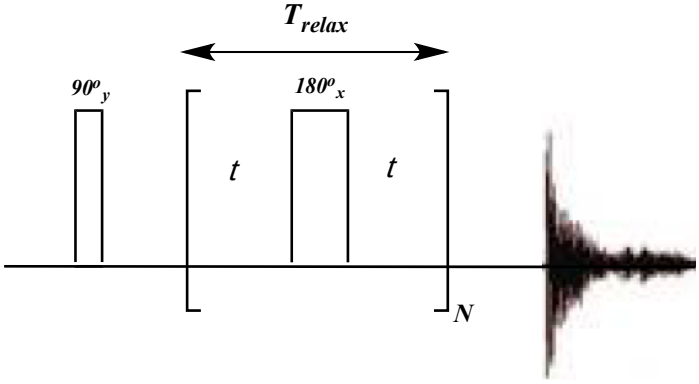

FIGURE 4.1: Spin echo pulse sequence

Relaxation dispersion studies exploit the dependence of the rate of magnetization decay ($R_{2,eff}$) during the CPMG sequence on the frequency (ν_{CPMG}) at which 180° pulses are applied during a constant time relaxation delay (T_{relax}). N 180° pulses are applied in $[\tau - 180^{\circ}_{x} - \tau\,]$ blocks such that $2\times N\times\tau_{cp} = T_{relax}$. $R_{2,eff}$ are quantified from the peak intensity, $I_{\nu_{CPMG}}$, of NMR spectra recorded with different numbers of repeats of $[\tau - 180^{\circ}_{x} - \tau\,]$ of CPMG blocks as shown in Eq. 4.3, where I_0 is the reference signal intensity recorded without a relaxation delay (T_{relax}) and T_{relax} is the constant time CPMG relaxation period. The exchange parameters can be obtained from the relaxation dispersion profiles based on a model for two-site exchange ($R_{2,eff}$ as a function of ν_{CPMG}). In the limit of fast exchange ($k_{ex} \gg \Delta\omega$, where $\Delta\omega$ is the chemical shift difference between the signals of the two exchanging conformations, $A \leftrightarrow B$), a simplified dependence of $R_{2,eff}$ on the CPMG pulse spacing can be used (Eq. 4) (145,147,148).

$$\nu_{CPMG} = {}^{1}/_{\tau_{cp}} \tag{4.2}$$

$$I_{\nu_{CPMG}} = I_0\, exp^{(-R_{2,eff}*T_{relax})} \tag{4.3}$$

$$R_{2,eff} = R_2^0 + \left[\frac{\Phi_{ex}}{k_{ex}}\right]\left[1 - \frac{2\tanh[k_{ex}\tau_c]}{2k_{ex}\tau_c}\right] \tag{4.4}$$

Where $\Phi_{ex} = [P_A P_B \Delta\omega^2]$, and P_A, P_B and $\Delta\omega$ can only be determined with additional independent measurements.

R_2^0 =Relaxation rate in the absence of exchange

P_A, P_B = Equilibrium populations for conformations A and B

$\Delta\omega$ = Chemical shift difference between two exchanging conformations

k_{ex} = Exchange rate constant ($k_{ex} = k_A + k_B$)

One-dimensional relaxation dispersion profiles of NR were obtained at 4°C, 25°C and 32°C on a Varian 600 MHz spectrometer. Amide spectra were collected using a TROSY (transverse relaxation optimized spectroscopy)-CPMG pulse sequence (Fig. 4.2, (148)) at a series of CPMG field strengths (ν_{CPMG}) ranging from 100 ($\tau_{cp} = 10\,ms$) –

1000 Hz ($\tau_{cp} = 1\ ms$) (100, 125, 166, 200, 303, 400, 500, 714, 833, 1000 Hz). Spectra were collected of ^{15}N Uniformly-labeled NR (0.8 mM) in 50 mM KH_2PO_4, 50 mM KCl, 1 mM DTT, 0.2 mM EDTA, 0.02% sodium azide (NaN_3), 10% (v/v) ^2H_2O at pH 7.50. Spectra were collected of ^{15}N transverse relaxation data were recorded using the first increment of a refocused HSQC-based sequence (148) with 1,024 accumulations.

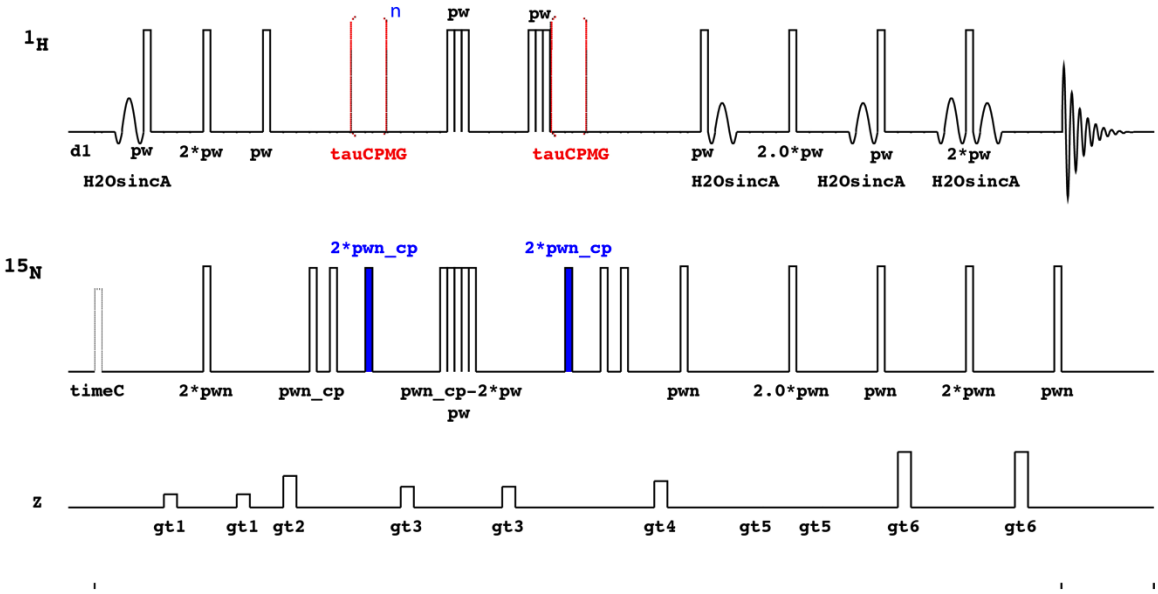

FIGURE 4.2: CPMG relaxation dispersion pulse sequences (148)

Oligomerization state of NR in solution by Dynamic Light Scattering (DLS) – The effect of temperature on the quaternary structure of wild-type and mutant NR can be determined using dynamic light scattering (DLS). DLS is a technique for measuring the translational diffusion coefficient (D_T) of macromolecules under Brownian motion in solution. Small and rapidly diffusing particles will produce rapid fluctuations whereas large and slowly moving particles will cause slow fluctuations in the scattering intensity. These intensity fluctuations are monitored by recording the intensity autocorrelation function $G(\tau)$ of the scattered light signal (Eq. 4.5) and subsequent analysis of $G(\tau)$ permits determination of the diffusion coefficient of the particles in solution (Eq. 4.6). Using the Stokes-Einstein equation and assuming spherical particles (in our simple analysis) the hydrodynamic radius of gyration (R_H) can be calculated (Eq. 4.7).

$$G(\tau) = < I_s(t) I_s(t+\tau) > \quad (4.5)$$

$I_s(t)$: scattered intensity at the time *t*

τ: short time interval

$$G(Q,\tau) = B\,[1 + ae^{(-2D_T Q^2 \tau)}] \quad (4.6)$$

$G(Q,\tau)$: the experimentally measured autocorrelation function

a ≤ 1: geometrical factor

Q: the scattering vector (depends on the polarizability of the macromolecule)

D_T: translational diffusion coefficient

$$D_\tau = \frac{k_B T}{(f_0)} = \frac{k_B T}{(6\pi\eta_0 R_H)} \quad (4.7)$$

k_B: Bolzmann constant

T: Temperature (Kelvin)

η_0: viscosity of the solvent

R_H: hydrodynamic radius of gyration (depends on the shape of the particle, but for NR, the two larger diameters of the dimer are within a factor of 2 of the smallest one.)

The measurements were performed with 134 μM NR in 50 mM potassium phosphate, 50 mM potassium chloride, pH 7.50 using a DynaPro DLS spectrometer equipped with temperature control, a 20 μL quartz cuvette and an avalanche photodiode, detecting photons scattered at a fixed angle of 90°. DLS is very sensitive to aggregation of the particles in solution; therefore all the samples measured in the experiment were filtered through a disposable 0.1 μm pore filters to remove dust and other contaminating particles, which significantly confound the measurement. To characterize the temperature dependence, measurements were made at the temperatures 4, 10, 15, 20, 25, 32, 37, and 45^{o}C.

4.4 RESULTS

4.4.1 Determination of the dissociation constant (K_d) for binding dicoumarol to NR at various temperatures

A growing number of enzymes are now being recognized as being 'promiscuous', that is of accepting numerous and sometimes diverse substrates. Protein dynamics associated with catalytic activity has been appreciated for a while now, thanks to the work of Wright and others (147,151-153). A comprehensive test across enzymes of the question: are promiscuous enzymes more dynamic? is beyond the scope of this project. Moreover there are numerous examples of enzymes that undergo considerable dynamics in the course of turnover yet are not promiscuous (151,153). Thus our objective is more modest: we wish to learn whether NR's promiscuity can be attributed to its dynamics.

To address this question we have several thrusts underway. We have made amino acid substitutions to permit formation of disulfide bond between monomers and thus potentially limit opening of the dimer interface. We have introduced amino acid substitutions designed to destabilize the dimer and found that some produced such sever affects that they are not amenable to study. We are exploiting the fact that NR appears to become more dynamic at low temperature, to allow us to study a single protein when it is more dynamic or less, and ask whether it is able to bind and turn over more diverse substrates when it has more dynamics (at lower temperature), than when its dynamics are quenched (at higher temperature).

To determine whether binding of the substrate analog dicoumarol is favoured by enhanced dynamics we measured the dissociation constant (K_d) at various temperatures. Meanwhile dynamics as a function of temperature, and moreover change in dynamics upon dicoumarol binding, was probed via ^{1}H-^{15}N HSQC NMR spectra over the same temperature range.

Binding of dicoumarol to wild-type enzyme was measured by monitoring the absorbance change of wild-type enzyme upon mixing with dioumarol in the diode array spectrophotometer. The maximum absorbance change upon binding to wild-type enzyme was at 530 nm and the change appears to be bathochromic shift (Fig. 4.3). The amplitude changes at 530 nm over the course of each titration were plotted versus dicoumarol concentration and the absorbance changes were hyperbolically dependent on the

concentration of dicoumarol present (Fig. 4.4). The plots were fitted to Eq. 4.1 giving the K_d value of the binding of dicoumarol to wild-type enzyme at the temperature used. The relationship between K_d values and temperature is shown in Fig. 4.5. The K_d value decreases with decreasing the temperature indicating that at low temperature dicoumarol binds more tightly to the wild-type enzyme.

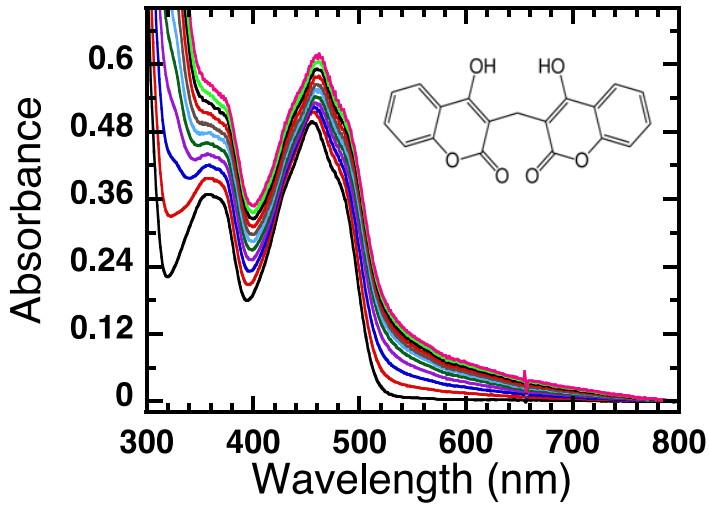

FIGURE 4.3: Absorption spectra observed at 37°C during the titration of dicoumarol into a solution of wild-type enzyme. The 35 μM protein was in 50 mM KH_2PO_4, 50 mM KCl at pH 7.50. The concentrations of dicoumarol corresponding to the spectra shown are from the lower graph to the top one: 4.4, 8.8, 13.2, 17.5, 21.7, 26.0, 30.2, 34.3, 38.5, 42.6, 46.6, 50.6, 54.6, 58.6, 62.5, 66.4, 70.2, 74.1, 77.9, and 81.6 μM.

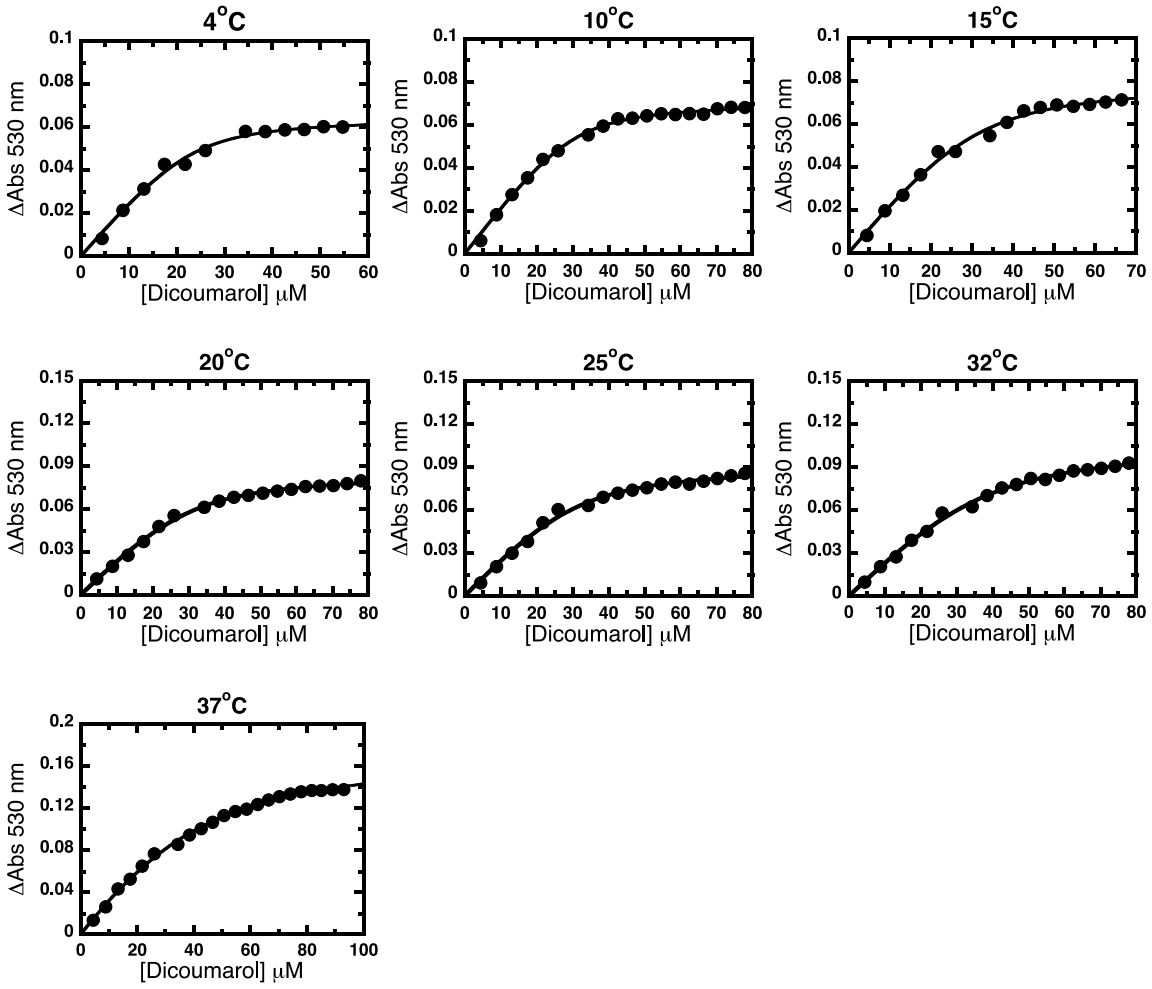

FIGURE 4.4: Binding of the inhibitor dicoumarol to wild-type enzyme observed over the temperature range of 4–37ºC. 35 μM wild-type enzyme was in 50 mM KH_2PO_4, 50 mM KCl at pH 7.50 (room temp). The maximum absorbance change at 530 nm was hyperbolically dependent on the concentration of dicoumarol present. The concentration of dicoumarol giving half-saturation represents the K_d value for the binding of dicoumarol to wild-type enzyme at observed temperature 4ºC (2.2 ± 1.4 μM), 10ºC (2.5 ± 0.7 μM), 15ºC (4.4 ± 2.2 μM), 20ºC (4.5 ± 1.1 μM), 25ºC (5.0 ± 1.9 μM), 32ºC (6.9 ± 2.3 μM), 37ºC (15.2 ± 3.5 μM). Standard errors of the fits are given in parentheses, the experimental uncertainty (due to pipetting etc.). The K_d was extracted by fitting the entire data set to Eq. 4.1.

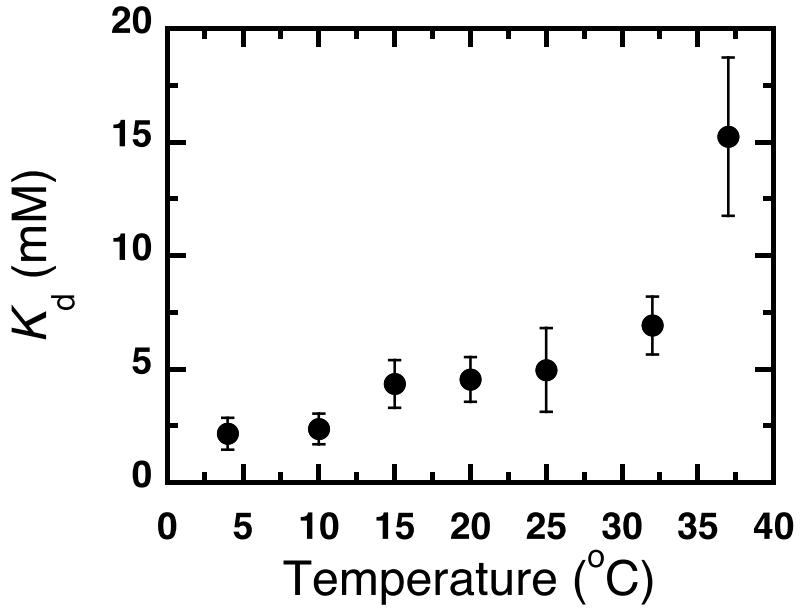

FIGURE 4.5: Plot of dissociation constants (K_d) of dicoumarol for WT NR as a function of temperatures 4, 10, 15, 20, 25, 32, and 37^{o}C, suggesting that the low temperature form of NR has a higher affinity for inhibitor binding.

4.4.2 Nuclear Magnetic Resonance Spectroscopy (NMR)

4.4.2.1 Dynamics and a possible relationship with substrate analog binding

For proteins, 1D proton NMR spectra are too complex for interpretation (Fig. 4.9B) due to spectral overlap. A protein the size of NR has more than 1500 H atoms and their individual line widths are relatively large. Even assuming 10 Hz line widths the signals would cover 15,000 Hz side-by-side, however they are clustered in smaller spectral regions on the basis of chemical type and therefore overlap heavily. By introduction another dimension (^{15}N), a set of nuclei other than ^{1}H can be detected and this facilitates the study of protein structure since the one-bond coupling ^{1}H-^{15}N is present in every non-proline amino acid residue, providing a diagnostic fingerprint of the protein (the N-terminal residue's signal is rarely observed due to facile proton exchange between amines and water). Additional signals may be attributed to the side chain amido, guanidinium, imidazole and indole functional groups of asparagine/glutamine, arginine, histidine and tryptophan residues, respectively. The HSQC does not reveal the primary sequence identity of side-chain resonances, nor does it give sequential connectivities between backbone resonances, but the dispersion pattern of ^{1}H, intensity, and number of observed cross peaks reports directly on the extent to which the protein persists in a specific folded state (well-dispersed), secondary structure (once assignments are made) and overall sample quality (number of peaks and uniformity of line widths). In previous studies from our group, we have assigned resonances to 102 of the 217 residues of [^{2}H, ^{13}C, ^{15}N]-labeled NR using conventional TROSY 3D solution NMR methods at 800 MHz (66). This backbone assignment NMR is very useful for further structural and functional studies. In this study, we analyzed the 2D ^{1}H-^{15}N HSQC NMR spectra of NR as a function of temperature in the range from 4^{o}C to 37^{o}C to monitor NR's dynamics in a qualitative way.

In the spectrum collected at 37^{o}C, the ^{1}H-^{15}N HSQC spectrum is characteristic of a unique persistent folded structure based on the good dispersion of chemical shifts in the proton dimension and the relatively uniform line widths and intensities (Fig. 4.7G). The 1D proton NMR spectrum also showed sharp peaks indicative of a well-defined protein structure (Fig. 4.9). Similarly, the HSQC spectrum exhibited a large number of peaks corresponding well to the number predicted from NR’s amino acid sequence (217 amino

acid residues). With decreasing temperature, the signals were distributed in a narrower range of ^{1}H chemical shifts and the intensities of most signals also decreased (Fig. 4.7). The 1D protein spectrum showed peak broadening indicating conformational averaging (more dynamic) or slower tumbling. The fact that ^{1}H dispersion in 1D spectra does not decrease indicates that the loss of dispersed resonances from the 2D spectra should be attributed to shorter T_2 times especially for dispersed resonances, as resonances in the range of 7.5-9 ppm are retained with more intensity.

To test for a possible coupling between structural flexibility and dicoumarol binding we compare NMR spectra of NR with and without dicoumarol present. If the more pronounced protein dynamics observed at low temperature aid in substrate binding (as opposed to lower substrate solubility at lower temperature) we would expect the converse as well: that substrate binding should result in greater protein dynamics.

1 mM dicoumarol (substrate analog) was added to 1 mM enzyme solution and spectra were collected over the same temperature range (4^{o}C to 37^{o}C) as was used to characterize substrate analog binding. The overlays of ^{1}H-^{15}N HSQC NMR spectra obtained with and without dicoumarol present (Fig. 4.10) indicated that at lower temperatures, especially at 4^{o}C (Fig. 4.10A) and 10^{o}C, (Fig. 4.10B) NR displays more conformational flexibility when dicoumarol binds than in the absence of dicoumarol, based on the narrower region of ^{1}H dispersion.

In addition, the tryptophan residue (the cross-peak at (δ (^{1}H) = 11.7 ppm and δ (^{15}N) = 135 ppm)) shifted 0.2 ppm downfield to 11.9 ppm in the ^{1}H dimension. Thus the indole proton NH resonance of this Trp is sensitive to dicoumarol binding and this downfield shift indicates stronger hydrogen bond interaction involving the indole proton NH group of tryptophan (hydrogen bonding causes “deshielding” due to electron density decrease at the proton site). There are three tryptophan residues per monomer, which are Trp46, Trp94, and Trp138. Based on our HSQC spectra of the effect of dicoumarol binding together with the crystal structure (Fig. 4.8) (52), we can propose that the Trp that responds to dicoumarol binding is Trp138, because this side chain is close to the substrate-binding site and indole proton NH of Trp138 hydrogen bonds to carboxyl side chain of Glu165 (Fig. 4.6). Thus we propose that the resonance at 11.9 ^{1}H ppm and 135

^{15}N ppm corresponds to Trp138 and that it responds to dicoumarol as part of dicoumarol binding.

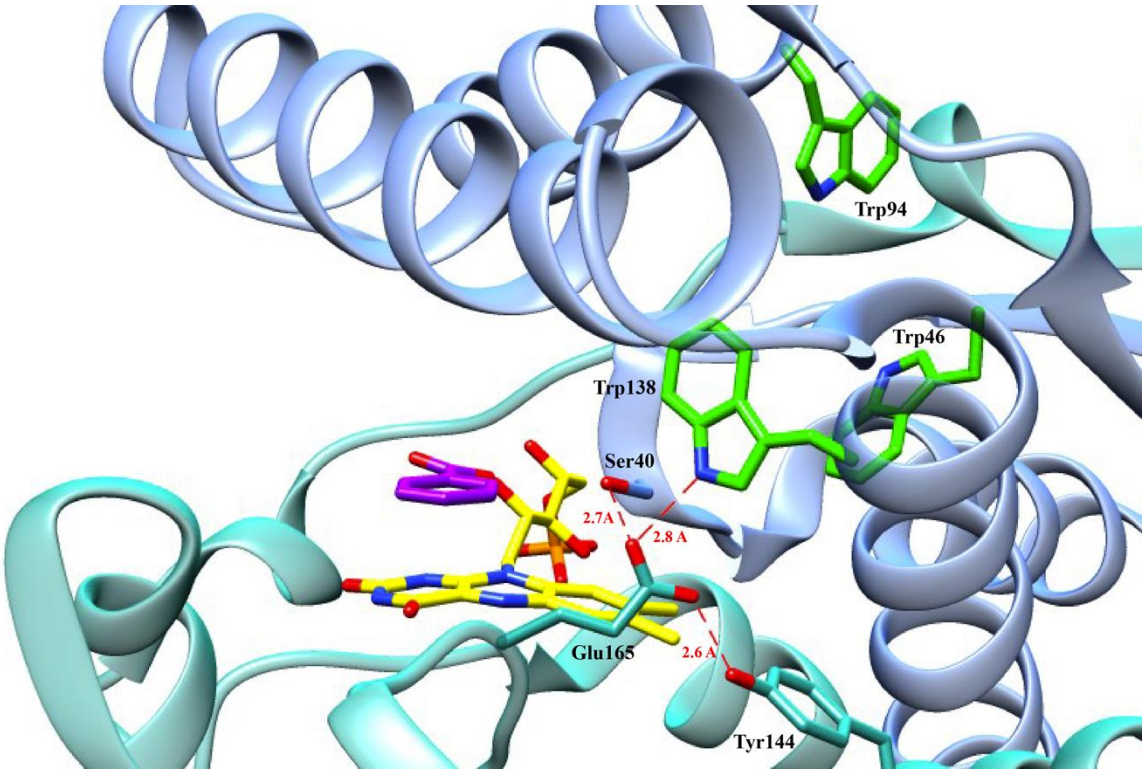

FIGURE 4.6: Crystal structure of NR showing the location of three tryptophan residues colored in green and the active site of NR in complex with benzoic acid (PDB: 1KQB).

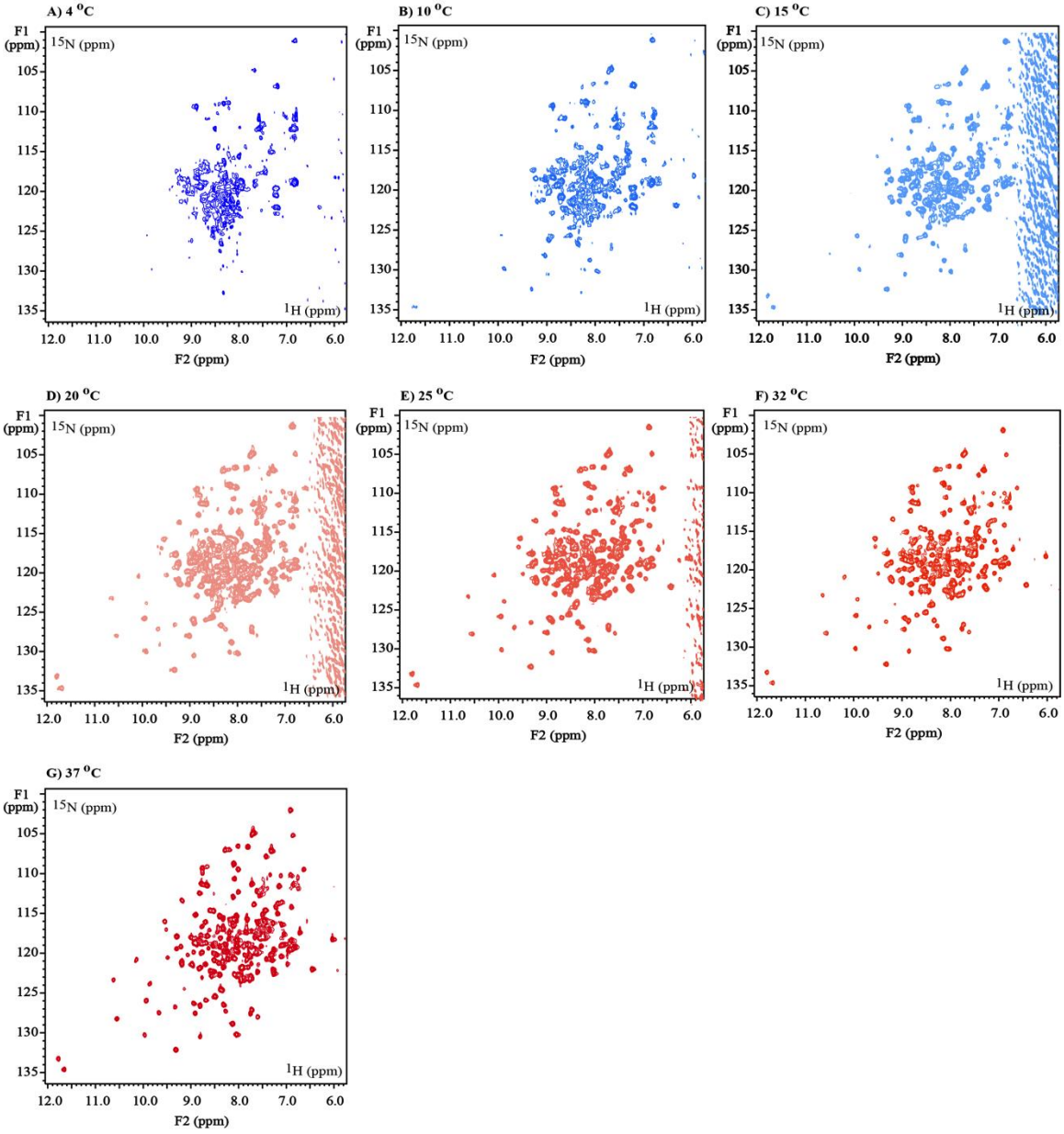

FIGURE 4.7: A series of ^{1}H-^{15}N HSQC spectrum of wild-type enzyme in 50 mM KH_2PO_4, 50 mM KCl, 0.2 mM EDTA, 1 mM DTT, 0.02% NaN_3, pH 7.50 at various temperatures A) 4°C, B) 10°C, C) 15°C, D) 20°C, E) 25°C, F) 32°C, G) 37°C. The spectra were contoured identically.

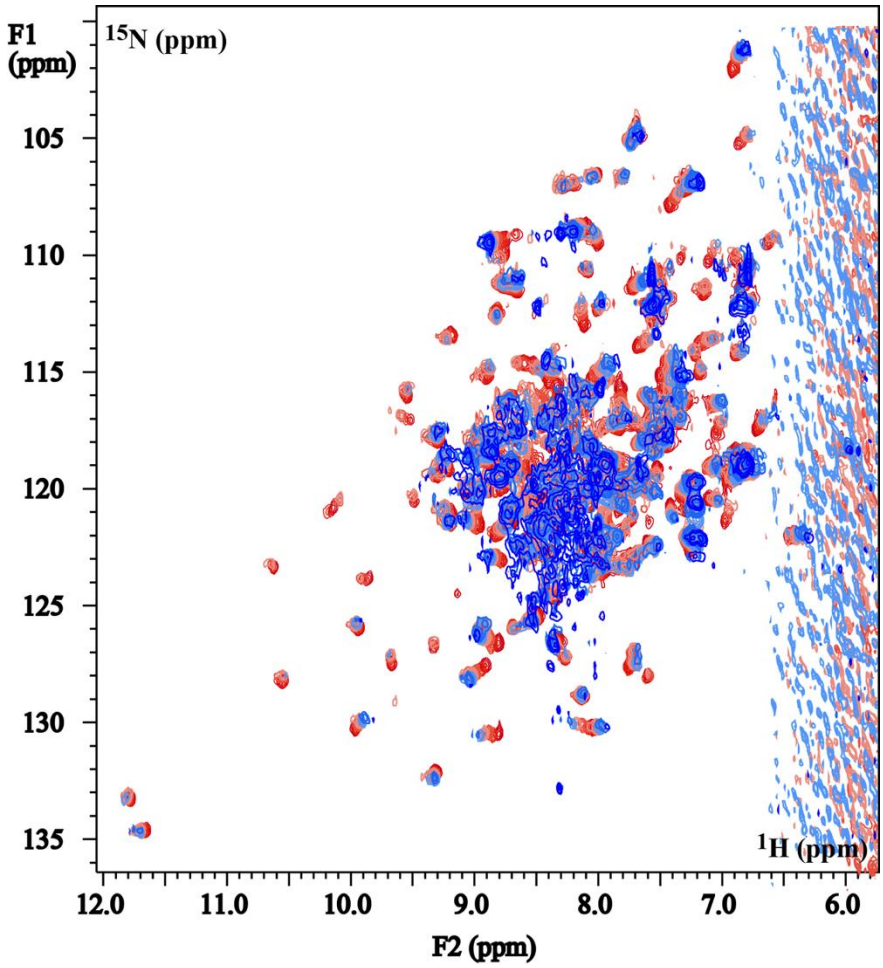

FIGURE 4.8: Overlay ^{1}H-^{15}N HSQC NMR spectra of wild-type enzyme in 50 mM KH_2PO_4, 50 mM KCl, 0.2 mM EDTA, 1 mM DTT, 0.02% NaN_3, pH 7.50 at various temperature, 4 ^{o}C (•), 10 ^{o}C (•), 15 ^{o}C (•), 20 ^{o}C (•), 25 ^{o}C (•), 32 ^{o}C (•), 37 ^{o}C (•).

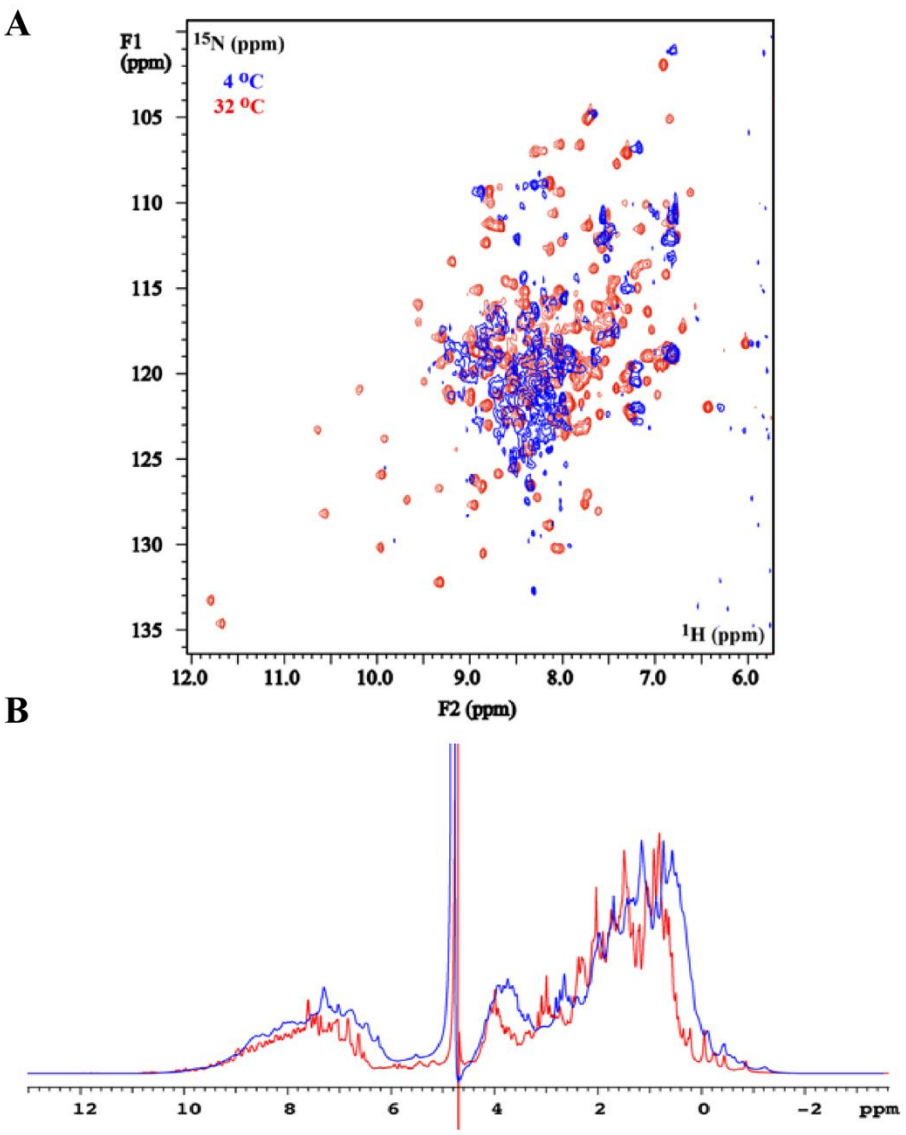

FIGURE 4.9: A) 2D ^{1}H-^{15}N Heteronuclear Single Quantum Coherence (HSQC) spectra of wild-type NR in 50 mM KH_2PO_4, 50 mM KCl, 0.2 mM EDTA, 1 mM DTT, 0.02% NaN_3, pH 7.50 at 4ºC (blue) and 32ºC (red). The axes of the HSQC indicate the chemical shift of hydrogen (F2) and the nitrogen (F1) nuclei. B) Proton 1D NMR spectra of wild-type enzyme at 4ºC (blue) and 32ºC (red).

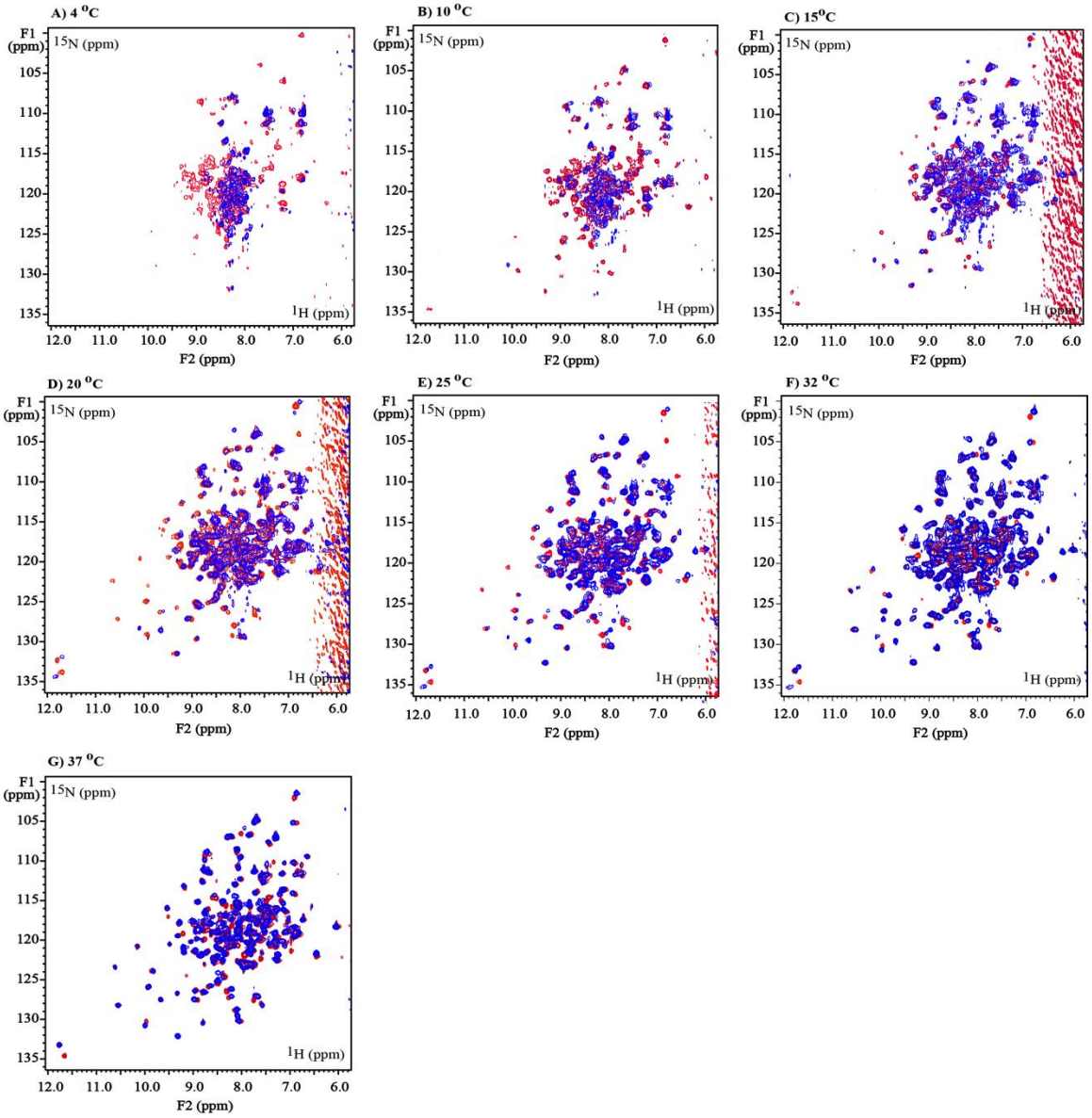

FIGURE 4.10: A series of ^{1}H-^{15}N HSQC spectra of wild-type enzyme with (blue) and without (red) 1 mM dicoumarol in 50 mM KH_2PO_4, 50 mM KCl, 0.2 mM EDTA, 1 mM DTT, 0.02% NaN_3, pH 7.50 at various temperatures A) 4ºC, B) 10ºC, C) 15ºC, D) 20ºC, E) 25ºC, F) 32ºC, G) 37ºC. The spectra were contoured identically.

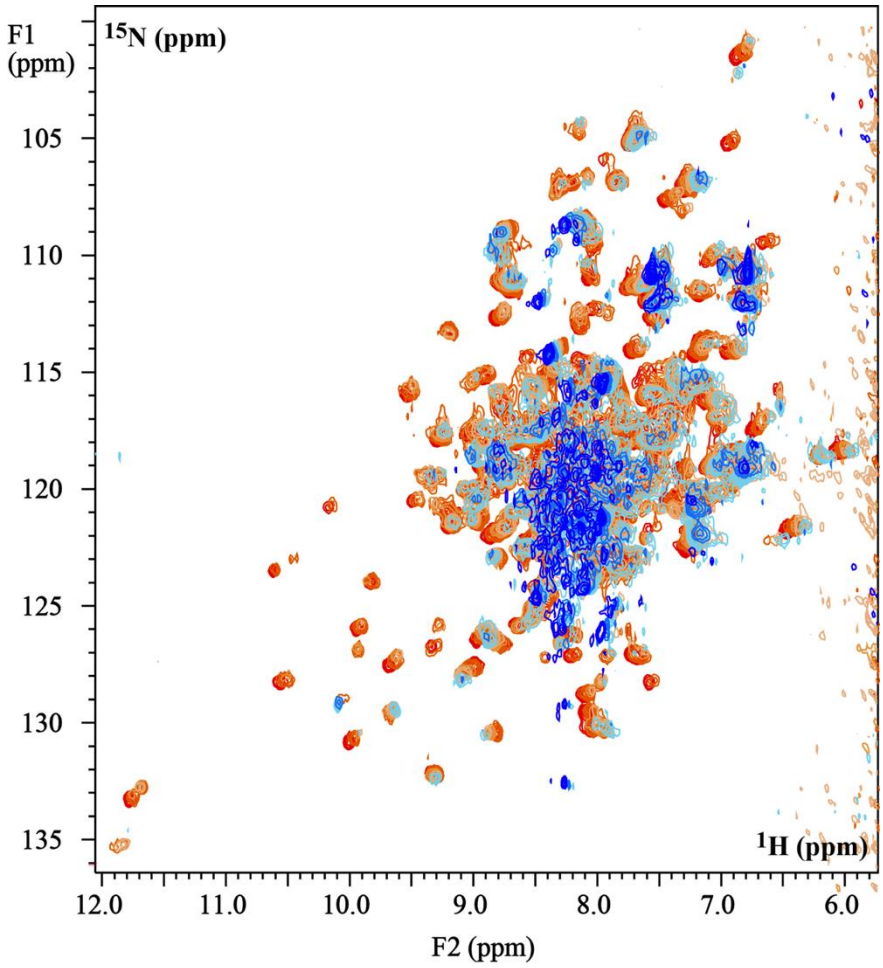

FIGURE 4.11: Overlay ^{1}H-^{15}N HSQC NMR spectra of wild-type enzyme in the presence of 1 mM dicoumarol in50 mM KH_2PO_4, 50 mM KCl, 0.2 mM EDTA, 1 mM DTT, 0.02% NaN_3, pH 7.50 at various temperature, 4^{o}C (•), 10^{o}C (•), 15^{o}C (•), 20^{o}C (•), 25^{o}C (•), 32^{o}C (•), 37^{o}C (•).

4.4.2.2 2D ^{1}H-^{15}N HSQC NMR for ^{15}N glycine-labeled NR

Protein labeling with NMR-detectable isotopes plays an important role in structural biology research. Selective labeling of a subset of amino acids provides the advantages of simpler spectra with better dispersion between resonances. This aids in the isolation and identification of signals of interest. Thus, the conformations and dynamics of specific regions or amino acid residues can be directly observed. When bacteria overexpressing the protein of interest are grown in media containing ^{15}N labeled glycine with all other amino acids provided in unlabeled form, they produce protein specifically labeled with ^{15}N glycine (157,158). NR contains total 12 glycine residues per monomer distributed throughout NR's structure at both interior and surface positions in the protein structure (Fig. 4.12). Fig. 4.13 shows the secondary structure assignment for NR indicating the location of Gly56 on helix C; Gly66 at the beginning of helix D; Gly106 in the loop between helix E and helix F; Gly120 at the middle of helix F; Gly148, Gly153 and Gly155 in helix G; Gly158 in the loop between helix G and β-stand 3; Gly166 in the loop between β-stand 3 and helix H; Gly177 in the turn of helix H; Gly182 at the end of the loop between helix H and β-stand 4 and Gly192 at the end of β-stand 4. These glycine residues are expected to provide excellent coverage of the protein in the sense that they will be found in regions that contribute in important ways to the structure or dynamics of the NR.

^{1}H-^{15}N HSQC spectra of ^{15}N glycine-labeled NR at various temperatures (4, 15, 25 and 32^{o}C) are shown in Fig. 4.14. The overlay of HSQC spectra at various temperatures shows the temperature dependence of Gly56, Gly66, Gly106, Gly120, Gly155, Gly158, Gly166, Gly177, Gly182, and Gly192, which are identified and enclosed in magenta rectangles in Fig. 4.15. In contrast, the resonances of Gly153 and Gly148, located in helix G, did not move appreciably due to changes in temperature indicating that the interface between monomers in the center of the NR's structure (helix G) is less affected by temperature. The rigidity of NR's monomer-monomer interface seems to be an important contributor to the integrity of the native folded structure, whereas a certain degree of flexibility from other protein's regions appears to be required for activity.

Ligand binding may be used as an external perturbation of protein flexibility and stability, permitting multivariable analysis that may reveal possible correlations in the variable of interest. The binding of ligand has been shown to both increase and decrease the dynamics of certain regions of protein (57,58). At low ligand concentrations, the free protein (*P*) makes the dominant contribution to spectra and is the "visible" ground state whereas ligand-bound protein (*PL*) is the "invisible" excited state. However, when saturating ligand is added ([*L*] >> K_d) to form the protein:ligand complex (*PL*), *PL* becomes the "visible" state and can be probed directly by NMR if the complex is in slow exchange relative to the NMR time scale (~ μ s – ms).

$$P + L \underset{k_{off}}{\overset{k_{on}}{\rightleftharpoons}} PL$$

^{1}H-^{15}N HSQC spectra of ^{15}N glycine-labeled NR with and without dicoumarol bound are shown in Fig. 4.16. Without dicoumarol binding, the NMR spectrum shows a single strong resonance from Gly120 (labeled as G120 in Fig. 4.16) at the cross-peak at (δ (^{1}H) = 8.04 ppm and δ (^{15}N) = 105.9 ppm); upon dicoumarol addition the former signal lost intensity and a new one (labeled as G120* in Fig. 4.16) was observed with a cross-peak and intensity that grew with the concentration of dicoumarol used. Therefore this resonance is inferred to represent the visible ground state of *PL* complex, and because no other Gly resonance was lost upon dicoumarol binding we presume that this resonance represents Gly120. Gly120 does not appear to interact with other residues outside the α helix in which it resides, arguing against its chemical shift change being the result of motion of other groups around it. Therefore our results indicate the presence of slow motion (~ μs – ms timescale) of helix F with associated with the binding of dicoumarol and also support published proposals that mobility of helix F accommodates binding of diverse substrates. Mobility of helix F can also be supported by the high B-factor value of this region reported with the crystal structure (Fig. 1.9E in Chapter 1) and molecular dynamics simulations of NR with nitrobenzene (57). The chemical shifts of Gly56, Gly155, Gly158, and Gly192 were also altered in response to dicoumarol binding, but the

resonances moved as a single peak each. Gly166, located in the NR's active site, shows less chemical shift change upon dicoumarol binding.

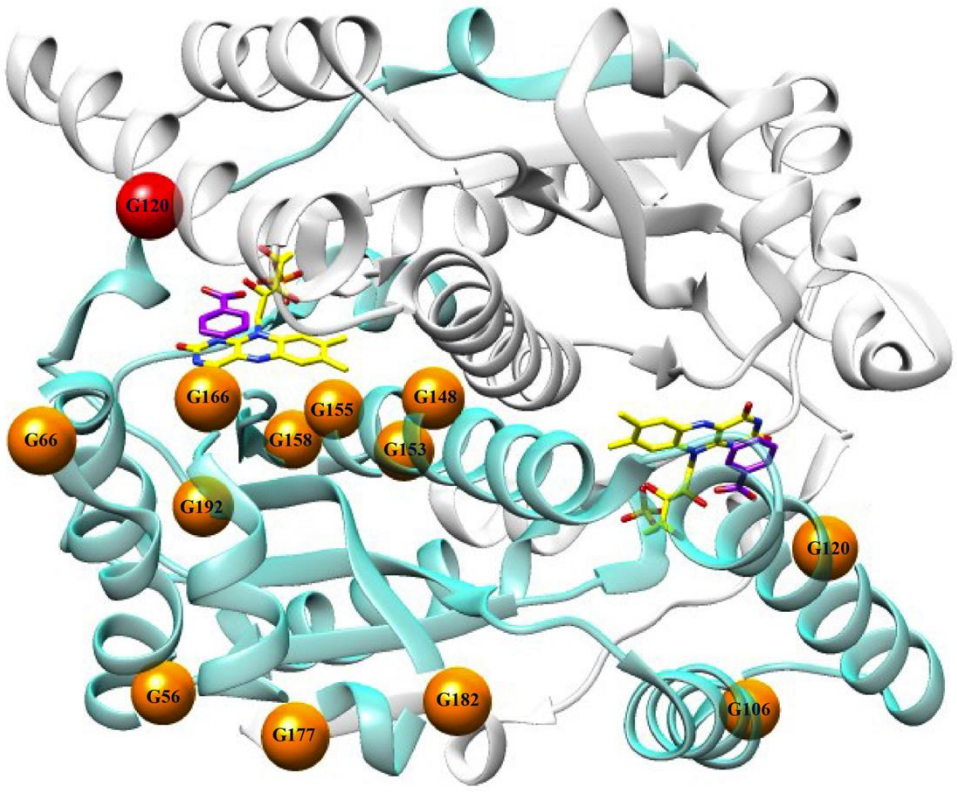

FIGURE 4.12: Structure of wild-type NR bound with benzoate (PDB:1KQB, (52)). The orange solid circles represent total 12 glycine residues per monomer and the red solid circle represents the Gly120 on helix F of another monomer.

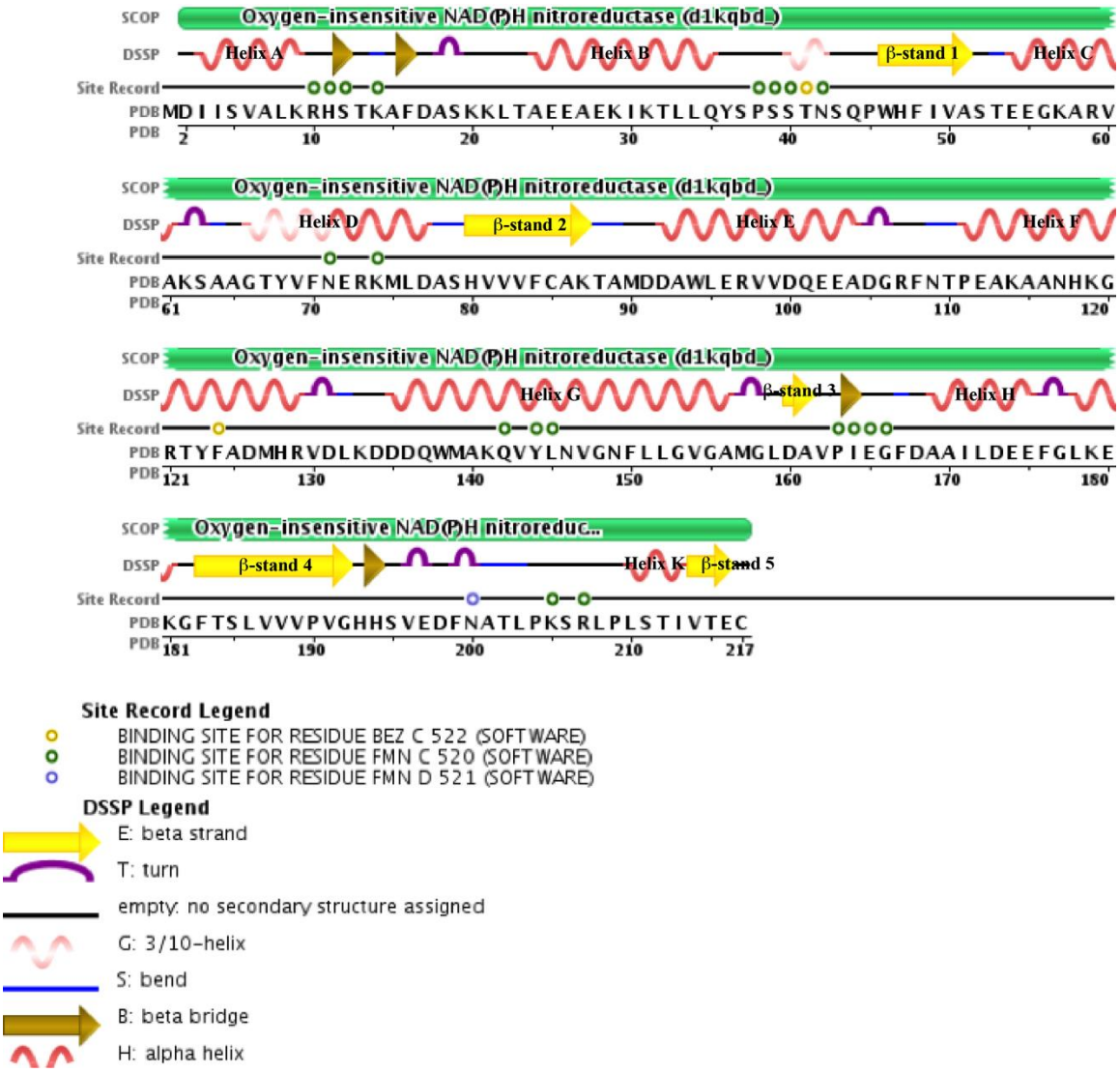

FIGURE 4.13: Secondary structure assignments for NR were assigned according to EBI SIFTS (159) (PDB to UniProt mapping). SCOP Domain Assignment: a structural classification of proteins database for the investigation of sequences and structures (160), DSSP Secondary Structure: Dictionary of protein secondary structure: pattern recognition of hydrogen-bonded and geometrical features (161), Site Record Structural Feature (MSDsite): a database search and retrieval system for the analysis and viewing of bound ligands and active site (162). This figure was created by PDB to UniProt mapping (UniProtKB Q01234) with some modifications by me.

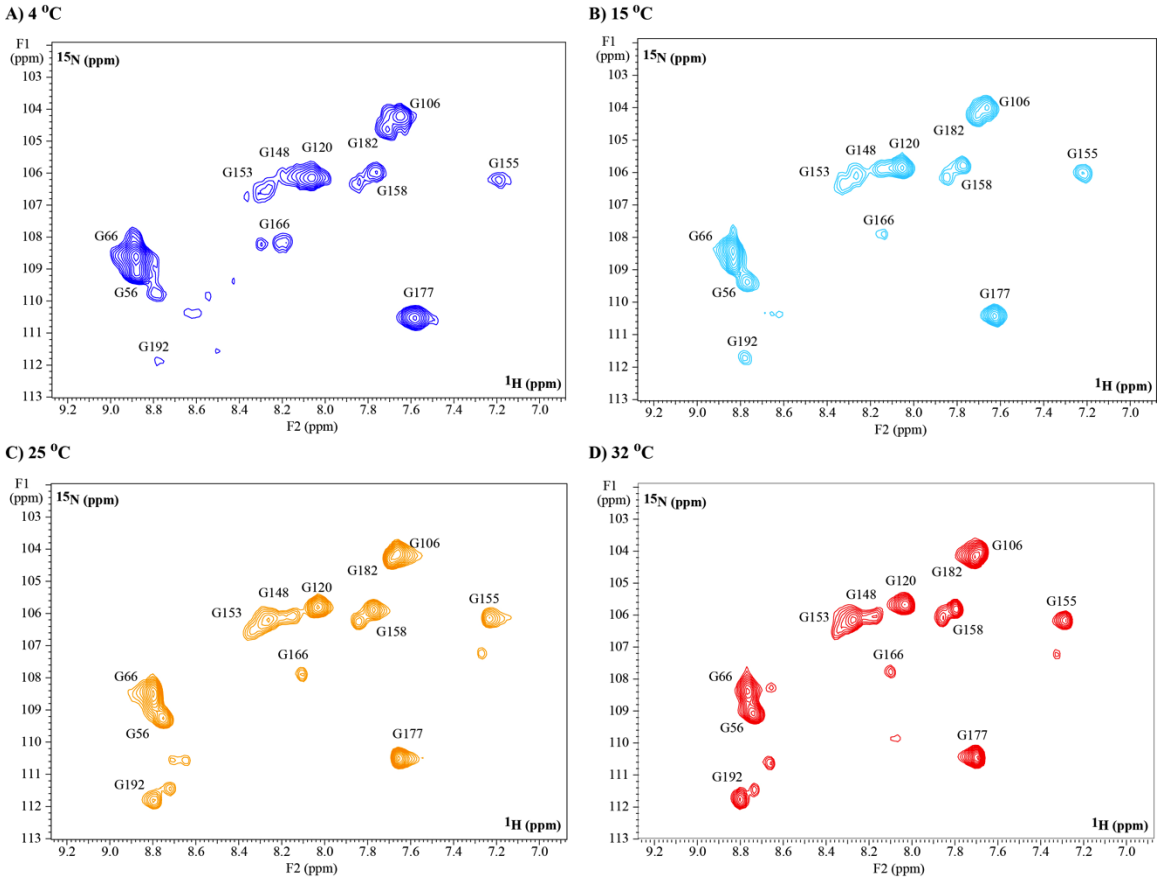

FIGURE 4.14: A series of ^{1}H-^{15}N HSQC spectrum of ^{15}N Glycine-labeled NR wild-type enzyme in 50 mM KH_2PO_4, 50 mM KCl, 0.2 mM EDTA, 1 mM DTT, 0.02% NaN_3, pH 7.50 at various temperatures A) 4°C (vs2d = 240,000), B) 15°C (vs2d = 60,000), C) 25°C (vs2d = 45,000), and D) 32°C (vs2d = 45,000).

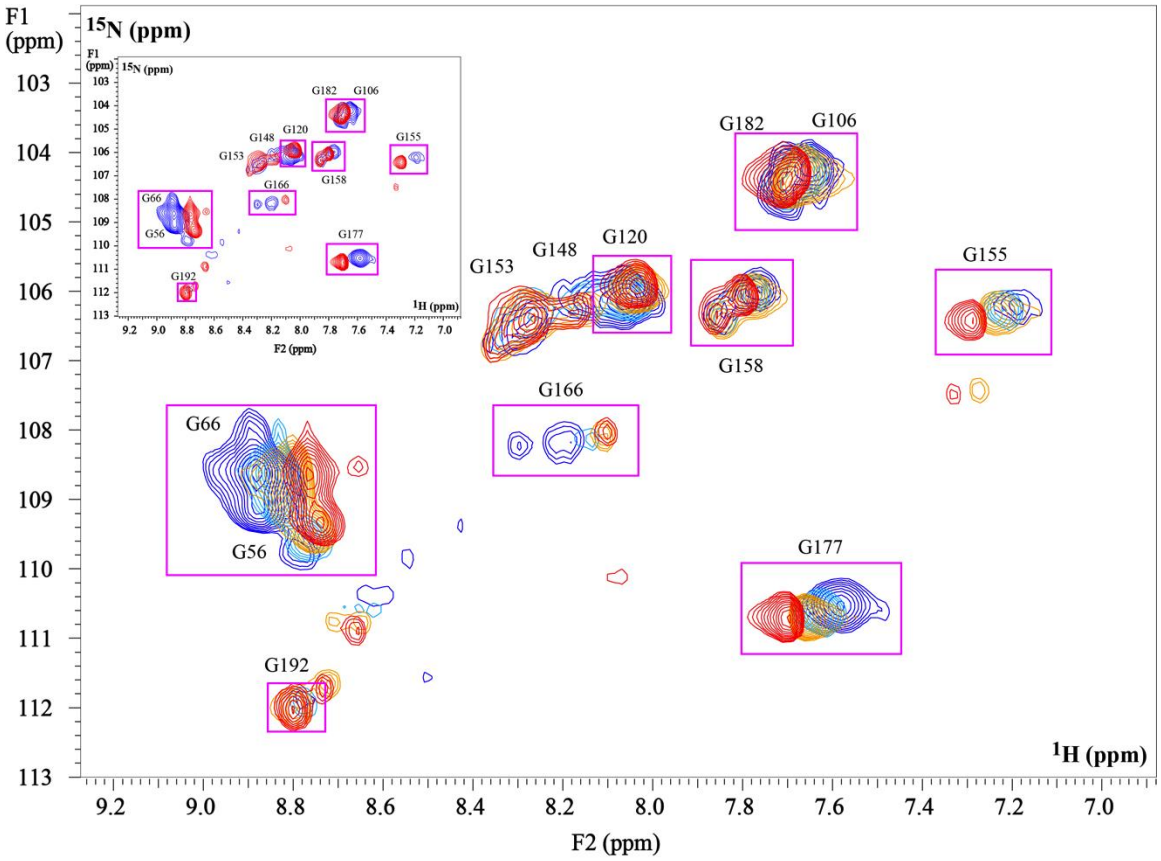

FIGURE 4.15: Overlay ^{1}H-^{15}N HSQC NMR spectra of ^{15}N Glycine-labeled NR wild-type enzyme in 50 mM KH_2PO_4, 50 mM KCl, 0.2 mM EDTA, 1 mM DTT, 0.02% NaN_3, pH 7.50 at various temperatures, 4 ^{o}C (•), 15 ^{o}C (•), 25 ^{o}C (•), and 32 ^{o}C (•).The residues that respond significantly to temperature are enclosed in margenta rectangles. The inset shows the overlay of the highest (32^{o}C, •) and the lowest (4^{o}C, •) temperatures. Note that the resonance of water shifts to higher field as temperature increases, so amide protons in rapid exchange with water are expected to likewise.

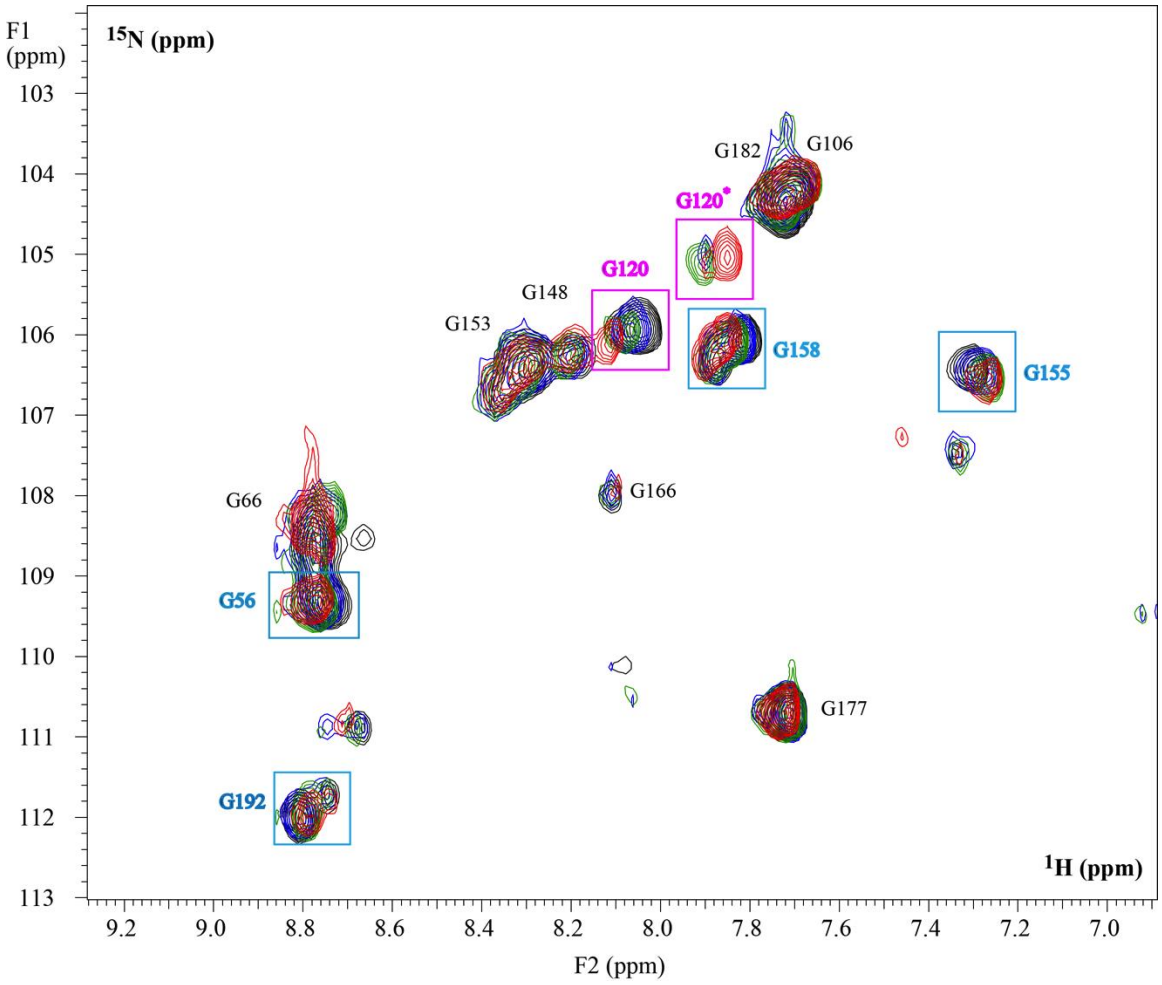

FIGURE 4.16: Overlay ^{1}H-^{15}N HSQC NMR spectra of ^{15}N Glycine-labeled NR wild-type enzyme bound with various concentrations of dicoumarol in 50 mM KH_2PO_4, 50 mM KCl, 0.2 mM EDTA, 1 mM DTT, 0.02% NaN_3, pH 7.50 at 32 ^{o}C, without dicoumarol (•), 0.5 mM dicoumarol (•), 1.0 mM dicoumarol (•), and 2.0 mM dicoumarol (•). Magenta retangles represent two strong peaks of Gly120 which responded strongly to dicoumarol binding in a slow-exchange regime (due to the large Δδ). Cyan retangles represent the glycine residues in which chemical shifts were shifted slightly with respect to dicoumarol binding, but shifted as a single peak in fast-exchange (due to the small Δδ).

4.4.2.3 1D Relaxation Dispersion Experiments

The relaxation dispersion (CPMG) experiments were applied to the backbone (N-H) of NR in order to test for and characterize dynamic processes (e.g. two state conformational change, $A \leftrightarrow B$) in the time range of microseconds to milliseconds based on a model of two state conformational exchange ($A \leftrightarrow B$). The effects of molecular motions that alter chemical shift are detected by monitoring the transverse relaxation rate ($R_{2,\text{eff}}$) of the ^{15}N nuclei for ^{1}H-^{15}N spin pairs. $R_{2,\text{eff}}$ can be obtained by measuring the decay of the NMR resonance signal during a CPMG spin-echo pulse element (τ-180^{o}- τ) where τ is a delay period (163). The first increments of HSQC experiments incorporating different total relaxation times (T_{relax}) show that the signal decreases in intensity as expected due to R_2 relaxation of the ^{15}N resonance, when τ_{cp} is held constant (Fig. 4.17). This is standard behavior as all resonances are subject to spin-spin cross relaxation. However examination of these spectra reveals that some resonances appear to decay faster than others. To determine the extent to which the observed R_2 reflects a contribution from conformational exchange (μs to ms motions, $R_{2,\text{obs}} = R_2^0 + R_{\text{ex}}$, where R_2^0 is $R_{2,\text{intrinsic}}$), we then varied τ_{cp} and thereby ν_{CPMG}.

We hypothesized that differences in overall R_2 reflected different magnitudes of R_{ex}. If R_{ex} reflects μs to ms motions it's contribution to relaxation expected to be suppressed by use of ν_{CPMG} values comparable to the rate of conformational exchange k_{ex}. Therefore we measured R_2 at a series of different ν_{CPMG} obtained by using different values of τ_{cp}. For each spectrum, the area of the ^{15}N-filtered ^{1}H spectrum was determined by integration and this was then plotted vs. T_{relax} to determine $R_{2,\text{obs}}$. The $R_{2,\text{obs}}$ values obtained based on different τ_{cp} were plotted vs. ν_{CPMG}. The experiments were repeated at 25° and 32° (Fig. 4.18 and 4.19, respectively).

Fig. 4.20 compares the relaxation dispersion plots of $R_{2,\text{obs}}$ vs. ν_{CPMG} at the two temperatures. $R_{2,\text{eff}}$ rates were found to be higher at the lower temperature (longer T_2 at higher Temperature) and shorter molecular correlation times at higher temperatures where the viscosity of water is lower.

Relaxation dispersion at 25°C and 32°C were fit with Eq. 4.4 (148,153), as well as the equation for fast exchange from Ishima (Eq. 4.8) (164). The data and the fits are shown in Fig. 4.20. The two different functions describing fast exchange fit the data

comparably well and yield parameters that agree with one another (solid lines). However the equation for slow exchange dynamics was not able to fit the data (dashed lines). This was true for the data collected at both temperatures. The parameters obtained from the fits have the values listed in Table 4.3.

$$R_{2,eff} = R_2^0 + P_a P_b \Delta\omega^2 k_{ex} / \left({k_{ex}}^2 + (2\pi \nu_{CPMG})^2 \right) \qquad (4.8)$$

R_2^0 =Relaxation rate in the absence of exchange

P_A, P_B = Equilibrium populations for conformations A and B

$\Delta\omega$ = Chemical shift difference between two exchanging conformations

k_{ex} = Exchange rate constant ($k_{ex} = k_A + k_B$)

Because this analysis treated all amide Hs at once, $\Delta\omega^2$ represents a phenomenological average over all backbone positions. Assuming P_a and P_b close to 0.5, we obtain $\Delta\omega \approx 300$ Hz. This value, equal to 5 ppm, is compatible with our spectral dispersion in the ^{15}N dimension and also the fast-exchange condition, since it is smaller than the value obtained for k_{ex} = 600 and 770 s^{-1}. However we note that where we have been able to track the shifting of individual residues, their displacement in the ^{15}N dimension has generally been modest. Nonetheless, $P_a P_b \Delta\omega^2$ is the parameter that differed the most between the two data sets. k_{ex} is marginally larger at the lower temperature, consistent with increased dynamics at lower temperature. However the rigid-body relaxation R_2^0 is essentially temperature independent, suggesting that internal motions play and important role in producing the temperature dependence of NR's relaxation rate.

The experiment was repeated in the presence of saturating dicoumarol at 25°C. This inhibitor binds quite tightly and could be expected to quench some active site motions as it does not undergo reaction and its binding is considerably tighter than that of common substrates. Indeed, its k_{ex} is not as large as that of NR alone at the same temperature. Its value of $P_a P_b \Delta\omega^2$ is intermediate between those of NR alone at 25°C vs. at 32°C. However in the presence of dicoumarol NR seems to have a significantly

enlarged R_2^0. This could indicate a change in shape resulting in a less compact structure that reorients more slowly in solution. Similarly, an expansion of the protein due to uptake of substrate analog and hydrating water, would be compatible with this result.

To address the latter possibilities, as well as the concern that NR might form larger aggregates, we evaluated the hydrodynamic radius as a function of temperature in the presence and absence of substrate analog.

TABLE 4.3: One-dimentional CPMG relaxation parameters for the fast time scales exchange process

Parameters	32°C	25°C	25°C with dicoumarol
		Ishima (Eq. 4.8)[a]	
R_2^0	21.0 ± 0.3 s^{-1}	21.2 ± 0.3 s^{-1}	24.0 ± 0.9 s^{-1}
$P_a P_b \Delta\omega^2$	12000 ± 700	20,000 ± 700	18,000 ± 3,000
k_{ex}	600 ±100	770 ± 80	600 ± 300
		Eq. 4.4[b]	
R_2^0	21.0 ± 0.3 s^{-1}	21.2 ± 0.3 s^{-1}	24.0 ± 0.9 s^{-1}
$P_a P_b \Delta\omega^2$	14000 ± 800	24000 ± 800	21000 ± 3000
k_{ex}	600 ± 100	780 ± 80	600 ± 300

Parameters were extracted by fitting the relaxation dispersion data to the model of two-state conformational exchange ($A \leftrightarrow B$).

[a] $R_{2,eff} = R_2^0 + P_a P_b \Delta\omega^2 k_{ex} / \left(k_{ex}{}^2 + (2\pi\nu_{CPMG})^2\right)$

[b] $R_{2,eff} = R_2^0 + \left[\frac{\Phi_{ex}}{k_{ex}}\right]\left[1 - \frac{2\tanh[k_{ex}\tau_c]}{2k_{ex}\tau_c}\right]$, Where $\Phi_{ex} = [P_A P_B \Delta\omega^2]$

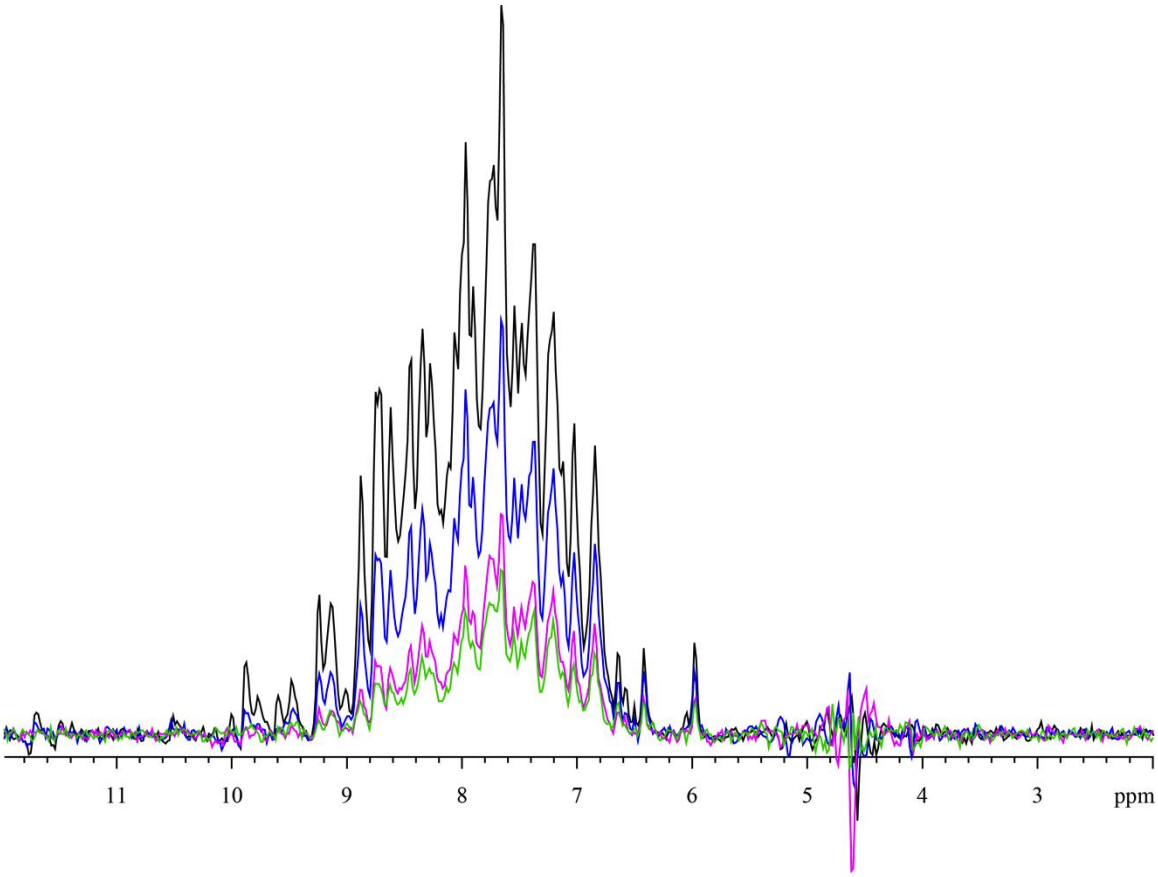

FIGURE 4.17: One-dimensional CPMG relaxation NMR spectra. Wild-type NR enzyme (0.8 mM) in 50 mM KH_2PO_4, 50 mM KCl, 0.2 mM EDTA, 1 mM DTT, 0.02% NaN_3, pH 7.50 at 32°C. The data were acquired using τ_{cp} = 10 ms and T_{relax} = 0.02 s (black), 0.04 (blue), 0.06 (pink), and 0.08 (green). All spectra were acquired with 1,024 accumulations at the same vertical scale (vs). The peaks at 4.65 ppm are the residual of the water peak after implementation of a 20 Hz ssfilter.

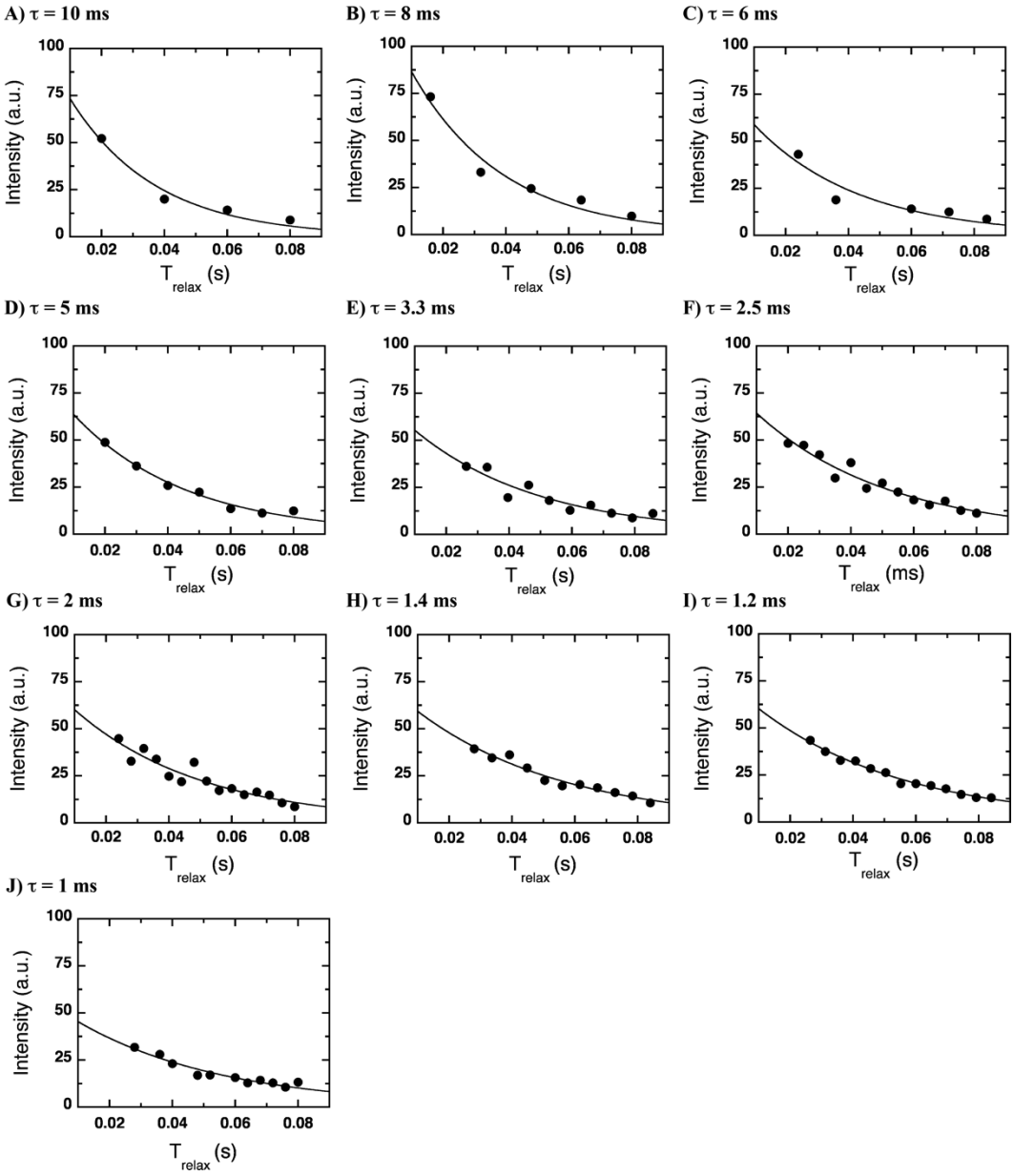

FIGURE 4.18: One-dimensional CPMG relaxation data for 0.8 mM wide-type NR in 50 mM KH_2PO_4, 50 mM KCl, 0.2 mM EDTA, 1 mM DTT, 0.02% NaN_3, pH 7.50 at **25ºC**. The data were acquired using τ_{cp} = 10 ms (A), 8 ms (B), 6 ms (C), 5 ms (D), 3.3 ms (E), 2.5 ms (F), 2 ms (G), 1.4 ms (H), 1.2 ms (I), and 1 ms (J). The relaxation rate constant ($R_{2,eff}$) obtained from the fitted curve (solid line) are 36.5 ± 2.4 s^{-1} (A), 34.3 ± 2.0 s^{-1} (B), 29.7 ± 2.2 s^{-1} (C), 27.8 ± 2.0 s^{-1} (D), 25.0 ± 3.5 s^{-1} (E), 23.8 ± 2.0 s^{-1} (F), 23.4 ± 2.7 s^{-1} (G), 21.4 ± 1.7 s^{-1} (H), 21.5 ± 0.8 s^{-1} (I) 21.4 ± 1.9 s^{-1} (J).

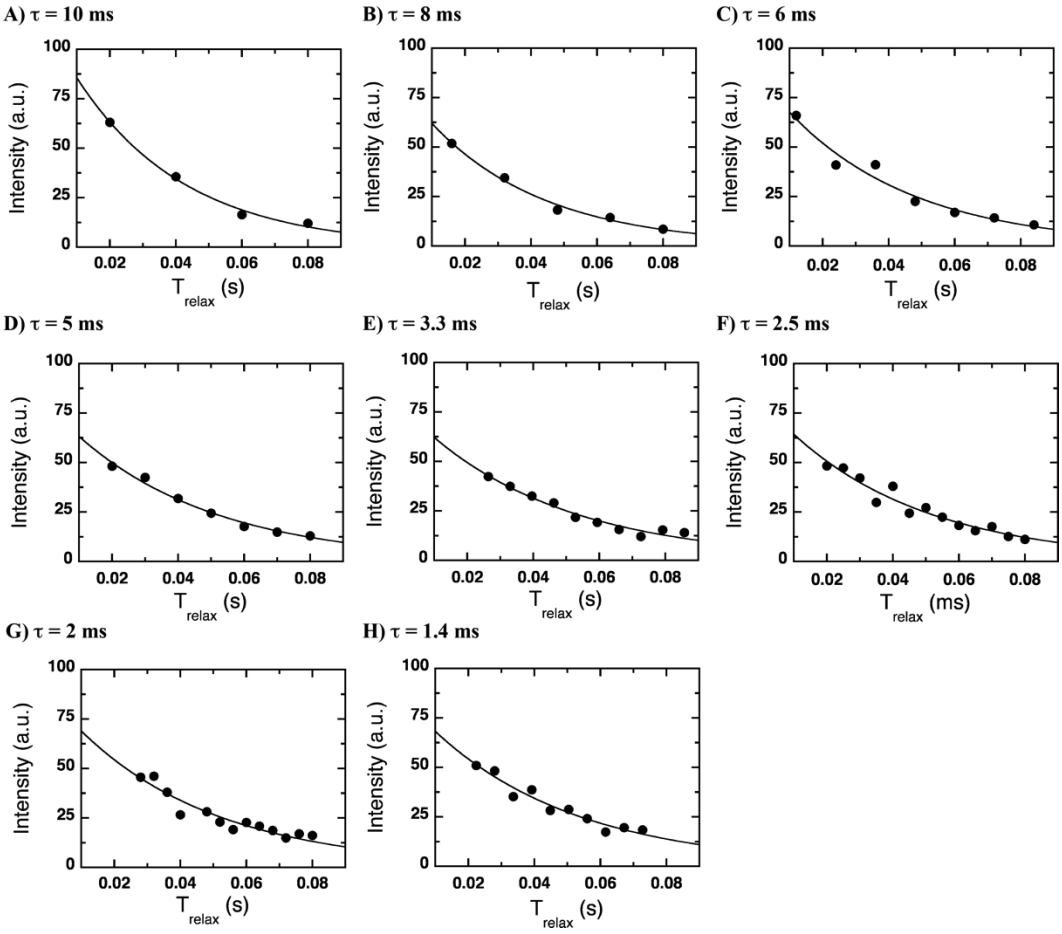

FIGURE 4.19: One-dimensional CPMG relaxation data for 0.8 mM Wild-type NR in 50 mM KH_2PO_4, 50 mM KCl, 0.2 mM EDTA, 1 mM DTT, 0.02% NaN_3, pH 7.50 at **32ºC**. The data were acquired using τ_{cp} = 10 ms (A), 8 ms (B), 6 ms (C), 5 ms (D), 3.3 ms (E), 2.5 ms (F), 2 ms (G), 1.4 ms (H). The relaxation rate constant ($R_{2,eff}$) obtained from the fitted curve (solid line) are 30.3 ± 2.2 s^{-1} (A), 28.7 ± 2.0 s^{-1} (B), 26.0 ± 2.8 s^{-1} (C), 24.1 ± 1.4 s^{-1} (D), 22.7 ± 1.6 s^{-1} (E), 21.6 ± 2.2 s^{-1} (F), 21.6 ± 2.3 s^{-1} (G), 21.8 ± 2.1 s^{-1} (H).

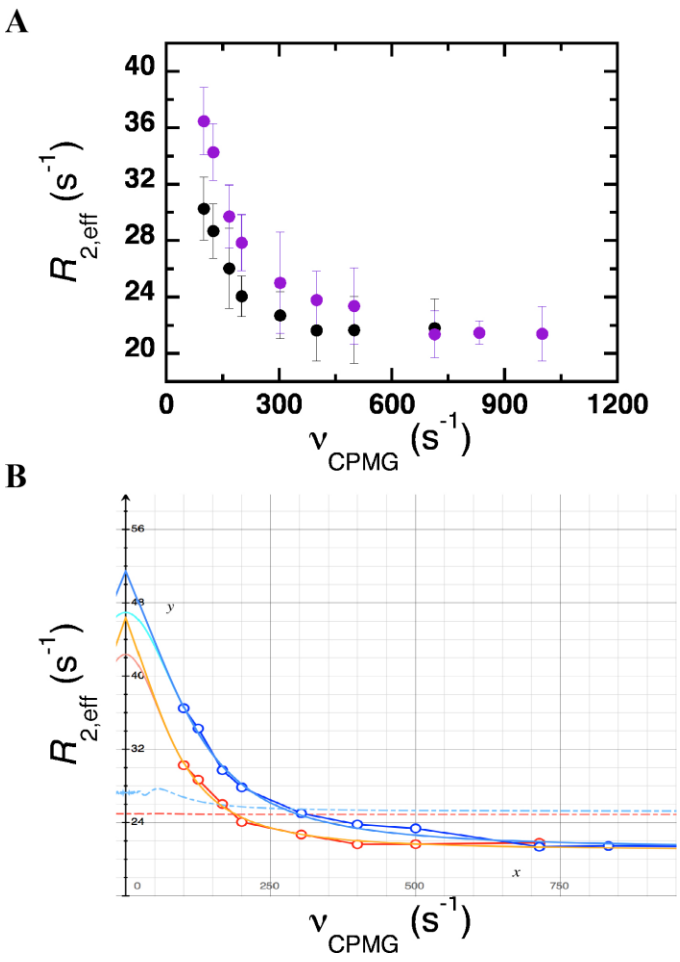

FIGURE 4.20: CPMG relaxation dispersion curves for wild-type NR enzyme. A) Values of $R_{2,eff}$ are plotted versus ν_{CPMG} ($1/\tau_{cp}$) for data obtained at 25ºC (magenta) and at 32ºC (black). B) Values of $R_{2,eff}$ are plotted versus ν_{CPMG} ($1/\tau_{cp}$) at 25ºC (blue) and 32ºC (red). Data could be simulated using either Eq. 4.4 for fast-exchange motion (powder blue or orange), or a function provided by Ishima: $R_{2,eff} = R_2^0 + P_a P_b \Delta\omega^2 k_{ex}/\left({k_{ex}}^2 + (2\pi\nu_{CPMG})^2\right)$ (light turquoise or coral). The equation for slow exchange was unable to fit the data $R_{2,eff} = R_2^0 + P_b k_{ex} - P_a k_{ex}\left(sin(\Delta\omega/4\nu_{CPMG})/(\Delta\omega/4\nu_{CPMG})\right)$ (dashed-dotted lines). Fitting was performed using Matlab and the parameters obtained are in Table 4.3.

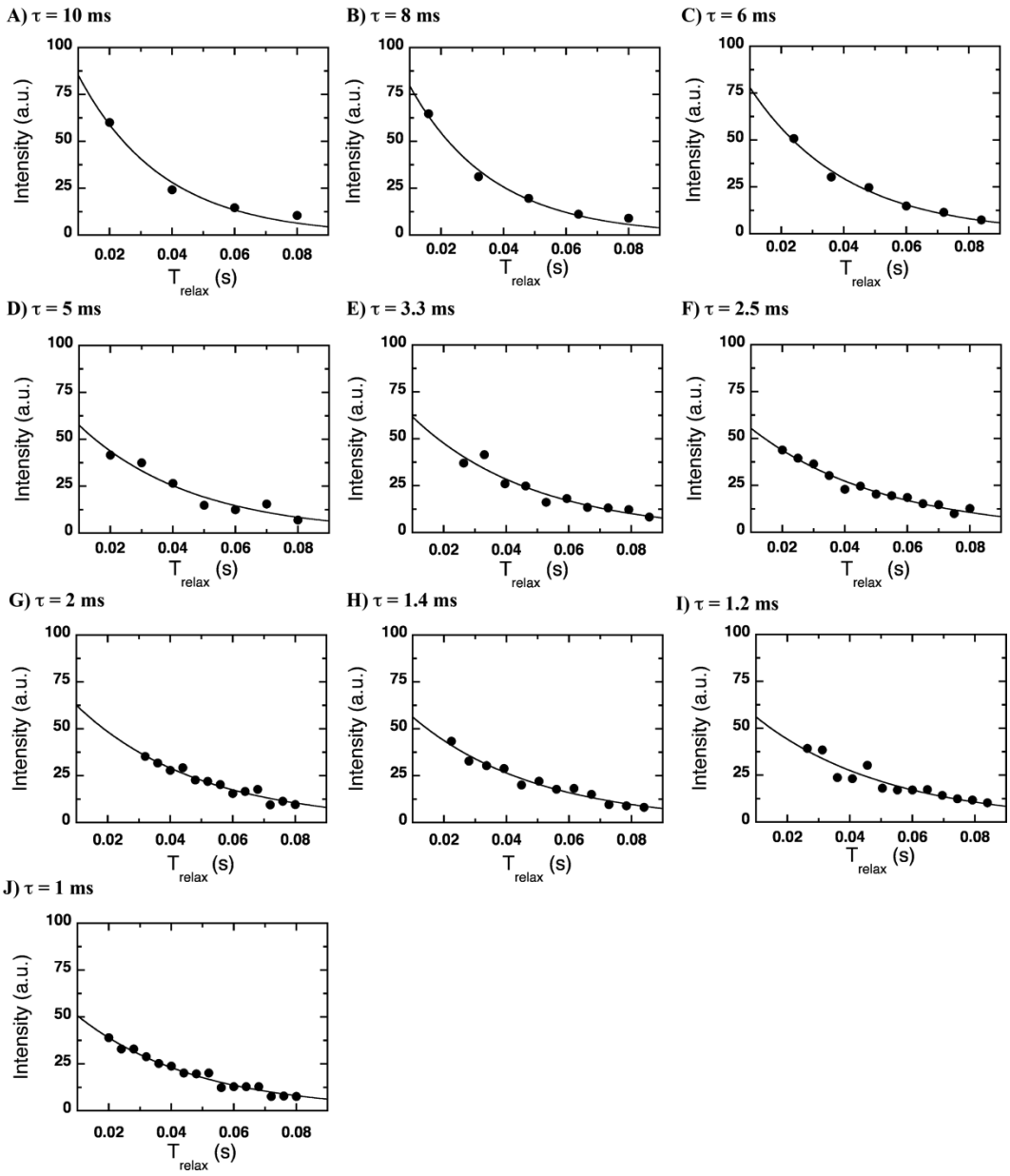

FIGURE 4.21: One-dimensional CPMG relaxation data for 0.8mM wild-type NR bound with 0.4 mM dicoumarol in 50 mM KH_2PO_4, 50 mM KCl, 0.2 mM EDTA, 1 mM DTT, 0.02% NaN_3, pH 7.50 at **25ºC**. The data were acquired using τ_{cp} = 10 ms (A), 8 ms (B), 6 ms (C), 5 ms (D), 3.3 ms (E), 2.5 ms (F), 2 ms (G), 1.4 ms (H), 1.2 ms (I), and 1 ms (J). The relaxation rate constant ($R_{2,eff}$) obtained from the fitted curve (solid line) are 36.9 ± 3.0 s^{-1} (A), 36.6 ± 3.3 s^{-1} (B), 32.3 ± 2.4 s^{-1} (C), 27.4 ± 3.8 s^{-1} (D), 25.8 ± 3.2 s^{-1} (E), 23.6 ± 2.8 s^{-1} (F), 25.5 ± 1.9 s^{-1} (G), 25.2 ± 1.8 s^{-1} (H), 23.7 ± 2.9 s^{-1} (I) 26.3 ± 1.3 s^{-1} (J).

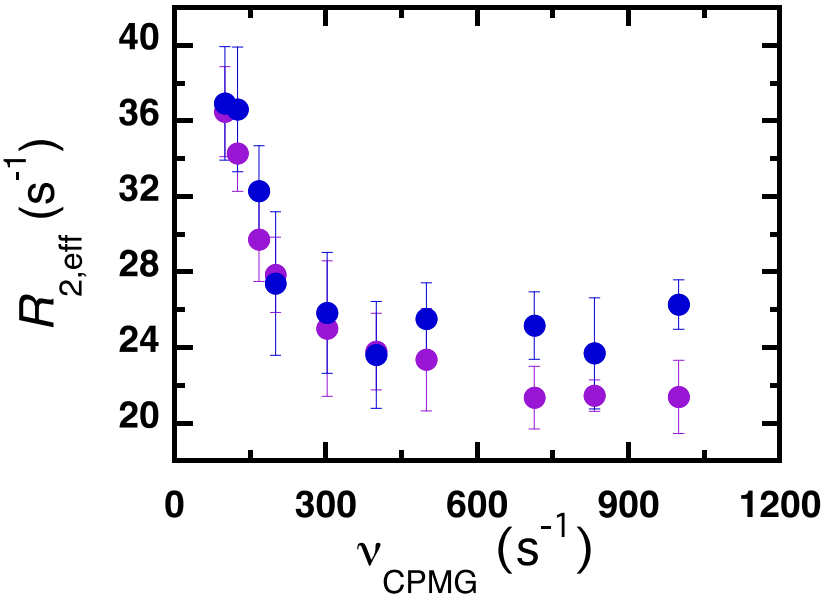

FIGURE 4.22: CPMG relaxation dispersion curves for 0.8 mM wild-type NR with (blue) and without (magenta) 0.4 mM dicoumarol at 25°C. Values of $R_{2,eff}$ are plotted versus ν_{CPMG} ($1/\tau_{cp}$) and the parameters obtained are provided in Table 4.3.

4.4.3 Oligomerization state of NR in solution

The temperature dependence of NR was investigated using proton 1D and 2D ^{1}H-^{15}N HSQC NMR at 4°C and 32°C. The results showed a well-resolved 2D ^{1}H-^{15}N HSQC NMR spectrum at 32°C, but revealed a much less intense spectrum characterized by broader lines at 4°C suggesting that NR undergoes more conformational averaging at 4°C. Shorter T_2 values at lower temperature could be explained by formation of higher-order aggregates at the lower temperature, and conformational averaging could involves interactions between the two monomers, rather than within them. Therefore, DLS and native gel electrophoresis can be used to clarify the oligomerization state of NR at different temperatures. The hydrodynamic diameters of the protein were measured by DLS at various temperatures: 4, 10, 15, 20, 25, 32, 37, and 45^{o}C as described in experimental procedures to be 2.90 ± 0.78 (4^{o}C), 2.61 ± 0.84 (10^{o}C), 2.84 ± 0.59 (15^{o}C), 2.58 ± 0.74 (20^{o}C), 2.73 ± 0.73 (25^{o}C), 2.82 ± 0.73 (32^{o}C), 2.82 ± 0.78 (37^{o}C), and 2.52 ± 0.90 (45^{o}C). The hydrodynamic radii are shown plotted versus temperature (Fig. 4.23) and the radius was found approximately the same for all the temperatures tried, with the average of 2.7 ± 0.8 nm. Overall, DLS and Native gel electrophoresis suggest the same oligomerization state of NR at low (4^{o}C) and high (32^{o}C) temperature.

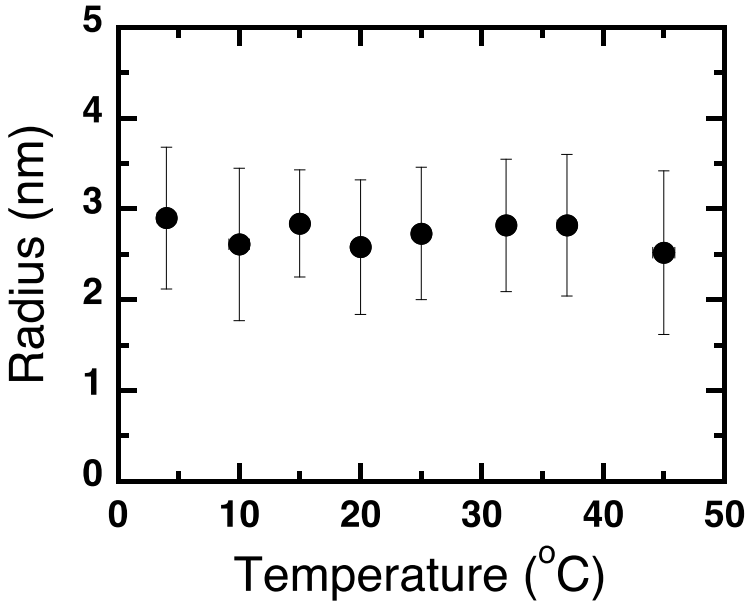

FIGURE 4.23: Temperature-dependence of hydrodynamic radius as determined by dynamic light scattering. The 134 μM wild-type enzyme was measured at various temperatures after filtration.

4.5 DISCUSSION

In this section, the contributions of conformational dynamics to substrate binding have been examined by 1D proton and HSQC NMR spectroscopy. We recorded HSQC spectra over a range of temperatures from 4 to 37^{o}C. Above 37^{o}C, the protein precipitated over a period of hours. Below this temperature, we observed a consistent increase in spectral resolution and peak intensities with increasing temperatures (Fig. 4.7). The HSQC spectra at 32^{o}C are well-resolved indicated well-defined rigid structure, but revealed a much less intense spectrum characterized by broader lines at 4°C, suggesting accelerated relaxation.

To address the possibility that residues are lost from the HSQC due to shorter T_2s produced by formation of higher oligomers of NR at lower temperatures, we used DLS. DLS showed that NR remains a dimer over the full temperature range of 4^{o}C – 32^{o}C. Moreover our DLS data also rule out the possibility that shorter T_2s at lower temperature are not the result of dimer dissociation.

Interestingly, dicoumarol binding produced HSQC NMR spectra that were narrower in the ^{1}H dimension, especially at lower temperatures (Fig. 4.10), corroborating the conclusion that dicoumarol binding is positively coupled to the dynamics that alter the HSQC (i.e. dicoumarol binding accentuates the effect). The reverse is also shown to be true by the tighter dicoumarol binding we observe at lower temperatures where the dynamics are greater (Fig. 4.5). These results motivate similar studies with additional substrate analogs.

The studies shown find changes in R_2 that are relatively modest compared to those documented in Kern's studies, where $R_{2,\text{eff}}$ changed by a factor of 5 as a function of the substrate concentration (165,166). However such large responses were observed only for certain residues and most of the residues' responses were much smaller. Our use of the first increment alone has averaged together the properties of any highly responsive residues with those of less responsive residues. The HSQC data moreover indicate that many residues undergo relatively small (if any) change in chemical shift. Thus they are not expected to experience accelerated relaxation. Finally, our use of saturating dicoumarol minimizes exchange between bound and free states of the protein. Thus we anticipate that the use of selectively ^{15}N-Gly labeled NR, to permit study of individual

resonances, and treatment with weaker-binding substrate analogs such as *p*-nitrobenzoic acid or lower concentration of dicoumarol, will improve our chances of observing relaxation signatures of dynamics.

A trivial explanation of the changes in the HSQCs, from well-dispersed resolved resonances to fewer resonances with larger linewidths, narrower dispersion and diminished amplitudes, is that NR's lines may all broaden and loose intensity in 2-D spectra due to slower tumbling at lower temperature, in combination with a loose structure. However if some small population or region of the protein is not folded, and is highly mobile, that small population of resonances would become visible at lower temperatures when the signals from the native protein dwindle. The possible dynamic population would be present at higher temperature but not be visible due to the dominance of the signal from the majority population of NR. Thus the spectra observed might represent two non-interconverting populations that are present together in the samples but dominate the spectra under different conditions. We do not have evidence for contaminating protein based on mass spectrometric analysis of NMR samples.

To test the alternative: that accelerated R_2 relaxation alone can explain the disappearance of the resolved spectrum, we need to extend our relaxation studies to lower temperatures. Because the signals are weak, we would forgo relaxation dispersion profiles but simply compare the $R_{2,\mathrm{eff}}$ values obtained with the longest value of τ_{CPMG} (lowest ν_{CPMG}).

The studies described focused on backbone resonances, however we note that the side-chain (indole) NH of Trp has a significant change in chemical shift upon dicoumarol binding. Thus that resonance is another candidate for exchange-mediated relaxation.

Our comparison of Gly resonances with and without dicoumarol present suggest that helix F experiences a change in environment. This is in agreement with crystallographic studies showing that this helix is displaced upon substrate binding, not only in NR (52) but also in the *E. coli* (NfsB) (60). The relative insensitivity of other Gly to substrate analog binding could be a consequence of the fact that all our work on substrate binding has used the oxidized state of NR, despite the fact that it is the reduced state that interacts productively with the quinones and nitroaromatics that dicoumarol mimics. Future efforts will therefore employ an inhibitor that competes with NADH for

the oxidized state, and will also try some of NR's bulkier substrates, which might therefore have a large effect on NRs structure. Protein dynamics may play a minor role in binding smaller substrates, but become more important when larger substrates are to be accommodated.

Concluding Remarks,

This work has not discovered striking evidence of dynamics associated with inhibitor binding to NR. However this does not mean the dynamics do not play a role, with some substrates, and certain aspects of turnover. We have ruled out some of the less interesting potential explanations for the chance in observed spectrum with temperature, such as aggregation or monomer dissociation. Thus future experiments could consider the effects of bulkier ligands, present at a concentration close to their K_d. All these experiments are made difficult by NR's large size, many signals and the short T_2 values that make total assignment difficult. Thus any future efforts will concentration on the selectively labeled samples that reveal at least one resonance that undergoes a large relocation upon substrate analog binding.

CHAPTER 5

AN APPROACH FOR FLEXIBILITY AND DIMERIZATION STATE OF NITROREDUCTASE MUTANTS

5.1 ABSTRACT

Besides mechanistic considerations dealt with above, NR's broad substrate repertoire must also entail binding of the different substrates in NR's active site, in the dimer interface. To address the appealing possibility that movement within the dimer interface, of one monomer relative to the other, may be involved in binding substrate analogs, we have worked on two sets of mutants. In one we have modified the C-terminal clamp that appears to provide a long-range tether that would prevent monomers from actually separating from one another but nonetheless allow reorganization of interactions within the interface. Deletion of residue 217 removes the backbone interactions as well as any benefits of the side chain. ΔC217-NR failed to accumulate in either the soluble fraction or even the insoluble debris after induction of the corresponding gene, indicating that deletion of the C-terminal residue greatly destabilized the protein. C217A-NR was similar to WT-NR in multiple respects but appears more dynamic based on more pronounced loss of dispersed HSQC resonances a low-temperature. Thus, interactions mediated by backbone functionalities of the C-terminal residue of NR help to stabilize its structure.

Another set of mutants directly perturbs the dimer interface to assess the importance of the small network of H-bonds observed there between Ser40A, Glu165B and Trp138A (as well as the symmetry-related network between Ser40B, Glu165A and Trp138B). Despite conserving volume, substitution of Glu165 with Leu greatly weakened FMN binding. In contrast to E165L-NR, S40A-NR was similar to wild-type enzyme with respect to stability and temperature dependence except that the resonance of the indole NH of Trp138 moves downfield shift in the ^{1}H dimension suggesting a stronger H-bond interaction between Glu165 and Trp138.

5.2 INTRODUCTION

Homo-oligomeric proteins have been proposed to provide increased stability by enabling a single amino acid sequence to bury more hydrophobes and assemble a larger total entity when self-associated in multiple copies than would be possible for monomeric versions. Homodimers can also match the symmetry required for binding to both strands of palindromic DNA double helices. The stability advantages of dimerization can be used to 'pay' for desirable protein properties that may be energetically disadvantageous. In the case of NR, the enzyme's polar hydrophobic substrates are best bound by residues that should normally be buried within a hydrophobic core. Thus, formation of an exposed binding site would involve solvation of non-polar side chains. Moreover in all members of the NR family for which liganded structures are available, the substrate (analog) is bound with its aromatic ring stacked against the flavin. Thus the sparingly polar flavin ring must be provided with a suitable protein contact surface, yet a site for substrate binding must be exposed to water. Thus the protein of NR would appear to present a non-polar surface to solvent, were it not a dimer.

When it binds, the substrate (analog) inserts between the flavin and the monomer with which it does not interact (Fig. 5.1B). This arrangement therefore resembles a wedge and suggests that an optimally stable dimer that provides good interactions with both faces of the flavin would not accommodate a ligand. Instead it appears that binding of the flavin ring and indeed the dimer interface *per se* is not optimized. FMN nonetheless binds with high affinity, presumably due to strong interactions between the protein and the ribityl phosphate side chain. Meanwhile the integrity of the dimer is ensured by extensive interactions between the two termini of each monomer with the body of the other monomer. In particular, the C-terminal, 4 amino acids, wraps around the other monomer and forms a strand of its central β sheet (Fig. 5.1C.), and the N-terminus forms a 9 residues α helix that packs against helix B of the other monomer (Fig. 5.1D). Such close association with the tertiary fold of the other monomer has been dubbed '3D domain-swapped-dimer' formation (54). Thus, NR's dimeric nature is tied to its ability to bind flavin and substrates and, we propose, to intimate associations between the termini of one monomer and the body of the other.

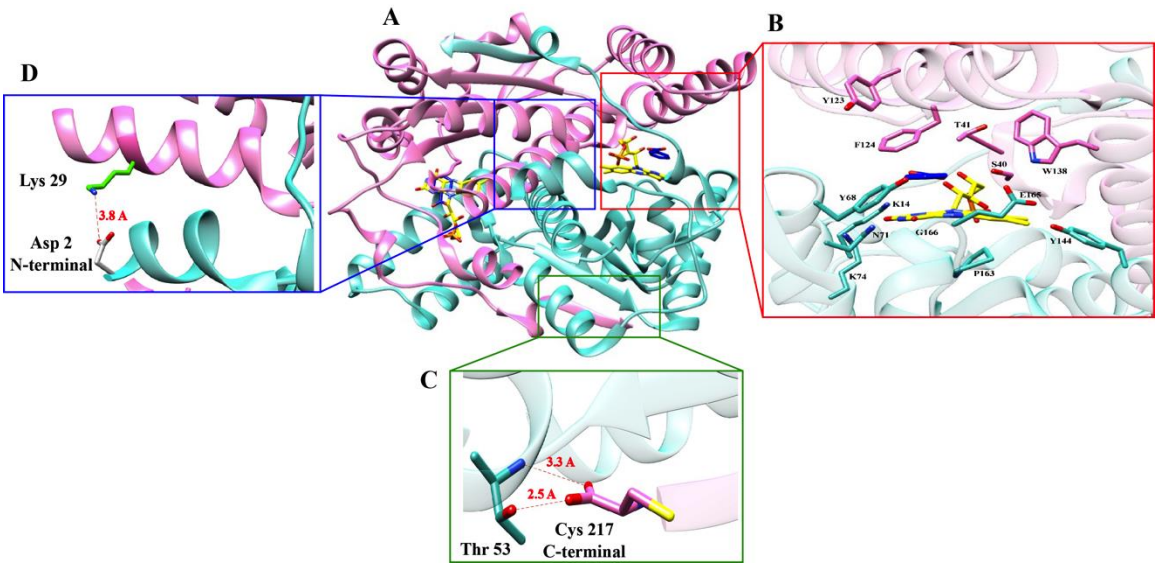

FIGURE 5.1: A) Nitroreductase (NR) structure from *E. cloacae* (PDB: 1KQB) in the oxidized state bound with FMN cofactor (yellow sticks) and benzoic acid (blue sticks). B) Interaction of FMN with amino acids from both subunits in the NR active site. C) C-terminal residue (Cys217) hydrogen bonds to hydroxyl (-OH) side chain and amide backbone of Thr53 of another subunit with 2.5 Å and 3.3 Å, respectively. D) N-terminal residue (Asp2) hydrogen bonds to ε-NH_2 of Lys29 of another subunit with 3.8 Å (52).

Dimers are by far the most abundant homotropic oligomeric state. Some two thirds of proteins for which reliable structural data exist are found to be oligo homomers, and two thirds of these are dimers (167). The prevalence of oligomers does not vary significantly between taxa, nor does the complexity of quaternary structure correlate with the complexity of the organism. There is a continuum of dimerization constants and dimer interface sizes, although most proteins have a binding interface that is close to 16% of the surface area of the monomeric unit. In most cases, the active site is contained in individual monomers (each monomer has one) (167).

Homo-multimers are very prevalent among human enzymes. Enzyme active sites are frequently located in the dimer interface (168), indeed approximately one sixth of oligomeric enzymes' active sites are found in interfaces between two separate polypeptide chains (169). In an early analysis of homotropic oligomers, interfaces between monomers in a dimer were found to have properties intermediate between those of

protein interiors and exteriors (170). The exposed surface area of the dimer was smaller than the sum of the two monomers conforming to the expectation that the surface area to mass ratio shrinks upon dimerization and that this may be a driving force for dimerization. The hydrophobicity of the interface was found to be intermediate between the interior and the exterior (171-173). Hydrophobes are somewhat enriched in the dimer interfaces, along with Arg, His Tyr and Phe. In general, dimer interfaces are circular planar hydrophobic patches with good shape complementarity. dimer interfaces ranges between 400 and 5000 $Å^2$.

Among homodimers, an interesting subset have been deemed 'domain-swapped dimers' (DSD), when a structural component of one monomer interacts closely with the other monomer in a fully reciprocal arrangement whereby the first monomer gains an identical interaction with the analogous component of the other monomer. The two interfaces are identical but are created by two separate protein molecules, although in principle each monomer could have supplied the partner polypeptide. Some proteins have indeed been found able to form either the intramonomer interactions or the intermonomer interactions (54,174). Although some domain swapped dimers may be artifacts of crystallization, the interaction interfaces of intramonomer interactions form ready-made surfaces at which intermonomer interactions can occur with comparatively minor adjustments needed, for example to linker or hinge regions between the participating regions in the primary sequence (54). Formation of a domain swapped dimer then creates a new interface between monomers that can bring together binding sites for multiple substrates, or for a cofactor and a substrate, making new catalytic activity possible (175). Indeed, the thiamine pyrophosphate dependent enzymes for which structures are known all employ at least a dimeric structure, in which different domains of the two monomers each contribute different binding functionality (176). Thiamine pyrophosphate-utilizing enzymes commonly bind the thiamine cofactor in the interface between monomers (177). In the case of NR, it is crucial that the dimer interface provides a non-polar surface which can associate closely with the catalytic flavin ring system. However such a surface would be destabilizing if it were presented on an exterior surface. Thus the dimer interface at which the symmetry-related relatively non-polar surfaces of two monomers associate provides a slot in which the flavin ring system

can insert without disrupting the hydrophobic core of an individual monomer.

The NR dimer can be considered to be a domain-swapped dimer, under the criteria of Eisenberg (54) because a strand of the β-sheet of one monomer is provided by a strand from the other (Fig. 5.1C). The NR domain-swapped dimer displays two features identified by Gronenborn: that the exchanged stretches of polypeptide occurs at the termini of the individual molecules and are connected to the folding core by hinge-loops (178). In studies on cyanovirin-N, Koharudin found evidence by size-exclusion chromatography and multi-angle light scattering for coexistence of diverse oligomeric forms upon refolding cyanovirin-N from concentrated solutions. Different crystal forms obtained upon crystallization under different conditions were indeed found to reflect different oligomeric forms. In the case of cyanovirin-N, refolding was performed at concentrations as high as 4 mM, which is likely to favor formation of higher oligomers (178). The different forms were sufficiently long-lived to be separated from one another chromatographically and crystallized separately, although HN-HSQC NMR spectra of one form revealed separate resonances from other forms co-existing with it. Most residues retained the same dihedral angles in the different oligomeric forms, consistent with swaps between similar domains or identical proteins, so many NMR resonances of the different forms may nonetheless have been superimposable. Thus the spectra of samples dominated by different oligomeric forms were strongly similar. Consistent with larger radii of gyration, the tetrameric forms displayed larger line widths. Nitroreductase illustrates a principle identified by Eisenberg, that domain-swapping may follow simply from the presence of C- and/or N-terminal extensions. However in the case of NR the extensions both appear to be a conserved suggesting that the swapped interactions are evolved properties of the protein not accidental, since they are shared by all the homologues with 33% identity or greater for which crystal structures of the dimer have been published (the major NAD(P)H:FMN oxidoreductase of *V. fischeri* (FRase I) shares only 33% identity, the minor O_2-insensitive nitroreductase of *E. Coli* (NfsB) shares 88% identity) (Fig. 5.2). Moreover because the dimer interface supports the active site, we consider that the dimerization mode is highly significant to function and likely subject to considerable evolutionary pressure. Thus we can expect that the protein will include specific features that reinforce this particular dimerization mode. We have set out to test

two in particular.

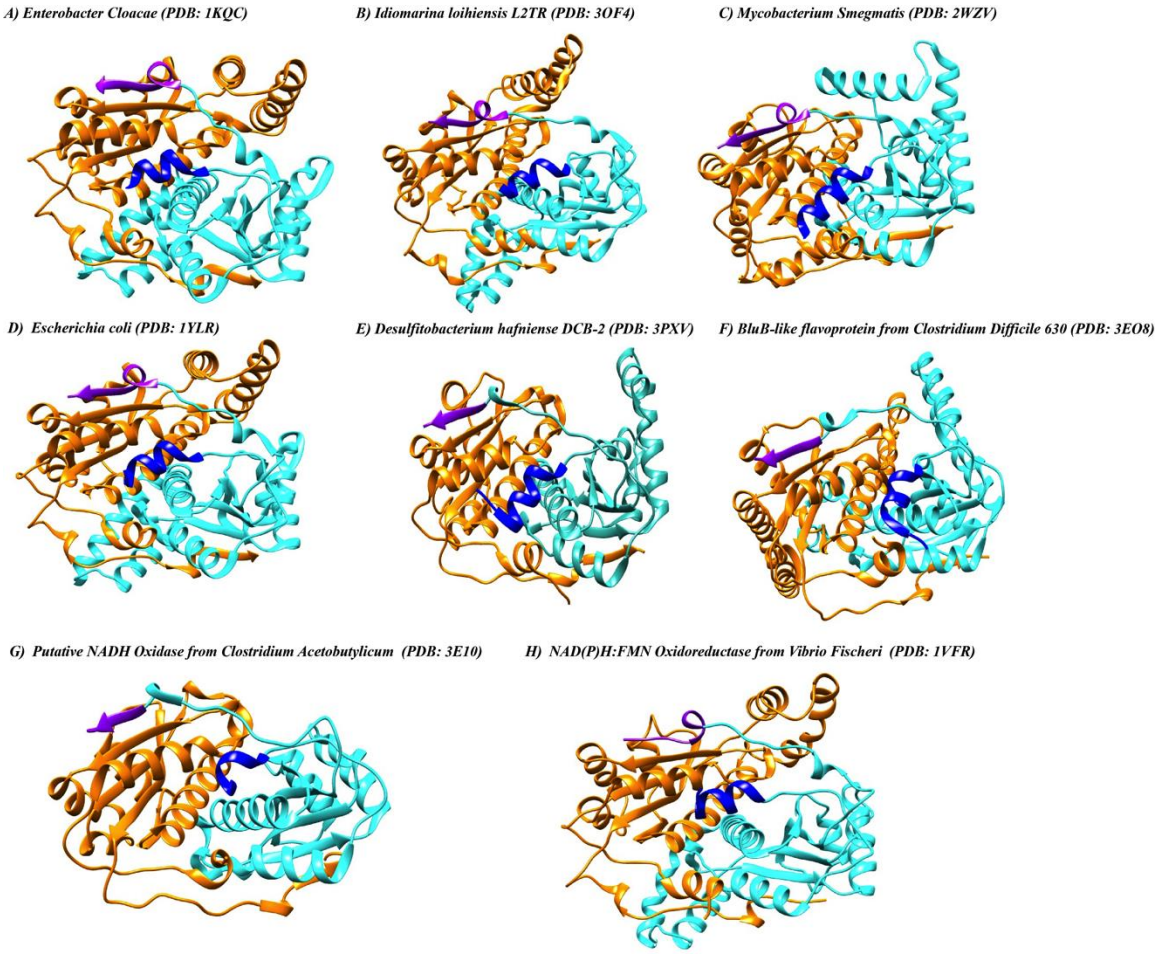

FIGURE 5.2: Ribbon diagrams of the structures of the nitroreductases family ((A) *Enterobacter cloacae* (PDB: 1KQC) (52), (B) *Idiomarina loihiensis* L2TR (PDB: 3OF4) (DOI:10.2210/pdb3of4/pdb), (C) *Mycobacterium Smegmatis* (PDB: 2WZV) (78), (D) *Escherichia coli* (PDB: 1YLR) (60), (E) *Desulfitobacterium hafniense* DCB-2 (PDB: 3PXV) (DOI: 10.2210/pdb3pxv/pdb), (F) BluB-like flavoprotein from *Clostridium Difficile* 630 (PDB: 3EO8) (DOI:10.2210/pdb3eo8/pdb), (G) Putative NADH Oxidase from *Clostridium Acetobutylicum* (PDB: 3E10) (DOI:10.2210/pdb3e10/pdb), (H) NAD(P)H:FMN Oxidoreductase from *Vibrio Fischeri* (PDB: 1VFR) (67)) with subunit A in cyan and subunit B in orange. The N- and C- termini of subunit A are indicated by blue and magenta color, respectively.

Side-directed mutagenesis was used to produce proteins in which amino acids of particular interest were replaced in order to learn what their contributions might be to

dynamics, the dimer interface and stability of the dimer. Amino acid substitutions were chosen based on published crystal structures (52). To clearly understand the role of C-terminal domain swapping for NR flexibility and dimerization, the C-terminal Cys217 residue was changed to Ala to investigate the role of the thiol group (-SH), or deleted altogether (ΔC217) to assess the significance of residue 217's backbone interactions. The hypothesis is that weakening this clamp, based entirely on non-covalent interactions, will destabilize the NR dimer, increase its propensity to dissociate and possibly unfold. Moreover, the role of the C-terminus' interactions with the other monomer in holding the dimer together vs. allowing motion of one monomer relative to the other was investigated by introducing a second Cys (Fig. 5.3) side chain positioned so as to be able to form a disulfide bond with the sulfhydryl of Cys217 and thereby crosslink the two monomers. The side chain of Ala51 from the other monomer is in close proximity to the Cys217. By introducing cysteine at this position, we propose that the oxidized A51C/C217 with the disulfide bond distance of 2.9 Å (Fig. 5.3) will decrease the conformational flexibility and also be less able to bind dicoumarol at low temperature.

The stability of the dimer interface and the significance of specific interactions within it was tested via substitution of residues located in the dimer interface which interact with residues in the other monomer: Glu165 and Ser40. The carboxyl side chain of Glu165 forms a 2.8Å hydrogen bond with the hydroxyl side chain of Ser40 of the other monomer (Fig. 5.1B). We constructed E165L-NR and S40A-NR to interrupt this hydrogen bond interaction by two independent means, to learn whether this hydrogen bond supports adaptive conformational flexibility. The redox potentials of wild type and all mutant enzymes were measured in order to investigate whether the electrostatic environments around the active site of the mutant enzymes play an important role in redox potentiation of the cofactor. Additionally, because the redox potential embodies the change in flavin binding affinity upon flavin reduction, the redox potential will reveal whether the active site's specificity for a particular oxidation state of the flavin has been altered.

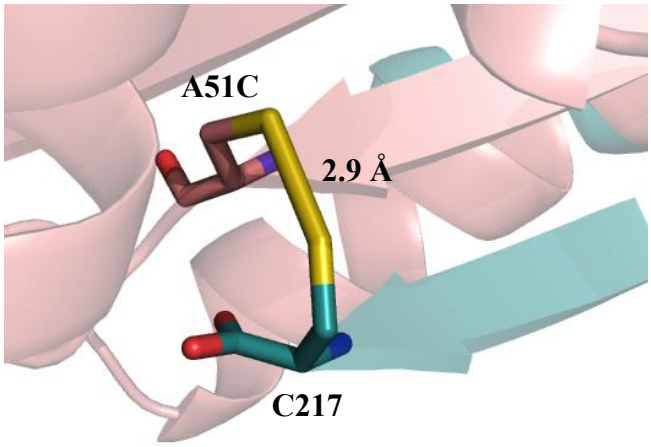

FIGURE 5.3: C-terminal residue (Cys217) cross-links to Ala51Cys (Modeling in PyMol (86))

5.3 EXPERIMENTAL PROCEDURES

5.3.1 Site-Directed Mutagenesis

Site directed mutagenesis at positions S40, A51, E165 and C217 was performed by using QuikChange® II XL Site-Directed Mutagenesis Kit (Agilent Technologies). The mutagenic forward primers:

5’-CTGCTGCAGTACAGCCCGTCCGCCACCAACTCCCAGCCGTGGCAC-3’ (S40A),
5’-CAGCCGTGGCACTTCATTGTATGCAGCACCGAGGAAGGAAAAGCG-3’ (A51C),
5’-GGTCTGGACGCGGTACCAATTCTGGGTTTCGACGCCGCTATTCTC-3’ (E165L),
5’-CTGAGCACGATTGTGACCGAGGCCTGAGCTCCTCTGGCACGCTGG-3’ (C217A),
5’-CTGAGCACGATTGTGACCGAGTGATGAGCTCCTCTGGCACGCTGG-3’ (ΔC217),

and the reverse primers:

5’-GTGCCACGGCTGGGAGTTGGTGGCGGACGGGCTGTACTGCAGCAG-3’ (S40A),
5’-CGCTTTTCCTTCCTCGGTGCTGCATACAATGAAGTGCCACGGCTG-3’ (A51C),
5’-GAGAATAGCGGCGTCGAAACCCAGAATTGGTACCGCGTCCAGACC-3’ (E165L),
5’-CCAGCGTGCCAGAGGAGCTCAGGCCTCGGTCACAATCGTGCTCAG-3’ (C217A),
5’- CCAGCGTGCCAGAGGAGCTCATCACTCGGTCACAATCGTGCTCAG -3’ (ΔC217),

were from IDT (Integrated DNA Technologies). The plasmid pRK1 was used as template for mutagenic PCR.

PCR reactions were carried out in a thermal cycler (GeneAmp PCR system 9700, Applied Biosystem). The reaction mixtures included primers (each at 125 ng), 10 ng of plasmid DNA, 1 µL dNTPs mix, 3 µL QuickSolution, and 2.5 units *PfuUltra* HF DNA polymerase and sterile distilled water to make up a volume of 50 µL. *PfuUltra* HF DNA polymerase was added to start the reaction. The reaction mixture was preheated at 95°C for 1 minute. Cycling parameters were as follows (18 cycles): denaturing at 95°C for 50 s, annealing at 60°C for 50 s and extending for 2 minutes at 68°C. At the end, the reaction was left at a final temperature of 68°C for 2 minutes. The amplified PCR products were separated by agarose gel electrophoresis and purified using HiSpeed® Plasmid Midi Kits (Qiagen). To confirm the accuracy of the mutations, the plasmid DNA was analyzed by sequencing using the forward primers 5'-TAATACGACTCACTATAGGG-3' (T7-Promoter) and the reverse primer 5'-GCTAGTTATTGCTCAGCGG-3' (T7-terminator). The DNA sequencing was performed by Eurofins MWG Operon Sequencing.

5.3.2 Non-denaturing (Native) Polyacrylamide Gel Electrophoresis

A gradient gel has an increasing concentration of acrylamide at increasing depth (distance travelled). This results in decreasing pore sizes in the direction of migration. The protein samples were run onto 4-20% gradient native gels (Mini-Protein® TGX™ Precast Gels BIO-RAD, 4-20%, 10-well comb, 30 µL/well Cat. #456-1093) and run at 4, 25, and 32ºC. Gels were equilibrated 1xTAE buffer at the desired temperature for 30 min prior to use.

5.3.3 Determinations of the reduction midpoint potential of NR

Standard reduction potentials (E_m^o) of mutant enzymes were measured by reducing NR in the presence of standard indicator dyes of known E_m^o according to the method of Massey (179). The reduction process was driven using the xanthine and xanthine oxidase system, which reduced the dye and enzyme by generating electrons from xanthine as shown in (Scheme 5.1). Optical analysis of the equilibrium formed between partially-reduced flavoenzyme and a similar concentration of a reference dye of known midpoint potential reveals the amount of each species that is oxidized. Since we know the total amount of each species we can calculate the amount of each that is reduced. This technique requires only a dye with a redox potential similar to that of the flavoprotein.

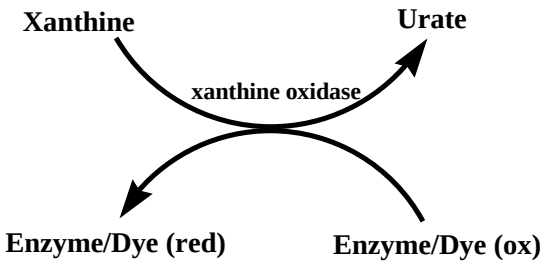

SCHEME 5.1: Xanthine/xanthine oxidase system

Measurements were carried out in a reaction mixture that included 400 µM xanthine, 3 nM xanthine oxidase (side arm), 2 µM benzyl viologen as a mediator, 18 µM standard dye (phenosafranine, E_m^0 = -252 mV (180) and 18 µM of wild-type or mutant NR in 50 mM KH_2PO_4, 50 mM KCl buffer pH 7.50 at 25ºC , wild-type and mutant NRs. The reaction mixture was placed in an anaerobic cuvette and made anaerobic by 50 cycles of removal of air and equilibration with Ar on an anaerobic gas train as previously described. After anaerobiosis had been established, the spectrum of the mixture in the oxidized state was recorded before the reaction was initiated by admixture of the xanthine oxidase from the side arm. During the reaction process, absorbance at wavelengths of 454 and 521 nm was used to calculate the amounts of oxidized NR and dye present, at frequent intervals (10 min time intervals per scan with total time ~12-14 hours). Because both dye and NR absorb at both wavelengths (454 and 521 nm), simultaneous Eq. 5.1 and 5.2 were used to calculate the concentrations C^D and C^E of oxidized dye and NR, respectively, based on their known extinction coefficients (ε) at the two wavelengths. The midpoint potential of the NR enzyme (E_e^o) can then be calculated from the standard Nernst equation (Eq. 5.3 and 5.4) where E_{ox} is the concentration of oxidized NR (= C^E above) and E_{red} is the concentration of reduced NR (= total concentration - oxidized concentration), D_{ox} and D_{red} are similarly defined for the dye and (E_d^o) is the reduction midpoint potential of the dye.

$$A_{445} = \epsilon_{445}^{E} C^{E} + \epsilon_{445}^{D} C^{D} \quad (5.1)$$

$$A_{521} = \epsilon_{521}^{E} C^{E} + \epsilon_{521}^{D} C^{D} \quad (5.2)$$

$$E_e = E_e^0 - (\frac{0.0592}{n_2}) \log(E_{red} / E_{ox}) \quad (5.3)$$

$$E_d = E_d^0 - (\frac{0.0592}{n_1}) \log(D_{red} / D_{ox}) \quad (5.4)$$

n_1 = number of electron involved in the dye reaction

n_2 = number of dye electron involved in the enzyme reaction

At equilibrium, $E_d = E_e$

$$\log(E_{red} / E_{ox}) = \frac{n_2}{n_1} \log(D_{red} / D_{ox}) + \frac{n_2}{0.0592}(E_e^0 - E_d^0) \quad (5.5)$$

The plot of $\log(E_{red} / E_{ox})$ versus $\log(D_{red} / D_{ox})$ provides a linear correlation (Eq. 5.5), and the intercept value can be used to calculate E_e^0 since E_d^0 is known. The number of electrons involved in the reduction can be identified from the slope of the plot, which is the ratio of the number of electrons involved in the enzyme reduction to the number of electrons involved in the dye reduction.

The values of molar absorption coefficients are follows:

ϵ_{445}^{E} $(oxidized\ NR\ at\ 445\ nm) = 14.3\ mM^{-1}cm^{-1}$

ϵ_{521}^{E} $(oxidized\ NR\ at\ 521\ nm) = 0.76\ mM^{-1}cm^{-1}$

ϵ_{445}^{D} $(oxidized$ phenosafranine $at\ 445\ nm) = 9.85\ mM^{-1}cm^{-1}$

ϵ_{521}^{D} $(oxidized$ phenosafranine $at\ 521\ nm) = 44.7\ mM^{-1}cm^{-1}$

5.3.4 Determination of the dissociation constant (K_d) for binding of dicoumarol to A51C-NR

The sulfhydryl groups of C217 and A51C are oxidized non-enzymatically to disulfides by H_2O_2. In brief, A51C-NR was expressed and purified as describe in experimental procedure in chapter 3 for wild-type NR except that no DTT was added. After purification, ~0.2 mM A51C-NR was incubated with 1% H_2O_2 for 1 hour at room

temperature, then the enzyme solution was loaded onto a PD-10 chromatography column and eluted with 50 mM potassium phosphate buffer pH 7.50. The dissociation constants of A51C-NR at 4 and 32^{o}C were performed as similar to those described in chapter 4 for the wild-type NR.

5.4 RESULTS

5.4.1 Site-Directed Mutagenesis

The correct mutations at Ser40, Ala51, Glu165, and Cys217 were confirmed by using DNA sequence analysis (Eurofins MWG Operon). The PCR products were run on 0.8% agarose gel and the results showed DNA of ~7 kb compared to the DNA molecular size markers.

5.4.2 Expression of NR mutants

NR wild-type and mutants were expressed in *E. coli,* BL21(DE3). Typically, about 110-120 mg of the purified enzyme was obtained from 8 L of cell culture. All wild-type and mutant enzymes expressed well and were found in the soluble fraction of the crude extract, except the deletion mutant (ΔC217). This result suggests that the backbone of Cys217 is important for NR stability, solubility or expression.

5.4.3 Purification of NR mutants

All NR wild-type and mutant proteins save ΔC217 were purified to homogeneity using the procedure described in "experimental procedures". After the gel filtration (S-200) purification step, the solutions of wild-type, S40A, A51C, and C217A-NR showed yellow color indicating that a flavin moiety was bound in the active site, whereas the solution of E165L-NR was colorless suggesting that there was no flavin bound in the active site of this mutant. E165L protein was confirmed to be present by SDS-PAGE and the molecular mass was ~23 kDa (Lanes 2-6 in Fig. 5.4) in agreement with the molecular mass of wild-type enzyme (Lane 1 in Fig. 5.4). All wild-type and mutated enzymes maintained full enzymatic activity upon storage in 50 mM KH_2PO_4, 50 mM KCl, 0.2 mM EDTA, 1 mM DTT, 0.02% NaN_3 pH 7.50 at 4°C.

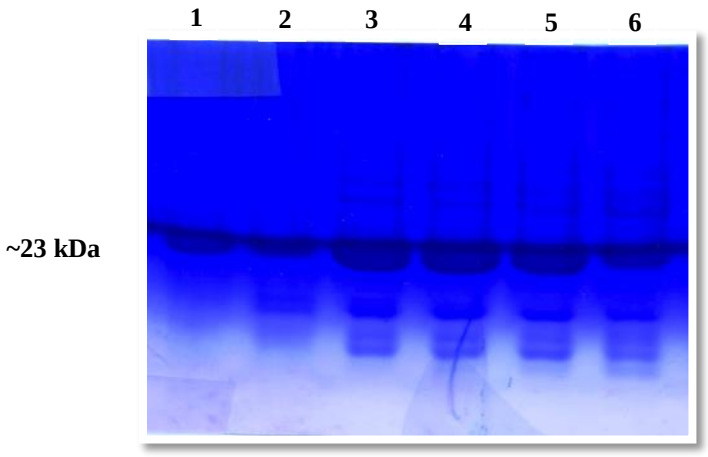

FIGURE 5.4: SDS-PAGE (12%) of wild-type and E165L mutant NR expressed in *E. coli*. Lane 1, wild-type NR; Lanes 2-6: E165L mutant after DEAE column

5.4.4 Dimer rigidification by interactions between one monomer's C-terminus and the beta sheet of the other monomer

To learn whether interaction between the C-terminal extension of one monomer and the other monomer's β-sheet acts to rigidify the dimer, and likewise to learn whether hydrogen bond interactions in the dimer interface correlate with decreased flexibility, we used NMR spectroscopy. 1D proton and 2D ^{1}H-^{15}N HSQC NMR experiments were conducted at low-temperature (4^{o}C) and higher-temperature (32^{o}C). Because the ^{1}H-^{15}N-HSQC spectra of wild-type enzyme (Fig. 4.7 in Chapter 4), were similar at 32^{o}C and 37^{o}C, 32^{o}C was used to observe the higher temperature state instead of 37^{o}C, because after the 21 hours needed for an NMR experiment with 256 transients, enzyme run at 32^{o}C was less precipitated than enzyme run at 37^{o}C. We can then use the same enzyme for further experiments (such as the effect of dicoumarol on the NMR spectra). The results showed that both 1D proton and 2D ^{1}H-^{15}N-HSQC NMR spectra of C217A-NR were only slightly different from those of wild-type enzyme at 32^{o}C (Fig. 5.5B). This indicates that the thiol group (-SH) of Cys217 doesn't have a significant effect on the structure of NR. However the spectra at 4 °C are visibly different (Fig. 5.5A). Both the WT- and the C217A-NR display fewer resonances in a narrower range of ^{1}H chemical shifts when observed at lower temperature. However many fewer backbone resonances were visible in the spectrum of C217A- than in WT-NR. Since ^{1}H-^{15}N-HSQC spectra have the property of being more sensitive to resonances with long T_2 values than to resonances with short T_2s, this implies that more backbone resonances in C217A-NR have short T_2s and we interpret the few very strong resonances as highly mobile side chains and loops of backbone. (Because all low-T ^{1}H-^{15}N-HSQCs were collected using the same number of transients we expect the noise floors to coincide with similar spectral intensities, and because the same concentration of samples were used we expect similar intensities for signals with similar T_2s.) Thus the decrease in the number of residues with T_2 values long enough to permit observation by 2D-NMR is more extreme for the mutant than for the WT. Consistent with an interpretation in terms of shortened T_2s, many of the resonances that remain visible are attributed to side chains on the basis of their characteristic chemical shifts (side chain amides and guanidinium). Thus, C217A-NR appears more prone to conformational exchange than is WT-NR.

We could not obtain NMR data for ΔCys217 because this mutant was not expressed well at all, as mentioned above. Such a change in behavior upon alteration of a single residue is often interpreted to indicate that the residue is important to the stability, folding or solubility of a protein. Such an interpretation is consistent with our findings for C217A that this residue's interactions rigidify the NR dimer.

5.4.5 Effects of the N-terminus

The crystal structure provides an obvious motivation for addressing a possible significance for the C-terminus as a clamp holding monomers together. However we also investigated the possible significance of the N-terminus. This was in part as a control and comparison to support work on the C-terminus and in part from a practical interest in being able to attach a tag to the N-terminus to facilitate purification of the protein. (Tagging the C-terminus was viewed as too likely to perturb the behavior of the protein based on the results described above). The effects of the N-terminal part of NR were studied by comparing the ^{1}H-^{15}N-HSQC spectra obtained from N-terminal His-tagged NR with those of untagged protein at 4°C and 32°C. The spectra shown in Fig. 5.6 indicate that addition of a His_6 tag to the N-terminus of NR via a Gly-Ser linker significantly decreases the T_2 of the protein. Thus we infer that it increases conformational averaging of the protein.

5.4.6 Dimer stabilization by interactions in the dimer interface

Based on the crystal structure (52), the side chain of Glu165 forms a hydrogen bond interaction with the side chain hydroxyl group (-OH) of Ser40 from the other monomer. We propose that disruption of the hydrogen bond between these residues may affect the stability of NR's dimer state and movement of one monomer relative to the other.

The ^{1}H-^{15}N-HSQC spectrum of S40A-NR at 32ºC (Fig. 5.7B) was similar to that of WT-enzyme except that one of the indole resonances shifts 0.5 ppm downfield to 12.1 ppm in the ^{1}H dimension. This resonance also responds to dicoumarol binding while none of the other resolved indole resonances responds to either the mutation or dicoumarol binding (Fig. 5.7B). Thus we infer that the responsive resonance is that of Trp138, the only Trp near the substrate-binding site and Ser40. This provides a tentative assignment of the side chain of Trp138 to the resonance at 11.9 ^{1}H ppm and 129 ^{15}N in

wild-type NR. The movement of the resonance further downfield indicates a stronger hydrogen bond interaction to the indole proton NH group of Trp138 in S40A-NR than in the WT-enzyme.

Apart from the shift of the W138 indole resonance, the ^{1}H-^{15}N-HSQC at 4°C is similar to that of the wild-type (Fig. 5.7A). This suggests that any H-bond between Ser40 and Glu165 does not restrict the slow motions or conformational exchange that are responsible for the loss of dispersed residues from our ^{1}H-^{15}N-HSQCs, since we would have expected much greater loss of the dispersed spectrum in the mutant had that been true.

In contrast to the effects of the S40A mutation, the E165L substitution made a large difference the behavior of NR (Fig. 5.8), most notably that the E165L mutant was not bound to FMN as-isolated. Therefore Fig. 5.9C shows NMR data acquired after addition of 1 mM FMN. The 1D proton and 2D ^{1}H-^{15}N HSQC NMR spectra at 32°C indicate that FMN does bind to E165L-NR, as the resulting NMR spectrum is more dispersed than that in the absence of FMN (Fig. 5.9C). However 1 mM FMN may not saturate all the active sites as the ^{1}H-^{15}N HSQC NMR spectrum is still not fully dispersed as in WT and also does not have the sharp uniform resonances seen for the WT (Fig. 5.9D). At 4°C it is not clear that FMN remains bound (Fig. 5.9A and 5.9B). This is interesting since for WT-NR FMN binding is tighter at 4°C than at 37°C, and the K_ds are 2.2 ± 1.4 μM at 4°C vs. 15.2 ± 3.5 μM at 37°C (Chapter 4).

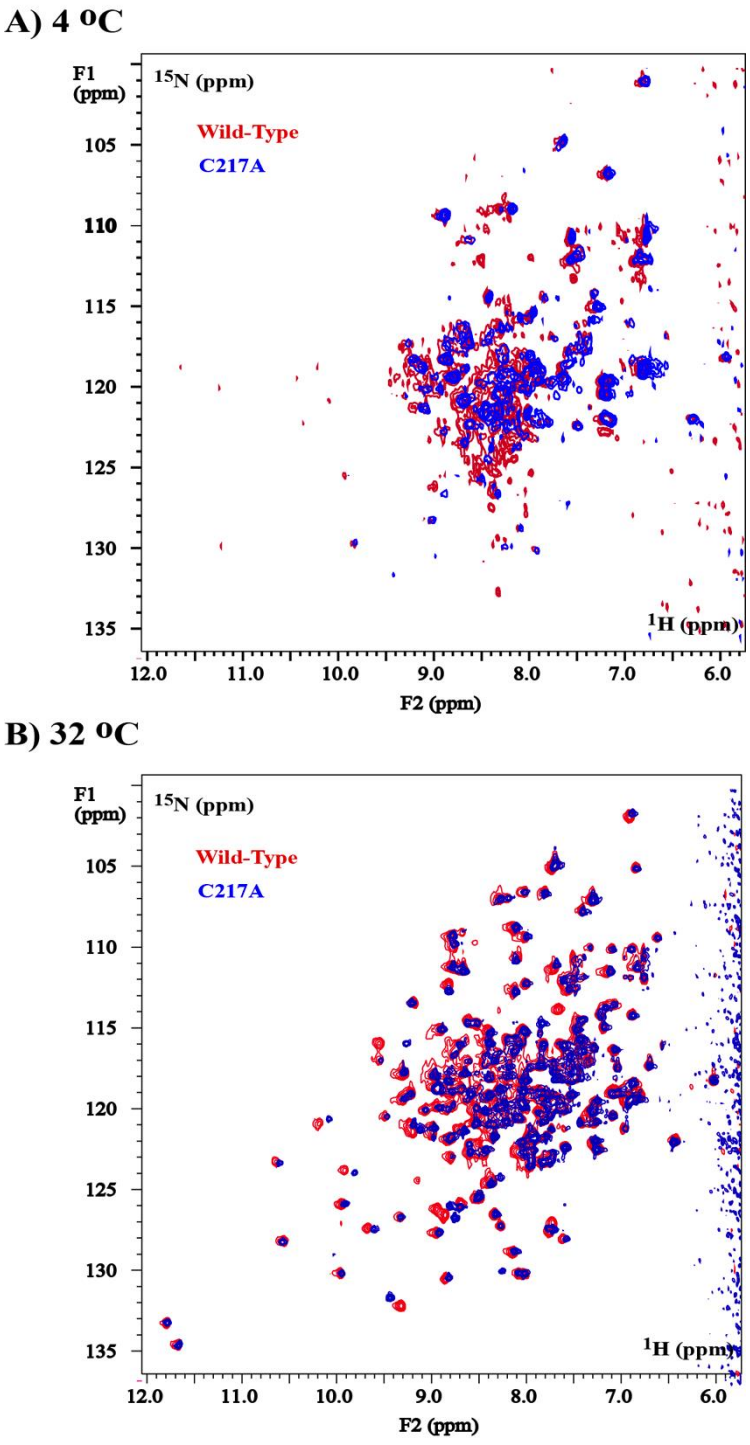

FIGURE 5.5: Overlay 2D ^{1}H-^{15}N HSQC spectra of C217A-NR (blue) with wild-type enzyme (red) in 50 mM KH_2PO_4, 50 mM KCl, 0.2 mM EDTA, 1 mM BME, 0.02% NaN_3, pH 7.50 at 4°C and 32°C.

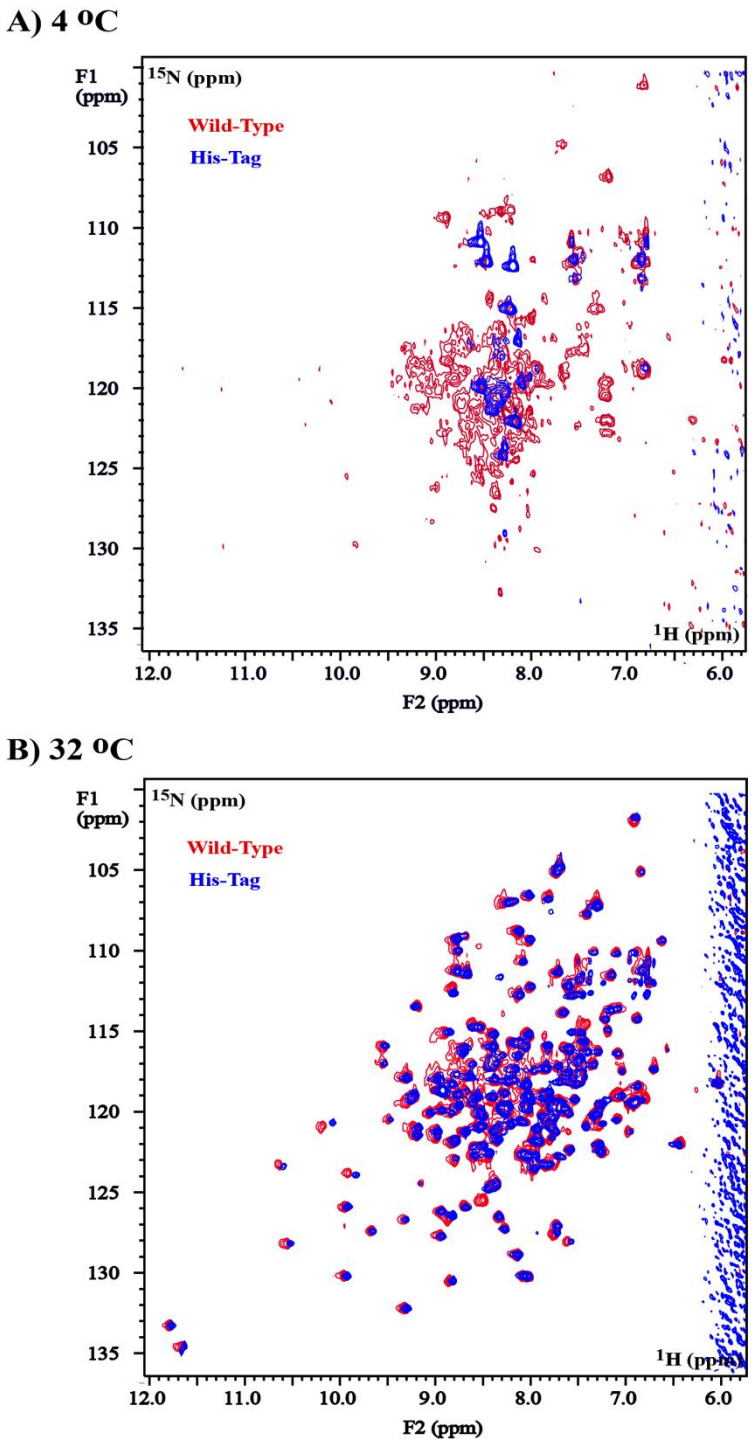

FIGURE 5.6: Overlay of 2D ^{1}H-^{15}N HSQC spectra of N-terminally His-tagged NR (blue) with wild-type enzyme (red) in 50 mM KH_2PO_4, 50 mM KCl, 0.2 mM EDTA, 1 mM BME, 0.02% NaN_3, pH 7.50 at 4°C and 32°C.

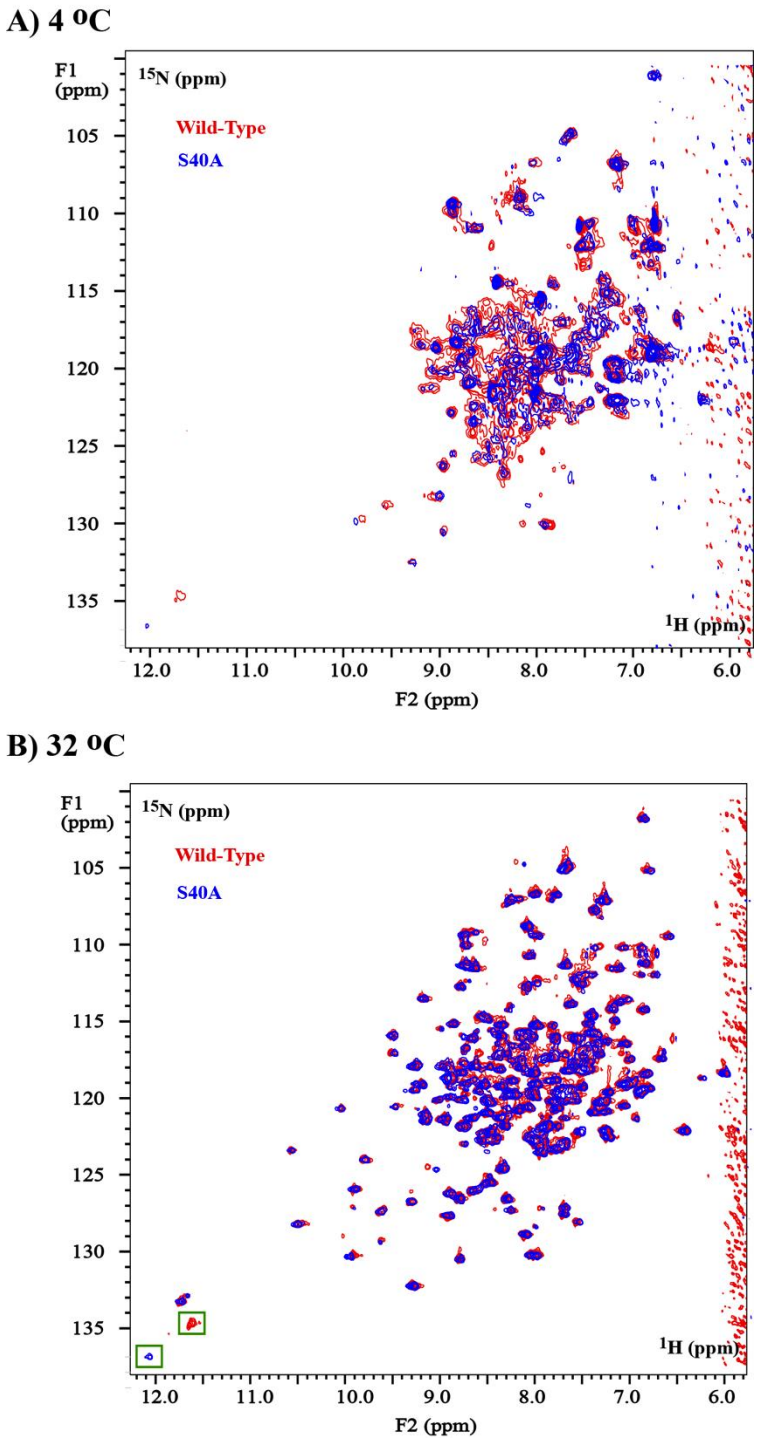

FIGURE 5.7: Overlay of 2D ^{1}H-^{15}N HSQC spectra of S40A-NR (blue) with wild-type enzyme (red) in 50 mM KH_2PO_4, 50 mM KCl, 0.2 mM EDTA, 1 mM BME, 0.02% NaN_3, pH 7.50 at 4°C and 32°C and the responsive tryptophan resonance is labeled green rectangular.

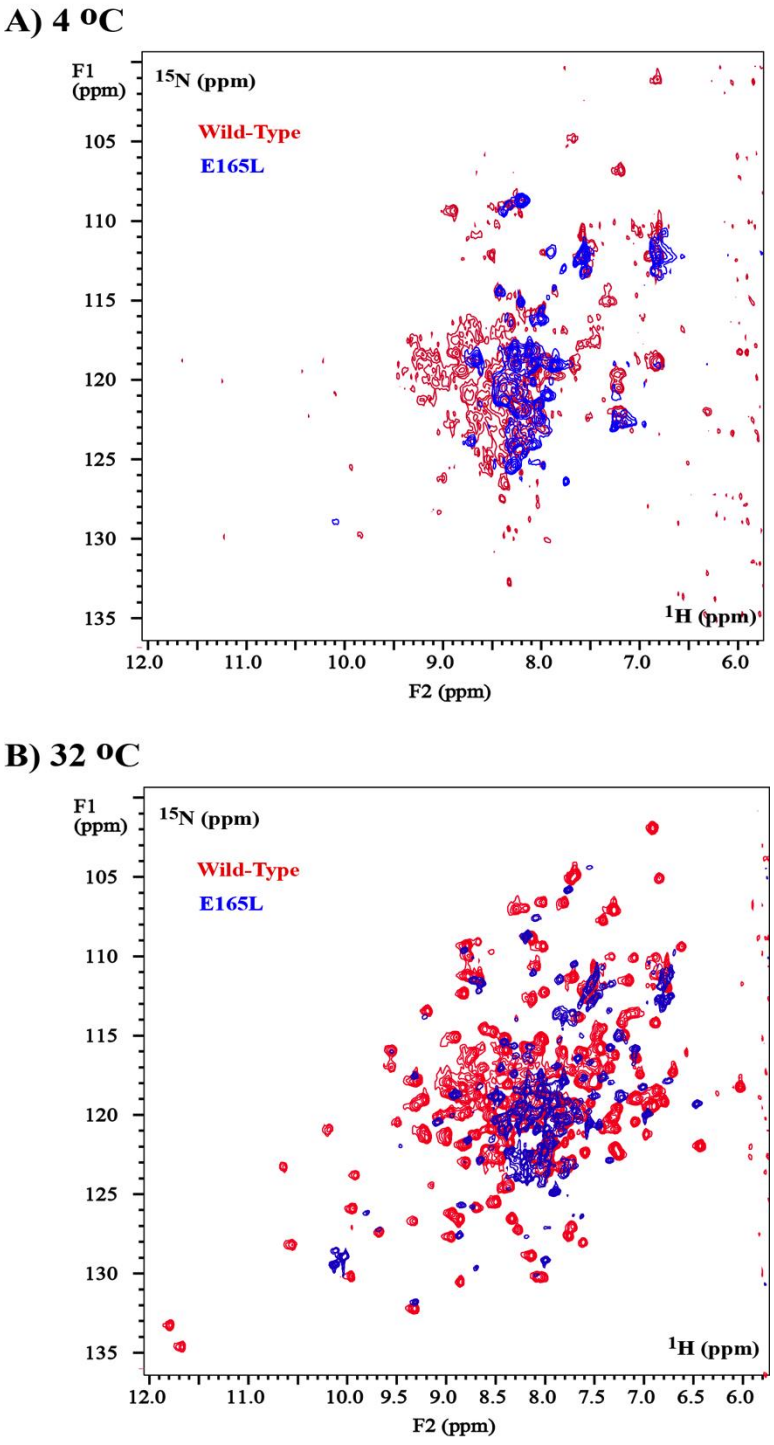

FIGURE 5.8: Overlay of 2D ^{1}H-^{15}N HSQC spectra of E165L-NR (blue) with wild-type enzyme (red) in 50 mM KH_2PO_4, 50 mM KCl, 0.2 mM EDTA, 1 mM BME, 0.02% NaN_3, pH 7.50 at 4°C and 32°C.

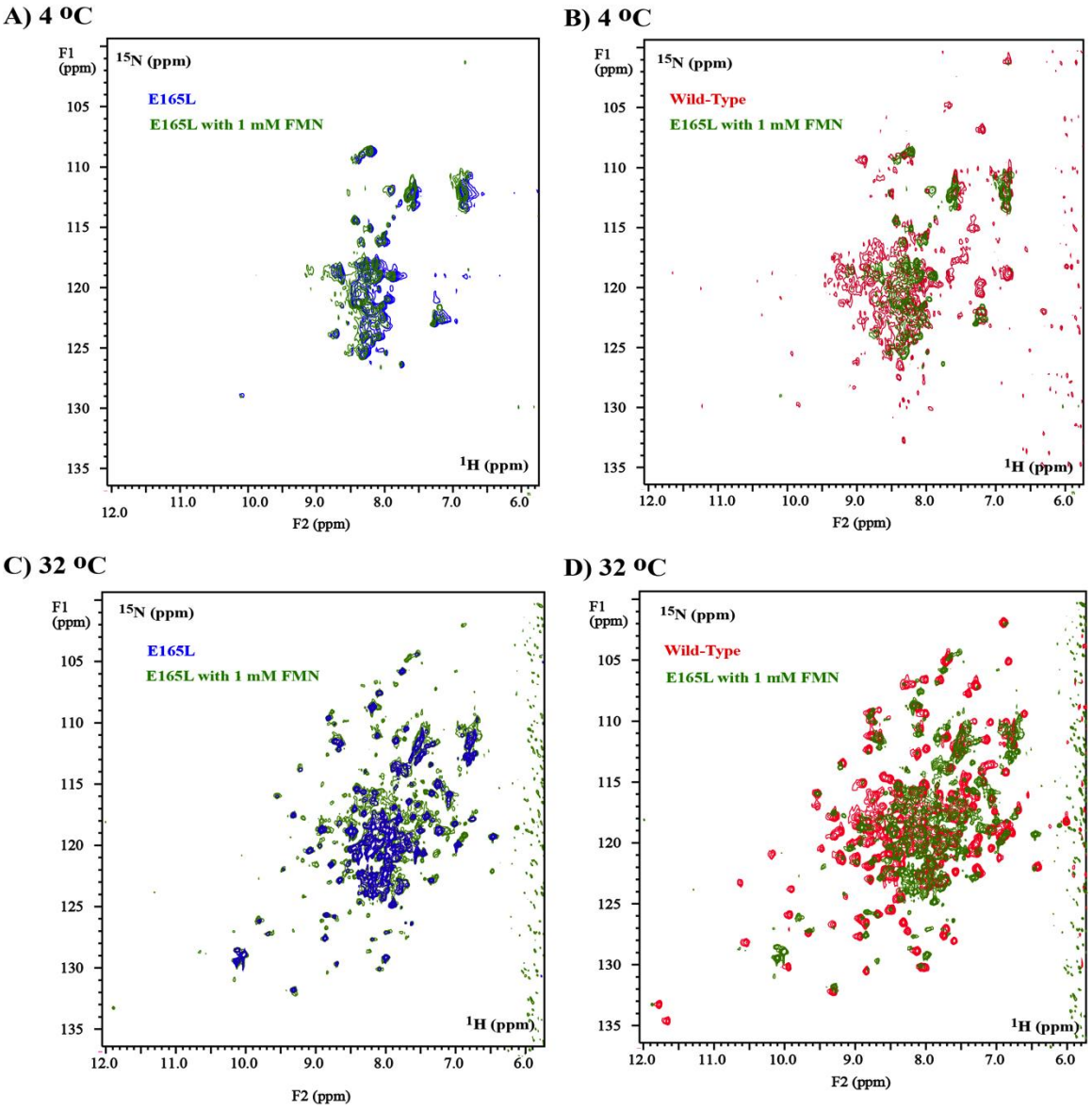

FIGURE 5.9: Overlay of 2D ^{1}H-^{15}N HSQC spectra of A) E165L-NR without (blue) and with (green) 1 mM FMN at 4ºC. B) E165L-NR with 1 mM FMN added (green) and wild-type enzyme (red) at 4ºC. C) E165L-NR without (blue) and with (green) 1 mM FMN at 32ºC. D) E165L-NR with 1 mM FMN (green) and wild-type enzyme (red) at 32ºC. All samples were prepared in 50 mM KH_2PO_4, 50 mM KCl, 0.2 mM EDTA, 1 mM BME, 0.02% NaN_3 at pH 7.50.

5.4.7 Oligomerization state of NR in solution

Mutation of E165 clearly affected FMN binding, and absence of FMN produced symptoms analogous to those of the mutation. Both FMN binding and Glu165 reside in the NR dimer interface. Therefore we investigated the oligomeric state of NR and selected mutants.

Native gel electrophoresis suggests that WR- and C217A-NR retain the same oligomerization state at low (4°C) and high (32°C) temperature. In contrast, C217A- and N-terminal His-tagged NR showed 2 bands at low temperature (4°C), but only one band was observed at high temperature (32°C) (Fig. 5.10) suggesting that both C217A and N-terminal Hig-tag affect the oligomeric state of NR at low temperature. These findings correlate well with the 2D ^{1}H-^{15}N HSQC results.

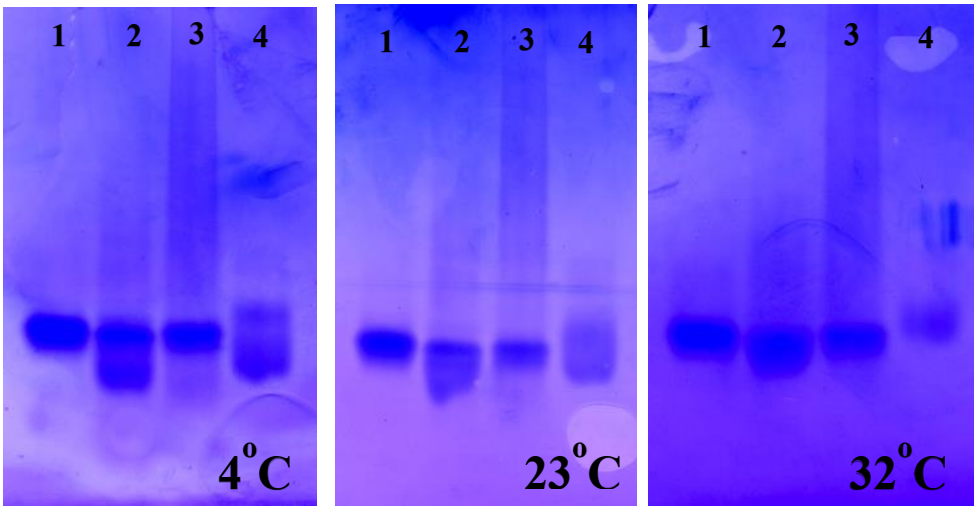

FIGURE 5.10: Native gel electrophoresis (4-20%) of 1: wild-type enzyme, 2: C217A, 3: S40A, and 4: N-terminal Hig-tagged-NR at 4, 23, 32°C.

5.4.8 Redox potential determination of wild-type and mutants NR

The above data indicate that both mutations of residues in the dimer interface and mutations affecting the termini both weaken dimerization and enhance slow internal motions or conformational exchange in NR. The E165L mutation also significantly weakened flavin binding, consistent with the fact that Glu165 is within the dimer interface and the flavin ring binds in the interface between monomers. Thus we have evidence that this mutation weakens interactions between the protein and the isoalloxazine ring. When these interactions favor one oxidation state of the isoalloxazine ring system over others, they shift the redox potentials of the flavin. Thus, the midpoint potential of FMN bound to the protein informs us as to the difference between the affinity for reduced FMN vs. that for oxidized FMN. Because the side chain of Ser40 is in the dimer interface and close to the flavin ring (Fig. 5.1A), it is possible that our replacement of this residue with the less polar Ala might influence the redox potential of the flavin. This is of course also true for the mutant in which Glu165 is replaced by Leu. Although oxidized FMN binds to E165L-NR more weakly than to WT-NR, it is possible that reduced FMN could bind to E165L- with similar affinity as to WT-NR and that the altered FMN binding site could be specific to the reduced state. Such an eventuality would produce an elevated redox potential.

To learn whether NR's preference for oxidized vs. reduced FMN has been altered by any of the mutations, we measured the redox potential of WT- and mutant NRs. The reduction potentials of wild-type and S40A-NR mutant were determined using phenosafranine as the reference dye (E_m^0 = -252 mV) as described in 'Experimental Procedures'. Data from a sample WT-NT titration are shown in Fig. 5.11 and spectra from a titration of S40A-NR are shown in Fig. 5.12. Absorbance at wavelengths of 454 and 521 nm was used to calculate the concentrations of oxidized enzyme and dye at each point in the titration, as described in 'Experimental Procedures'. The results showed that WT- and S40A-NR as well as the dye were reduced by the xanthine/xanthine oxidase system via a two-electron reduction process because slopes from the plots of $\log(E_{red}/E_{ox})$ vs. $\log(D_{red}/D_{ox})$ were ~1.0 and 1.4 (inset to Fig. 5.11 and Fig. 5.12). The midpoint potentials (E_m^0) calculated form the plots are -213 mV for wild-type NR and -215 mV for S40A-NR, which are within error of one another.

The reduction midpoint potential of the C217A-NR and A51C-NR were also determined using phenosafranine as the standard dye. Even though Cys217 and the cross-linking of C217/A51C are not located in the active site of NR, substitution of these residues could affect the stability and flexibility of the dimer via the interactions of one domain's C-terminus and the beta sheet of the other. Since the flavin is in the dimer interface, it could in turn be affected (Fig. 5.1A) (52). C217A-NR or A51C-NR and dye were reduced by xanthine/xanthine oxidase and absorbance at 454 and 521 nm was used to calculate the amount of the oxidized enzyme and dye, as above. The slope from the plot was ~1.2 for C217A-NR (inset to Fig. 5.13) and 1.0 for A51C-NR (inset to Fig. 5.14) and the midpoint potentials of the NR variants (E_m^0) were calculated to be -217 mV for C217A-NR and -215 mV for A51C-NR, unchanged from the wild-type enzyme, indicating that C217A substitution and cross linking C217A/A51C either cause negligible effects on the flavin binding site or cause the energies of the reduced and oxidized states change in the same way. The former is consistent with the lack of any effect on the absorption maximum.

TABLE 5.1: Reduction potentials (E_m^0) of wild-type and mutant NRs at 25°C, pH 7.50.

	(E_m^0), mV
Wild-type	-213
S40A	-215
C217A	-217
A51C (without DTT)	-215

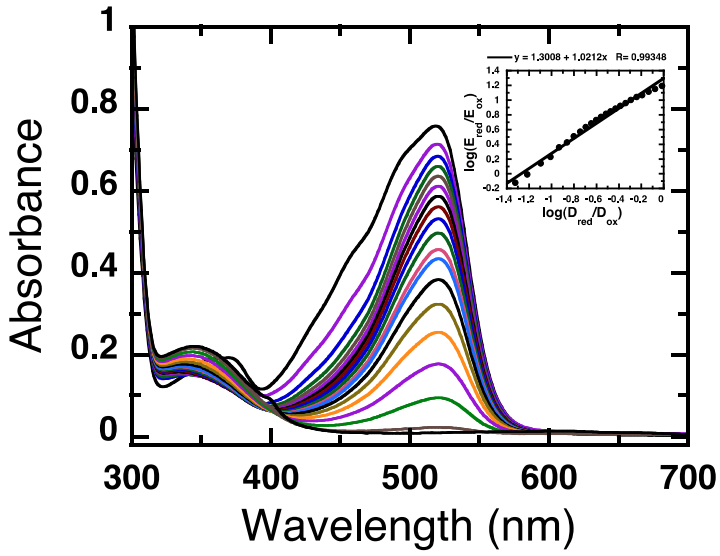

FIGURE 5.11: Redox potential determination of wild-type enzyme using phenosafranine as the standard dye. The reaction contained 400 µM xanthine, 3 nM xanthine oxidase (side arm), 2 µM benzyl viologen, 18 µM wild-type enzyme and 18 µM phenosafranine. Enzyme and dye were slowly reduced under anaerobic conditions by the xanthine/xanthine oxidase system. The top spectrum is that of a mixture of the fully oxidized enzyme and dye, and the bottom absorption spectrum is that of the fully reduced enzyme and dye. The inset shows a plot of $\log(E_{red}/E_{ox})$ versus $\log(D_{red}/D_{ox})$. The slope of the plot of $\log(E_{red}/E_{ox})$ *versus* $\log(D_{red}/D_{ox})$ is 1.0, indicating that two electrons are involved in the reduction of the enzyme and the dye. The redox potential ($E^{o'}_{m}$) for WT-NR is –213 mV.

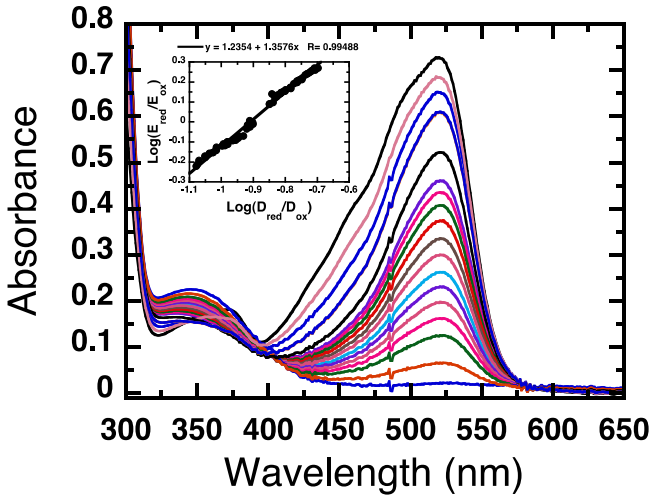

FIGURE 5.12: Redox potential determination of S40A-NR using phenosafranine as the standard dye. The reaction contained 400 µM xanthine, 3 nM xanthine oxidase (side arm), 2 µM benzyl viologen, 18 µM Ser40Ala mutant and 18 µM phenosafranine. Enzyme and dye were slowly reduced under anaerobic conditions by the xanthine/xanthine oxidase system. The top spectrum is that of a mixture of the fully oxidized enzyme and dye, and the bottom absorption spectrum is that of the fully reduced enzyme and dye. The inset shows a plot of $\log(E_{red}/E_{ox})$ versus $\log(D_{red}/D_{ox})$. The slope of the plot of $\log(E_{red}/E_{ox})$ *versus* $\log(D_{red}/D_{ox})$ is 1.4, indicating that two electrons are involved in the reduction of enzyme and dye. The redox potential ($E^{o'}_{m}$) for S40A-NR is –215 mV.

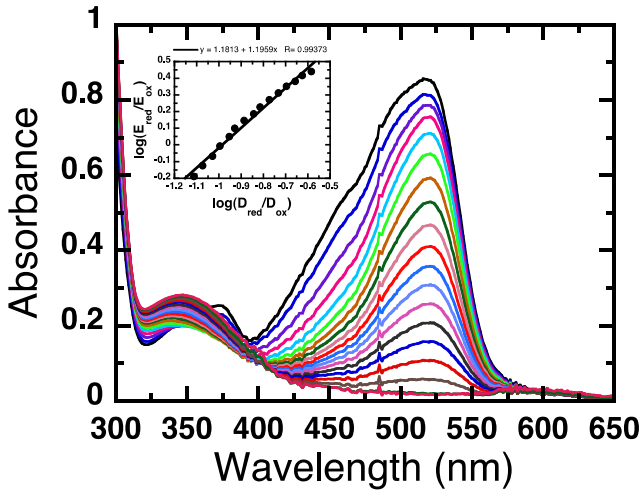

FIGURE 5.13: Redox potential determination of C217A-NR using phenosafranine as the standard dye. The reaction contained 400 µM xanthine, 3 nM xanthine oxidase (side arm), 2 µM benzyl viologen, 18 µM C217A-NR and 18 µM phenosafranine. Enzyme and dye were slowly reduced under anaerobic conditions by the xanthine/xanthine oxidase system. The top spectrum is that of a mixture of the fully oxidized enzyme and dye, and the bottom absorption spectrum is that of the fully reduced enzyme and dye. The inset shows a plot of log(E_{red}/E_{ox}) versus log(D_{red}/D_{ox}). The slope of the plot of log(E_{red}/E_{ox}) *versus* log(D_{red}/D_{ox}) is 1.2, indicating that two electrons are involved in the reduction of enzyme and dye. The redox potential ($E^{o'}_{m}$) for C217A-NR is -217 mV.

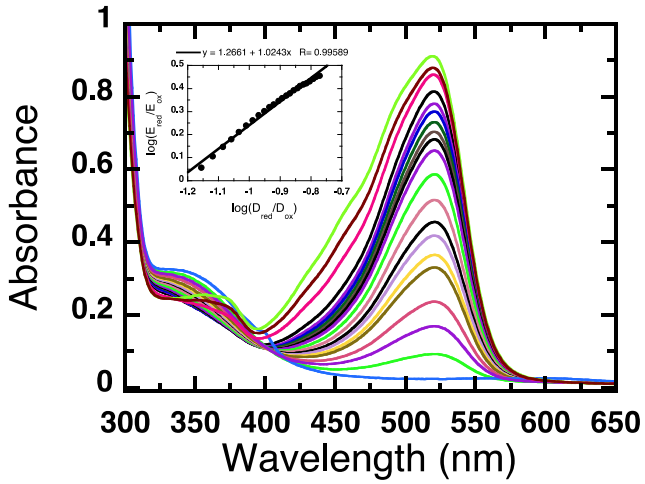

FIGURE 5.14: Redox potential determination of A51C-NR in the absence of 1mM DTT using phenosafranine as the standard dye. The reaction contained 400 µM xanthine, 3 nM xanthine oxidase (side arm), 2 µM benzyl viologen, 18 µM A51C-NR and 18 µM phenosafranine. Enzyme and dye were slowly reduced under anaerobic conditions by the xanthine/xanthine oxidase system. The top spectrum is that of a mixture of the fully oxidized enzyme and dye, and the bottom absorption spectrum is that of the fully reduced enzyme and dye. The inset shows a plot of $\log(E_{red}/E_{ox})$ versus $\log(D_{red}/D_{ox})$. The slope of the plot of $\log(E_{red}/E_{ox})$ *versus* $\log(D_{red}/D_{ox})$ is 1.2, indicating that two electrons are involved in the reduction of enzyme and dye. The redox potential ($E^{o'}_{m}$) for A51C-NR is -215 mV.

5.4.9 Determination of the dissociation constant (K_d) for binding of dicoumarol to A51C-NR

We would like to understand the role of C-terminal domain swap. This motif is conserved in all the NRs of the same class for which crystal structures are available. We would like to know whether this feature has any special purpose for conformational flexibility? For example the C-terminus' participation in the β sheet of the other monomer could serve to hold the two monomers together providing stability for the dimer, but it could do so independent of the contents of the dimer interface where the flavin ring and substrates bind. Thus it could provide a device that could free the dimer interface to accommodate more diverse ligands at lower cost to dimer stability.

We addressed this question by making a specific cross-link with another thiol group in the other monomer, thus making the interaction between monomers permanent and rigid. To achieve this, we studied the protein structure and discovered that the side chain of C217 is very close to the methyl of Ala51 from the other monomer (3.6 Å). We have mutated Ala51 to Cys, which can lock together the folded conformations of two monomers by cross-linking. Disulfide cross-linking was introduced as described in the 'Experimental Procedures'. We hypothesized that formation of a disulfide bond between monomers may diminish the ability of this protein to bind dicoumarol. However, the results showed that the dissociation constants (K_d) determined at 4^{o}C and 32^{o}C were 3.3 ± 1.3 μM and 6.5 ± 1.5 μM, respectively (Fig. 5.15), which were similar to those observed in wild-type NR (4^{o}C = 2.2 ± 1.4 μM and 32^{o}C = 6.9 ± 2.3 μM) indicating that the movement of C-terminal domain was not significantly contributed to the flexibility around the NR's active site. However the mutant's sensitivity to temperature as indicated by the change in K_d, 6.5/3.3 ≈ 2, is smaller than that of WT, 6.9/2.2 ≈ 3, consistent with rigidification due to the introduction of a cross-link. Based on our ^{1}H-^{15}N HSQC spectra of ^{15}N glycine-labeled NR, the regions of NR most affected by substrate binding are on the F helix (Fig. 4.16 in chapter 4), as also indicated by B-factors from the crystal structure (52) and MD simulation (57).

A) 4°C

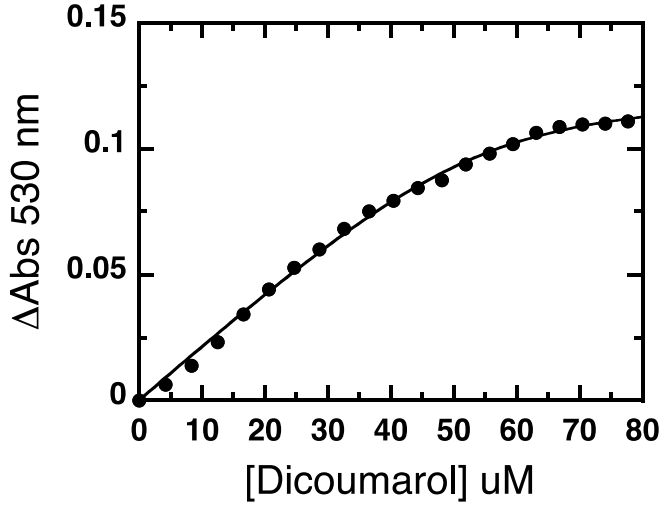

B) 32°C

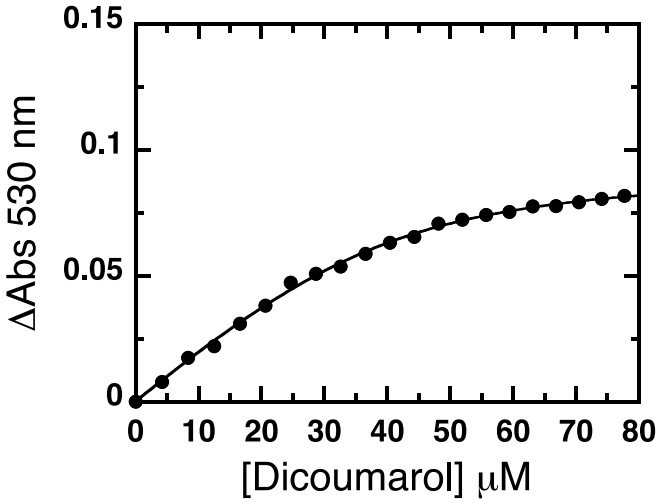

Figure 5.15: Binding of the inhibitor dicoumarol to A51C-NR in the presence of H_2O_2 observed at temperature 4 °C (A) and 32°C (B). 35 μM wild-type enzyme was in 50 mM KH_2PO_4, 50 mM KCl at pH 7.50. The maximum absorbance change at 530 nm was hyperbolically dependent on the concentration of dicoumarol present. The concentration of dicoumarol giving half-saturation represents the K_d value for the binding of dicoumarol to A51C-NR at observed temperature 4°C (3.3 ± 1.3 μM) and 32°C (6.5 ± 1.5 μM). Standard errors of the fits are given in parentheses, the experimental uncertainty (due to pipetting etc.). The K_d extracted by fitting the entire data set to Eq. 4.1 in Chapter

5.5 DISCUSSION

Full-length NR has 217 amino acid residues, with cysteine at the C-terminal end. An intriguing and clearly visible feature of the dimeric form of NR is a domain-swapped strand whereby the C-terminal (Cys217) contributes to the fifth β-stand of the other monomer by lying parallel to that β-stand (Fig. 1.6A in Chapter 1). This swap may contribute to dimer stability. We hypothesize that the presence of this strand preserves the dimeric structure even when interactions within the dimer interface are weakened or altered to accommodate substrate binding. Thus the presence of the C-terminus' interactions may be crucial to the possibility of active site flexibility at the same time as dimer stability.

Mutation of Cys217 to Ala has allowed us to assess the importance of the thiol group (-SH) at the C-terminus. The expression results show that C217A-NR expressed and accumulated as well as the wild-type enzyme, and removal of the thiol group at the C-terminus in the C217A-NR does not make any significant change in the 32°C HSQC but does appear to modulate the severity of the low-temperature effect on the HSQC (Fig. 5.5), with the result that the loss of apparent dispersion was somewhat more severe. There is no nearby Cys residue that could form a disulfide with Cys217 in WT-NR and the Cys side chain appears to be solvent-exposed, which is normally taken to suggest that the side chain will not exert an effect on the structure of the protein. However the presence of a polar group in this exposed position may increase the stability of the folded structure over the C217A-mutant, which presumably exposes the methyl of Ala to solution (although the Ala side chains are not normally considered strongly non-polar). The other big difference is that the Cys side chain is much more polarizable than the methyl of Ala.

In contrast, deletion of Cys217 produced a protein that could not be over-expressed into the soluble fraction in significant yields, unlike all the other variants studied here. This suggests that the C-terminal backbone is critical for protein stability or solubility. The crystal structure shows that carboxyl group of Cys217 forms a hydrogen bond with the NH backbone of Ser52 (2.9 Å) and the hydroxyl side-chain of Thr53 (2.5 Å), both of the other monomer (Fig. 5.3). These non-covalent interactions may help to fix one monomer in a specific orientation relative to the other, in essence limiting rotation

relative to the axis perpendicular to the dimer interface. Thus we propose that the interactions between the backbone functionalities of Cys217 limit enzyme dynamics and control the flexibility around the active site preventing NR's monomers from coming apart when NR binds certain of substrates.

Not only the C-terminus, but also the N-terminus is important to NR's dynamics. Addition of a His-tag to the N-terminus of also affects the dynamics, as the low-temperature HSQC was much more depleted of dispersed resonances than that of the wild-type NR although spectra obtained at higher temperatures were almost the same as those observed in wild type enzyme (Fig. 5.6).

For mutations affecting residues in the dimer interface (Glu165 and Ser40), protein expression levels remained high and protein was found in the crude extract suggesting WT-like protein solubility. However E165L-NR did not bind FMN even though the latter was provided at the time of cell breakage. This indicates that Glu165 is significant for FMN binding. Indeed when FMN was provided to purified E165L-NR at a concentration of 1 mM FMN, NMR spectra of the protein and fluorescence of the flavin indicated that the protein did not bind it. Replacing the polar side chain of Glu with the non-polar side-chain of Leu may alter the backbone's interactions with the nearby residues with which it normally H-bonds (Ser40 and Trp138) and change the electrostatic environment around the flavin binding site. However we were surprised by the magnitude of the effect since the side chain of residue 165 is directed away from the FMN binding site (Fig. 5.1A). Moreover the NR homologue NADH oxidase (NADOX) from *Thermus thermophilus* employs a Leu residue in the place of NR's Glu. Indeed, the indole group of Trp138 hydrogen bonds to the carboxyl side-chain of Glu165 (2.9 Å) in WT-NR. The indole may retain the ability to interact with Leu, but now via hydrophobic interactions as in NADOX in which Leu158 interact with Ala46, Trp131, and Tyr137 via hydrophobic interactions (Fig. 5.16). This may be a reason why removal of the hydrogen bond interaction between hydroxyl group of Ser40 and carboxyl side-chain of Glu165 did not affect enzyme expression.

Given the drastic consequences of mutating Glu165, we were surprised that mutation of the H-bonding partner Ser40 has only relatively subtle effects on the HSQC, even at lower temperature. We propose that this is because Trp138 is present and able to

satisfy Glu165's H-bonding potential. Indeed, we observed that the indole group of Trp138 shifts downfield shift (Fig. 5.7B) indicating a stronger H-bond interaction with Glu165 in the absence of an H-bond from Ser40. It would be interesting to know the pK_a of this Glu. Glu165, Ser40 and Trp138 are all conserved in the NR from *E. coli*. However the homologous enzyme of *Thermus thermophilus* replaces Glu165 and Ser40 with Leu and Ala, respectively (Fig. 5.16), thus replacing a polar interaction with a non-polar one.

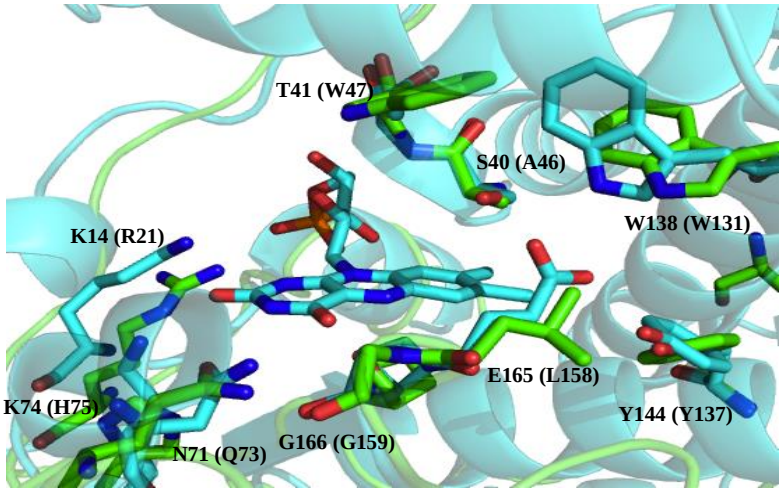

FIGURE 5.16: Overlay of the active site of NR (cyan, PDB 1NEC) and NADOX (green). The NADOX's residues are displayed within parentheses.

The redox potentials of C217A-NR ($E^{o'}_m$ = -217 mV), A51C-NR ($E^{o'}_m$ = -215 mV) and S40A-NR ($E^{o'}_m$ = -215 mV) mutant enzymes were similar to that of wild-type enzyme ($E^{o'}_m$ = -213 mV) indicating that the C-terminal C217A-NR mutant and the cross-linking C217A/A51C did not significantly affect the electrostatic nature of the active site around the flavin ring, as this would cause conversion of neutral oxidized FMN to anionic reduced FMN to be associated with a different energy change. Ser40 which is on the ^{39}S-S-T-N^{42} loop located near the active site of NR helps to mediate substrate binding, but does not participate in any interaction with the isoalloxazine ring. This is consistent with the absence of a role in modulation of flavin's redox potential.

CHAPTER 6

CONCLUSIONS AND FUTURE WORK

In summary, we have completed the first comprehensive study of the transient kinetics of NR. We find that the kinetic mechanism is a very simple one, for both reduction and oxidation. This can allow NR to transform a wide range of substrates. The results of our NMR investigation suggest that NR displays more dynamics in the presence of substrate analog and the movement of helix F helps this enzyme to accommodate diverse substrates. Although the NMR data might be taken to suggest that NR changes conformation in the course of turnover, the kinetic studies argue that any conformational change is only part of the basis for NR's promiscuity. Such information is critical to our understanding of the link between enzyme functional dynamics and the kinetic mechanism underlying NR's broad substrate repertoire.

For full insight, analogous studies should be conducted with a selection of other substrates chosen to represent the span of sizes and functionalities represented among NR's substrates.

This work has a much broader significance than simply reduction of nitroaromatics. It addresses fundamental questions applicable to other enzymes' ability to transform very different substrates. It also addresses evolution of new enzymes from old, in which an enzyme with a specialized function can be evolved to acquire new needed function. If we can understand these adaptive mechanisms, perhaps we can use this insight to engineer enzymes for other non-natural substrates.

Now that we have observed a connection between ligand binding and dynamics we aim to understand the loss of dispersed resonances from the 2D spectra, despite their retention in 1D spectra. This phenomenon is consistent with faster T_2 relaxation for resonances in exchange with an exchange partner separated by a larger chemical shift difference. Moreover the apparent loss of dispersion affects the ^{1}H dimension much more than the ^{15}N dimension. This is reasonable since the dispersion of ^{15}N chemical shifts is believed to reflect the distinct identities of amino acids more strongly whereas ^{1}H

chemical shifts are more sensitive to interactions such as H-bonding and the local environment. Similar loss of dispersion in the ^{1}H dimension has been observed in other cases, such as the drk domain studied by Forman-Kay and Kay. We hypothesize that the resonances observed in our HSQCs are more susceptible to relaxation than side chain resonances we observed because backbone amides have the capacity to exchange protons with water. The resonances further from that of water are strongly represented among the first to be lost (as the temperature is decreased). Thus we hypothesize that exchange with water accelerates at lower temperature and this results in shortened T_2s that in turn cause the HSQC to detect a smaller subset of all backbone positions. The 1D spectra shown throughout this section demonstrate that the dispersion of amide protons *per-se* is not diminished, just the dispersion of those observed in 2D. Production of Val, Ile (δ1), and Leu methyl-protonated ^{15}N-, ^{13}C, ^{2}H-labeled protein using proteated amino acids and amino acid precursors ([3,3-$^{2}H_2$]α-Ketobutyrate to generate (^{1}H-δ1 Methyl)-Isoleucine and [3-2H]α-Ketoisovalerate to generate (1H-γ Methyl)-Valine and (1H-δ Methyl)-Leucine) in a D_2O media (181,182) can be used to generate protein for ^{13}C-^{1}H HSQC spectrum of the methyl region of Val, Ile (δ1), and Leu of NR. The strategy of this selective protonation is to increase T_2s for better resolution and sensitivity at lower temperature HSQC NMR. Thus we will test the hypothesis that accelerated exchange with water shortens the T_2s of amide protons at lower temperature, because this mechanism should not affect the side chain methyl Hs, whereas relaxation mediated by conformational change should affect at least a fraction of methyl Hs.

2D ^{1}H-^{15}N HSQC NMR for ^{15}N glycine-labeled NR showed a resonance shift consistent with slow dynamics in helix F when oxidized NR was bound with the substrate analog dicoumarol, so **Ex**change **S**pectroscop**y** (EXSY) or the zz exchange experiment ($k_{ex} \approx 0.2 – 100\ s^{-1}$; $k_{ex} << \Delta\nu$) (145,183) will be used to probe this dynamic process. The dependence of peak intensities for resonances affected by two-state exchange (A↔B) will be plotted vs. exchange time to determine the exchange rate constants k_a and k_b. Thus we will learn whether the conformational change we observe could be catalytically competent.

REFERENCES

1. Massey, V., and Ghisla, S. (1983). in *Biological Oxidations*, Colloq.-Mosbach (Sund, H. & Ullrich, V., eds), Springer-Verlag Berlin. pp 114–139
2. Ghisla, S., and Massey, V. (1989) Mechanisms of Flavoprotein-Catalyzed Reactions. *Eur J Biochem* **181**, 1-17
3. Bernstein, F. C., Koetzle, T. F., Williams, G. J., Meyer, E. F., Jr., Brice, M. D., Rodgers, J. R., Kennard, O., Shimanouchi, T., and Tasumi, M. (1977) The Protein Data Bank: a computer-based archival file for macromolecular structures. *J Mol Biol* **112**, 535-542
4. Fischbach, M. A., and Walsh, C. T. (2006) Assembly-line enzymology for polyketide and nonribosomal Peptide antibiotics: logic, machinery, and mechanisms. *Chem Rev* **106**, 3468-3496
5. Walsh, C. T., and Wencewicz, T. A. (2013) Flavoenzymes: Versatile catalysts in biosynthetic pathways. *Nat Prod Rep* **30**, 175-200
6. Ghisla, S., and Massey, V. (1986) New Flavins for Old - Artificial Flavins as Active-Site Probes of Flavoproteins. *Biochem J* **239**, 1-12
7. Pettersen, E. F., Goddard, T. D., Huang, C. C., Couch, G. S., Greenblatt, D. M., Meng, E. C., and Ferrin, T. E. (2004) UCSF chimera - A visualization system for exploratory research and analysis. *J Comput Chem* **25**, 1605-1612
8. Massey, V., and Palmer, G. (1966) On the existence of spectrally distinct classes of flavoprotein semiquinones. A new method for the quantitative production of flavoprotein semiquinones. *Biochemistry* **5**, 3181-3189
9. Unno, H., Yamashita, S., Ikeda, Y., Sekiguchi, S., Yoshida, N., Yoshimura, T., Kusunoki, M., Nakayama, T., Nishino, T., and Hemmi, H. (2009) New Role of Flavin as a General Acid-Base Catalyst with No Redox Function in Type 2 Isopentenyl-diphosphate Isomerase. *Journal of Biological Chemistry* **284**, 9160-9167
10. Massey, V. (1995) Flavoprotein Structure and Mechanism - Introduction. *Faseb J* **9**, 473-475

11. van Berkel, W., Benen, JA., Eppink, MH., Fraaije, MW. . (1999) Flavoprotein kinetics. in *Methods Mol Biol.* . pp 61-85
12. Entsch, B., Ballou, D. P., and Massey, V. (1976) Flavin-oxygen derivatives involved in hydroxylation by p-hydroxybenzoate hydroxylase. *The Journal of biological chemistry* **251**, 2550-2563
13. Entsch, B., and Ballou, D. P. (1989) Purification, properties, and oxygen reactivity of p-hydroxybenzoate hydroxylase from Pseudomonas aeruginosa. *Biochimica et biophysica acta* **999**, 313-322
14. Arunachalam, U., and Massey, V. (1994) Studies on the Oxidative Half-Reaction of P-Hydroxyphenylacetate 3-Hydroxylase. *Journal of Biological Chemistry* **269**, 11795-11801
15. Engel, P. C. (1992) Acyl-coenzyme A dehydrogenases. in *Chemistry and Biochemistry of Flavoenzyme (Müller, F., ed)*, CRC Press, Boca Raion, Florida. pp 597-655
16. Kohn, L. D., and Kaback, H. R. (1973) Mechanisms of Active-Transport in Isolated Bacterial Membrane Vesicles .15. Purification and Properties of Membrane-Bound D-Lactate Dehydrogenase from Escherichia-Coli. *Journal of Biological Chemistry* **248**, 7012-7017
17. Ackrell, A., Johnson, MK., Gunsalus, PR., and Cecchini, G. (1992). in *Chemistry and Biochemistry of Flavoenzymes (Muller, F., ed)* CRC Press, Boca Raton, FL. . pp 229-297
18. Sucharitakul, J., Prongjit, M., Haltrich, D., and Chaiyen, P. (2008) Detection of a C4a-hydroperoxyflavin intermediate in the reaction of a flavoprotein oxidase. *Biochemistry* **47**, 8485-8490
19. Friedman, J. E., Watson, J. A., Jr., Lam, D. W., and Rokita, S. E. (2006) Iodotyrosine deiodinase is the first mammalian member of the NADH oxidase/flavin reductase superfamily. *J. Biol. Chem* **281**, 2812-2819
20. Bryant, C., Hubbard, L., and McElroy, W. D. (1991) Cloning, nucleotide sequence, and expression of the nitroreductase gene from Enterobacter cloacae. *J. Biol. Chem* **266**, 4126-4130

21. Bryant, C., and DeLuca, M. (1991) Purification and Characterization of an Oxygen-Insensitive NAD(P)H Nitroreductase from Enterobacter cloacae. *J. Biol. Chem.* **266**, 4119-4125

22. Bryant, D. W., Mccalla, D. R., Leeksma, M., and Laneuville, P. (1981) Type-I Nitroreductases of Escherichia-Coli. *Can J Microbiol* **27**, 81-86

23. Peterson, F. J., Mason, R. P., Hovsepian, J., and Holtzman, J. L. (1979) Oxygen-Sensitive and Oxygen-Insensitive Nitroreduction by Escherichia-Coli and Rat Hepatic Microsomes. *Journal of Biological Chemistry* **254**, 4009-4014

24. Smyth, G. E., and Orsi, B. A. (1989) Nitroreductase Activity of Nadh Dehydrogenase of the Respiratory Redox Chain. *Biochem J* **257**, 859-863

25. Marchler-Bauer, A., Zheng, C., Chitsaz, F., Derbyshire, M. K., Geer, L. Y., Geer, R. C., Gonzales, N. R., Gwadz, M., Hurwitz, D. I., Lanczycki, C. J., Lu, F., Lu, S., Marchler, G. H., Song, J. S., Thanki, N., Yamashita, R. A., Zhang, D., and Bryant, S. H. (2013) CDD: conserved domains and protein three-dimensional structure. *Nucleic Acids Res* **41**, D348-352

26. Huson, D. H., Richter, D. C., Rausch, C., Dezulian, T., Franz, M., and Rupp, R. (2007) Dendroscope: An interactive viewer for large phylogenetic trees. *Bmc Bioinformatics* **8**

27. Watanabe, M., Ishidate, M., and Nohmi, T. (1990) Nucleotide-Sequence of Salmonella-Typhimurium Nitroreductase Gene. *Nucleic Acids Res* **18**, 1059-1059

28. Somerville, C. C., Nishino, S. F., and Spain, J. C. (1995) Purification and Characterization of Nitrobenzene Nitroreductase from Pseudomonas Pseudoalcaligenes Js45. *J Bacteriol* **177**, 3837-3842

29. Elanskaya, I. V., Chesnavichene, E. A., Vernotte, C., and Astier, C. (1998) Resistance to nitrophenolic herbicides and metronidazole in the Cyanobacterium Synechocystis sp PCC6803 as a result of the inactivation of a nitroreductase-like protein encoded by drgA gene. *Febs Lett* **428**, 188-192

30. Liu, D., Thomson, K., and Anderson, A. C. (1984) Identification of nitroso compounds from biotransformation of 2,4-dinitrotoluene. *Appl Environ Microbiol* **47**, 1295-1298

31. Koder, R. L., and Miller, A. F. (1998) Steady-state kinetic mechanism, stereospecificity, substrate and inhibitor specificity of Enterobacter cloacae nitroreductase. *Biochimica et biophysica acta* **1387**, 395-405

32. Zenno, S., Koike, H., Tanokura, M., and Saigo, K. (1996) Gene cloning, purification, and characterization of NfsB, a minor oxygen-insensitive nitroreductase from Escherichia coli, similar in biochemical properties to FRase I, the major flavin reductase in Vibrio fischeri. *Journal of biochemistry* **120**, 736-744

33. Hecht, H. J., Erdmann, H., Park, H. J., Sprinzl, M., and Schmid, R. D. (1995) Crystal-Structure of Nadh Oxidase from Thermus-Thermophilus. *Nat Struct Biol* **2**, 1109-1114

34. Tanner, J. J., Lei, B., Tu, S. C., and Krause, K. L. (1996) Flavin reductase P: structure of a dimeric enzyme that reduces flavin. *Biochemistry* **35**, 13531-13539

35. Parkinson, G. N., Skelly, J. V., and Neidle, S. (2000) Crystal structure of FMN-dependent nitroreductase from Escherichia coli B: a prodrug-activating enzyme. *J Med Chem* **43**, 3624-3631

36. Kobori, T., Sasaki, H., Lee, W. C., Zenno, S., Saigo, K., Murphy, M. E. P., and Tanokura, M. (2001) Structure and site-directed mutagenesis of a flavoprotein from Escherichia coli that reduces nitrocompounds - Alteration of pyridine nucleotide binding by a single amino acid substitution. *Journal of Biological Chemistry* **276**, 2816-2823

37. Lovering, A. L., Hyde, E. I., Searle, P. F., and White, S. A. (2001) The structure of Escherichia coli nitroreductase complexed with nicotinic acid: three crystal forms at 1.7 A, 1.8 A and 2.4 A resolution. *J Mol Biol* **309**, 203-213

38. Knox, R. J., Boland, M. P., Friedlos, F., Coles, B., Southan, C., and Roberts, J. J. (1988) The Nitroreductase Enzyme in Walker Cells That Activates 5-(Aziridin-1-Yl)-2,4-Dinitrobenzamide (Cb-1954) to 5-(Aziridin-1-Yl)-4-Hydroxylamino-2-Nitrobenzamide Is a Form of Nad(P)H Dehydrogenase (Quinone) (Ec-1.6.99.2). *Biochemical Pharmacology* **37**, 4671-4677

39. Knox, R. J., Friedlos, F., Biggs, P. J., Flitter, W. D., Gaskell, M., Goddard, P., Davies, L., and Jarman, M. (1993) Identification, Synthesis and Properties of 5-

(Aziridin-1-Yl)-2-Nitro-4-Nitrosobenzamide, a Novel DNA Cross-Linking Agent Derived from Cb1954. *Biochemical Pharmacology* **46**, 797-803

40. Knox, R. J., Friedlos, F., Sherwood, R. F., Melton, R. G., and Anlezark, G. M. (1992) The bioactivation of 5-(aziridin-1-yl)-2,4-dinitrobenzamide (CB1954)--II. A comparison of an Escherichia coli nitroreductase and Walker DT diaphorase. *Biochem Pharmacol* **44**, 2297-2301
41. Xu, G., and McLeod, H. L. (2001) Strategies for enzyme/prodrug cancer therapy. *Clin Cancer Res* **7**, 3314-3324
42. Chung-Faye, G., Palmer, D., Anderson, D., Clark, J., Downes, M., Baddeley, J., Hussain, S., Murray, P. I., Searle, P., Seymour, L., Harris, P. A., Ferry, D., and Kerr, D. J. (2001) Virus-directed, enzyme prodrug therapy with nitroimidazole reductase: A phase I and pharmacokinetic study of its prodrug, CB1954. *Clin Cancer Res* **7**, 2662-2668
43. Young, J. G., Leung, H. Y., Searle, P. F., Mautner, V., Howie, A., Horne, M., Ellis, J., Gilbert, J., Neal, D. E., Harris, P., Doherty, A. P., Wallace, D. M. A., and James, N. D. (2002) Direct injection of adenovirus for enzyme prodrug therapy of prostate cancer. *Brit J Cancer* **86**, S30-S30
44. Knox, R. J., Friedlos, F., and Boland, M. P. (1993) The Bioactivation of Cb-1954 and Its Use as a Prodrug in Antibody-Directed Enzyme Prodrug Therapy (Adept). *Cancer Metast Rev* **12**, 195-212
45. Helsby, N. A., Wheeler, S. J., Pruijn, F. B., Palmer, B. D., Yang, S., Denny, W. A., and Wilson, W. R. (2003) Effect of nitroreduction on the alkylating reactivity and cytotoxicity of the 2,4-dinitrobenzamide-5-aziridine CB 1954 and the corresponding nitrogen mustard SN 23862: distinct mechanisms of bioreductive activation. *Chem Res Toxicol* **16**, 469-478
46. Springer, C. J., and Niculescu-Duvaz, I. (2000) Prodrug-activating systems in suicide gene therapy. *The Journal of clinical investigation* **105**, 1161-1167
47. Rigg, A., and Sikora, K. (1997) Genetic prodrug activation therapy. *Molecular medicine today* **3**, 359-366
48. Niculescu-Duvaz, I., Spooner, R., Marais, R., and Springer, C. J. (1998) Gene-directed enzyme prodrug therapy. *Bioconjugate chemistry* **9**, 4-22

49. Prosser, G. A., Copp, J. N., Syddall, S. P., Williams, E. M., Smaill, J. B., Wilson, W. R., Patterson, A. V., and Ackerley, D. F. (2010) Discovery and evaluation of Escherichia coli nitroreductases that activate the anti-cancer prodrug CB1954. *Biochem Pharmacol* **79**, 678-687

50. Cui, W., Gusterson, B., and Clark, A. J. (1999) Nitroreductase-mediated cell ablation is very rapid and mediated by a p53-independent apoptotic pathway. *Gene Ther* **6**, 764-770

51. Knox, R. J., Friedlos, F., Jarman, M., and Roberts, J. J. (1988) A new cytotoxic, DNA interstrand crosslinking agent, 5-(aziridin-1-yl)-4-hydroxylamino-2-nitrobenzamide, is formed from 5-(aziridin-1-yl)-2,4-dinitrobenzamide (CB 1954) by a nitroreductase enzyme in Walker carcinoma cells. *Biochem Pharmacol* **37**, 4661-4669

52. Haynes, C. A., Koder, R. L., Jr., Miller, A.-F., and Rodgers, D. W. (2002) Structures of Nitroreductase in Three States: Effects of Inhibitor Binding and Reduction. *J. Biol. Chem.* **277**, 11513-11520

53. Koder, R. L., Haynes, C. A., Rodgers, M. E., Rodgers, D. W., and Miller, A. F. (2002) Flavin thermodynamics explain the oxygen insensitivity of enteric nitroreductases. *Biochemistry* **41**, 14197-14205

54. Bennett, M. J., Schlunegger, M. P., and Eisenberg, D. (1995) 3d Domain Swapping - a Mechanism for Oligomer Assembly. *Protein Science* **4**, 2455-2468

55. Yang, K. Y., and Swenson, R. P. (2007) Modulation of the redox properties of the flavin cofactor through hydrogen-bonding interactions with the N(5) atom: Role of alpha Ser254 in the electron-transfer flavoprotein from the methylotrophic bacterium W3A1. *Biochemistry* **46**, 2289-2297

56. Pitsawong, W., Sucharitakul, J., Prongjit, M., Tan, T. C., Spadiut, O., Haltrich, D., Divne, C., and Chaiyen, P. (2010) A conserved active-site threonine is important for both sugar and flavin oxidations of pyranose 2-oxidase. *J. Biol. Chem.* **285**, 9697-9705

57. Isayev, O., Crespo-Hernandez, C. E., Gorb, L., Hill, F. C., and Leszczynski, J. (2012) In silico structure-function analysis of E. cloacae nitroreductase. *Proteins* **80**, 2728-2741

58. Christofferson, A., Zhao, L. F., and Pei, Q. (2012) Dynamic Simulations as a Complement to Experimental Studies of Enzyme Mechanisms. *Adv Protein Chem Str* **87**, 293-335

59. Johansson, E., Parkinson, G. N., Denny, W. A., and Neidle, S. (2003) Studies of the nitroreductase produg-activating system. Crystal structures of complexes with the inhibitor dicoumarol and dinitrobenzamide prodrugs and of the enzyme active form. *J. Med. Chem.* **46**, 4009-4020

60. Race, P. R., Lovering, A. L., Green, R. M., Ossor, A., White, S. A., Searle, P. F., Wrighton, C. J., and Hyde, E. I. (2005) Structural and mechanistic studies of Escherichia coli nitroreductase with the antibiotic nitrofurazone - Reversed binding orientations in different redox states of the enzyme. *J. Biol. Chem* **280**, 13256-13264

61. Wouters, J., Durant, F., Champagne, B., and Andre, J. M. (1997) Electronic properties of flavins: Implications on the reactivity and absorption properties of flavoproteins. *Int J Quantum Chem* **64**, 721-733

62. Barna, T. M., Khan, H., Bruce, N. C., Barsukov, I., Scrutton, N. S., and Moody, P. C. E. (2001) Crystal structure of pentaerythritol tetranitrate reductase: "Flipped" binding geometries for steroid substrates in different redox states of the enzyme. *Journal of Molecular Biology* **310**, 433-447

63. Nivinskas, H., Staskeviciene, S., Sarlauskas, J., Koder, R. L., Miller, A. F., and Cenas, N. (2002) Two-electron reduction of quinones by Enterobacter cloacae NAD(P)H:nitroreductase: quantitative structure-activity relationships. *Arch Biochem Biophys* **403**, 249-258

64. Nivinskas, H., Koder, R. L., Anusevicius, Z., Sarlauskas, J., Miller, A. F., and Cenas, N. (2000) Two-electron reduction of nitroaromatic compounds by Enterobacter cloacae NAD(P)H nitroreductase: description of quantitative structure-activity relationships. *Acta Biochim Pol* **47**, 941-949

65. Race, P. R., Lovering, A. L., White, S. A., Grove, J. I., Searle, P. F., Wrighton, C. W., and Hyde, E. I. (2007) Kinetic and structural characterisation of Escherichia coli nitroreductase mutants showing improved efficacy for the prodrug substrate CB1954. *J. Mol. Biol* **368**, 481-492

66. Zhang, P. (2007) *Nitroreductase: evidence for a fluxional low-temperature state and its possible role in enzyme activity.* Doctoral Dissertations, Kentucky

67. Koike, H., Sasaki, H., Kobori, T., Zenno, S., Saigo, K., Murphy, M. E. P., Adman, E. T., and Tanokura, M. (1998) 1.8 angstrom crystal structure of the major NAD(P)H : FMN oxidoreductase of a bioluminescent bacterium, Vibrio fischeri: Overall structure, cofactor and substrate-analog binding, and comparison with related flavoproteins. *Journal of Molecular Biology* **280**, 259-273

68. Ghisla, S., and Wenz, A. . (1980) Colin Thorpe Suicide Substrates as Irreversible Inhibitors of Flavoenzymes. in *Enzyme Inhibitors: proceedings of a meeting held in Basel, on 20 and 21 March 1980 / ed.* , Urs Brodbeck. Weinheim, Verl. Chemie. pp 43-60

69. Palfey, B. A., Barrieentsch, B., Ballou, D. P., and Massey, V. (1994) Changes in the Catalytic Properties of P-Hydroxybenzoate Hydroxylase Caused by the Mutation Asn300asp. *Biochemistry* **33**, 1545-1554

70. Koder, R. L., and Miller, A. F. (1998) Overexpression, isotopic labeling, and spectral characterization of Enterobacter cloacae nitroreductase. *Protein Expr Purif* **13**, 53-60

71. Nivinskas, H., Koder, R. L., Anusevicius, Z., Sarlauskas, J., Miller, A. F., and Cenas, N. (2001) Quantitative structure-activity relationships in two-electron reduction of nitroaromatic compounds by Enterobacter cloacae NAD(P)H:nitroreductase. *Arch Biochem Biophys* **385**, 170-178

72. Kim, H. Y., and Song, H. G. (2005) Purification and characterization of NAD(P)H-dependent nitroreductase I from *Klebsiella* sp. C1 and enzymatic transformation of 2,4,6-trinitrotoluene. *Appl Microbiol Biotechnol* **68**, 766-773

73. Yanto, Y., Hall, M., and Bommarius, A. S. (2010) Nitroreductase from Salmonella typhimurium: characterization and catalytic activity. *Org. Biomol. Chem.* **8**, 1826-1832

74. Goodwin, A., Kersulyte, D., Sisson, G., van Zanten, S. J. O. V., Berg, D. E., and Hoffman, P. S. (1998) Metronidazole resistance in Helicobacter pylori is due to null mutations in a gene (rdxA) that encodes an oxygen-insensitive NADPH nitroreductase. *Molecular Microbiology* **28**, 383-393

75. Upcroft, P., and Upcroft, J. A. (2001) Drug targets and mechanisms of resistance in the anaerobic protozoa. *Clin Microbiol Rev* **14**, 150-+

76. Whitmore, G. F., and Varghese, A. J. (1986) The Biological Properties of Reduced Nitroheterocyclics and Possible Underlying Biochemical-Mechanisms. *Biochemical Pharmacology* **35**, 97-103

77. Goldman, P., Koch, R. L., Yeung, T. C., Chrystal, E. J. T., Beaulieu, B. B., Mclafferty, M. A., and Sudlow, G. (1986) Comparing the Reduction of Nitroimidazoles in Bacteria and Mammalian-Tissues and Relating It to Biological-Activity. *Biochemical Pharmacology* **35**, 43-51

78. Manina, G., Bellinzoni, M., Pasca, M. R., Neres, J., Milano, A., Ribeiro, A. L. J. L., Buroni, S., Skovierova, H., Dianiskova, P., Mikusova, K., Marak, J., Makarov, V., Giganti, D., Haouz, A., Lucarelli, A. P., Degliacomi, G., Piazza, A., Chiarelli, L. R., De Rossi, E., Salina, E., Cole, S. T., Alzari, P. M., and G., R. (2010) Biological and structural characterization of the *Micobacterium smegmatis* nitroreductase NfnB, and its role in benzothiozinone resistance. *Mol. Microbiol.* **77**, 1172-1185

79. LinWu, S. W., Wu, C. A., Peng, F. C., and Wang, A. H. (2012) Structure-based development of bacterial nitroreductase against nitrobenzodiazepine-induced hypnosis. *Biochem Pharmacol* **83**, 1690-1699

80. Mast, N., Norcross, R., Andersson, U., Shou, M. G., Nakayama, K., Bjorkhem, I., and Pikuleva, I. A. (2003) Broad substrate specificity of human cytochrome P450 46A1 which initiates cholesterol degradation in the brain. *Biochemistry* **42**, 14284-14292

81. Guengerich, F. P. (2001) Common and uncommon cytochrome P450 reactions related to metabolism and chemical toxicity. *Chem Res Toxicol* **14**, 611-650

82. Khan, H., Harris, R. J., Barna, T., Craig, D. H., Bruce, N. C., Munro, A. W., Moody, P. C., and Scrutton, N. S. (2002) Kinetic and structural basis of reactivity of pentaerythritol tetranitrate reductase with NADPH, 2-cyclohexenone, nitroesters, and nitroaromatic explosives. *J. Biol. Chem* **277**, 21906-21912

83. French, C. E., Nicklin, S., and Bruce, N. C. (1996) Sequence and properties of pentaerythritol tetranitrate reductase from Enterobacter cloacae PB2. *J Bacteriol* **178**, 6623-6627

84. Lu, Z. B., Dunaway-Mariano, D., and Allen, K. N. (2011) The X-ray crystallographic structure and specificity profile of HAD superfamily phosphohydrolase BT1666: Comparison of paralogous functions in B. thetaiotaomicron. *Proteins* **79**, 3099-3107

85. Jarrom, D., Jaberipour, M., Guise, C. P., Daff, S. N., White, S. A., Searle, P. F., and Hyde, E. I. (2009) Steady-state and stopped-flow kinetic studies of three *Escherichia coli* NfsB mutants with enhanced activity for the prodrug CB1954. *Biochemistry* **48**, 7665-7672

86. Delano, W. L. (2010) The PyMOL Molecular Graphics System, version 1.3rl, Schrödinger, LLC, New York.

87. Defoin, A. (2004) Simple preparation of nitroso benzenes and nitro benzenes by oxidation of anilines with H2O2 catalysed with molybdenum salts. *Synthesis-Stuttgart*, 706-710

88. Cleland, W. W. (1979) Substrate inhibition. *Methods Enzymol* **63**, 500-513

89. Cornish-Bowden, A. (1995) Fundamentals of Enzyme Kinetics. *Portland Press, London*

90. Smallcombe, S. H., Patt, S. L., and Keifer, P. A. (1995) WET solvent suppression and its applications to LC NMR and high-resolution NMR spectroscopy. *J Magn Reson Ser A* **117**, 295-303

91. Ogata, Y., and Takagi, Y. (1958) Kinetics of the Condensation of Anilines with Nitrosobenzenes to Form Azobenzenes. *J Am Chem Soc* **80**, 3591-3595

92. Zhao, R., Tan, C., Xie, Y., Gao, C., Liu, H., and Jiang, Y. (2011) One step synthesis of azo compounds from nitroaromatics and anilines. *Tetrahedron Letters* **52**, 3805-3809

93. Sone, T., Tokuda, Y., Sakai, T., Shinkai, S., and Manabe, O. (1981) Kinetics and Mechanisms of the Bamberger Rearrangement .3. Rearrangement of Phenylhydroxylamines to Papa-Aminophenols in Aqueous Sulfuric-Acid-Solutions. *J Chem Soc Perk T 2*, 298-302

94. Yost, Y. (1969) Oxidation of Fluorenamines and Preparation of 2,2'- and 4,4'-Azofluorene. *Journal of Medicinal Chemistry* **12**, 961-&

95. Gasparic, J., Svobodova, D., and Pospisilova, M. (1977) Investigation of color-reaction of phenols with mbth reagent - identification of organic-compounds .86. *Mikrochimica Acta* **1**, 241-250

96. Elkommos, M. E., and Emara, K. M. (1987) Spectrophotometric Determination of Certain Local-Anesthetics Using 3-Methylbenzothiazolin-2-One Hydrazone. *Analyst* **112**, 1253-1256

97. Campbell, G. R. O., Taga, M. E., Mistry, K., Lloret, J., Anderson, P. J., Roth, J. R., and Walker, G. C. (2006) Sinorhizobium meliloti bluB is necessary for production of 5,6-dimethylbenzimidazole, the lower ligand of B-12. *P Natl Acad Sci USA* **103**, 4634-4639

98. Pérez-Reinado, E., Roldán, M. D., Castillo, F., and Moreno-Vivián, C. (2008) The NprA nitroreductase required for 2,4-dinitrophenol reduction in Rhodobacter capsulatus is a dihydropteridine reductase. *Env. Micro.* **10**, 3174-3183

99. Johansson, E., Parkinson, G. N., Denny, W. A., and Neidle, S. (2003) Studies on the nitroreductase prodrug-activating system. Crystal structures of complexes with the inhibitor dicoumarol and dinitrobenzamide prodrugs and of the enzyme active form. *Journal of Medicinal Chemistry* **46**, 4009-4020

100. Gamage, N. U., Tsvetanov, S., Duggleby, R. G., McManus, M. E., and Martin, J. L. (2005) The structure of human SULT1A1 crystallized with estradiol - An insight into active site plasticity and substrate inhibition with multi-ring substrates. *Journal of Biological Chemistry* **280**, 41482-41486

101. Yasutake, Y., Yao, M., Sakai, N., Kirita, T., and Tanaka, I. (2004) Crystal structure of the Pyrococcus horikoshii isopropylmalate isomerase small subunit provides insight into the dual substrate specificity of the enzyme. *J. Mol. Biol.* **344**

102. Tomatis, P. E., Fabiane, S. M., Simona, F., Carloni, P., Sutton, B. J., and Vila, A. J. (2008) Adaptive protein evolution grants organismal fitness by improving catalysis and flexibility. *Proc Natl. Acad. Sci. USA.* **105**, 20605-20610

103. Hou, L., Honaker, M. T., Shireman, L. M., Balogh, L. M., Roberts, A. G., Ng, K. C., Nath, A., and Atkins, W. M. (2007) Functional promiscuity correlates with conformational heterogeneity in A-class glutathione S-transferases. *Journal of Biological Chemistry* **282**, 23264-23274

104. Frederick, K. K., and Palfey, B. A. (2005) Kinetics of proton-linked flavin conformational changes in p-hydroxybenzoate hydroxylase. *Biochemistry* **44**, 13304-13314

105. Palfey, B. A., Moran, G. R., Entsch, B., Ballou, D. P., and Massey, V. (1999) Substrate recognition by "password" in p-hydroxybenzoate hydroxylase. in *Biochemistry*

106. Bollinger, J. M., Jr., and Krebs, C. (2006) Stalking intermediates in oxygen activation by iron enzymes: Motivation and method. *J. Inorg. Biochem.* **100**, 586-605

107. Solomon, E. I., Brunold, T. C., Davis, M. I., Kemsley, J. N., Lee, S.-K., Lehnert, N., Neese, F., Skulan, A. J., Yang, Y.-S., and Zhou, J. (2000) Geometric and electronic structure/function correlations in non-heme iron enzymes. *Chem. Rev.* **100**, 235-349

108. Schenzle, A., Lenke, H., Spain, J. C., and Knackmuss, H. J. (1999) 3-hydroxylaminophenol mutase from Ralstonia eutropha JMP134 catalyzes a Bamberger rearrangement. *J Bacteriol* **181**, 1444-1450

109. Spain, J. C. (1995) Biodegradation of Nitroaromatic Compounds. *Annu Rev Microbiol* **49**, 523-555

110. Smallcombe, S. H., Patt, S. L., and Keifer, P. A. (1995) WET solvent suppression and its applications to LC NMR and high-resolution NMR spectroscopy,. *J. Magn. Reson. A* **117**, 295-303

111. Hammes-Schiffer, S. (2002) Comparison of hydride, hydrogen atom, and proton-coupled electron transfer reactions. *Chemphyschem* **3**, 33-42

112. Pitsawong, W., Hoben, J. P., and Miller, A. F. (2014) Understanding the Broad Substrate Repertoire of Nitroreductase Based on Its Kinetic Mechanism. *Journal of Biological Chemistry* **289**, 15203-15214

113. Fraaije, M. W., and Mattevi, A. (2000) Flavoenzymes: diverse catalysts with recurrent features. *TIBS* **25**, 126-132

114. Page, C. C., Moser, C. C., Chen, X. X., and Dutton, P. L. (1999) Natural engineering principles of electron tunnelling in biological oxidation-reduction. *Nature* **402**, 47-52

115. Bianchet, M. A., Faig, M., and Amzel, L. M. (2004) Structure and mechanism of NAD[P]H : Quinone acceptor oxidoreductases (NQO). *Method Enzymol* **382**, 144-174

116. Gassner, G., Wang, L. H., Batie, C., and Ballou, D. P. (1994) Reaction of Phthalate Dioxygenase Reductase with Nadh and Nad - Kinetic and Spectral Characterization of Intermediates. *Biochemistry* **33**, 12184-12193

117. Nijvipakul, S., Ballou, D. P., and Chaiyen, P. (2010) Reduction kinetics of a flavin oxidoreductase LuxG from Photobacterium leiognathi (TH1): half-sites reactivity. *Biochemistry* **49**, 9241-9248

118. Mayhew, S. G. (1971) Studies on flavin binding in flavodoxins. *Biochimica et biophysica acta* **235**, 289-302

119. Cui, D. (2010) *15N Solid-State NMR Detection of Flavin Perturbation by H-Bonding in Models and Enzyme Active Sites*Doctoral Dissertations, University of Kentucky

120. Glascoe, P. K., Long, F.A. (1960) Use of glasselectrode to measure acidities in deuterium oxide. *J. Phys. Chem.* **64**, 188-191

121. Tinikul, R., Pitsawong, W., Sucharitakul, J., Nijvipakul, S., Ballou, D. P., and Chaiyen, P. (2013) The Transfer of Reduced Flavin Mononucleotide from LuxG Oxidoreductase to Luciferase Occurs via Free Diffusion. *Biochemistry* **52**, 6834-6843

122. Xu, H. Y., Alguindigue, S. S., West, A. H., and Cook, P. F. (2007) A proposed proton shuttle mechanism for saccharopine dehydrogenase from Saccharomyces cerevisiae. *Biochemistry* **46**, 871-882

123. Vashishtha, A. K., West, A. H., and Cook, P. F. (2009) Chemical Mechanism of Saccharopine Reductase from Saccharomyces cerevisiae. *Biochemistry* **48**, 5899-5907

124. Schowen, K. B., and Schowen, R. L. (1982) Solvent isotope effects of enzyme systems. *Methods Enzymol* **87**, 551-606

125. Quinn, D. M., and Sutton, L. D. (1991) Theoretical Basis and Mechanistic Utility of Solvent Isotope Effects. in *Enzyme mechanism from isotope effects* (Cook, P. F. ed.), CRC Press, Boca Raton. pp 73-126

126. Schowen, R. L. (1977) Solvent Isotope Effects on Enzymic Reactions. in *Isotope effects on enzyme-catalyzed reactions* (Cleland, W. W., O'Leary, M. H., and Northrop, D. B. ed.), University Park Press, Baltimore, MD. pp 64-99

127. Karsten, W. E., Lai, C. J., and Cook, P. F. (1995) Inverse Solvent Isotope Effects in the Nad-Malic Enzyme Reaction Are the Result of the Viscosity Difference between D2o and H2o - Implications for Solvent Isotope Effect Studies. *J Am Chem Soc* **117**, 5914-5918

128. Chang, F. C., and Swenson, R. P. (1999) The midpoint potentials for the oxidized-semiquinone couple for Gly57 mutants of the Clostridium beijerinckii flavodoxin correlate with changes in the hydrogen-bonding interaction with the proton on N(5) of the reduced flavin mononucleotide cofactor as measured by NMR chemical shift temperature dependencies. *Biochemistry* **38**, 7168-7176

129. Basran, J., Harris, R. J., Sutcliffe, M. J., and Scrutton, N. S. (2003) H-tunneling in the multiple H-transfers of the catalytic cycle of morphinone reductase and in the reductive half-reaction of the homologous pentaerythritol tetranitrate reductase. *The Journal of biological chemistry* **278**, 43973-43982

130. Pudney, C. R., Hay, S., and Scrutton, N. S. (2009) Bipartite recognition and conformational sampling mechanisms for hydride transfer from nicotinamide coenzyme to FMN in pentaerythritol tetranitrate reductase. *Febs J* **276**, 4780-4789

131. Hermes, J. D., Roeske, C. A., Oleary, M. H., and Cleland, W. W. (1982) Use of Multiple Isotope Effects to Determine Enzyme Mechanisms and Intrinsic Isotope Effects - Malic Enzyme and Glucose-6-Phosphate-Dehydrogenase. *Biochemistry* **21**, 5106-5114

132. Belasco, J. G., Albery, W. J., and Knowles, J. R. (1983) Double Isotope Fractionation - Test for Concertedness and for Transition-State Dominance. *J Am Chem Soc* **105**, 2475-2477

133. Pudney, C. R., Hay, S., Sutcliffe, M. J., and Scrutton, N. S. (2006) Alpha-secondary isotope effects as probes of "tunneling-ready" configurations in enzymatic H-tunneling: insight from environmentally coupled tunneling models. *J Am Chem Soc* **128**, 14053-14058

134. Shen, A. L., Sem, D. S., and Kasper, C. B. (1999) Mechanistic studies on the reductive half-reaction of NADPH-cytochrome P450 oxidoreductase. *The Journal of biological chemistry* **274**, 5391-5398

135. Sanchez-Azqueta, A., Catalano-Dupuy, D. L., Lopez-Rivero, A., Tondo, M. L., Orellano, E. G., Ceccarelli, E. A., and Medina, M. (2014) Dynamics of the active site architecture in plant-type ferredoxin-NADP(+) reductases catalytic complexes. *Bba-Bioenergetics* **1837**, 1730-1738

136. Wang, Z., Roston, D., Kohen, A. (2012) Experimetal and theoretical studies of enzyme-catalyzed hydrogen-transfer reactions. in *Adv Protein Chem Str* (Christov, C., Karabencheva-Christova, T. ed.), Elsevier Academic Press Inc, San Diego, CA, USA. pp 155-180

137. Westheimer, F. H. (1961) The Magnitude of the Primary Kinetic Isotope Effect for Compounds of Hydrogen and Deuterium. *Chem Rev* **61**, 265-273

138. Gannavaram, S., and Gadda, G. (2013) Relative Timing of Hydrogen and Proton Transfers in the Reaction of Flavin Oxidation Catalyzed by Choline Oxidase. *Biochemistry* **52**, 1221-1226

139. Franken, H. D., Ruterjans, H., and Muller, F. (1984) Nuclear-magnetic-resonance investigation of 15N-labeled flavins, free and bound to Megasphaera elsdenii apoflavodoxin. *Eur J Biochem* **138**, 481-489

140. Macheroux, P., Ghisla, S., Sanner, C., Ruterjans, H., and Muller, F. (2005) Reduced flavin: NMR investigation of N5-H exchange mechanism, estimation of ionisation constants and assessment of properties as biological catalyst. *BMC biochemistry* **6**, 26

141. Meah, Y., and Massey, V. (2000) Old Yellow Enzyme: Stepwise reduction of nitro-olefins and catalysis of aci-nitro tautomerization. *P Natl Acad Sci USA* **97**, 10733-10738

142. Vihinen, M. (1987) Relationship of Protein Flexibility to Thermostability. *Protein Eng* **1**, 477-480

143. Shoichet, B. K., Baase, W. A., Kuroki, R., and Matthews, B. W. (1995) A Relationship between Protein Stability and Protein Function. *P Natl Acad Sci USA* **92**, 452-456

144. Tang, K. E. S., and Dill, K. A. (1998) Native protein fluctuations: The conformational-motion temperature and the inverse correlation of protein flexibility with protein stability. *J Biomol Struct Dyn* **16**, 397-411

145. Kleckner, I. R., and Foster, M. P. (2011) An introduction to NMR-based approaches for measuring protein dynamics. *Biochimica et biophysica acta* **1814**, 942-968

146. Loria, J. P., Berlow, R. B., and Watt, E. D. (2008) Characterization of enzyme motions by solution NMR relaxation dispersion. *Accounts Chem Res* **41**, 214-221

147. Palmer, A. G. (2004) NMR characterization of the dynamics of biomacromolecules. *Chem Rev* **104**, 3623-3640

148. Loria, J. P., Rance, M., and Palmer, A. G. (1999) A relaxation-compensated Carr-Purcell-Meiboom-Gill sequence for characterizing chemical exchange by NMR spectroscopy. *J Am Chem Soc* **121**, 2331-2332

149. Neudecker, P., Lundstrom, P., and Kay, L. E. (2009) Relaxation dispersion NMR spectroscopy as a tool for detailed studies of protein folding. *Biophys J* **96**, 2045-2054

150. Mittermaier, A., and Kay, L. E. (2006) New tools provide new insights in NMR studies of protein dynamics. *Science* **312**, 224-228

151. Boehr, D. D., McElheny, D., Dyson, H. J., and Wright, P. E. (2006) The dynamic energy landscape of dihydrofolate reductase catalysis. *Science* **313**, 1638-1642

152. Fierke, C. A., Johnson, K. A., and Benkovic, S. J. (1987) Construction and Evaluation of the Kinetic Scheme Associated with Dihydrofolate-Reductase from Escherichia-Coli. *Biochemistry* **26**, 4085-4092

153. Eisenmesser, E. Z., Millet, O., Labeikovsky, W., Korzhnev, D. M., Wolf-Watz, M., Bosco, D. A., Skalicky, J. J., Kay, L. E., and Kern, D. (2005) Intrinsic dynamics of an enzyme underlies catalysis. *Nature* **438**, 117-121

154. Cai, M. L., Huang, Y., Sakaguchi, K., Clore, G. M., Gronenborn, A. M., and Craigie, R. (1998) An efficient and cost-effective isotope labeling protocol for proteins expressed in Escherichia coli. *Journal of Biomolecular Nmr* **11**, 97-102

155. Muchmore, D. C., McIntosh, L. P., Russell, C. B., Anderson, D. E., and Dahlquist, F. W. (1989) Expression and nitrogen-15 labeling of proteins for proton and nitrogen-15 nuclear magnetic resonance. *Methods Enzymol* **177**, 44-73

156. Baxter, N. J., and Williamson, M. P. (1997) Temperature dependence of 1H chemical shifts in proteins. *J Biomol NMR* **9**, 359-369

157. Curley, R. W., Jr., Panigot, M. J., Hansen, A. P., and Fesik, S. W. (1994) Stereospecific assignments of glycine in proteins by stereospecific deuteration and 15N labeling. *J Biomol NMR* **4**, 335-340

158. Wahjudi, P. N., Xiao, G. G., Lee, W. N. P., Nowak, M. W., and Shiva, N. (2010) Determination of Protein Synthesis In-Vivo with N-15-Glycine Labeling and MALDI-TOF Spectrum Analysis. *Faseb J* **24**

159. Velankar, S., Dana, J. M., Jacobsen, J., van Ginkel, G., Gane, P. J., Luo, J., Oldfield, T. J., O'Donovan, C., Martin, M. J., and Kleywegt, G. J. (2013) SIFTS: Structure Integration with Function, Taxonomy and Sequences resource. *Nucleic Acids Res* **41**, D483-D489

160. Murzin, A. G., Brenner, S. E., Hubbard, T., and Chothia, C. (1995) Scop - a Structural Classification of Proteins Database for the Investigation of Sequences and Structures. *Journal of Molecular Biology* **247**, 536-540

161. Kabsch, W., and Sander, C. (1983) Dictionary of Protein Secondary Structure - Pattern-Recognition of Hydrogen-Bonded and Geometrical Features. *Biopolymers* **22**, 2577-2637

162. Golovin, A., Dimitropoulos, D., Oldfield, T., Rachedi, A., and Henrick, K. (2005) MSDsite: A database search and retrieval system for the analysis and viewing of bound ligands and active sites. *Proteins* **58**, 190-199

163. Meiboom, S., and Gill, D. (1958) Modified Spin-Echo Method for Measuring Nuclear Relaxation Times. *Rev Sci Instrum* **29**, 688-691

164. Ishima, R. (2012) Recent Developments in 15N NMR Relaxation Studies that Probe Protein Backbone Dynamics. in *Topics in Current Chemistry: NMR of*

Proteins and Small Biomolecules (Zhu, G. ed.), Springer-Verlag Berlin Heidelberg. pp 99-122

165. Labeikovsky, W., Eisenmesser, E. Z., Bosco, D. A., and Kern, D. (2007) Structure and dynamics of Pin1 during catalysis by NMR. *Journal of Molecular Biology* **367**, 1370-1381
166. Eisenmesser, E. Z., Bosco, D. A., Akke, M., and Kern, D. (2002) Enzyme dynamics during catalysis. *Science* **295**, 1520-1523
167. Lynch, M. (2013) Evolutionary diversification of the multimeric states of proteins. *P Natl Acad Sci USA* **110**, E2821-E2828
168. Marianayagam, N. J., Sunde, M., and Matthews, J. M. (2004) The power of two: protein dimerization in biology. *Trends Biochem Sci* **29**, 618-625
169. Ali, M. H., and Imperiali, B. (2005) Protein oligomerization: How and why. *Bioorgan Med Chem* **13**, 5013-5020
170. Jones, S., and Thornton, J. M. (1995) Protein-Protein Interactions - a Review of Protein Dimer Structures. *Prog Biophys Mol Bio* **63**, 31-&
171. Jones, S., and Thornton, J. M. (1997) Prediction of protein-protein interaction sites using patch analysis. *Journal of Molecular Biology* **272**, 133-143
172. Xu, D., Lin, S. L., and Nussinov, R. (1997) Protein binding versus protein folding: The role of hydrophilic bridges in protein associations. *Journal of Molecular Biology* **265**, 68-84
173. Yonehara, M., Minami, Y., Kawata, Y., Nagai, J., and Yahara, I. (1996) Heat-induced chaperone activity of HSP90. *Journal of Biological Chemistry* **271**, 2641-2645
174. Liu, Y., and Eisenberg, D. (2002) 3D domain swapping: as domains continue to swap. *Protein science : a publication of the Protein Society* **11**, 1285-1299
175. Huma, Z. E., Ludeman, J. P., Wilkinson, B. L., Payne, R. J., and Stone, M. J. (2014) NMR characterization of cooperativity: fast ligand binding coupled to slow protein dimerization. *Chem Sci* **5**, 2783-2788
176. Andrews, F. H., Rogers, M. P., Paul, L. N., and McLeish, M. J. (2014) Perturbation of the Monomer-Monomer Interfaces of the Benzoylformate Decarboxylase Tetramer. *Biochemistry* **53**, 4358-4367

177. Duggleby, R. G. (2006) Domain relationships in thiamine diphosphate-dependent enzymes. *Acc Chem Res* **39**, 550-557

178. Koharudin, L. M. I., Liu, L., and Gronenborn, A. M. (2013) Different 3D domain-swapped oligomeric cyanovirin-N structures suggest trapped folding intermediates. *P Natl Acad Sci USA* **110**, 7702-7707

179. Massey, V. (1991) A Simple Method for the Determination of Redox Potentials. in *Flavins and Flavoproteins* (Curti, B., Rochi, S., and Zanetti, G., Eds. ed.), Water DeGruyter & Co., Berlin. pp 59-66

180. Loach, P. A. (1973) Oxidation-reduction potentials: Absorbance bands and molar absorbance of compounds used in biochemical studies. in *Handbook of Biochemistry Selected Data for Molecular Biology* (Sorber, H. A., Ed. ed.), The Chemical Rubber Co. (CRC Press), Cleveland, OH. pp J-33 - J-40

181. Gardner, K. H., and Kay, L. E. (1997) Production and incorporation of N-15, C-13, H-2 (H-1-delta 1 methyl) isoleucine into proteins for multidimensional NMR studies. *J Am Chem Soc* **119**, 7599-7600

182. Goto, N. K., Gardner, K. H., Mueller, G. A., Willis, R. C., and Kay, L. E. (1999) A robust and cost-effective method for the production of Val, Leu, Ile (delta 1) methyl-protonated N-15-, C-13-, H-2-labeled proteins. *Journal of Biomolecular Nmr* **13**, 369-374

183. Religa, T. L., Sprangers, R., and Kay, L. E. (2010) Dynamic Regulation of Archaeal Proteasome Gate Opening As Studied by TROSY NMR. *Science* **328**, 98-102

VITA

Warintra Pitsawong

EDUCATION

Mahidol University, Bangkok, Thailand

B.Sc. in Chemistry (First Class Honors: top 10% of graduating class) **2007**

Mahidol University, Bangkok, Thailand

M.Sc. in Biochemistry **2010**

Thesis: Investigation the role of Threonine 169 in the reaction catalyzed by pyranose 2-oxidase from *Trametes Multicolor*

PROFESSIONAL EXPERIENCE

Undergraduate Honors Research: Department of Biochemistry, Mahidol University, Bangkok, Thailand, 2005-2007, (research advisor: Prof. Pimchai Chaiyen)

- Development of enzyme assay for detection of glycerol
- Purification of bacterial luciferase from *Photobacterium sp*.

Master research: Department of Biochemistry, Mahidol University, Bangkok, Thailand, 2007-2010, (research advisor: Prof. Pimchai Chaiyen)

- Investigation on the role of Threonine 169 in the reaction catalyzed by pyranose 2-oxidase
- The transfer of reduced flavin mononucleotide from LuxG oxidoreductase to luciferase occurs via free diffusion

Doctoral Research: Department of Chemistry, University of Kentucky, 2010-2014, (research advisor: Prof. Anne-Frances Miller)

- The unusual broad substrate repertoire of nitroreductase (NR), which may be related to protein dynamics (flexibility).
- Integrated computational approach to the analysis of ^{15}N and ^{13}C NMR in active site of flavodoxin.
- Use of ^{19}F NMR to probe the pK_a changes upon binding in enzyme active sites.

HONORS AND AWARDS

2003-present: Scholarship from Royal Government of Thailand "**D**evelopment and **P**romotion of **S**cience and **T**echnology talents project (DPST)"

2006: 1. "Honor Program" of Chemistry Dept., Mahidol University, Bangkok, Thailand

2. Scholarship from **J**unior **S**cience **T**alent **P**roject (JSTP), Thailand

2009: Thesis Publication Award from the Graduate School, Mahidol University

2013-2014: 1. **R**esearch **C**hallenge **T**rust **F**und (RCTF) fellowship from University of Kentucky

2. Travel Award from Graduate School, University of Kentucky

2014 1. Vince Massey Award from 18th International Symposium on Flavins and Flavoproteins.

2. Travel Award from Graduate School, University of Kentucky

PUBLICATIONS

1. **Pitsawong, W.**, Sucharitakul, J., Prongjit, M., Tan, T-C., Spadiut, O., Haltrich, D., Divne, C., and Chaiyen, P. (2010) A Conserved active-Site threonine is important for both sugar and flavin oxidation of pyranose 2-oxidase. *J. Biol. Chem.* 285, 9697- 705.
2. Tan, T-C., **Pitsawong, W.**, Wongnate, T., Spadiut, O., Haltrich, D., Chaiyen, P., and Divne, C. (2010) H-bonding and positive charge at the N(5)/O(4) locus are critical for covalent flavin attachment in trametes pyranose 2-oxidase. *J. Mol. Biol.* 402, 578-594.
3. Tinikul, R.*, **Pitsawong, W.***, Sucharitakul, J., Nijvipakul, S., Ballou, DP., and Chaiyen, P. (2013) The transfer of reduced flavin mononucleotide from LuxG oxidoreductase to luciferase occurs via free diffusion. *Biochemistry* 52, 6834-6843. (*Equal contribution)
4. **Pitsawong, W.**, Hoben JP., and Miller, AF. (2014) Understanding and exploiting the broad substrate repertoire of nitroreductase via kinetic mechanism**.** *J. Biol. Chem.* 289, 15203-14.
5. **Pitsawong, W.**, Chenprakhon, P., Dhammaraj, T., Medhanavyn, D., Sucharitakul, J., Chaiyen, P., and Miller, AF. Depression and Reversal of Substrate pK_as upon Binding

to the Oxygenase Components of *p*-Hydroxyphenylacetate 3-Hydroxylase or 3-Hydroxybenzoate 6-Hydroxylase. (experiments complete, writing in progress)

6. **Pitsawong, W.**, Haynes, CA., Koder, RL., Rodgers, DW., and Miller, AF. Rate-contributing proton transfers of the two half-reactions of the flavoenzyme nitroreductase. (experiments complete, writing in progress)

RESEARCH PRESENTATIONS

Selected Oral Presentations

1. **Pitsawong, W.**, Suadee, C., and Chaiyen, P. (2007) Development of enzyme assay for detection of glycerol. Honor Program in Chemistry Dept., Mahidol University, Bangkok, Thailand.
2. **Pitsawong, W.**, Sucharitakul, S., Prongjit, M., Tan, T-C., Spadiut, O., Haltrich, D., Divne, C., and Chaiyen, P. (2009) A conserved active-Site threonine is important for both half-reactions of pyranose 2-oxidase. Pure and Applied Chemistry International Conference (PACCON2010), Sunee Grand Hotel and Convention Center, Ubon Ratchathani, Thailand.
3. **Pitsawong, W.**, Sucharitakul, S., Prongjit, M., Tan, T-C., Spadiut, O., Haltrich, D., Divne, C., and Chaiyen, P. (2010) A conserved active-site threonine is important for both half-reactions of pyranose 2-oxidase. University of Graz, Graz, Austria, 25th - 26th March.
4. **Pitsawong, W.**, Miller, AF. (2012) Integrated computational approach to the analysis of ^{15}N and ^{13}C NMR in active site of flavodoxin. Third Annual Southeast Enzyme Conference (SEC), Georgia State University, 14th April.
5. **Pitsawong, W.**, Chenprakhon, P., Dhammaraj, T., Medhanavyn, D., Sucharitakul, J., Chaiyen, P., and Miller, AF. (2014) Depression and Reversal of Substrate pK_as upon Binding to the Oxygenase Components of *p*-Hydroxyphenylacetate 3-Hydroxylase or 3-Hydroxybenzoate 6-Hydroxylase. 18th International Symposium on Flavins and Flavoproteins, Phechaburi, Thailand, 27th July – 1st August.

Selected Poster Presentations

1. **Pitsawong, W.**, Suadee, C., and Chaiyen, P. (2007) Development of enzyme assay for detection of glycerol. The 8th Science Project Exhibition, Mahidol University, Bangkok, Thailand.
2. **Pitsawong, W.**, Nijvipakul, S., and Chaiyen, P. (2008) Probing interaction between bacterial luciferase and LuxG protein. 16th International symposium on flavins and flavoproteins. Palacio de Congresos, Jaca, Spain.
3. **Pitsawong, W.**, Sucharitakul, J., Prongjit, M., Haltrich, D., and Chaiyen, P. (2009) Investigation the role of Threonine 169 in the reaction catalyzed by pyranose 2-oxidase from *Trametes Multicolor*. The 4th Annual Symposium of Protein Society of Thailand Protein Research from Basic Studies to Applications in Health Science, Chulabhorn Research Institute Conference Center, Vibhavadee Rangsit Highway, Bangkok, Thailand.
4. **Pitsawong, W.**, Jeerus Sucharitakul, Sarayut Nijvipakul, David P. Ballou, and Pimchai Chaiyen. (2011) Reduced FMN transfer from LuxG to LuxAB is mediated through transient protein-protein interaction. 17th International Flavin and flavoproteins Symposium, University of California, Berkeley, California
5. **Pitsawong, W.**, Miller, AF. (2012) Integrated Computational Approach to the Analysis of ^{15}N and ^{13}C NMR in Active Site of Flavodoxin. Naff Symposium, University of Kentucky, Lexington, KY, 4th May.
6. **Pitsawong, W.**, Miller, AF. (2012) A Moving Target: Transient kinetics, temperature dependent dynamics and substrate analog binding in nitroreductase. The 32nd Midwest Enzyme Chemistry Conference (MECC). University of Illinois at Chicago (UIC), Chicago, IL, 13rd October.
7. **Pitsawong, W.**, Miller, AF. (2012) A Basic for Breadth: The kinetic mechanism of nitroreductase. NSF-I/UCR Center for Pharmaceutical Development (CPD), Georgia Institute of Technology, Atlanta, GA, 8th-9th November.
8. **Pitsawong, W.**, Miller, AF. (2013) Solvent kinetic isotope effect (SKIE) and proton inventory for nitroreductase. NSF-I/UCR Center for Pharmaceutical Development (CPD), University of Kentucky, 14th-15th May.

9. **Pitsawong, W.**, Miller, AF (2013) Transient kinetics of nitroreductase from *Enterobacter cloacae* and kinetic isotope effects as a tool for probing hydride transfer. 246th American Chemical Society (ACS) National Meeting in Indianapolis, Indiana, 8th -12th September.
10. **Pitsawong, W.**, Chenprakhon, P., Dhammaraj, T., Medhanavyn, D., Sucharitakul, J., Chaiyen, P., and Miller, AF. (2014) Depression and Reversal of Substrate pK_as upon Binding to the Oxygenase Components of *p*-Hydroxyphenylacetate 3-Hydroxylase or 3-Hydroxybenzoate 6-Hydroxylase. 18th International Symposium on Flavins and Flavoproteins, Phechaburi, Thailand, 27th July – 1st August.

Warintra Pitsawong

November 24th, 2014